

**Fiber Reinforced Elastomeric Isolators
for Bridge Applications**

Fiber Reinforced Elastomeric Isolators for Bridge Applications

By

YASSER MOHAMMED AL-ANANY

B.Sc., M.Sc.

A Thesis Submitted to the School of Graduate Studies
in Partial Fulfilment of the Requirements for the Degree of

DOCTOR OF PHILOSOPHY

McMaster University

© Copyright by Yasser Al-Anany

September 2016

Doctor of Philosophy (2016)
(Civil Engineering)

McMaster University
Hamilton, Ontario

TITLE: Fiber Reinforced Elastomeric Isolators for Bridge Applications

AUTHOR: Yasser Mohammed Mohammed Al-Anany

SUPERVISOR: Dr. Michael J. Tait

NUMBER OF PAGES: XV,213

Abstract

Bridge structures are considered a critical component in transportation systems. Bridges are divided into two main components, the superstructure and the substructure. Often the superstructure is integrated with the substructure. However, this type of integrated connection results in a direct transmission of straining actions developed within the superstructure to the substructure and vice versa. This consequently leads to a significant increase in the demand capacity of both elements. Examples of various actions that can develop in the superstructure include thermal expansion/contraction, pre-stress shortening/camber and creep. Deformation induced from ground motions during a seismic event is an example of an action that develops in the substructure. It has been proposed to isolate the superstructure and substructure by implementing bearings/isolators between these two components in order to reduce the transmission of straining actions. If the elements are used only to transfer the vertical loads as well as to accommodate the rotational and/or lateral deformations then it is referred as a bearing. However, if the bearings are also used for seismic isolation of the bridge then they are defined as isolators. Thus, isolators also act as bearings, but bearings may not be capable of acting as isolators.

Elastomeric bearings/isolators are among the most common and widely used bearing type. Traditional elastomeric bearings are comprised of elastomer layers reinforced with steel plates/shims and are called Steel Reinforced Elastomeric Isolators (SREI). However, the application of these bearings has been limited to high-importance structures. This is due to the fact that SREI are characterized by their high cost and weight. These features result from labour intensive manufacturing costs and significant weight of the steel shims and end plates. As such, it has been proposed that a reduction in weight and cost could be achieved if the steel reinforcement was replaced with another type of material having comparable mechanical properties to steel, such as fiber fabric sheets. This relatively new type of isolator is called a Fiber Reinforced Elastomeric Isolators (FREI). FREI can be constructed without thick steel end plates and are placed, unfastened, between the superstructure and the substructure. In this case, the isolator is denoted as an unbonded-FREI (U-FREI). In addition to the expected reduction in weight and potential cost, U-FREI can be manufactured and cut to the desired shape and size from large sheets using a standard band saw. Furthermore, U-FREI are able to detach from the contact supports by rollover and lift-off under excessive deformations in the lateral and rotational direction, respectively. This is due to the unbonded boundary conditions and the negligible flexural rigidity of the fiber reinforcement.

Research studies have revealed that U-FREI have desirable performance characteristics for building applications. This dissertation investigates the feasibility of extending the use of U-FREI to bridge applications. Experimental testing was carried out to study U-FREI behaviour under a wide range of bridge loading conditions in the vertical, rotational, and lateral directions. Numerical studies were also completed to assess the resulting stress and strain state within U-FREI. Finally, the seismic performance of a bridge, equipped with a U-FREI isolation system was evaluated via non-linear time history analysis using a large suite of earthquake motions.

Acknowledgments

All praise and gratitude be to the one and only God: **ALLAH** the Most Gracious, the Most Compassionate and the Most Merciful, exalted in Power and Knowledge and who's blessing on us cannot be counted. Also, my deepest gratitude and appreciation to the all-time teacher, the **Prophet Mohammed**, the last messenger of **ALLAH** who said: *“When a person follows a path looking for knowledge, Allah will ease for him the way to paradise”*.

This thesis would have been impossible without the support and mentoring of my supervisor **Dr. Michael Tait**. I appreciate all his contributions of time, ideas, and funding to make my Ph.D. experience productive and stimulating. The joy and enthusiasm he has for his research was motivational for me, even during tough times in the Ph.D. pursuit. **Dr. Tait** teaches by setting a great example of how to think, to design, to evaluate, and to write well. I have never learned as much professionally from any other person. His friendship and professional collaboration means a great deal to me.

I would like to express my sincere appreciation to my supervisory committee members, **Drs. Konstantinidis, Sivakumaran and Veldhuis**. Thank you so much for your motivation, invaluable comments and advice throughout this research work. Your guidance and encouragement have sustained me in my research from the very beginning and throughout. I am also extremely grateful to **Dr. Wael El-Dakhkhni** for his guidance and encouragement during my Ph.D. studies. Finally, I gratefully acknowledge **Dr. James Kelly** for his kind acceptance to review my thesis, for his insightful feedback and valuable suggestions.

I am also extremely grateful to **Mark Torrie** for his invaluable help in building and controlling the experimental test apparatus. I would also like to thank the technical staff members of Applied Dynamics laboratory (ADL): **Peter Koudys, Kent Wheeler, and Paul Heerema** for their support

with technical issues with the test set-up. In addition, I would like to extend my gratitude to all my friends and colleagues whom I met during my journey at **McMaster University**.

It has been a great honour to get my Bachelor Degree and spend eight years (2004-2012) in the Construction and Building Department at **Arab Academy for Science, Technology and Martine Transport (AASTMT)**. Its faculty and staff will always remain dear to me. Many thanks also go to the professors in **Cairo University**, particularly **Dr. Mashhour Ghoneim** and **Dr. Osman Ramadan**, whom taught me a lot about structural engineering and helped me pursue my Master of Science degree.

I greatly appreciate the sacrifices, encouragement and support done by my father and mother: **Mohammed** and **Amany**; sisters and brother: **Alaa-Allah, Nagya, Mariam, Amany**, and **Esmail**; and my brother-in-law: **Dr. Mohammed Ali** for helping me pursue my Doctoral degree. Thus, my highest appreciation goes to them for all what they did for me throughout my life in general and the last four years in particular. I owe to them every success I have in my life. I would also like to extend my thanks to my parents-in-law: **Mohammed** and **Ola** for all their support.

Finally, and most importantly, I would like to thank my lovely wife **Nourhane** for helping me through many of the challenging times I encountered during this doctoral dissertation and for making me smile the whole way through. Her support, encouragement, quiet patience and indescribable love were undeniably the bedrock upon which the past three years of my life have been built. Her tolerance of my occasional vulgar moods is a testament in itself of her unyielding devotion and love. She was always there cheering me up and stood by me through my ups and downs.

Table of Contents

Chapter 1:

INTRODUCTION	1
1.1. Overview Background	1
1.1.1. Seismic Isolation for Bridges Structures	2
1.1.2. Commonly employed Seismic Isolators	3
1.1.3. Fiber-Reinforced Elastomeric Isolators (FREIs)	4
1.1.4. Previous Research on U-FREI	5
1.2. Research Objectives and Impetus	7
1.3. Thesis Structure.....	8
References	10

Chapter 2:

EXPERIMENTAL INVESTIGATION ON THE VERTICAL AND LATERAL BEHAVIOUR OF UNBONDED FIBER REINFORCED ELASTOMERIC ISOLATORS	18
Abstract	18
2.1. Introduction	19
2.2. Background	20
2.2.1. Analytical Solutions	23
2.3. Experimental Program	24
2.3.1. Specimens	24
2.3.2. Test Program	25
2.3.2. Experimental Apparatus	26
2.4. Experimental Results	26
2.4.1. Effect of Loading Rate on Vertical Stiffness	26
2.4.2. Effect of Lateral Offset on Vertical Stiffness	28
2.4.3. Lateral Cyclic Tests	30
2.4.4. Normalized Vertical Deformation and Lateral Displacement	34
2.5. Conclusion	35
Acknowledgments	36
References	36

Chapter 3:

A NUMERICAL STUDY ON THE COMPRESSIVE AND ROTATIONAL BEHAVIOUR OF FIBER REINFORCED ELASTOMERIC ISOLATORS (FREI)	54
Abstract	54
3.1. Introduction	55
3.2. Finite Element Model.....	60
3.3. Vertical Behaviour	62
3.4. Rotational Behaviour	65
3.4.1. Moment-Rotation Response	65
3.4.2. Code Evaluation for Lift-off in Unbonded Isolators	69
3.5. Stresses in Elastomer	70
3.6. Shear Strain	74
3.7. Tensile Strain in Fiber reinforcement	75
3.8. Comparison of Stresses and Strains in Bonded and Unbonded Isolators	76
3.9. Discussion and Conclusions.....	78
Acknowledgments	79
References	80

Chapter 4:

EXPERIMENTAL ASSESSMENT OF FIBER REINFORCED ELASTOMERIC ISOLATORS FOR BRIDGE APPLICATIONS	107
Abstract	107
4.1. Introduction	108
4.2. Background	110
4.3. Experimental Test Program	113
4.3.1. Properties of Bearing Specimens	113
4.3.2. Employed Test apparatus	114
4.3.3. Organization of the Test program	114
4.4. Experimental Results	115
4.4.1. Phase 1: The effect of axial load on vertical response	115
4.4.2. Phase 2: The effect of lateral offset on vertical response	118
4.4.3. Phase 3: The effect of static rotation on vertical response.....	119
4.4.4. Phase 4: The effects of axial load and angle of rotation on rotational response	120
4.5. Comparison of Measured and Theoretical Vertical Stiffness	121
4.6. Conclusion	123
Acknowledgments	124

References	124
------------------	-----

Chapter 5:

FIBER REINFORCED ELASTOMERIC ISOLATORS FOR THE SEISMIC ISOLATION OF BRIDGES	140
Abstract	140
5.1. Introduction	141
5.2. Background	143
5.3. Experimental Program	145
5.3.1. Isolator Specimens	145
5.3.2. Test apparatus	146
4.3.3. Test program	146
5.4. Experimental Program - Results and Discussion	147
5.4.1. Effects of rotational deformation on lateral stiffness	148
5.4.2. Effects of rotational deformation on lateral damping	149
5.5. Finite Element Modeling	150
5.5.1. Model description and evaluation	150
5.6. Results and Discussions of FE Modeling	151
5.6.1. Normal stresses σ_{11} , σ_{22} , and σ_{33}	151
5.6.2. Shear strain γ_{12}	153
5.7. Conclusion	153
Acknowledgments	155
References	155

Chapter 6:

MODELING AND EVALUATION OF SEISMICALLY ISOLATED BRIDGE USING UNBONDED FIBER REINFORCED ELASTOMERIC ISOLATORS	172
Abstract	172
6.1. Introduction	173
6.2. Bridge and Isolator Model	177
6.2.1. Idealization of the bridge substructure and superstructure	177
6.2.2. Idealization of the U-FREI Behaviour	178
6.3. Ground Motion Records	182
6.4. Results and Discussion	183
6.4.1. Response Histories	184
6.4.2. Seismic Demands Comparison	186

6.5. Summary and Conclusions.....	189
Acknowledgments	191
References	191

Chapter 7:

SUMMARY, CONCLUSIONS AND RECOMMENDATIONS.....	207
7.1. Summary	207
7.2. Conclusions.....	208
7.3. Recommendations for future studies	212
References	213

List of Tables

Table 2-1:	Specifications of the test specimen	39
Table 2-2:	Results of vertical testing on all isolators at the third cycle with no lateral offset	39
Table 2-3:	Comparison of the analytical solution to the experimental results	40
Table 2-4:	Influence of lateral testing on the vertical response of isolators	40
Table 2-5:	Results of the lateral cyclic testing on all isolators	40
Table 3-1:	Material Properties of the isolators	84
Table 3-2:	Geometric properties of the isolators	84
Table 3-3:	Vertical Stiffness value obtained from finite element analysis and analytical solutions	84
Table 3-4:	Ratio of maximum stress and strain in a bonded isolator relative to unbonded isolator	85
Table 4-1:	Test Specimen Specifications.....	128
Table 4-2:	Material Properties of the bearings	128
Table 4-3:	Comparison of the experimental results with the analytical solution	128
Table 5-1:	Geometric properties of the test specimen	158
Table 5-2:	Fundamental isolated period for the ¼ scaled isolators in seconds.....	159
Table 5-3:	Material Properties of the modeled isolators.....	159
Table 5-4:	Error in (%) for the calculated stiffness between the Experimental and FEM results	159
Table 6-1:	Specifications of the U-FREI specimen	194
Table 6-2:	Parameters of the Takeda-Elastic Model	194
Table 6-3:	Comparison of the predicted analytical response solution to the experimental results.....	194
Table 6-4:	The selected ground motion records	195

List of Figures

Figure 1-1:	A typical seismically-isolated bridge: (a) elevation; and (b) section II-II	13
Figure 1-2:	A comparison between: (a) non-isolated bridges and (b) isolated bridges	14
Figure 1-3:	The reduction in seismic demand due to the elongation of bridge period	14
Figure 1-4:	The influence of reinforcement on enhancing the vertical stiffness of elastomeric isolators	15
Figure 1-5:	Free body diagram of laterally deformed Bonded-FREI	15
Figure 1-6:	Deformation criteria of U-FREI	16
Figure 1-7:	Free body diagram of laterally deformed U-FREI	16
Figure 1-8:	The 3 DOF test-rig employed in the experimental program	17
Figure 2-1:	Lateral deformation of an U-FREI showing (a) rollover and (b) full rollover ..	41
Figure 2-2:	Sketch of the three isolators cut from a single pad	41
Figure 2-3:	The vertical input signal time history at vertical frequency of 0.1 Hz	42
Figure 2-4:	The input signal time history for the vertical tests with a lateral offset (vertical frequency = 0.1 Hz, lateral offset varies)	42
Figure 2-5:	The lateral input signal.....	43
Figure 2-6:	Multi-load test apparatus: (a) photograph; (b) schematic	44
Figure 2-7:	Vertical behaviour of considered isolators	45
Figure 2-8:	Average vertical stress versus normalized vertical displacement loops for Isolator 1	46
Figure 2-9:	Vertical stiffness as a function of frequency and loading cycle (no lateral offset)	46
Figure 2-10:	Influence of the lateral offset on the initial vertical displacement of the isolators	47
Figure 2-11:	Influence of the lateral offset on the vertical stiffness	47
Figure 2-12:	Influence of the normalized lateral offset on the stress-normalized vertical displacement loops of Isolator 1	48
Figure 2-13:	Lateral hysteresis loops for each isolator	49
Figure 2-14:	Lateral hysteresis loop at lateral displacement of $2.50 t_r$ (3 rd cycle).....	51
Figure 2-15:	Relation between lateral displacement (t_r) and reduction in (a) lateral stiffness; (b) lateral damping of the third cycle (i.e. scragged) (results are normalized to values at $0.25 t_r$).....	52
Figure 2-16:	The increase in the normalized vertical deformation during the lateral testing ..	53
Figure 3-1:	Deformation patterns of U-FREI	86
Figure 3-2:	Influence of aspect ratio on vertical response	86
Figure 3-3:	Variation of normalized compression modulus (E_c/E) with mean vertical pressure (P).	87
Figure 3-4:	Deformation progress of Isolator 4	88
Figure 3-5:	Moment-rotation response under different compressive loads	89
Figure 3-6:	Moment-rotation response under pure rotation (i.e. no axial loads).....	92
Figure 3-7:	Compressive stress distribution along the top surface of the isolators under a rotation of 0.001 radians (vertical displacement control)	93
Figure 3-8:	Normalized stresses (σ_{22} / P) in Isolator 3 under average compressive stress of 7 MPa	94

Figure 3-9:	Profile of normalized stress (σ_{22} / P) distribution along the intermediate elastomer layer for Isolator 3 ($P = 7$ MPa)	95
Figure 3-10:	Normalized stresses (σ_{11} / P) in Isolator 3 under an average compressive stress of 7 MPa	96
Figure 3-11:	Profile of normalized stress (σ_{11} / P) distribution along the intermediate elastomer layer for Isolator 3 ($P = 7$ MPa)	97
Figure 3-12:	Profile of normalized peak stresses (σ / P) in the bonded isolators	98
Figure 3-13:	Profile of normalized peak stresses (σ / P) in the unbonded isolators	99
Figure 3-14:	Shear strains (γ_{12}) in Isolator 3 under average compressive stress of 7 MPa	100
Figure 3-15:	Variation of peak shear strain (γ_{12}) in the bonded isolators	101
Figure 3-16:	Variation of peak shear strain (γ_{12}) in the unbonded isolators	102
Figure 3-17:	Deformation of isolator and resulting strain in fiber reinforcement	103
Figure 3-18:	Reinforcement strains ($\% \epsilon_{\text{fiber}}$) in Isolator 3 ($P = 7$ MPa)	104
Figure 3-19:	Variation of peak fiber strain ($\% \epsilon_{\text{fiber}}$) in the bonded isolators	105
Figure 3-20:	Variation of peak fiber strain ($\% \epsilon_{\text{fiber}}$) in the unbonded isolators	106
Figure 4-1:	(a) Lateral and (b) rotational deformation patterns of U-FREI	129
Figure 4-2:	U-FREI specimens tested in the study	129
Figure 4-3:	The 3 DOF test apparatus: (a) photograph; (b) schematic	130
Figure 4-4:	Applied vertical load time history for phase 1	132
Figure 4-5:	Vertical compressive load (P) versus vertical displacement (Δ_V) response curves for Bearing 1	132
Figure 4-6:	Vertical hysteresis loops for Bearing 1 under different axial loads	133
Figure 4-7:	Influence of applied vertical load on the: (a) vertical stiffness; (b) vertical damping	133
Figure 4-8:	Applied vertical and lateral load time histories for phase 2	133
Figure 4-9:	Influence of lateral offset on the vertical stiffness	133
Figure 4-10:	Vertical hysteresis loops for Bearing 1 corresponding to different vertical loads and lateral offsets	135
Figure 4-11:	Lateral response of Bearing 1 up to lateral displacement amplitude of $0.50 t_r$	135
Figure 4-12:	Applied vertical and lateral load time histories for phase 3	136
Figure 4-13:	Influence of static rotation on the vertical stiffness	136
Figure 4-14:	Vertical hysteresis loops for Bearing 1 corresponding to different static rotations under (a) 9.8kN and (b) 49kN vertical loads	137
Figure 4-15:	Applied rotational loading time history for phase 4	137
Figure 4-16:	Moment-rotation response for Bearing 1	139
Figure 4-17:	Influence of axial load and angle of rotation on the (a) rotational stiffness; (b) rotational damping	139
Figure 5-1:	Typical seismically isolated bridge	160
Figure 5-2:	Deformation patterns of U-FREI (i.e. unbonded)	160
Figure 5-3:	Deformation patterns of B-FREI (i.e. bonded)	161
Figure 5-4:	Sketch of the original pad before cutting the isolators	162
Figure 5-5:	Photograph of the three-degree of freedom test apparatus	162
Figure 5-6:	Schematic of the three-degree of freedom test apparatus	163
Figure 5-7:	The input signal time history	163

Figure 5-8:	Lateral hysteresis loops	164
Figure 5-9:	Variation in lateral stiffness (K_L) for all isolators	165
Figure 5-10:	Variation in isolator lateral damping (ξ_L)	166
Figure 5-11:	Definition of Stresses	167
Figure 5-12:	Contours of normalized stresses (σ / σ_v) in Isolator 1	168
Figure 5-13:	Contours of normalized stresses (σ / σ_v) in Isolator 2	169
Figure 5-14:	Contours of normalized stresses (σ / σ_v) in Isolator 3	170
Figure 5-15:	Contours of shear strain (γ_{12})	171
Figure 6-1:	A comparison between: (a) non-isolated bridges; and (b) isolated bridges	196
Figure 6-2:	Deformation progress of rollover in U-FREI under lateral deformation	196
Figure 6-3:	The two types of bridges considered in the study: (a) non-isolated; (b) isolated	197
Figure 6-4:	The three-dimensional bridge model: (a) non-isolated, (b) isolated.....	198
Figure 6-5:	(a) A typical OpenSees fiber-section defined for RC circular column; (b) the stress-strain relationship of: (i) concrete-02; (ii) steel-02 as defined in OpenSees	199
Figure 6-6:	Schematic illustration of typical load-displacement curve of an unbonded FREI	200
Figure 6-7:	Illustration of the proposed Takeda-Elastic model	200
Figure 6-8:	(a) The 3DOF employed test apparatus; (b) Comparison of the experimentally obtained response of the U-FREI with the prediction of the Takeda-Elastic model	201
Figure 6-9:	(a) Scaled pseudo-acceleration response spectra of the 20 selected ground motions (Damping = 5%); (b) comparison of the mean scaled acceleration response spectrum of the selected ground motions with the CHBDC (2014) design response spectrum at Victoria City Hall, Canada.....	201
Figure 6-10:	Longitudinal and transverse response histories of normalized base shear when subjected to Earthquake 11 at MCE level	202
Figure 6-11:	Longitudinal and transverse response histories of deck acceleration when subjected to Earthquake 11 at MCE level	202
Figure 6-12:	Deck drift ratio for non-isolated bridge when subjected to Earthquake 11 at MCE level	203
Figure 6-13:	Deck drift ratio for isolated bridge when subjected to Earthquake 11 at MCE level	203
Figure 6-14:	Comparison of the mean values from all 20 ground motions of the normalized peak bent base shear for the longitudinal and transverse directions	204
Figure 6-15:	(a) Force-displacement; (b) moment-curvature relationship for a single bent cap of both bridges when subjected to Earthquake 11 at MCE level	204
Figure 6-16:	Comparison of the mean values of the peak acceleration at the deck level from all 20 ground motions for the longitudinal and transverse directions	205
Figure 6-17:	Reduction (%) in the seismic demand of the bridge in both longitudinal and transverse directions	205
Figure 6-18:	Normalized peak isolation displacement for each of the considered 20 ground motions	206

Co-Authorship

This thesis has been prepared in accordance with regulations for a "**Sandwich thesis**" format or as a compilation of papers stipulated by the Faculty of Graduate Studies at McMaster University. The thesis chapters two through six has been co-authored as following:

Chapter 2: Experimental investigation on the vertical and lateral behaviour of unbonded fiber reinforced elastomeric isolators

Authors: Al-Anany Y., Van Engelen, N. and Tait M.

The setup preparation, experimental testing and data analysis were carried out by Yasser Al-Anany under the supervision of Dr. Michael Tait. The manuscript was prepared by Yasser Al-Anany under the supervision of Dr. Michael Tait and in consultation with Niel Van-Engelen. Modifications and revisions were made by all contributing authors.

This chapter has been submitted for publication in ASCE Journal of Composites for Construction.

Chapter 3: A numerical study on the compressive and rotational behavior of fiber reinforced elastomeric isolators (FREI)

Authors: Al-Anany Y. and Tait M.

The finite element modeling and data analysis were carried out by Yasser Al-Anany under the supervision of Dr. Michael Tait. The manuscript was written by Yasser Al-Anany and modifications were completed under the supervision of Dr. Michael Tait.

This chapter has been published in Composite Structures (Vol. 133, pages: 1249-1266).

Chapter 4: Experimental Assessment of Fiber Reinforced Elastomeric Isolators for Bridge Applications

Authors: Al-Anany Y. and Tait M.

Fabrication of the isolators, setup preparation, experimental testing and data analysis were carried out by Yasser Al-Anany under the supervision of Dr. Michael Tait. The manuscript was written by Yasser Al-Anany and modifications were completed under the supervision of Dr. Michael Tait.

This chapter has been submitted for publication in Composites Part B: Engineering.

Chapter 5: Fiber Reinforced Elastomeric Isolators for the Seismic Isolation of Bridges

Authors: Al-Anany Y. and Tait M.

Fabrication of the isolators, setup preparation, experimental testing and data analysis were carried out by Yasser Al-Anany under the supervision of Dr. Michael Tait. The manuscript was written by Yasser Al-Anany and modifications were completed under the supervision of Dr. Michael Tait.

*This chapter has been submitted for publication in **Composite Structures**.*

Chapter 6: Modeling and Evaluation of Seismically Isolated Bridge Using Unbonded Fiber Reinforced Elastomeric Isolators

Authors: Al-Anany Y., Moustafa M. and Tait M.

The finite element modeling and data analysis were carried out by Yasser Al-Anany under the supervision of Dr. Mohamed Moustafa from University of Nevada at Reno and Dr. Michael Tait. The manuscript was written by Yasser Al-Anany under the supervision of Dr. Michael Tait and Dr. Mohamed Moustafa. Modifications and revisions were made by all contributing authors.

*This chapter has been submitted for publication in **Earthquake Spectra**.*

Chapter ONE

INTRODUCTION

1.1. Overview Background

Bridges are employed to facilitate traffic flow on highways as well as for crossing obstacles and are one of the major elements in transportation infrastructure systems. The major components of bridges are the superstructure and the substructure along with the connecting elements between them. The superstructure (e.g. girder, deck ... etc.) is primarily responsible for supporting the different types of loads and transferring these loads to the substructure. Bridge bearings are typically installed in the transition zone between the superstructure and substructure (see Fig. 1-1) in order to isolate the bridge substructure from lateral and/or rotational deformations that are developed in the superstructure. The lateral and rotational deformations that may be experienced by the bridge superstructure are primarily due to traffic loading, creep, prestressing and temperature loading due to thermal expansion and contraction that occurs within the superstructure as a result of its large span.

Bridge bearings are responsible for transferring the vertical loads from the superstructure to substructure and accommodating the lateral and rotational deformations that are experienced by the bridge superstructure (CHBDC 2014). Accelerated bridge deterioration/damage can occur as a result of failure in the bridge bearings (AASHTO 2012). As previously mentioned, bridge bearings are subjected to loads/deformation in the vertical, lateral and rotational direction. However, each of the bearing types developed by bridge engineers has different capacities in each direction (Lee 1994). Hence, the bearing type is selected according to several factors, including the predicted loading, geometry, maintenance, available clearance, deflection, displacement and rotation demands, availability, policy, designer preference, and cost (Caltrans 1994).

1.1.1. Seismic Isolation for Bridges Structures

The ability of a bridge bearing to accommodate other types of loading, such as seismic loads which do not occur frequently but can induce substantial damage, has been investigated extensively (Priestley et al. 1996; Duggal 2007; Chen and Duan 2014). In this case, bridge

bearings are called seismic isolators and the bridge is referred to as a seismically isolated bridge. The main idea behind seismic isolation is similar to the idea behind the use of bridge bearing but in a reverse manner. Bridge bearings isolate the substructure from lateral and rotational deformations in the superstructure, while seismic isolators are used to uncouple/isolate the bridge superstructure from excessive lateral movements induced in the substructure during seismic events (Constantinou et al. 2011). Thus, for a seismically isolated bridge the seismic isolators are employed to handle the excessive lateral displacements that occur in the substructure as shown in Fig. 1-2.

The main advantage of base/seismic isolation is that it improves the seismic response of the bridge by mitigating the seismic demand on the bridge (Ghobarah and Ali 1988; Wesolowsky and Wilson 2003; Jangid 2004; Buckle et al. 2006; Constantinou et al. 2007; Siqueira et al. 2014). Seismic isolation leads to a near-rigid response motion of the superstructure during an earthquake, and as a result drift induced structural damage is significantly reduced or completely avoided. Seismic isolation can be achieved by introducing elements having low lateral stiffness (compared to substructure), which lengthen the fundamental natural vibration period of the bridge to a value that is larger than the predominant ground motion periods of the earthquake. This subsequently leads to a significant reduction in the seismic demand of the bridge elements as shown in Fig. 1-3. Accordingly, for little additional cost (compared to the overall cost of the bridge), a well-designed seismic isolator allows the entire bridge to remain within the elastic range (i.e. no damage or subsequent strengthening) during a seismic event. Thus, considering the previously mentioned benefits, seismic isolation is considered to be a “cost-effective technique for seismic protection” and as a result it has been employed in thousands of bridges around the globe (Buckle et al. 2011, Skinner et al. 1993).

1.1.2. Commonly employed Seismic Isolators

In general, seismic isolators are classified as either sliding or elastomeric (Naeim and Kelly 1999). The concept of the sliding isolation system is to place a medium with a low friction coefficient between the superstructure and substructure (Tsopelas et al. 1996). The lower the friction coefficient, the lower the shear forces that are transferred to the superstructure. Typically, sliding isolators are either pure friction isolators with flat sliding surfaces or friction pendulum isolators (FP), which depending on the number of its sliding surfaces can be single,

double, or triple FP. The FP isolators have spherical sliding surfaces that allow the development of restoring forces as a result of the pendulum action of the superstructure weight. An example of a Canadian bridge that is seismically isolated using FP isolators is the White River Bridge in Yukon, Canada.

Elastomeric isolators are the most common type of seismic isolator. This type of isolator consists of layers of natural or synthetic elastomer that are reinforced with an appropriate type of material. The reinforcing layers play a crucial role in developing sufficient vertical stiffness in the isolator by limiting the bulging in the elastomer layers as shown in Fig. 1-4. An unreinforced (i.e. plain) elastomeric isolator would possess comparable vertical and lateral stiffness. If employed as an isolator the superstructure could experience rocking during an earthquake event (Kelly and Konstantinidis 2011). As such, the addition of reinforcement is important as it significantly increases the vertical stiffness of the isolator (i.e. doesn't affect the lateral stiffness), which eliminates coupling with rocking modes of vibration.

Typically steel reinforcing shims are used, however some disadvantages are associated with the use of steel, including an increase in both the weight and cost of an isolator. The increase in weight is due to the steel shims as well as the two thick end-plates that are used to fasten the isolator top and bottom to the upper and lower contact supports. The increase in cost is due to the labour intensive manufacturing process. As such, a typical steel-reinforced elastomeric isolator can weigh up to one ton and cost in excess of \$10,000 (Kelly and Konstantinidis 2007). Thus, conventional steel-reinforced isolators have been limited to use in high importance structures. Their high cost has been a barrier to implementation in typical structures (e.g. housing and commercial buildings) and also in buildings in developing countries, although major loss of life due to earthquakes occurs in these countries (Kelly 2002).

Ordinary steel-reinforced elastomeric isolators (SREI) are typically fastened to the upper and lower contact supports, and as a result they are subjected to tensile stresses under lateral and rotational deformations. Tensile stresses occur under lateral deformation due to the fixation in boundary conditions and the point of application of the vertical load point - these stresses develop in order to maintain equilibrium, outside the overlap region between top and bottom surfaces as shown in Fig. 1-5. Tensile stresses increase the likelihood of isolator damage as a result of delamination of the elastomer from the reinforcement, particularly for aged elastomeric

isolators (Angelilli 2007). Finally, it should be noted that damaged elastomeric isolators are not repairable they can only be replaced (Pritchard 1994).

1.1.3. *Fiber Reinforced Elastomeric Isolators (FREIs)*

In order to overcome some of the limitations associated with steel reinforced isolators, the most recent version of bridge design codes (e.g. CHBDC 2014) allow the replacement of steel with a suitable alternative material, which has comparable mechanical properties to that of steel. Consequently, a relative reduction in both weight and manufacturing costs can be achieved if the alternative type of reinforcement is lighter and less expensive to manufacture

Extensive research efforts have revealed that such advantages are found in *fiber* material. When fiber material is used instead of steel as the reinforcement, the elastomeric isolators are called Fiber-Reinforced Elastomeric Isolators (FREIs). FREI can be constructed without rigid end plates and simply placed between the superstructure and its foundation - the shear forces are transferred between the isolator and the contact supports (i.e. the contact interfaces) by friction. When installed in this manner the isolator is referred to as an Unbonded-FREI (U-FREI). If the U-FREI is able to maintain a positive tangential stiffness over its entire lateral displacement range it is defined as a Stable Unbonded-FREI (SU-FREI) (Toopchi-Nazhad et al. 2008).

Thus, replacing the steel reinforcement with lighter fiber material along with removing the rigid end plates can result in a significant reduction in weight. Additionally, another possible reduction in manufacturing cost can be achieved since the fiber reinforcement and elastomer can be bonded together using a cold-vulcanized bonding compound without the need of a mold. Furthermore, FREI can be easily manufactured in large sheets and then subsequently cut to the required shape and size, which is not possible with steel-reinforced isolators. Moreover, for U-FREI, large tensile stresses do not develop since the top and bottom surfaces can roll off the supports when subjected to large lateral and rotational deformations as shown in Fig. 1-6. The *rollover* occurs under lateral deformation (see Fig. 1-6a) in U-FREI due to the lack of flexural rigidity in fiber layers as well as unbonded boundary conditions. The rollover deformation subsequently leads to an offset of the vertical resultant forces according to the level of lateral deformation, (i.e. the resultant stresses in any elastomeric layer has a maximum value at the pressed end and decreases moving towards the opposite free end). Thus, the unbalanced

moments caused by shear loads are resisted by this offset in the vertical resultant forces as shown in Fig. 1-7. Furthermore, *lift-off* that occurs under large rotational deformation (see Fig. 1-6b), which allows the uncompressed side of the isolator to detach from the contact supports so that isolator is only subjected only to compressive stresses.

1.1.4. Previous Research on U-FREI

Kelly (1999) carried out one of the earliest studies on fiber-reinforced elastomeric isolators. An important conclusion drawn from this study was confirming the viability of producing elastomeric isolators with efficient mechanical properties when reinforced with fiber instead of steel. Moon et al. (2002) compared the vertical response of FREI with conventional SREI, and found that the fiber reinforcement was effective in preventing bulging in the elastomer layers, resulting in isolators with high vertical stiffness.

Toopchi-Nezhad et al. (2008) conducted an experimental parametric study on U-FREI for their potential application in typical (normal importance) low-rise buildings. It was observed that the aspect ratio, defined as ratio of total length/width to total height, was the controlling parameter for the stable response of U-FREI under lateral deformation. A key finding was that U-FREI can maintain lateral stability (positive tangential stiffness) over a large range of lateral displacements if the aspect ratio is larger than approximately 2.60. Additionally, vertical compression testing revealed that the vertical frequency of U-FREI is significantly larger (at least 20 times) than the maximum expected lateral frequency associated with the base isolated building, which minimizes the contribution of rocking vibration modes. Moreover, negligible vertical stiffness degradation and no visible damage were found to have occurred to the isolator after completion of the lateral cyclic testing. De Raaf et al. (2011) experimentally investigated the lateral stability of U-FREI under a range of vertical loads. The objective of this study was to find the critical buckling load corresponding to zero lateral tangential stiffness (i.e. rollout instability). U-FREI were found to be able to maintain their lateral stability under large compressive stresses (e.g. up to 18.5 MPa) and large lateral displacements (up to $3.50 t_r$, where t_r is the total rubber thickness), which indicate that U-FREI are resistant to buckling instability. Russo et al. (2013a) showed that sliding instability occurs only under low compressive stresses (i.e. < 0.5 MPa). Russo et al. (2013b) also performed a comparative study on the lateral and vertical response of U-FREI with different fiber reinforcement directions (i.e bi-directional and

quadri-directional). This study concluded that U-FREI reinforced with quadri-directional carbon fiber reinforcement have higher vertical stiffness, lateral stiffness, and lateral damping.

In addition to the lateral stiffness of the isolator, which controls the effective isolation period, the level of energy dissipation (i.e. damping) of SU-FREI was also investigated by Toopchi-Nezhad et al. (2008) as it influences the displacement demand experienced by the isolator. It was found that if unfilled soft neoprene compound having a damping ratio of approximately 5% was used instead of natural rubber, the effective lateral damping was found to range from 8% to 16% depending on the lateral displacement amplitude. As the neoprene rubber was expected to have a value of 5% damping, it was postulated that additional energy dissipation was provided by the carbon fiber reinforcement.

Since FREI can be easily cut from a large sheet, different isolator geometries were also explored. For example, Van Engelen et al. (2012) found that introducing holes in strip U-FREI resulted in a decrease in the effective lateral stiffness of the isolator as well as an increase in the equivalent viscous damping. Additional studies had also shown the influence of altering the isolator geometry on the vertical behaviour (Van Engelen et al. 2014) and lateral behaviour (Osgooei et al. 2015) of U-FREI.

Toopchi-Nezhad et al. (2011) performed a finite element study to investigate the benefits of using U-FREI by comparing their vertical and lateral response with a similar bonded-FREI. Findings show that the main advantage in the lateral response of U-FREI was in the large reduction in lateral stiffness compared to that of the B-FREI, which reveals an increase in the seismic isolation efficiency for isolators with unbonded boundary conditions. Furthermore, the stress demand on the rubber material, fiber reinforcement, and bond between rubber and fiber was found to be considerably lower in U-FREI compared to B-FREI.

1.2. Research Objectives and Impetus

The primary objective of this dissertation is to investigate the feasibility of extending the U-FREI usage to bridge applications as defined by CHBDC (2014) and AASHTO (2012) as a: *"a structural device that transmits loads while facilitating translation and/or rotation"*.

As described in the previous section, previous research on FREI has focused mainly on the usage of this type of isolator for ordinary low-rise buildings. As such, the maximum vertical pressure has been limited 4 to MPa in most cases, which is insufficient for bridge applications. However, CHBDC (2014) specifies the service limit states for the compressive stresses on a bridge bearing to be within 4.5MPa – 7MPa, while 10MPa is the upper limit considered for ultimate limit state design. As such, this dissertation investigates the vertical and lateral response of U-FREI under a range of vertical compressive stresses up to 10MPa.

Extending the applications of U-FREI to bridges also requires the evaluation of the vertical and lateral responses under different loading scenarios that are expected over the life span of the bridge. These loading scenarios include the expansion and contraction of the superstructure, which leads to lateral deformations when implemented in bridges. Furthermore, the rotational deformation of a bridge superstructure under traffic and dead loads is another important loading scenario that should be considered. As an example, Stanton et al. (2007) reported that rotational deformations on bridge bearings are responsible for some of the most common bridge design problems. However, to date, no experimental or numerical data is available in the literature for the behaviour of U-FREI when subjected to rotational deformations as well as the influence of rotational deformation on the vertical and lateral response.

One of the primary reasons there is a limited number of studies reported in the literature that include the effect of rotation, particularly experimental, is due to the cost and challenges associated with the design, development, and construction of a suitable test apparatus (Stanton et al. 2007). To complete the required tests a 3-degree of freedom (3DOF) bearing test apparatus was designed and constructed as shown in Fig. 1-8, which is capable of applying vertical, rotational, and lateral loads/deformations, both separately and in combination.

In addition to experimental testing of U-FREI, a numerically study comparing the rotational response of U-FREI and B-FREI has been carried out. Finally, a mathematical model that can be readily implemented into commercially available general-purpose structural analysis software in order to simulate the lateral response of U-FREI has been developed. This model has subsequently been employed to evaluate the seismic response of a typical highway bridge that is seismically isolated using U-FREI.

1.3. Thesis Structure

This dissertation is comprised of five stand-alone chapters (i.e. chapters 2 to 6), which are published, in-press, or submitted in well-recognized journals. Each stand-alone chapter includes its own introduction, background, body, conclusions and references. As a result, some overlap may be observed in the introduction of each chapter as a result of how the sandwich thesis is structured. The contribution by the author of the thesis to each of the papers had been described above (see Co-Authorship section).

Chapter 2 presents an experimental study on the vertical and lateral response of unbonded FREI with different shape factors and aspect ratios. The aspect ratio and shape factor are of particular importance because the first strongly influence the vertical response, while the latter controls the lateral response. Accordingly, this chapter includes the evaluation of the mechanical properties (i.e. vertical/lateral stiffness and damping) of U-FREI through vertical cyclic tests on U-FREI under different vertical loading frequencies and lateral offset as well as lateral cyclic testing.

Chapter 3 investigates and compares the vertical and rotational response of bonded and unbonded FREI. Comprehensive 2D finite element modelling was conducted on infinitely long strip FREI with different aspect ratios using the commercially available general-purpose finite element program MSC Marc. This analytical study included the application of different vertical loads and angles of rotation. Results obtained from the finite element model study are compared to the values obtained from available closed-form analytical solutions and are found to be in excellent agreement.

Chapter 4 contains an experimental evaluation of the feasibility of employing U-FREI as a bridge bearing. This chapter includes an experimental investigation of the vertical and rotational response of U-FREI under different loading conditions expected in bridge applications, including high vertical loads, static rotation and static lateral offsets. The test program also presented the rotational response of U-FREI under cyclic rotation.

Chapter 5 includes an experimental evaluation of the lateral response U-FREI under a range of vertical loads and rotational deformations in order to determine their suitability as a seismic isolator for bridges. The shape factor of the three isolators tested in this study was maintained, while the aspect ratio was varied. The lateral stiffness and damping were computed

experimentally under different levels of vertical load, angles of rotations and lateral deformations. Additionally, the resulting stress and strain state within the isolators under peak deformations were also evaluated numerically via 3D modeling and are presented in this study.

Chapter 6 introduces a hysteretic model, which is based on a model initially proposed by Osgooei et al. (2016), in order to simulate the lateral response of FREI. The proposed *Takeda-nonlinear elastic* model combines the advantage of being non-iterative and can accurately predict the effective stiffness and damping of the isolator over a range of lateral displacement amplitudes. This model does not require fitting over the entire experimentally obtained hysteresis loops. The *Takeda-nonlinear elastic* model consists of a Bilinear Takeda Hysteresis Model and a nonlinear elastic model in parallel. Both models are represented by simplified parameters. Furthermore, the proposed model is employed in a comparative time history analysis of the seismic response of typical highway bridges that are non-isolated and isolated with U-FREI. The primary goal of this comparative study is to evaluate the reduction in base shears, accelerations, and displacements developed in the piers and girders of the isolated bridge using U-FREI.

References

- AASHTO. (2012). *American Association of State Highway and Transportation Officials. LRFD Bridge Design Specifications*, Washington, D.C.
- Angelilli C. (2007). *Surveillance of the Performance of Elastomeric Bearings on Maryland's Concrete Bridges*. ProQuest.
- Buckle I., Constantinou M., Dicleli M., Ghasemi H. (2006). *Seismic Isolation of Highway Bridges*. Special Publication MCEER-06-SP07, Multidisciplinary Center for Extreme Events Research, University at Buffalo, Buffalo NY.
- Buckle I., Moustafa A., Eric M. (2011). *Seismic isolation design examples of highway bridges* NCHRP Project: 20-7.
- Caltrans. (1994). *Bridge Memo to Designers, Section 7: Bridge Bearings*. California Department of Transportation, Sacramento, California.
- CHBDC. (2014). *Canadian Highway Bridge Design Code. CSA-S6-14*. Canadian Standard Association. Ontario.
- Chen W., Duan L. (2014). *Bridge Engineering Handbook: Construction and Maintenance*. CRC press.
- Constantinou M., Whittaker A. , Fenz D., Apostolakis G. (2007). *Seismic Isolation of Bridges*, Report Submitted to the State of California Department of Transportation.
- Constantinou M., Kalpakidis I., Filiatrault A., Ecker Lay R. (2011). *LRFD-based analysis and design procedures for bridge bearings and seismic isolators*. Report No. MCEER-11-0004, Multidisciplinary Center for Earthquake Engineering Research, University at Buffalo, State University of New York, Buffalo, New York.
- De Raaf M., Tait M., Toopchi-Nezhad H. (2011). Stability of fiber reinforced elastomeric bearings in an unbonded application. *Journal of Composite Materials*; 45(18): 1873-1884.
- Duggal, S. (2007). *Earthquake-resistant Design of Structures*, Oxford University Press.
- Ghobarah A., Ali H. (1988). "Seismic performance of highway bridges", *Engineering Structures*; 10(3): 157-166.
- Jangid R. (2004). "Seismic response of isolated bridges", *ASCE Journal of Bridge Engineering*; 9(2): 156-166.
- Kelly J. (1999). "Analysis of Fiber-reinforced Elastomeric Isolators", *Journal of Seismology and Earthquake Engineering*; 2(1): 19-34.

Kelly J., Konstantinidis D. (2007). “Low-cost seismic isolators for housing in highly seismic developing countries”, *ASISI 10th World conference on seismic isolation, energy dissipation and active vibrations control of structures*, Istanbul, 28-31 May 2007.

Kelly J., Konstantinidis D. (2011). *Mechanics of rubber bearings for seismic and vibration isolation*. Wiley.

Kelly J. (2012). “Seismic isolation systems for developing countries”, *Earthquake Spectra*, 18(3): 385-406.

Lee D. (1994). *Bridge Bearings and Expansion Joints*. E & FN Spon, London.

Moon B., Kang G., Kang B., Kelly J. (2002). “Design and Manufacturing of Fiber Reinforced Elastomeric Isolator for Seismic Isolation”, *Journal of Materials Processing Technology*, 130(131): 145-150.

Naeim F, Kelly J. (1999). *Design of Seismic Isolated Structures: From Theory to Practice*. John Wiley & Sons.

Osgooei P., Van Engelen N., Konstantinidis D., Tait M. (2015). “Experimental and finite element study on the lateral response of modified rectangular fiber-reinforced elastomeric isolators (MR-FREIs)”, *Engineering Structures*; 85: 293-303.

Osgooei P. (2016). *Advanced Numerical Modeling of Fiber-Reinforced Elastomeric Isolators (FREIs)*. Ph.D. thesis, McMaster University, Hamilton, Ontario.

Priestley M., Seible F., Calvi G. (1996). *Seismic design and retrofit of bridges*. John Wiley & Sons, New York.

Pritchard, B. (Ed.). (1994). *Continuous and integral bridges*. CRC Press.

Russo G., Pauletta M., Cortesia A. (2013). A study on experimental shear behavior of fiber-reinforced elastomeric isolators with various fiber layouts, elastomers and aging conditions. *Engineering Structures*; 52: 422-433.

Russo G., Pauletta M. (2013). “Sliding instability of fiber-reinforced elastomeric isolators in unbonded applications”, *Engineering Structures*; 48: 70-80.

Siqueira, G., Sanda A., Paultre P., Padgett J. (2014). “Fragility curves for isolated bridges in eastern Canada using experimental results”, *Engineering Structures*; 74: 311-324.

Skinner R., Robinson W., McVerry G. (1993). *An Introduction to Seismic Isolation*. Wiley.

Stanton J., Roeder C., Mackenzie-Helnwein P., White C., Kuester C., Craig B. (2007). *Rotation Limits for Elastomeric Bearings*. Report No. NCHRP 596, Transportation Research Board, National Cooperative Highway Research Program, Washington, D.C.

Toopchi-Nezhad H, Tait MJ, Drysdale RG. (2008). “Lateral response evaluation of fiber reinforced neoprene seismic isolators utilized in an unbonded application”, *ASCE Journal of Structural Engineering*; 134(10): 1627–37.

Toopchi-Nezhad H., Tait M., Drysdale R. (2011). “Bonded versus unbonded strip fiber reinforced elastomeric isolators: finite element analysis”, *Composite Structures*; 93(2): 850–9.

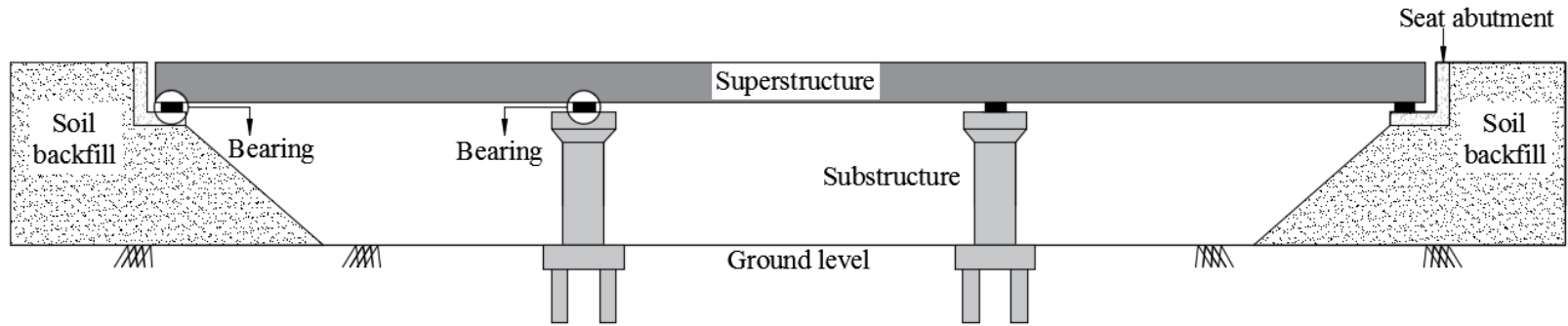
Tsopelas P., Constantinou M., Okamoto S., Fujii S., Ozaki D. (1996). “Experimental study of bridge seismic sliding isolation systems”, *Engineering Structures*; 18(4), 301-310.

Van Engelen N., Tait M., Konstantinidis D. (2012). “Lateral Behavior of Stable Unbonded Fiber Reinforced Elastomeric Isolators (SU-FREIs) with Holes”, *15th World Conference on Earthquake Engineering*. Lisbon, Portugal, 24–28 September 2012.

Van Engelen N., Osgooei P., Tait M., Konstantinidis D. (2014). “Experimental and finite element study on the compression properties of Modified Rectangular Fiber-Reinforced Elastomeric Isolators (MR-FREIs)”, *Engineering Structures*; 74: 52-64.

Wesolowsky M., Wilson J. (2003). “Seismic isolation of cable-stayed bridges for near-field ground motions”, *Earthquake Engineering and Structural Dynamics*; 32: 2107–26.

(a)



(b)

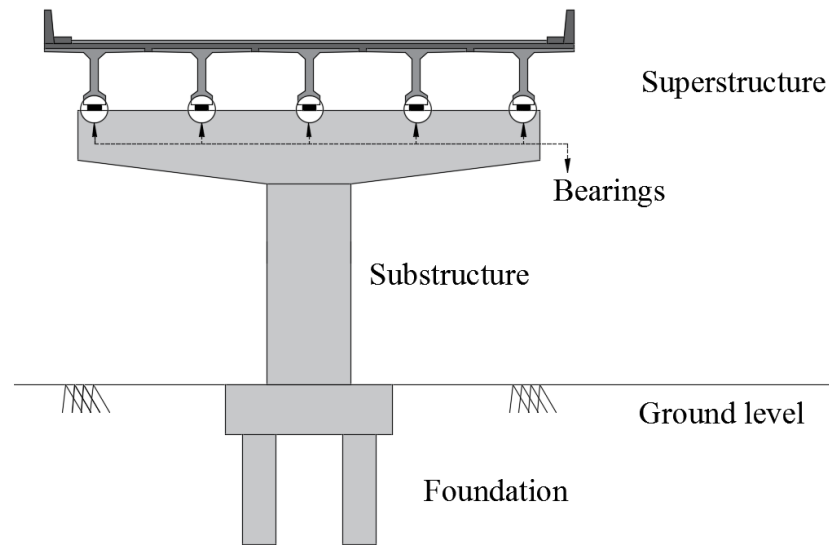


Fig. 1-1: A typical seismically-isolated bridge: (a) elevation; and (b) section II-II

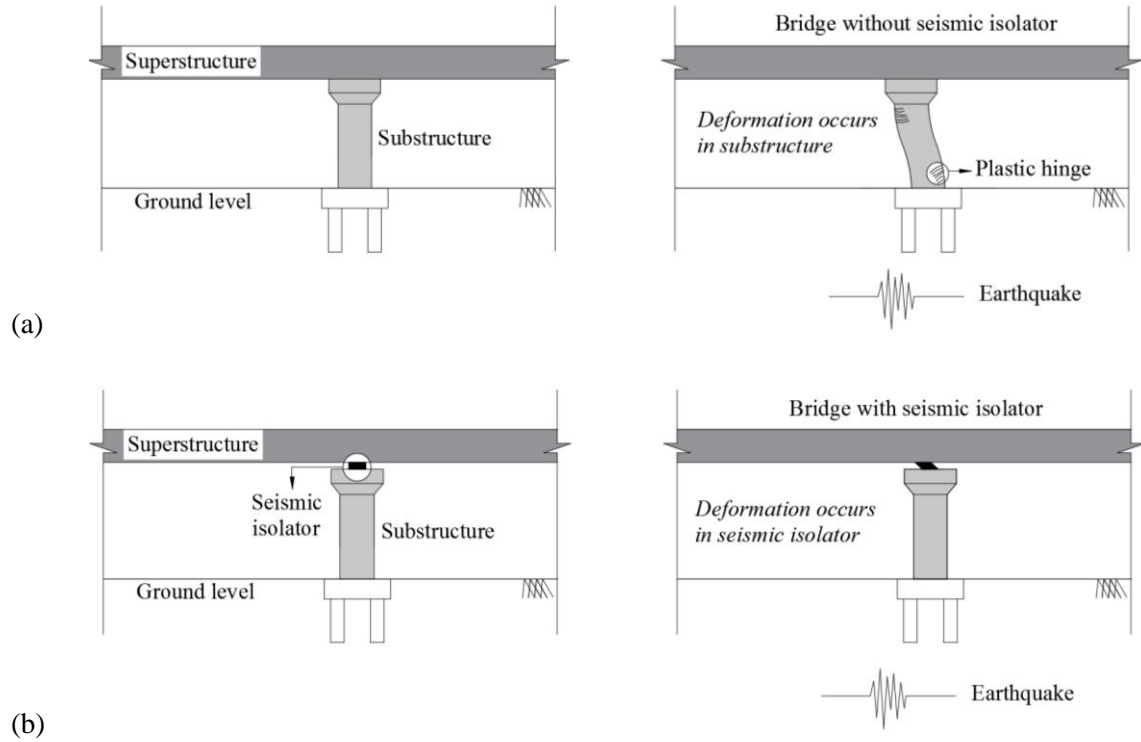


Fig. 2-2: A comparison between: (a) non-isolated bridges and (b) isolated bridges

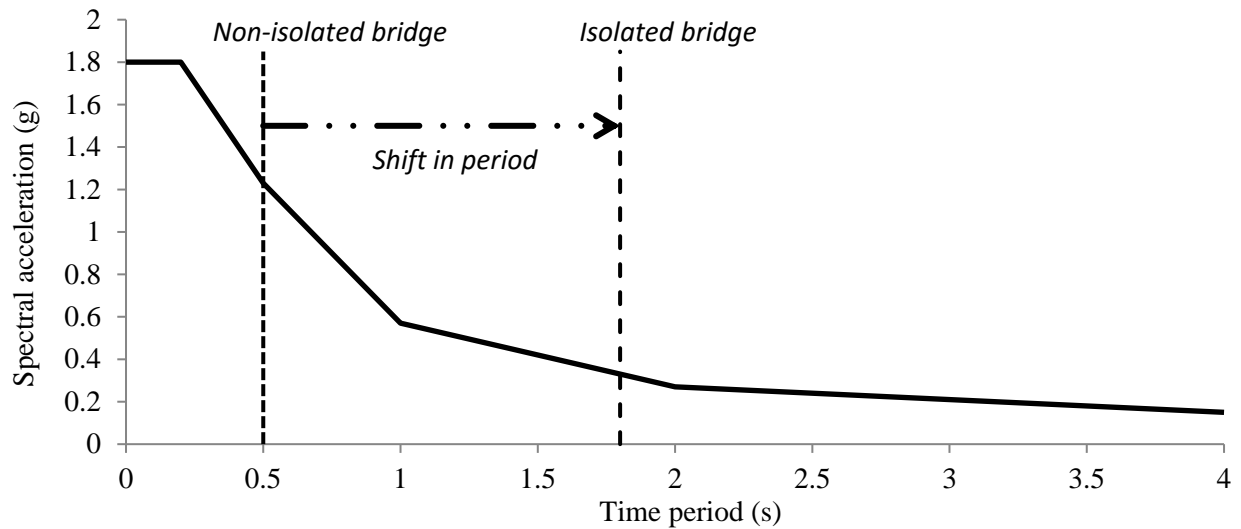


Fig. 3-3: The reduction in seismic demand due to the elongation of bridge period

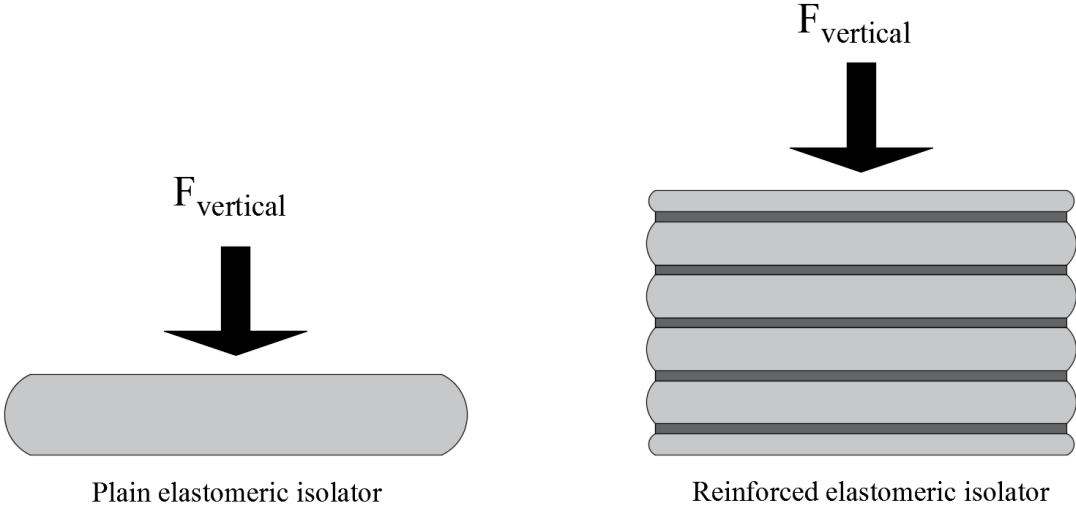


Fig. 4-4: The influence of reinforcement on enhancing the vertical stiffness of elastomeric isolators

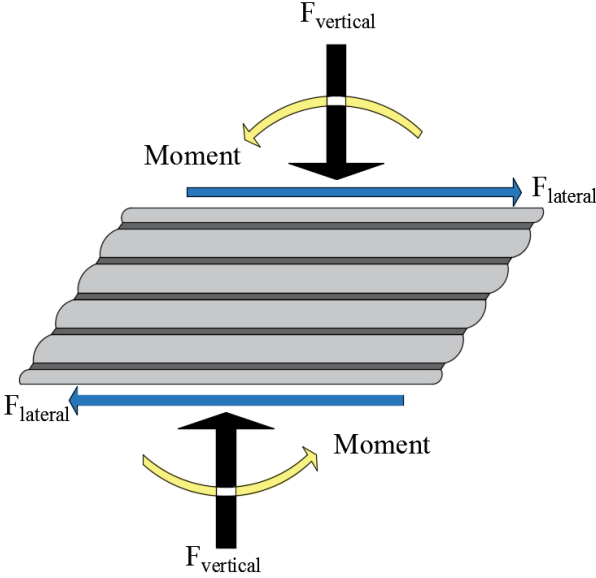


Fig. 5-5: Free body diagram of laterally deformed Bonded-FREI

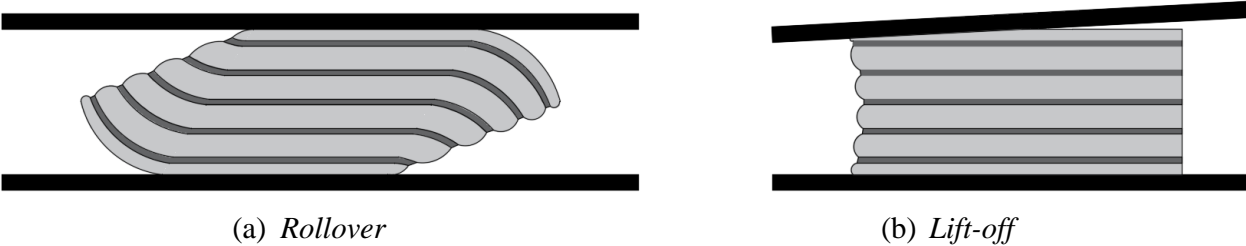


Fig. 6-6: Deformation criteria of U-FREI

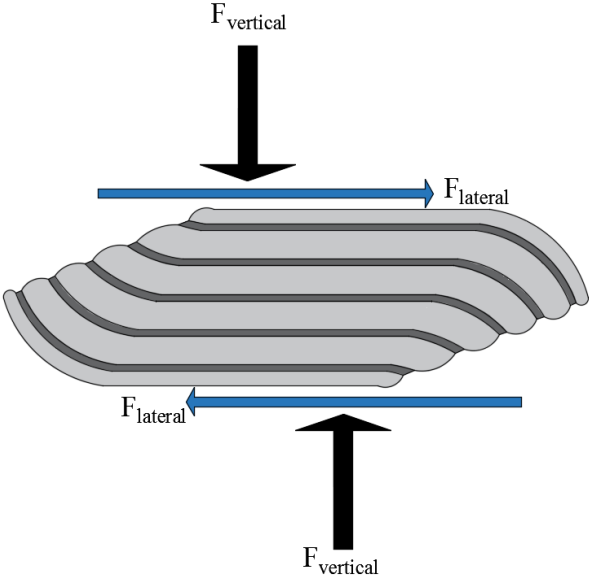


Fig. 7-7: Free body diagram of laterally deformed U-FREI

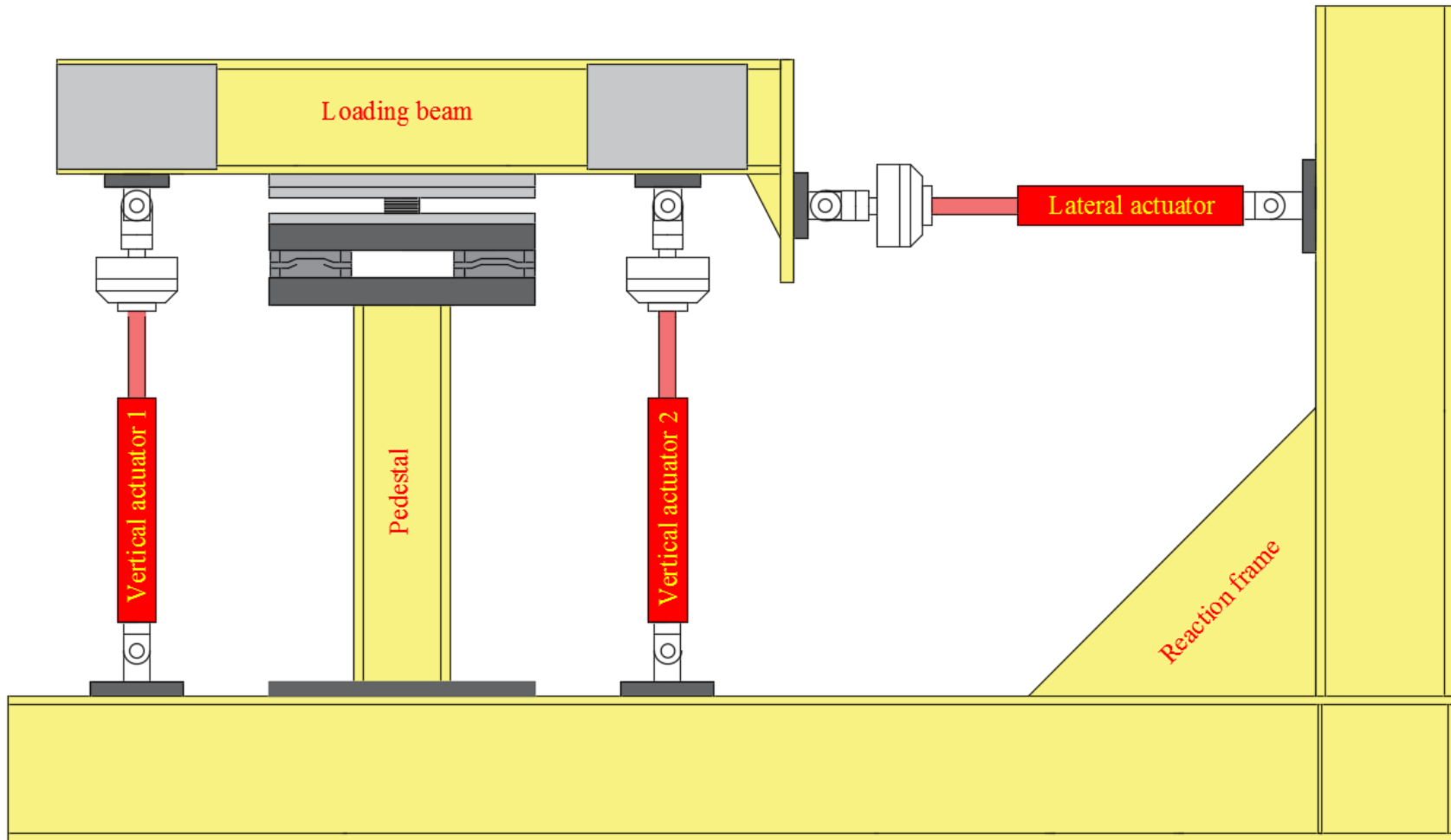


Fig. 8-8: The 3 DOF test apparatus employed in the experimental program

Chapter TWO

Experimental Investigation on the Vertical and Lateral Behaviour of Unbonded Fiber Reinforced Elastomeric Isolators

Abstract

Fiber reinforced elastomeric isolators (FREIs) have been proposed as an alternative to conventional steel reinforced elastomeric isolators (SREIs). FREIs are relatively light-weight and can be cut to the required size from larger pads. FREIs are typically categorized as either bonded or unbonded (U-FREI). In the unbonded case, the large steel end plates typically used to mechanically fasten the isolator to the supports are removed. The two major parameters that influence the vertical and horizontal response of U-FREIs are the shape factor and the aspect ratio. The vertical response is strongly influenced by the shape factor, while the aspect ratio is the controlling parameter for the stable response (i.e. maintaining a positive tangential lateral stiffness) of U-FREIs under lateral deformation. This paper describes an experimental study on the vertical and lateral response of unbonded FREIs under different loading conditions. Three U-FREIs, with different aspect ratios and shape factors, were tested using a multi-load test apparatus. Results from vertical tests indicate that, in addition to the shape factor, the vertical stiffness is influenced by the vertical rate of loading. Furthermore, it was found that the static lateral offset did not significantly affect the vertical stiffness of the isolators considered.

2.1. Introduction

Originally proposed as a potentially low-cost alternative to conventional steel reinforced elastomeric isolators (SREIs), fiber reinforced elastomeric isolators (FREIs) have been shown to demonstrate unique and potentially advantageous characteristics relative to SREIs (Kelly and Takhirov 2001; Kelly 2002; Toopchi-Nazhad et al. 2008a; Mordini and Strauss 2008; Kelly and Calabrese 2012; Dezfuli and Alam 2013; Van Engelen et al. 2016; Al-Anany et al. 2016). Fiber reinforcement has comparable tensile elastic material properties to steel, is light-weight, and allows isolators to be cut from larger pads. In light of the intended low-cost applications, it has been proposed that FREIs could be placed unbonded between the upper and lower supports to eliminate the large steel end-plates generally used to mechanically fasten the isolator to the upper and lower supports. Early investigations revealed that unbonded FREIs (U-FREIs) experience a unique *rollover* deformation when displaced laterally, illustrated in Fig. 2-1(a). Rollover occurs as a consequence of the unbonded application and the lack of flexural rigidity of the fiber reinforcement.

The volume of elastomer that experiences rollover is proportional to the lateral displacement (Van Engelen et al. 2014). The lateral resistance of the rollover section is less than an equivalent volume in simple shear (Toopchi-Nazhad 2014). Thus, as lateral displacement occurs, the lateral stiffness of the isolator reduces (softens). The reduction in lateral stiffness continues until the isolator reaches *full rollover*, where the initially vertical faces of the isolator rotate and contact the upper and lower supports (see Fig. 2-1(b)). Full rollover prevents additional rollover from occurring, stiffening the isolator with additional lateral displacement. U-FREIs that maintain a positive tangential stiffness over all levels of imposed lateral displacement are denoted as stable unbonded-FREIs (SU-FREIs) (Toopchi-Nazhad et al. 2009; Pauletta et al.

2015). Due to the characteristic softening and stiffening SU-FREIs are considered to be an adaptive device, which can be tailored to the expected earthquake hazard level.

A key requirement for any isolation system is a sufficiently high vertical stiffness (Kelly 1997; Naeim and Kelly 1999). A high vertical stiffness is required to suppress potential rocking modes. As a SU-FREI is displaced laterally, rollover results in a reduced load-bearing area (see Fig. 2-1(a)). While many studies have investigated the lateral or vertical properties of unbonded FREIs, none have investigated the sensitivity of the vertical properties to a lateral offset. A lateral offset is the lateral displacement applied to the specimen after applying the vertical load but before cycling the vertical load on the specimen. In this paper, the sensitivity of the vertical and lateral response of FREIs to the aspect ratio, defined as the ratio of the length in the direction of lateral loading to total height, is investigated. Experimental testing was conducted on three FREI specimens with aspect ratio values of 2.60, 3.60, and 5.00. The aspect ratio is considered to be an important parameter in the design of U-FREIs as it influences its lateral stability. Thus, it is important that the aspect ratio remains larger than approximately 2.5 (Toopchi-Nazhad et al. 2008a; Van Engelen et al. 2014; Toopchi-Nazhad 2014) in order to maintain lateral stability (i.e. maintain a positive lateral tangential stiffness).

The main objective of this study is to investigate the vertical and the coupled vertical-lateral response of U-FREIs under different loading conditions. The following tests were carried in order to achieve this objective: (1) vertical cyclic tests to study the effect of vertical loading frequency on the vertical mechanical properties, including the vertical stiffness and damping of U-FREI, (2) vertical cyclic tests with a lateral offset to study the influence of a lateral offset on the above properties and (3) lateral cyclic tests to study the vertical response and the lateral stiffness and damping of U-FREIs.

2.2. Background

The viability of replacing steel reinforcement in traditional elastomeric isolators with different types of reinforcing material, such as carbon fiber and glass fiber, has been investigated by a number of researchers (Kelly 1992; Moon et al. 2002). Kelly (1999) conducted an analytical study on FREIs in order to investigate the mechanical properties, particularly the vertical and lateral stiffness values of this type of elastomeric isolator. Based on the findings from this study, it was concluded that producing elastomeric isolators reinforced with fiber matching the behaviour of steel-reinforced isolators was viable. Moon et al. (2002) evaluated the efficiency of using FREIs by comparing their behaviour to conventional SREIs. It was reported that the vertical stiffness of the FREI investigated, which utilized carbon fiber reinforcement, was 3 times higher than the vertical stiffness of the corresponding SREI. It was also found that the equivalent damping of an FREI was 2.5 times higher than the SREI considered.

Toopchi-Nezhad et al. (2008b) evaluated the lateral response of U-FREIs manufactured using a neoprene elastomer reinforced with bi-directional plain weave carbon fiber fabric. An experimental study was conducted on U-FREIs with identical geometric properties cut from larger fiber reinforced elastomeric pads. The $\frac{1}{4}$ scale bearings had an aspect ratio of 2.8 and a shape factor of 11. The shape factor is defined as the ratio of the loaded area to the unloaded area of a single layer of elastomer. Test results showed that there was a significant decrease in the effective lateral stiffness due to rollover over a displacement range of $1.00 t_r$ to $2.00 t_r$, where t_r is the total thickness of the elastomer. A significant increase in the effective lateral stiffness was then found to occur at larger lateral displacements (i.e. beyond $2.00 t_r$), due to full rollover. Additionally, an increase in the lateral loading rate resulted in an increase in the effective lateral stiffness and damping.

Toopchi-Nezhad et al. (2009) performed a parametric study on a $\frac{1}{4}$ scale model SU-FREI to investigate their lateral and vertical response. The study found that the vertical frequency of the considered SU-FREI was at least 20 times larger than the maximum base isolated frequency expected from the bearing. Negligible vertical stiffness degradation occurred after the bearing specimen was subjected to lateral cyclic testing. At least 8% damping was achieved under the largest lateral displacement. The unscragged effective lateral stiffness and damping values were a maximum of 10% and 19%, respectively, larger than the average response values obtained from the scragged loops. Additionally, a 50% increase in the vertical stress resulted in a 10% increase in the effective damping.

De Raaf et al. (2011) studied the stability of fiber reinforced elastomeric bearings in an unbonded application through two experimental tests on three isolators matching those investigated by Toopchi-Nezhad et al. (2008b, 2009). The first test investigated the lateral stability under lateral cyclic excitation by incrementally increasing the axial load. The objective of this test was to calculate the buckling load corresponding to zero transverse stiffness. The second test investigated the ultimate shear properties of SU-FREIs under the design axial load by monotonically increasing the lateral displacement. Based on findings from the study it was concluded the value of the critical buckling load was inversely proportional to the amplitude of lateral displacement. Moreover, the critical buckling loads were found to be approximately 10 times larger than the design axial loads. The isolators were laterally displaced up to $3.50 t_r$ without showing any lateral instability.

Warn and Whittaker (2006) experimentally investigated the influence of lateral displacement on the mechanical properties of bonded SREIs, particularly the vertical stiffness. A series of various loading conditions, including different vertical stress levels, vertical loading

rates, and lateral displacements were applied. It was found that the vertical stiffness was inversely proportional to the level of lateral displacement. Moreover, the vertical stiffness increased when the vertical loading rate was increased. The vertical effective damping for the SREI investigated was found to be approximately 1%.

2.2.1. Analytical Solution

The analytical solution for the compression modulus of a rectangular pad, which includes the compressibility of the elastomer and extensibility of the reinforcement, based on the assumptions of the pressure solution, has been presented by Angeli et al. (2013) and Kelly and Van Engelen (2015). Angeli et al. (2013) assumed that the fiber reinforcement layer thickness can be divided by two, which is representative of the weave being of equal thickness in the two perpendicular directions, and presented the solution as a double Fourier series. In Kelly and Van Engelen (2015), an alternative solution based on a rapidly convergent single Fourier series solution was derived. In Kelly and Van Engelen (2015), the thickness of the fiber reinforcement layer was assumed to represent the thickness of the fibers as a matrix, while the value of the elastic modulus of the fiber reinforcement represented the effective modulus in the respective direction. Kelly and Van Engelen (2015) express the compression modulus, E_c , of a rectangular pad with a width of a and length of $2b$ as:

$$E_c = 96GS^2 \left(2 + \frac{a}{b}\right)^2 \sum_{n=1,3,5,\dots}^{\infty} \frac{1}{(n\pi)^2 \left((\alpha^2 + \beta^2) + \left(2 + \frac{a}{b}\right)^2 + (n\pi)^2 \right)} \frac{1}{(n\pi)^2} \left(1 - \frac{\tanh(\lambda)}{\lambda}\right) \quad (1)$$

The dimensionless parameters are defined as:

$$\alpha^2 = \frac{24 G S^2 t}{E_f t_f} \quad (2)$$

$$\beta^2 = \frac{12 G S^2}{t^2 K} \quad (3)$$

$$\lambda = \sqrt{\frac{(\alpha^2 + \beta^2) + \left(2 + \frac{a}{b}\right)^2 + (n\pi)^2}{\frac{a}{b}}} \quad (4)$$

where

$$S = \frac{ab}{t(a + 2b)} \quad (5)$$

is the shape factor, G is the shear modulus of the elastomer, K is the bulk modulus of the elastomer, t is the thickness of a single layer of elastomer, t_f is the thickness of the reinforcement, and E_f is the effective elastic modulus of the reinforcement.

Note that the dimensionless parameters α and β represent the sensitivity of E_c to the extensibility of the reinforcement and the compressibility of the elastomer, respectively. Equation (1) is equally sensitive to α and β , indicating that both parameters can have a pronounced effect on the compression modulus, even with low-to-moderate shape factors.

2.3. Experimental Program

2.3.1. Specimens

Three ¼ scale specimens were cut from a laminated fiber reinforced elastomeric sheet (see Fig. 2-2). The U-FREI specimens all had the same total height (h) of approximately 22.4 mm. All specimens comprised of five interior neoprene layers with a thickness of 3.18 mm and two exterior neoprene layers with a thickness of 1.59 mm. The total thickness of the elastomeric layers was approximately 19 mm. The plain weave bi-directional carbon fiber reinforcement had a thickness of approximately 0.55 mm when bonded to the elastomeric layers. The dimensions of the specimens are summarized in Table 2-1. All of the specimens had the same out of plan

dimension of 60 mm, but a different in-plane dimension (lateral loading direction), which determines the aspect ratio (see Table 2-1).

2.3.2. Test program

The test program was divided into three phases. The first test phase investigated the effect of vertical loading rate on the vertical response using three different frequencies (0.01, 0.1, and 1 Hz), as shown in Fig. 2-3. For each frequency, the isolators were monotonically loaded up to the desired vertical stress, σ_v , of 2 MPa under load control. This was followed by three cycles of $\pm 20\% \sigma_v$. Since the considered isolators had a different loaded area, axial loads of 13.4, 9.6, 6.8 kN were applied, respectively. Note that these axial loads were maintained during the three phases of this study. Thus, the maintained vertical stress of 2 MPa was considered the average stress based on the total plan area. The vertical loading conducted during the first phase of the test program was in accordance with procedures outlined in ISO-22762 (ISO 2010).

The second testing phase investigated the effect of lateral displacement on the vertical response. During this phase a vertical loading rate of 0.1 Hz was maintained, but lateral offsets were varied by values of: 0.25, 0.50, 1.00, and 1.50 of the total rubber thickness (t_r). The loading procedure for this phase is shown in Fig. 2-4. The isolator was first displaced laterally under displacement control after the vertical load was applied under load control. The vertical load was then cycled three times, identical to the first phase.

The third phase investigated the lateral and vertical response of U-FREIs under lateral cyclic loading. The lateral loading rate was maintained at 76 mm/s, while a total of six amplitudes were considered (0.25, 0.50, 1.00, 1.50, 2.00, and 2.50 t_r) as shown in Fig. 2-5. Each specimen was visually inspected for damage after each experiment.

2.3.3. Experimental Apparatus

The experimental program was conducted using a 3 degree-of-freedom bearing test apparatus, shown in Fig. 2-6. The self-reacting test apparatus consists of a loading beam, an isolator pedestal, and a reaction frame. The isolator pedestal supports a thick bottom platen. A cold-rolled plate, which is located directly above the bottom platen, supports the isolator and represents the lower contact surface. Vertical load/displacement is applied to the top of the isolator specimen through a cold-rolled steel plate, which is attached at the mid-span of the loading beam. Roller guides on both side of the loading beam provide out-of-plane stability.

The loading beam is displaced using three hydraulic actuators. There are two vertical actuators located at either end of the loading beam, which permit the application of vertical loads and/or rotations on the test specimen. A lateral actuator, which is used to apply lateral displacements, is located between one end of the loading beam and the vertical reaction arm. Two three-axis load cells are used to measure the vertical and lateral loads. The vertical deflection of the isolators during testing is measured using four laser displacement transducers attached at the four corners of the loading platen.

2.4. Experimental Results

2.4.1. Effect of Loading Rate on Vertical Stiffness

Figure 2-7 presents the relationship between the vertical stress and normalized vertical deformation for the three vertical loading rates considered. All isolators initially experienced some degree of run-in prior when the vertical load was applied. The run-in effect is considered to be one of the recognized differences between steel-reinforced elastomeric isolators and fiber reinforced elastomeric isolators (Kelly 2008). It primarily occurs due to the lack of straightness

of the individual fibers (Kelly 2008). As a vertical load is applied, the lateral bulging in the elastomer develops a tensile stress in the fiber reinforcement that pulls the individual fibers taut, which consequently results in a higher vertical stiffness as the restraint on the elastomeric layers is increased.

Results from the third vertical cycle (ISO 2010) completed on each isolator for Phase 1 (i.e. no lateral offset) are listed in Table 2-2. The vertical stiffness was calculated using the vertical displacements corresponding to the maximum and minimum vertical forces observed over the cycle under consideration as follows (ISO 2010)

$$K_v = \frac{F_{v,max} - F_{v,min}}{\delta_{v,max} - \delta_{v,min}} \quad (6)$$

where $F_{v,max}$ and $F_{v,min}$ are the maximum and minimum forces and $\delta_{v,max}$ and $\delta_{v,min}$ are the corresponding maximum and minimum vertical displacements, respectively, determined from the vertical hysteresis loops of the third cycle.

The compression modulus (E_c) of an elastomeric isolator with a plan area (A) can be expressed as

$$E_c = \frac{K_v t_r}{A} \quad (7)$$

The vertical damping ratio (ζ_v) for each isolator tested was calculated based on the area within the hysteresis loops (W_D) using the following (Chopra 2002)

$$\zeta_v = \frac{1}{2\pi} \left[\frac{W_D}{(|F_{v,max} - F_{v,min}| |\delta_{v,max} - \delta_{v,min}|)} \right] \quad (8)$$

Additionally, the vertical frequency (f_v) was calculated as follows

$$f_v = \frac{1}{2\pi} \sqrt{\frac{k_v g}{P A}} \quad (9)$$

where g is the gravitational acceleration, and P is the vertical load.

As listed in Table 2-2, the damping ratio was found to range between approximately 1% and 3%, which provides an energy dissipation mechanism for vertical vibrations. A previous experimental study completed by Warn and Whittaker (2006) found that the vertical damping ratio corresponding to other types of isolators, particularly lead-rubber (LR) and low-damping rubber (LDR) isolators was approximately 1% and 2%, respectively.

As anticipated, the vertical stiffness was directly proportional to the shape factor for each isolator, where isolators with a higher shape factor were found to have a higher vertical stiffness. An increase in the vertical stiffness was also observed at higher loading frequencies, and was particularly significant for the isolator with the lowest shape factor. The increase in vertical stiffness due to an increase in the vertical rate of loading from 0.01 Hz to 1 Hz was found to be approximately 13.6%, 18.9%, and 20.9% for Isolator 1, 2, and 3, respectively.

The aforementioned influence of the loading rate (0.01, 0.1, and 1 Hz) on the vertical response of Isolator 1 is shown in Fig. 2-8. The variation in vertical stiffness during the three loading cycles under the different loading rates considered is shown in Fig. 2-9. The change in the vertical stiffness from one cycle to another is minimal, regardless of isolator aspect ratio and vertical loading rate.

Table 2-3 compares the experimentally obtained value of E_c to the theoretical values obtained from Eq. (1). In Eq. (1), it was assumed that $K = 2000$ MPa and $E_f = 20,000$ MPa. The value of G was selected as 0.4 MPa based on the experimental results for the average of the three isolators at a lateral displacement of $0.25 t_r$. As shown in Table 2-3, the ratio of the analytical solution to the experimental values were found to range between 0.88 and 1.10, demonstrating overall good agreement.

2.4.2. Effect of Lateral Offset on Vertical Stiffness

This section presents the results from vertical testing completed in order to investigate the effect of lateral offset (Δ_L) on the vertical response of an U-FREI. The influence of varying lateral offset on the vertical displacement and the vertical stiffness is presented in Figs. 2-10 and 2-11, respectively. The vertical stiffness shown in Fig. 2-11 was a result of vertical cyclic loading applied to the isolators after the occurrence of some vertical deformation in the isolator under lateral displacement, which was normalized in Fig. 2-11 with respect to t_r . Lateral displacement reduces the contact area between the isolator and the supports as rollover occurs. As the bearing is displaced laterally, there is an increase in vertical deformation as shown in Fig. 2-10. However, it can be observed from Fig. 2-11 that the vertical stiffness remains relatively constant with lateral displacement. This implies that the vertical compression modulus increases with lateral displacement to offset the reduction in the contact area. This is a complex problem due to the significant material and geometric non-linearity. In a finite element investigation conducted by Toopchi-Nezhad et al. (2011), it was found that lateral displacement in U-FREIs resulted in a relatively small increase in the peak vertical stress when compared to a bonded isolator. It is postulated that the increased vertical deformation, coupled with the moderate increase in vertical stress, increases the lateral bulging which subsequently increases the tautness of the fiber reinforcement as the reinforcement matrix is strained. Thus, the expected reduction in vertical stiffness due to the loss of contact area is mitigated by an increase in the compression modulus resulting from fibers tautness as well as geometric nonlinearity.

According to Fig. 2-11, the change in the vertical stiffness due to an increase in lateral offset is 11% or less, independent of the aspect ratio. This observed behaviour for a U-FREI is different than that found for bonded steel reinforced isolators, where a lateral offset leads to a

reduction in the vertical stiffness as indicated by the following expression given by Warn et al. (2007):

$$k_v = k_{vo} \left[\frac{1}{1 + \frac{3A}{I} \left(\frac{\Delta_L}{\pi} \right)^2} \right] \quad (10)$$

where k_{vo} is the initial vertical stiffness before the application of lateral displacement and I is the isolator second moment of area.

Fig. 2-12 shows the vertical stress-strain curves for Isolator 1 under a constant vertical load, and varying normalized lateral displacement values of 0, 0.25, 0.50, 1.00 and 1.50 t_r . The figure presents the response for the three loading cycles (see Fig. 2-4) under a vertical loading rate of 0.1 Hz. It can be observed that the vertical stiffness is nearly constant for Isolator 1 at the different levels of lateral offset considered.

After completion of the lateral offset tests, a vertical test with no lateral offset was repeated on each isolator in order to check if any reduction in the vertical stiffness occurred due to internal damage. According to the experimental results, listed in Table 2-4, the reduction in vertical stiffness of Isolator 1, 2, and 3 due to the lateral offset testing was 4.8%, 4.2%, 6.4%, respectively. Additionally, it was found that the additional strain from one cycle to the next in the stress-strain relationship was retained in the isolator vertical behaviour as seen in Fig. 2-11. All isolators were visually inspected after each test, and no external damage was observed in any isolator. Stanton et al. (2007) have suggested using the damping as a way for measuring the damage in elastomeric bearings. No significant change in damping was found to have occurred in any of the three specimens tested.

2.4.3. Lateral Cyclic Tests

The objective of this section was to study the effect of the aspect ratio on the effective lateral stiffness (K_L), effective lateral damping (ζ_L), and vertical response on lateral cyclic loading of U-FREIs. Eighteen lateral consecutive cycles, consisting of six ascending normalized displacement amplitude (Δ_L/t_r) of 0.25, 0.50, 1.00, 1.50, 2.00, and 2.50 (see Fig. 2-5), under displacement control were applied under a lateral loading rate of 76 mm/s and an average vertical stress of 2 MPa. The lateral stiffness was computed using the same method employed to evaluate the vertical response, where the lateral stiffness was calculated from the peak responses from the lateral load-displacement hysteresis loops, using the following relation (ISO 2010)

$$k_L = \frac{F_{L,max} - F_{L,min}}{U_{max} - U_{min}} \quad (11)$$

where $F_{L,max}$ and $F_{L,min}$ are the maximum and minimum lateral forces computed at each cycle, respectively, and U_{max} and U_{min} are the maximum and minimum lateral displacements experienced by the isolator during each cycle, respectively. The lateral damping was determined from the hysteresis loops using the following relationship (Chopra 2002)

$$\zeta_L = \frac{2}{\pi} \left[\frac{W_D}{k_L(|U_{max}| + |U_{min}|)^2} \right] \quad (12)$$

Fig. 2-13 shows the lateral load-displacement relationship (hysteresis loops) of the isolators. The lateral load was normalized with respect to the isolator loading area (A) and the average shear modulus of the isolators (G) of 0.4 MPa. According to the results presented in Fig. 2-13, the lateral response of the isolators can be divided into three stages. In the first stage, at small lateral displacements where the isolator remains in full contact with the loading supports, the lateral-load response is similar to a bonded isolator. In the second stage, as the lateral displacement increases, a nonlinear decrease in the effective lateral stiffness of the isolator

occurs due to rollover. The third stage occurs under larger lateral displacements (approximately $2.00 t_r$) where the initially vertical face of the isolator contacts the supports, which leads to an increase in the effective lateral stiffness of the isolator (Toopchi-Nazhad et al. 2008a).

It can be observed from Fig. 2-13 that the displacement initiating any of the aforementioned three stages is insignificantly related to the aspect ratio of the isolator (Van Engelen et al. 2014). For example, Isolator 1 with the largest aspect ratio maintained the behaviour associated with stage 1 (similar to bonded isolators), before the occurrence of stiffening behaviour of stage 3. Observable stiffening begins when Δ_L/t_r exceeds 2.00, which corresponds to approximately when full rollover occurred. Additionally, the isolators maintained stable behaviour up to the largest considered normalized lateral displacement of 2.50 as shown in Fig. 2-14. With a larger aspect ratio, the volume of rollover is small in comparison to the total volume of the isolator; thus, the amount of softening observed is reduced (e.g. Isolator 1). As the aspect ratio decreases, the volume of rollover becomes large in comparison to the total volume of the isolator, and significant softening occurs (e.g. Isolator 3). For very small aspect ratios (generally below 2.5), the softening due to rollover may lead to horizontal instability in the lateral force-displacement relationship prior to the occurrence of full rollover (Toopchi-Nazhad et al. 2008a; Van Engelen et al. 2014).

Table 2-5 contains the resulting equivalent lateral stiffness and damping ratio values corresponding to the three loading cycles. The highest value for the equivalent mechanical properties (stiffness and damping) of the isolator is higher than the following cycles. This phenomena is primarily because the initial loading causes a breakage of links inside the elastomer material (Mullins effect) (Marckmann et al. 2002). The increase in the difference between the first and the third cycle for the tested isolators is related to the applied lateral

displacement. For instance, at a lateral displacement $0.25 t_r$, the difference in the lateral stiffness between the first and third cycle is approximately 4.3%, 3.9%, and 4.5% for Isolator 1, 2, and 3, respectively. However, at a lateral displacement $2.50 t_r$, the difference is found to be 11.4%, 13.7%, and 11.7%. It is important to note that these variations are within the limit of 15% stated in ASCE (2013).

Table 2-5 also shows that the values for damping are significantly larger than the elastomer supplier specified damping ratio of 5%, which is believed to be attributed to the slippage (friction) between the individual strands in the fiber bundle during the lateral rollover deformation of the isolator (Kelly 1992). Table 2-5 shows that the damping decreases with increasing lateral displacement, however, a slight increase was observed at $2.50 t_r$.

Figure 2-15 (a) and (b) present the effect of lateral displacement on the lateral stiffness and damping ratio, corresponding to the third cycle of lateral cyclic testing at each displacement amplitude. Cycle 3 is selected in order to compare the lateral response between isolators after being scragged. The lateral displacement resulted in a reduction in the lateral stiffness and damping ratio prior to the occurrence of full rollover, which theoretically occurs at a lateral displacement amplitude of $1.67 h$ (Kelly and Konstantinidis 2007). After the occurrence of full rollover, both the lateral stiffness and damping ratio increased.

Test results presented in Fig. 2-15 show that the reduction in lateral stiffness was more significant for isolators with a lower aspect ratio. The reduction in the damping ratio was more pronounced for isolators with a higher aspect ratio. For instance, at a normalized lateral displacement amplitude of 1.50 (i.e. before the occurrence of full rollover), Isolator 1, 2, and 3, showed a reduction in lateral stiffness of 44 %, 49 %, and 58 %, respectively, when compared to values at a normalized lateral displacement amplitude of $0.25 t_r$.

2.4.4. Normalized Vertical Deformation and Lateral Displacement

One of the major advantages of using U-FREIs is the ability to undergo rollover, which leads to a reduction in the lateral stiffness. However, the loss of contact leads to a reduction in loading area, which is expected to result in an increase in the vertical deformation due to an increase in average stress. The normalized vertical deformation is defined here as the ratio of vertical deformation at zero lateral displacement to the vertical deformation at the defined lateral displacement.

Figure 2-16 presents the effect of lateral displacement amplitude on the variation in the normalized vertical deformation of isolators during their lateral rollover. For normalized lateral displacement amplitudes up to $2.00 t_r$, an increase in the normalized vertical deformation occurs. The relationship between normalized vertical deformations during lateral cyclic testing is inversely proportional to the value of the aspect ratio. For example, when all isolators were displaced to a normalized lateral displacement of $1.50 t_r$, the factor of increase in normalized vertical deformation in Isolator 1, 2, and 3 when compared to their initial state (i.e. at zero lateral displacement) was approximately 1.23, 1.35, and 1.72, respectively (this value is an average of the both directions during the third cycle). However, some vertical deformation is recovered at larger lateral displacements of $2.50 t_r$, due to the occurrence of full rollover (see Fig. 2-2), particularly for isolator with high aspect ratios, which results in a slight increase in the vertical stiffness of the isolator. As an example, when exceeding full rollover (i.e. $2.50 t_r$), it was observed that the normalized vertical deformation was approximately 1.02, 1.58 and 2.54 in Isolator 1, 2, and 3, respectively, which means an almost full recovery of vertical displacement for high aspect ratio isolators.

2.5. Conclusion

Three U-FREI specimens with different aspect ratios were tested under several loading conditions in both the vertical and lateral direction. The loading conditions varied were the vertical loading rate, the lateral static offset, and the lateral cyclic amplitude. The mechanical properties evaluated during each stage were the stiffness and damping in both vertical and lateral directions.

The following conclusions were drawn:

- 1- The vertical damping ratio of the tested isolators was determined to range between approximately 1% and 3%, while the lateral damping ratio ranged between 9% and 14%.
- 2- The relationship between the vertical loading frequency and the vertical stiffness was found to be directly proportional, particularly for isolators with lower shape factor.
- 3- The analytical solution derived by Kelly and Van Engelen (2015) based on the assumptions of the pressure solution was in good agreement with experimental results. The difference was found to be within $\pm 10\%$.
- 4- For all isolators considered, it was found that the influence of the static lateral offset on the vertical stiffness was insignificant. It was postulated that this was partially because the tautness of the fiber reinforcement increases with vertical deformation, which increases the compression modulus and offsets the reduction in area.

This study is part of a larger research program investigating the viability of FREIs as a lightweight and low-cost bearing for structural applications. Ongoing research is currently being carried out to investigate the behaviour of FREIs in the vertical and lateral directions under static rotations, which is of significant importance for bridge applications.

Acknowledgements

Financial support for this study was provided by the McMaster University Centre for Effective Design of Structures (CEDs) funded through the Ontario Research and Development Challenge Fund (ORDCF) as well as an Early Researcher Award (ERA) grant, both of which are programs of the Ministry of Research and Innovation (MRI). The support of the Natural Sciences and Engineering Research Council of Canada and a Vanier Canada Graduate Scholarship is gratefully acknowledged.

References

- Al-Anany Y., Van Engelen N., Tait M., Konstantinidis D. (2016). "Examination of Fiber Reinforced Elastomeric Isolators for Bridge Applications", *International Joints and Bearings Research Council*, Atlanta, Georgia, USA, 25-29 September, 2016.
- Angeli P., Russo G., Paschini A. (2013). "Carbon Fiber-Reinforced Rectangular Isolators with Compressible Elastomer: Analytical Solution for Compression and Bending", *International Journal of Solids and Structures*; 50(22): 3519-3527.
- ASCE. (2013). *Minimum design loads for buildings and other structures*, ASCE/SEI 7-10, New York.
- Chopra A. (2002). *Dynamics of structures: Theory and Applications to Earthquake Engineering*. Fourth edition. Prentice Hall, New Jersey.
- De Raaf M., Tait M., Toopchi-Nezhad H. (2011). Stability of fiber reinforced elastomeric bearings in an unbonded application. *Journal of Composite Materials*; 45(18): 1873-1884.
- Dezfuli F., Alam M. (2013). "Multi-criteria optimization and seismic performance assessment of carbon FRP-based elastomeric isolator". *ASCE Journal of Structural Engineering*; 49: 525-540.
- ISO. (2010). *Elastomeric seismic-protection isolators*, ISO 22762, Geneva.
- Kelly J. (1997). *Earthquake-resistant design with rubber*. 2nd ed. London: Springer-Verlag.

- Kelly J. (1999). "Analysis of fiber-reinforced elastomeric isolators". *Journal of Seismology and Earthquake Engineering*; 2(1): 19–34.
- Kelly J., Takhirov S. (2001). *Analytical and Experimental Study of Fiber-Reinforced Elastomeric Isolators*. Pacific Earthquake Engineering Research Center, PEER, Berkeley, California; 2001/11.
- Kelly J. (2002). *Seismic isolation systems for developing countries*. *Earthquake Spectra*; 18(3):385–406.
- Kelly J., Konstantinidis D. (2007). "Low-cost seismic isolators for housing in highly seismic developing countries", *ASSISI 10th World Conference on Seismic Isolation, Energy Dissipation and Active Vibrations Control of Structures*, Istanbul, 28-31 May 2007.
- Kelly J. (2008). "Analysis of the run-in effect in fiber-reinforced isolators under vertical load", *Journal of Mechanics of Materials and Structures*; 3(7):1383–401.
- Kelly J., Calabrese A. (2012). *Mechanics of fiber reinforced bearings*. Pacific Earthquake Engineering Research Center, PEER, Berkeley, California; 2012/101.
- Kelly, J., Van Engelen N. (2015). *Single Series Solution for the Rectangular Fiber-Reinforced Elastomeric Isolator Compression Modulus*. Pacific Earthquake Engineering Research Center, PEER, Berkeley, California; 2015/03.
- Marckmann G., Verron E. , Gornet L., Chagnon G., Charrier P., Fort P. (2002). "A theory of network alteration for the Mullins effect." *Journal of the Mechanics and Physics of Solids*; 50(9): 2011–2028.
- Moon B., Kang G., Kang B., Kelly J. (2002). "Design and manufacturing of fiber reinforced elastomeric isolator for seismic isolation", *Journal of Materials Processing Technology*; 130(131): 145–150.
- Mordini, A., and Strauss, A. (2008) "An innovative earthquake isolation system using fibre

reinforced rubber bearings”, *Engineering Structures*; 30(10), 2739–2751.

Naeim F., Kelly J. (1999). *Design of Seismic Isolated Structures: From Theory to Practice*. John Wiley & Sons Inc., New York.

Pauletta M., Cortesia A., Russo G. (2008). “Roll-out instability of small size fiber-reinforced elastomeric isolators in unbonded applications”. *Engineering Structures*; 102: 358-368.

Stanton J., Roeder C., Mackenzie-Helnwein P., White C., Kuester C., Craig B. (2007). *Rotation Limits for Elastomeric Bearings*. Report No. NCHRP 596, Transportation Research Board, National Cooperative Highway Research Program, Washington, D.C.

Toopchi-Nezhad H., Tait M., Drysdale R. (2008a). “Testing and modeling of square carbon fiber reinforced elastomeric seismic isolators”, *Structure Control and Health Monitoring*; 15(6): 876–900.

Toopchi-Nezhad H., Tait M., Drysdale R. (2008b). “Lateral response evaluation of fiber reinforced neoprene seismic isolators utilized in an unbonded application”, *ASCE Journal of Structural Engineering*; 134(10):1627–37.

Toopchi-Nezhad H., Drysdale R., Tait M. (2009). “Parametric study on the response of stable unbonded fiber-reinforced elastomeric isolators (SU-FREIs)”, *Journal of Composite Materials*; 43(15): 1569–87.

Toopchi-Nezhad H., Tait M., Drysdale R. (2011). “Bonded versus unbonded strip fiber reinforced elastomeric isolators: finite element analysis”. *Composite Structures*; 93(2): 850–9.

Toopchi-Nezhad H. (2014). “Horizontal stiffness solutions for unbonded fiber reinforced elastomeric bearings”, *Structural Engineering and Mechanics*; 49(3): 395-410.

Van Engelen N., Tait, M., Konstantinidis D. (2014). “Model of the Shear Behavior of Unbonded Fiber-Reinforced Elastomeric Isolators”, *ASCE Journal of Structural Engineering*; 141(7): 04014169.

Van Engelen N., Konstantinidis D., Tait M. (2016). “Structural and Nonstructural Performance of a Seismically Isolated Building using Stable Unbonded Fiber-Reinforced Elastomeric Isolators”, *Earthquake Engineering and Structural Dynamics*; 45(3): 421–439.

Warn G. and Whittaker A. (2006). *A Study of the Coupled Horizontal-Vertical Behavior of Elastomeric and Lead-Rubber Seismic Isolation Bearings*. Rept. No. MCEER-06-0011; Multidisciplinary Center for Earthquake Engineering Research, State University of New York at Buffalo.

Warn G. and Whittaker A., and Constantinou M. (2007). “Vertical Stiffness of Elastomeric and Lead–Rubber Seismic Isolation Bearings”. *ASCE Journal of Structural Engineering*; 133(9): 1227–1236.

Table 2-1: Test specimen specifications (all units are in mm)

	Isolator 1	Isolator 2	Isolator 3
Width (a)	112	80	57
Length ($2b$)	60	60	60
Total height of bearing (h)	22.4	22.4	22.4
Aspect ratio (R)	5.0	3.6	2.6
Shape Factor (S)	6.1	5.4	4.6

Table 2-2: Results of vertical testing on all isolators (third cycle) with no lateral offset

Isolator	Vertical Loading Frequency (Hz)	k_v ($\frac{\text{kN}}{\text{mm}}$)	f_v (Hz)	ζ_v (%)
1	0.01	33.0	24.7	1.1
	0.1	35.7	25.7	1.1
	1	37.5	26.3	2.6
2	0.01	20.1	22.8	1.3
	0.1	21.6	23.7	1.5
	1	23.9	24.9	2.3
3	0.01	11.0	20.0	1.4
	0.1	11.9	20.8	1.5
	1	13.3	22.0	2.9

Table 2-3: Comparison of the analytical solution to the experimental results

Isolator	Vertical Loading Frequency (Hz)	E_c		Ratio
		Exp. (MPa)	Theor. (MPa)	
1	0.01	93.7		1.10
	0.1	101.4	102.7	1.01
	1	106.4		0.97
2	0.01	79.8		1.07
	0.1	86.0	85.8	1.00
	1	95.1		0.90
3	0.01	61.2		1.07
	0.1	66.3	65.4	0.99
	1	74.0		0.88

Table 2-4: Influence of lateral testing on the vertical response of isolators

Isolator	Before				After			
	k_v ($\frac{\text{kN}}{\text{mm}}$)	E_c (MPa)	f_v (Hz)	ζ_v (%)	k_v ($\frac{\text{kN}}{\text{mm}}$)	E_c (MPa)	f_v (Hz)	ζ_v (%)
1	33.8	95.9	25.0	1.4	32.2	91.3	24.4	1.5
2	21.5	85.5	23.6	1.5	20.6	81.9	23.1	1.6
3	11.7	65.4	20.6	1.4	11.0	61.1	20.0	1.5

Table 2-5: Results of the lateral cyclic testing

Lateral Displacement (t_r)	Cycles	Isolator 1		Isolator 2		Isolator 3	
		K_L ($\frac{\text{N}}{\text{mm}}$)	ζ_L (%)	K_L ($\frac{\text{N}}{\text{mm}}$)	ζ_L (%)	K_L ($\frac{\text{N}}{\text{mm}}$)	ζ_L (%)
0.25	1	227.1	12.5	147.8	12.6	93.4	13.4
	2	219.4	12.2	143.3	12.6	90.0	13.1
	3	217.3	12.0	142.0	12.3	89.2	12.9
0.50	1	177.8	10.6	115.3	11.0	71.2	11.9
	2	172.8	10.3	112.0	10.7	68.6	11.5
	3	171.3	10.2	110.9	10.7	67.8	11.5
1.00	1	138.9	9.5	86.9	10.3	49.9	11.7
	2	134.7	8.9	84.1	9.5	47.8	10.9
	3	132.7	8.8	83.0	9.5	47.0	10.9
1.50	1	129.3	8.6	77.4	9.6	40.4	10.6
	2	124.0	7.9	74.3	8.8	38.1	10.8
	3	121.7	7.8	72.9	8.7	37.2	9.8
2.00	1	138.4	8.2	83.6	8.9	43.7	10.3
	2	129.2	7.3	77.4	8.1	40.6	9.4
	3	125.3	7.2	75.1	8.0	39.2	9.4
2.50	1	142.0	8.5	85.0	9.2	46.2	10.1
	2	130.7	7.8	77.0	8.8	42.3	9.6
	3	125.8	7.7	73.3	8.8	40.8	9.7

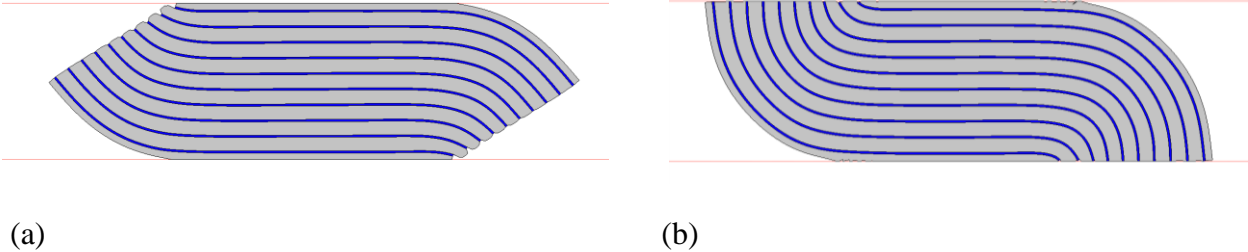


Fig. 2-1: Lateral deformation of an U-FREI showing (a) rollover and (b) full rollover

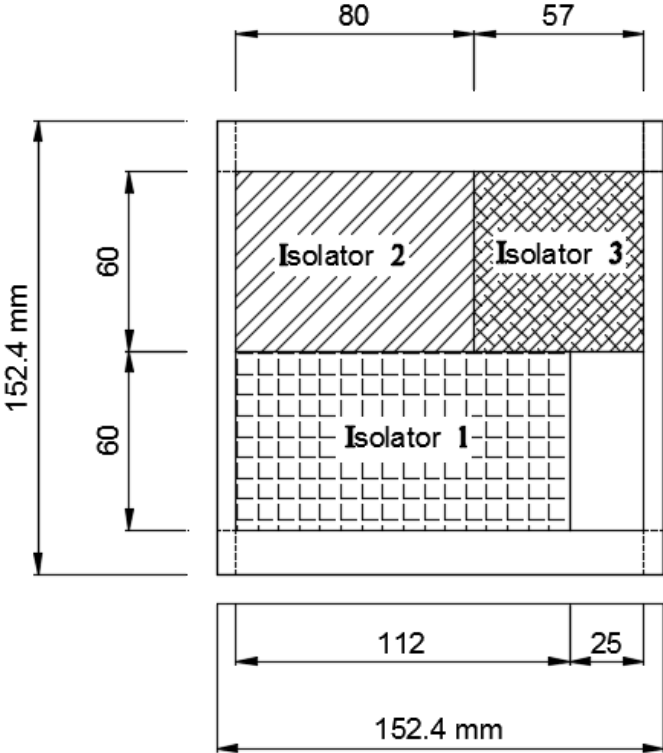


Fig. 2-2: Sketch of the three isolators cut from a single pad

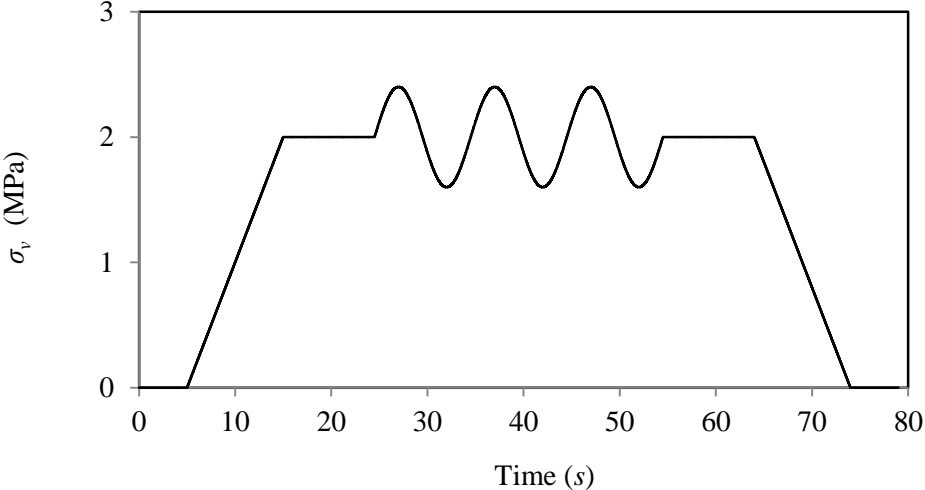


Fig. 2-3: The vertical input signal time history at vertical frequency of 0.1 Hz

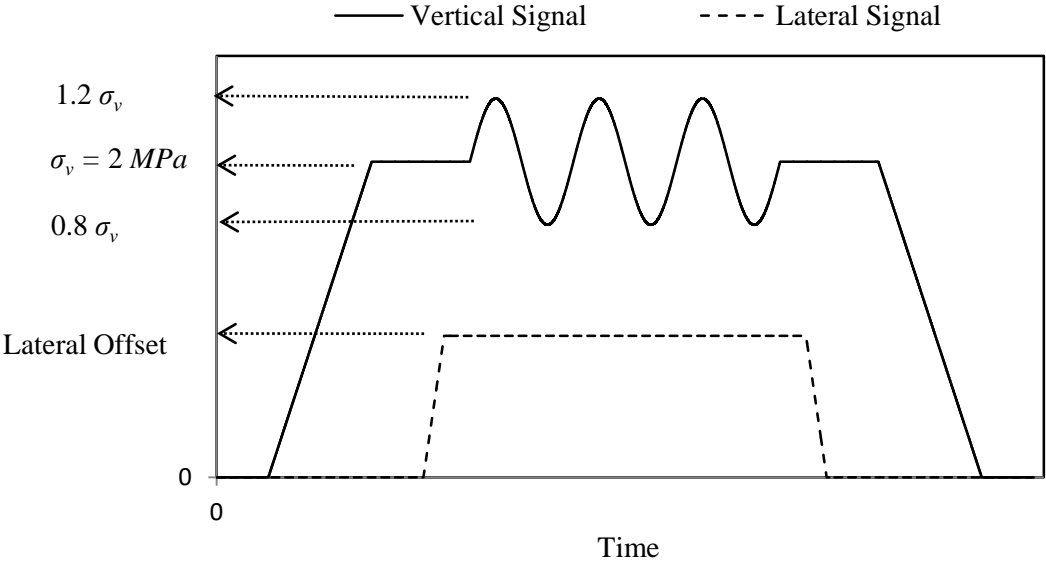


Fig. 2-4: The input signal time history for the vertical tests with a lateral offset (vertical frequency = 0.1 Hz, lateral offset varies)

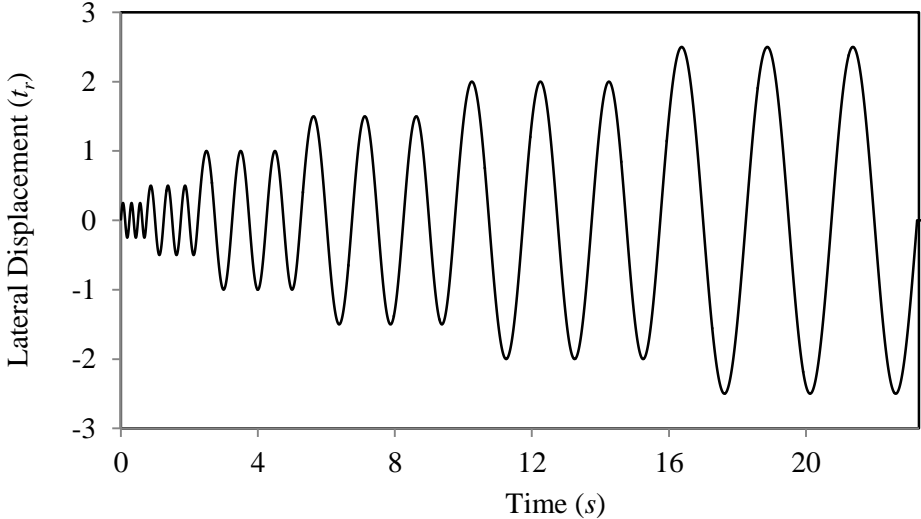
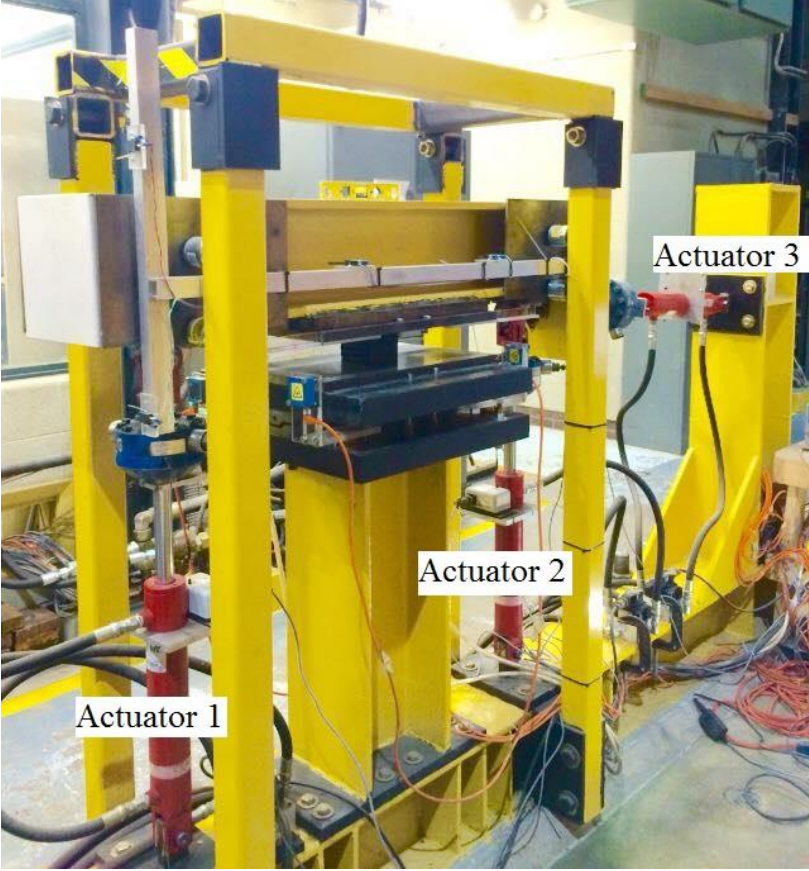
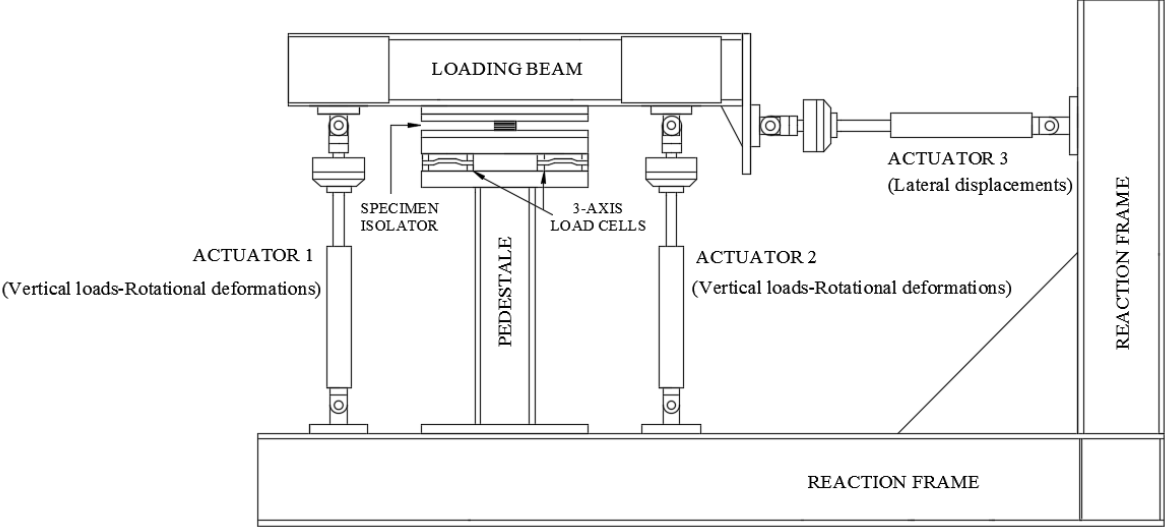


Fig. 2-5: The lateral input signal



(a)



(b)

Fig. 2-6: Multi-load test apparatus: (a) photograph; (b) schematic

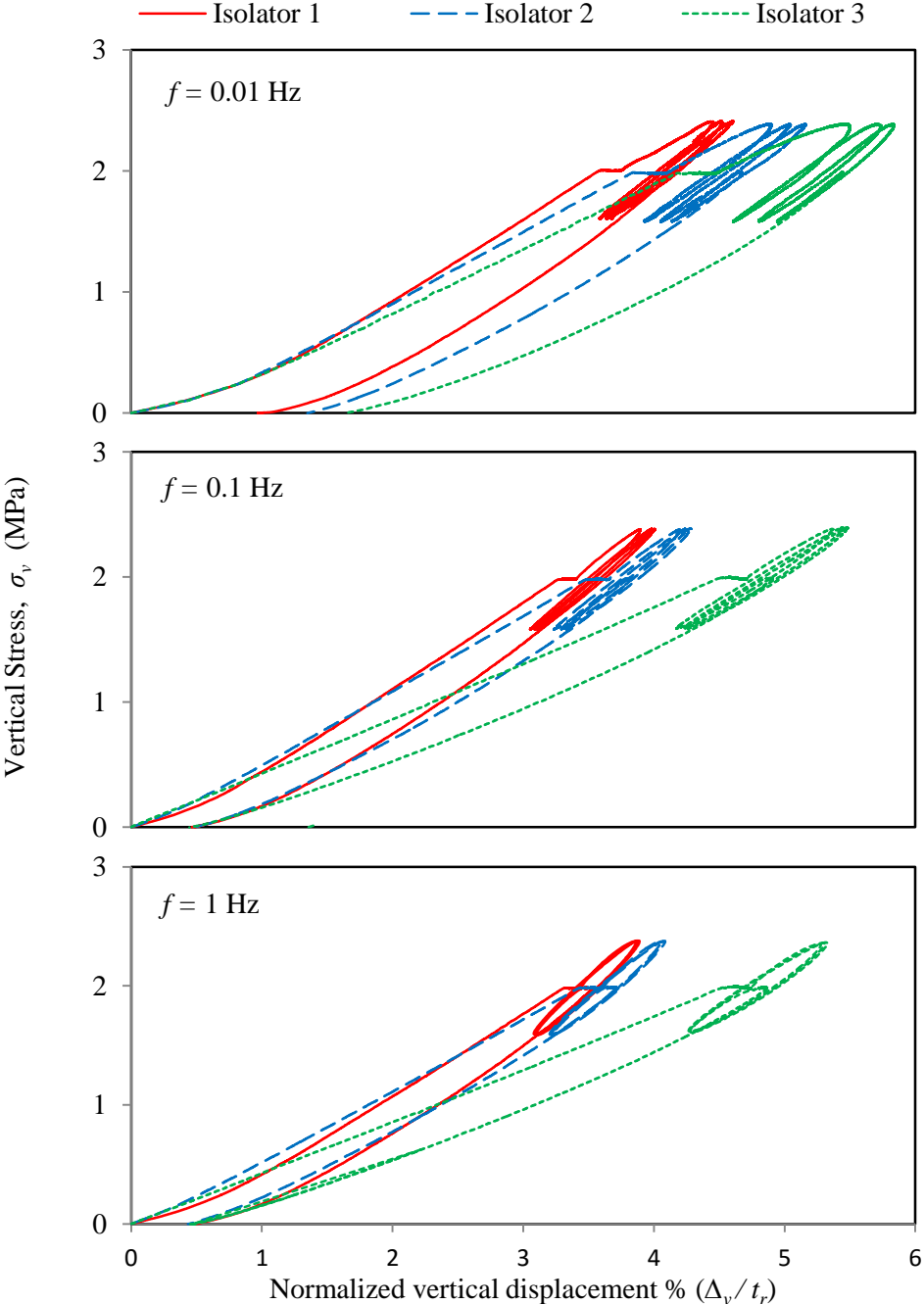


Fig. 2-7: Vertical behaviour of considered isolators

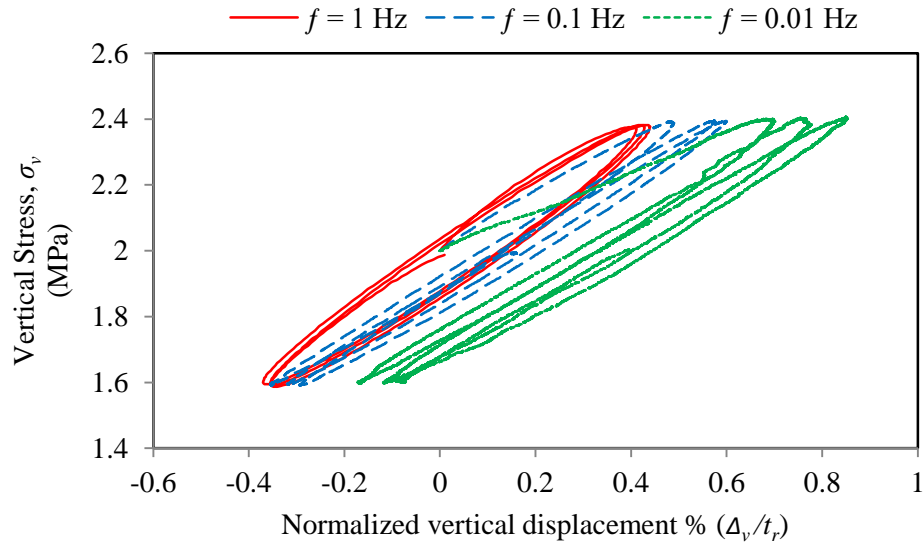


Fig. 2-8: Average vertical stress versus normalized vertical displacement loops for Isolator 1

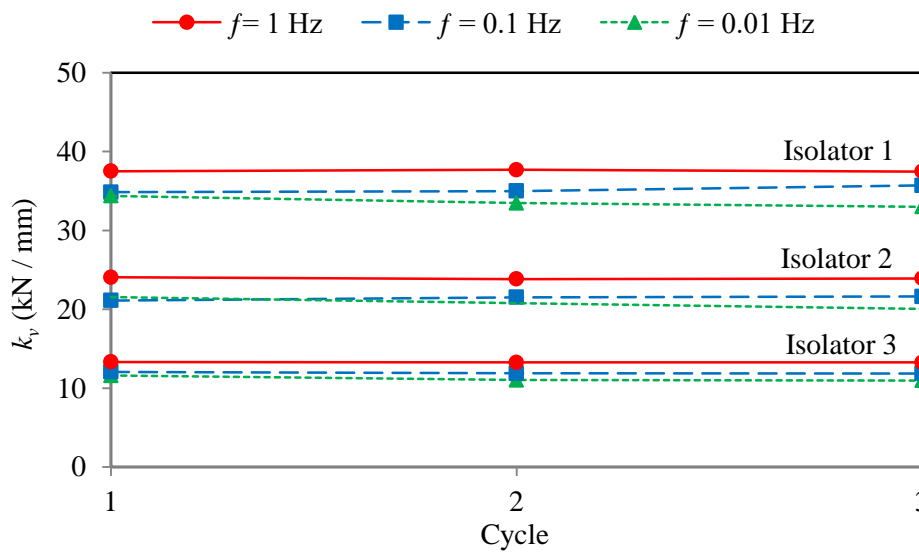


Fig. 2-9: Vertical stiffness as a function of frequency and loading cycle (no lateral offset)

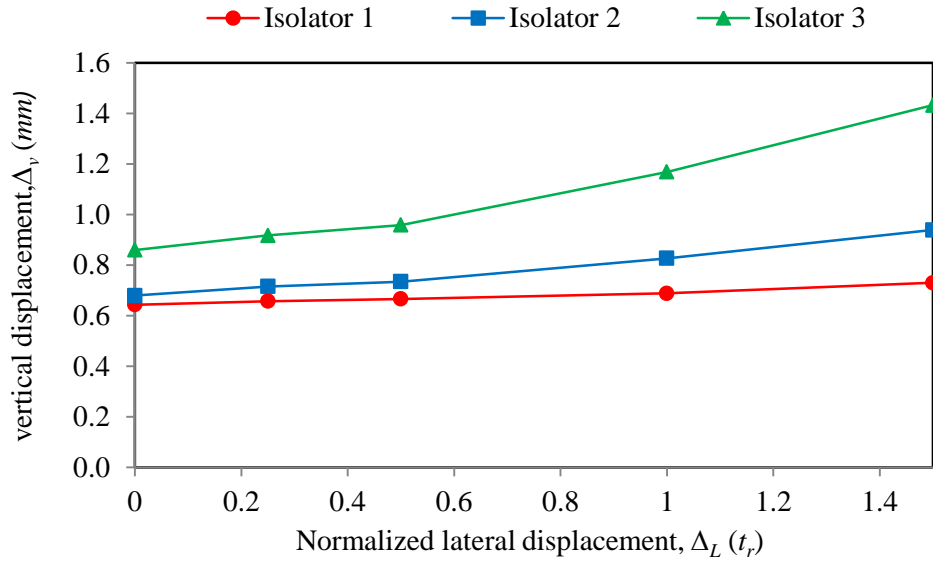


Fig. 2-10: Influence of the lateral offset on the initial vertical displacement of the isolators

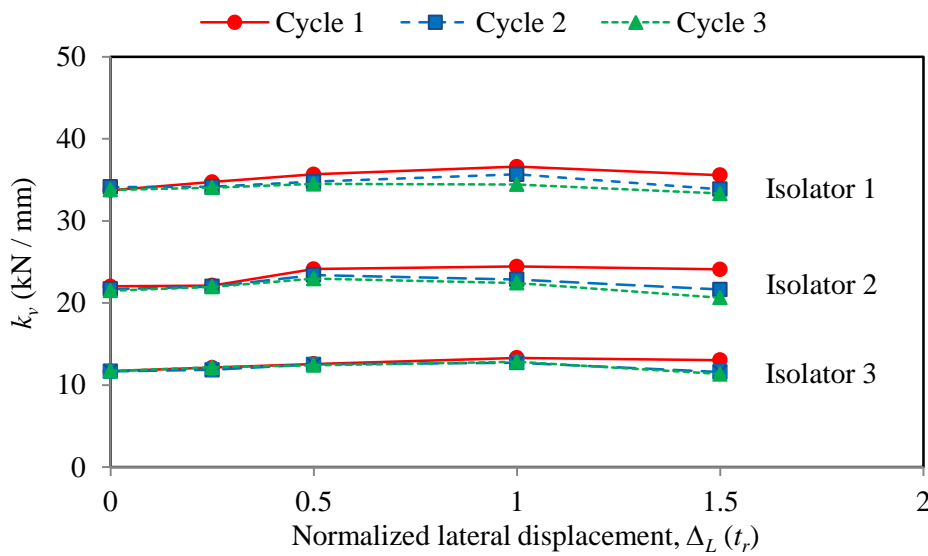


Fig. 2-11: Influence of the lateral offset on the vertical stiffness

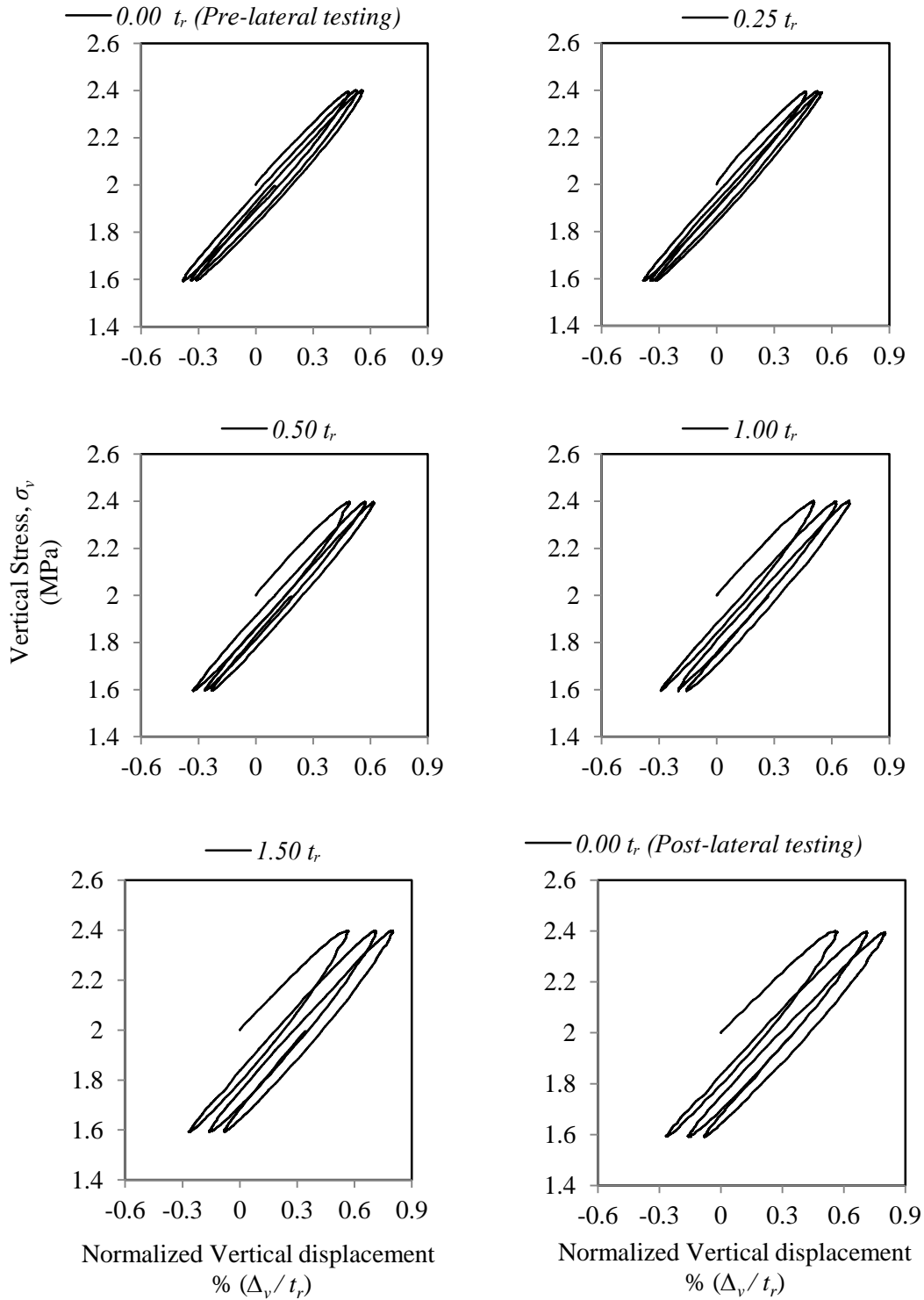


Fig. 2-12: Influence of the normalized lateral offset on the stress-normalized vertical displacement loops of Isolator 1

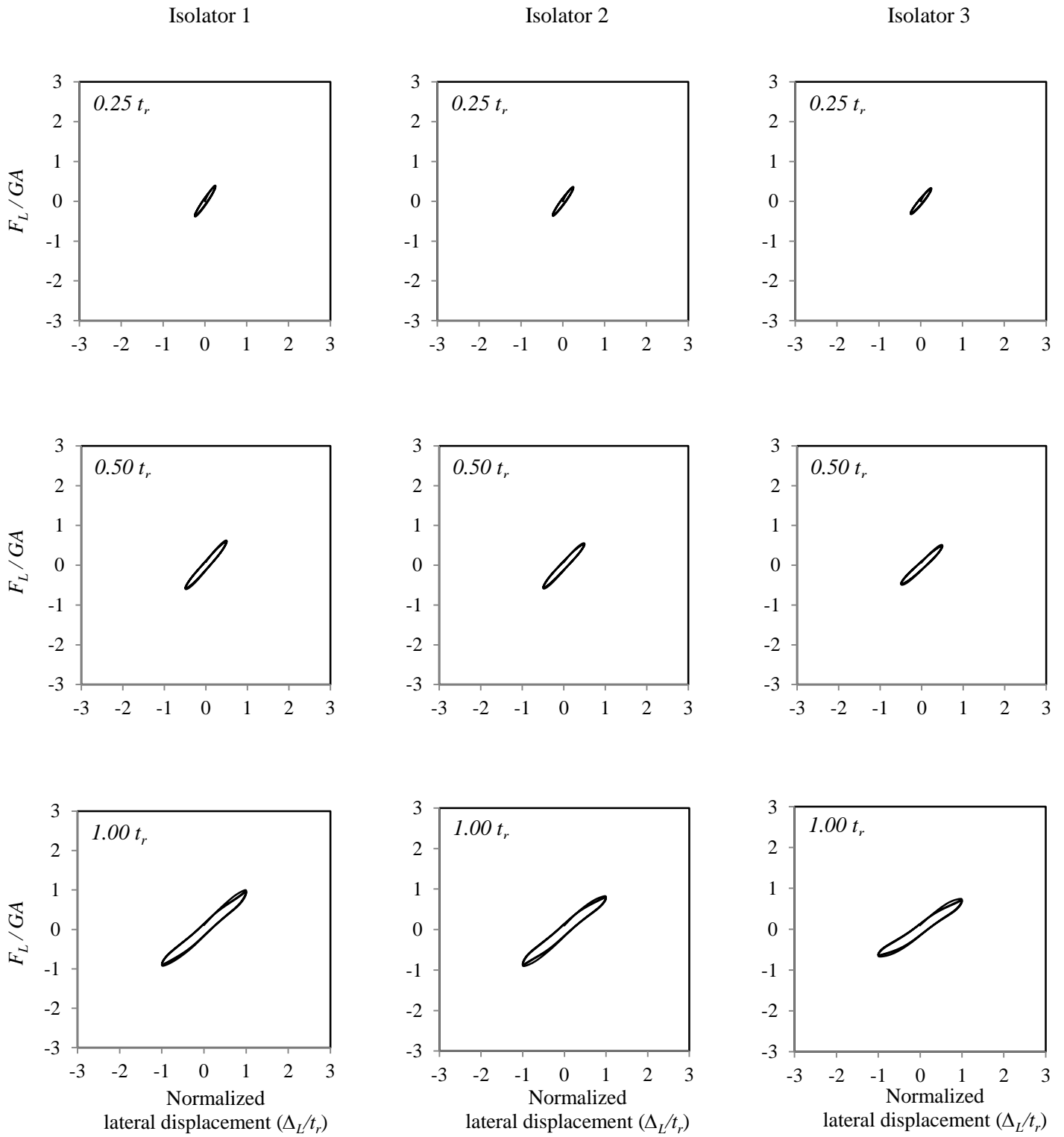


Fig. 2-13. Lateral hysteresis loops for each isolator

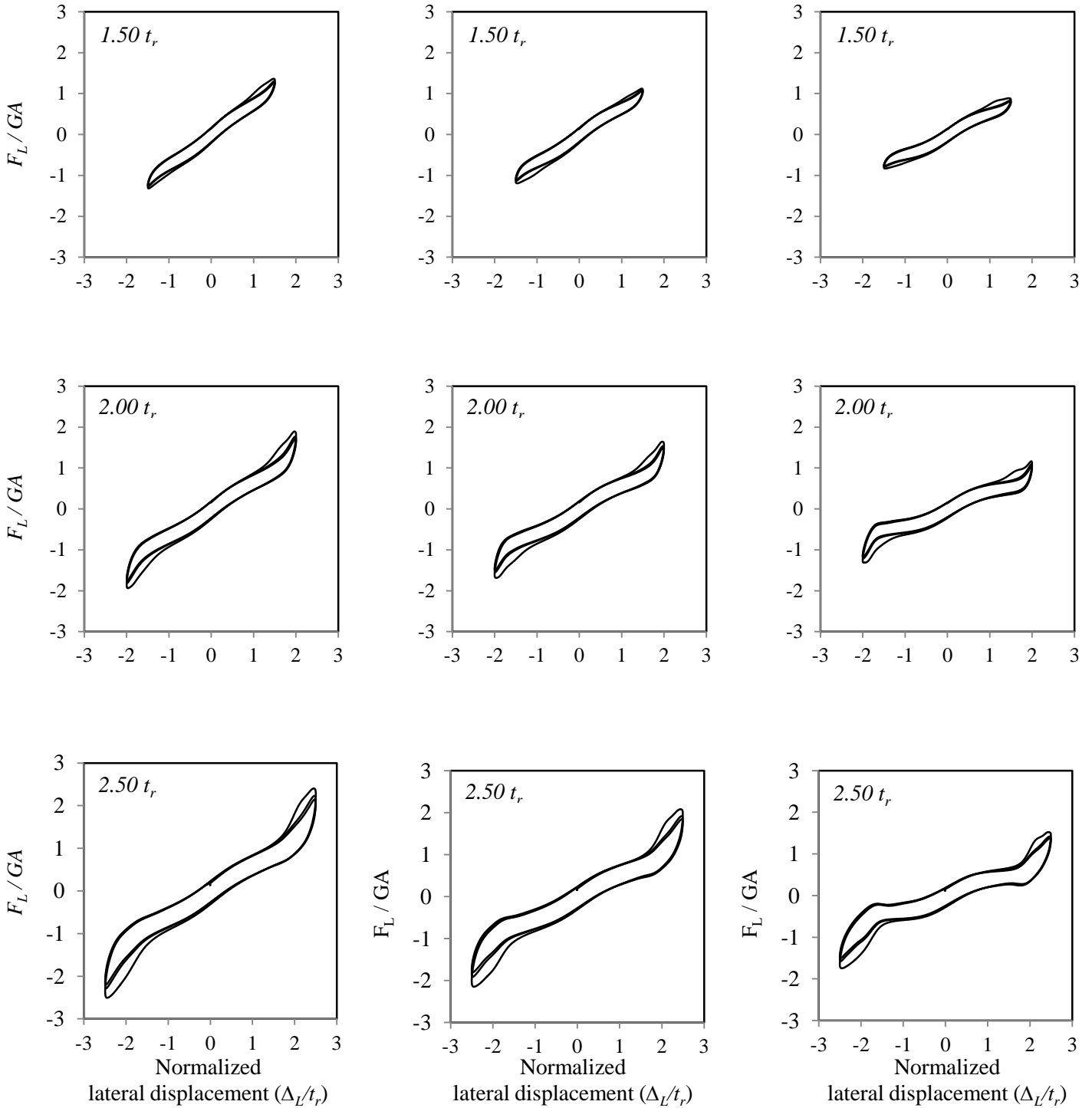


Fig. 2-13. Lateral hysteresis loop for each isolator (continued)

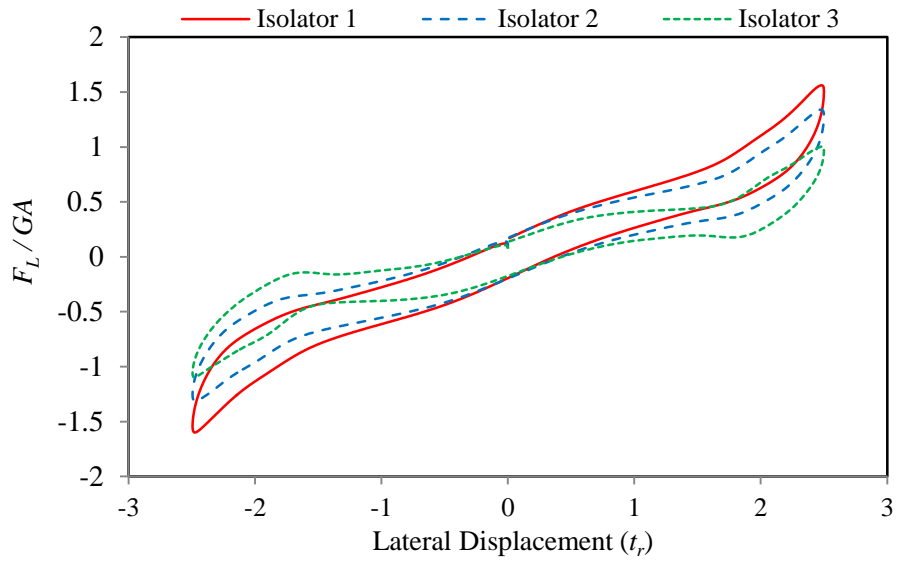


Fig. 2-14. Lateral hysteresis loop at lateral displacement of $2.50 t_r$ (3^{rd} cycle)

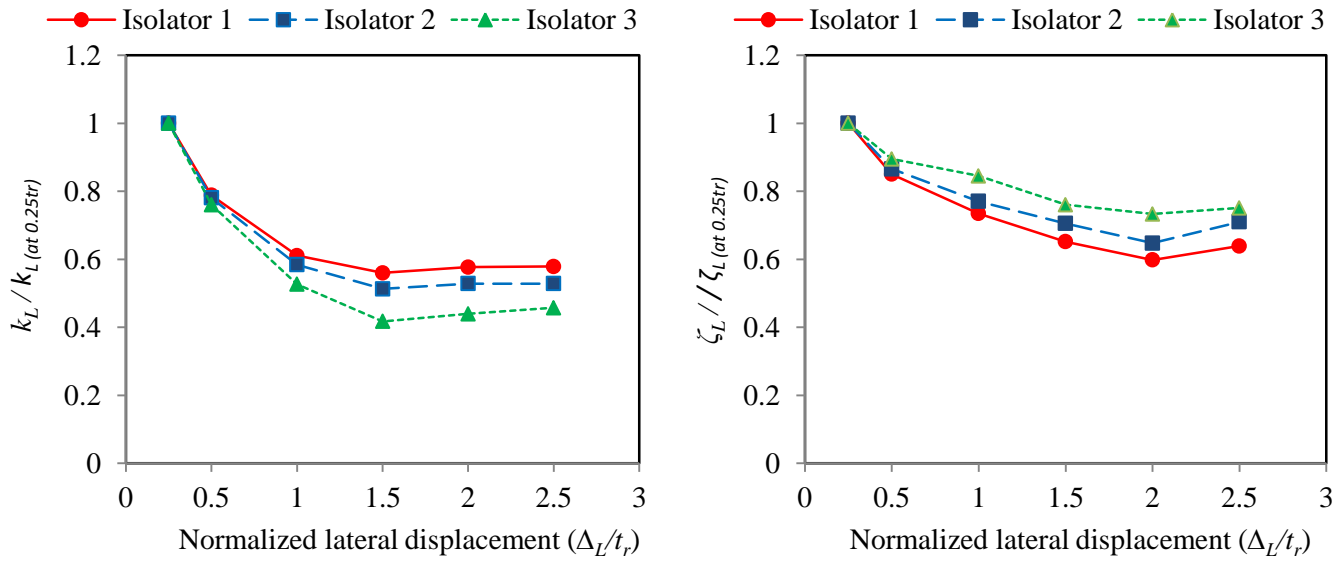


Fig 2-15: Relation between lateral displacement (t_r) and reduction in
 (a) lateral stiffness; (b) lateral damping of the third cycle (i.e. scragged)
 (results are normalized to values at $0.25 t_r$)

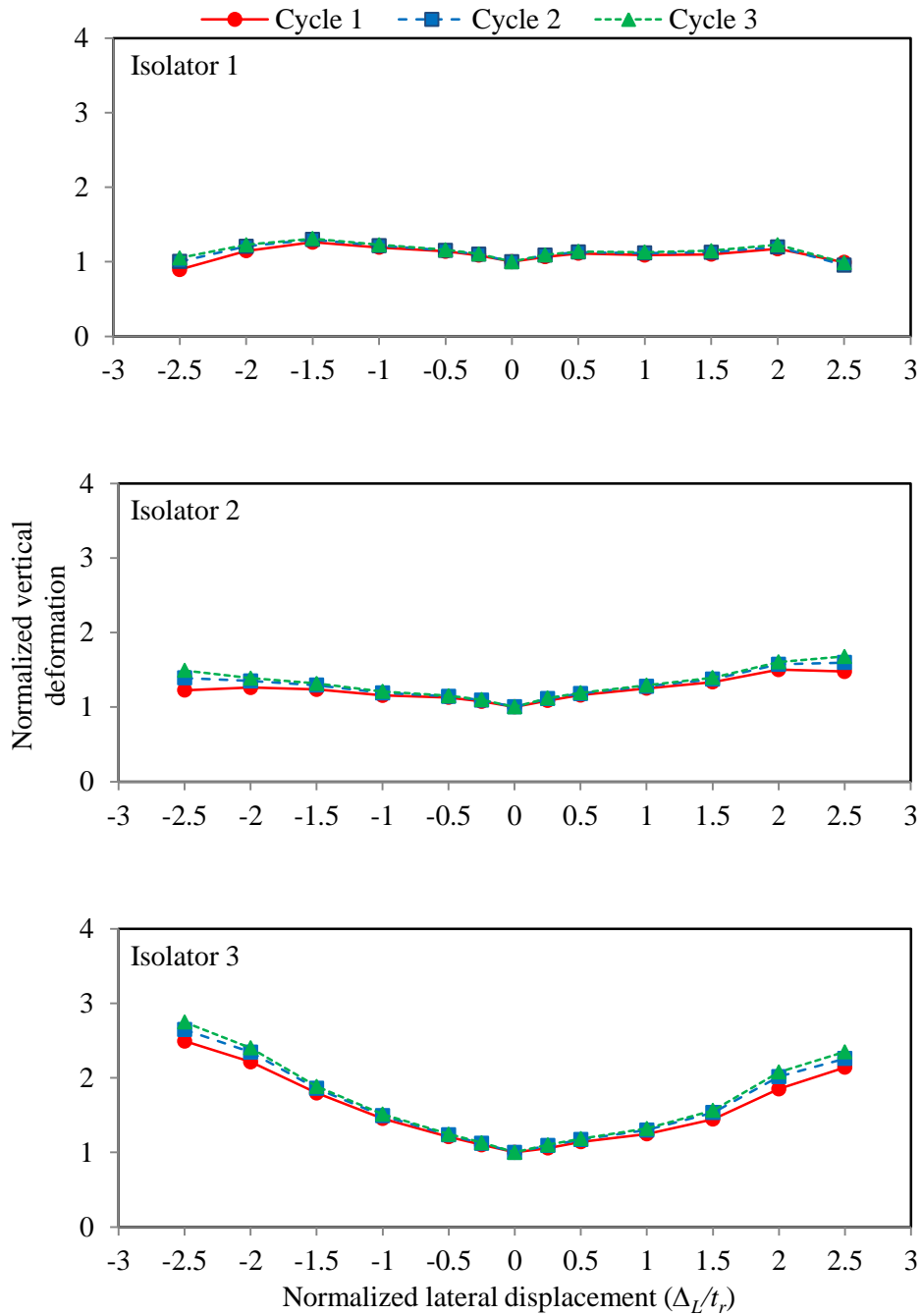


Fig. 2-16: The increase in the normalized vertical deformation during the lateral testing

Chapter THREE

A numerical study on the compressive and rotational behaviour of fiber reinforced elastomeric isolators (FREI)

Abstract

Fiber reinforced elastomeric isolators (FREI) possess unique characteristics relative to traditional steel reinforced elastomeric isolators (SREI). FREI can be classified as either bonded or unbonded according to the connection type employed. An understanding of the behavior of FREI under these loading configurations is needed in order to extend the application of FREI to bridges. The objective of this study is to investigate the response of FREI when vertical and rotational deformations are applied separately as well as in combination. Finite element modeling is carried out on five FREI having the same material properties but possessing different geometrical properties. The mean vertical pressure values employed in this studied are 1, 4.5, 7 and 10 MPa, which represent the specified upper and lower limits presented in CAN/CSA-S6 and AASHTO-LRFD. The behavior of the isolators under different angles of rotation is investigated up to a maximum value of 0.05 radians. Results obtained from the finite element model study and values obtained from available closed-form analytical solutions are found to be in excellent agreement. In addition, results show that U-FREI experience lower normal stresses and shear strains in the elastomer and lower strains in the reinforcement relative to B-FREI.

3.1. Introduction

When a structure is subjected to a significant earthquake event, this can result in substantial direct financial losses (i.e. building replacement/repair cost), indirect financial losses (i.e. business interruption) and casualties (injuries/loss of life) (Constantinou et al. 2010). One of the most effective ways to reduce the seismic demand on a structure is through seismic isolation (Naeim and Kelly 1999). Typically, seismic isolation involves the introduction of low lateral stiffness elements between the superstructure and substructure of a building or between the girders and piers/abutments of a bridge. These flexible elements, which reduce and redistribute the earthquake induced lateral forces, are referred to as isolators or bearings. Bridge isolators must accommodate the vertical, lateral and rotational load/deformation demands that are expected to occur over the lifetime of the bridge (Lee 1994; CAN/CSA-S6-06; AASHTO/LRFD 2012). Bridge isolators should possess adequate vertical stiffness to resist and transmit gravity loads from the superstructure to substructure. However, they must also have sufficient flexibility in the lateral direction in order to accommodate thermal expansion/contraction, pre-stress shortening, shrinkage, creep, traffic, as well as seismic action (Caltrans 1994). Additionally, the isolators must be able to accommodate rotations induced by both dead and live loads. It is important to note that the rotational deformations experienced by isolators in building applications can often be neglected; however rotations need to be considered when isolators are employed in bridges and are considered to be a substantial aspect in bridge isolator design (LaFave et al. 2013; Konstantinidis et al. 2008; Stanton et al. 2007; Muscarella et al. 1995). Moreover, isolators are considered to be a critical element in the bridge design as they are the only link between the bridge superstructure (girders) and substructure (piers/abutments) (Ramberger 2002).

The most common types of bridge isolators in use are elastomeric isolators and high load multi-rotational bearings (pot, spherical, and disk) (Ramberger 2002). According to the Caltrans Bridge Memo to Designers (Caltrans 1994), the selection of a bearing type depends on several factors, including the loading, geometry, maintenance, available clearance, deflection, displacement and rotation demands, availability, policy, designer preference, and cost. It also states that reinforced elastomeric bearings: “should be considered the preferred type of bearing for all structures”.

Elastomeric isolators are typically divided into three main categories: low-damping natural and synthetic rubber (LDR) isolators, lead-plug rubber (LPR) isolators and high-damping natural rubber (HDR) isolators (Naeim and Kelly 1999). Traditionally, steel plates/shims are used to limit the bulging in the elastomer layers of the isolator. This type of isolator, which possesses high vertical stiffness, is called a steel reinforced elastomeric isolator (SREI). When fiber material is used as the reinforcement, as an alternative to steel, the isolator is called a fiber reinforced elastomeric isolator (FREI). SREI can be relatively heavy and costly to manufacture (Konstantinidis and Kelly 2012) compared to FREI. The increase in weight is primarily due to the thick steel rigid end plates and reinforcement, which result in isolators weighing up to one ton or more. The high cost is a result of the labor intensive manufacturing process, as the steel plates for each isolator must be cut, sand-blasted and acid-cleaned and the compounded mold of rubber and steel must be heated under high pressure for several hours (Kelly and Konstantinidis 2007). Alternatively, a significant reduction in both weight and manufacturing cost are possible with FREI. Replacing the steel reinforcement with lighter fiber material, along with the removal of the rigid end plates when employed in an unbonded application, can result in a significant

reduction in weight. The elimination of the steel end plates also allows individual isolators to be cut from large sheets, resulting in reduced manufacturing costs (Toopchi-Nezhad et al. 2008a).

FREI can be employed as either bonded or unbonded in terms of the connection between its upper and lower surfaces to the substructure and superstructure. Bonded-FREI (B-FREI) have rigid steel end plates located at the top (upper surface) and bottom (lower surface) of the isolator, which are used to fasten it to the superstructure and the substructure. Unbonded-FREI (U-FREI) are constructed without rigid steel end plates and are simply placed (unfastened) between the superstructure and the foundation. An unbonded FREI experiences rollover under large lateral deformations as shown in Fig. 3-1(a), and lift-off when subjected to large rotational deformations as shown in Fig. 3-1(b).

One of the earliest analytical studies on FREI, carried out by Kelly (1999) investigated the mechanical characteristics, such as vertical and horizontal stiffness of multilayer elastomeric isolators reinforced by flexible fiber layers. It was concluded that producing a fiber reinforced isolator that can match the behavior of a steel-reinforced isolator is viable. In addition, theoretical analysis carried out by Kelly (2002) indicated that it is feasible to produce a fiber-reinforced strip isolator that matches the behavior of a steel-reinforced isolator and test results confirmed that the concept is feasible.

A number of numerical studies involving finite element analysis have been performed in order to investigate the response of FREI. Toopchi-Nezhad et al. (2011) carried out a finite element analysis study on B-FREI and U-FREI in order to evaluate and compare their lateral load–displacement response with given geometric and material properties. It was found that U-FREI, relative to B-FREI, possess higher seismic isolation efficiency, and lower stress demand on the elastomer and fiber reinforcement. Toopchi-Nezhad et al. (2012) also studied the

influence of the thickness of individual elastomer layers (shape factor, S) on the lateral response of U-FREI. The shape factor (also referred to as the first shape factor) is a dimensionless measure of the elastomer layer slenderness and is defined as the ratio between the loaded area and the area free to bulge. A comprehensive 2D-finite element study on strip isolators with different first and second shape factors was performed. The second shape factor is defined as the ratio of isolator width to the total thickness of the elastomer layers (Kelly and Lai J. 2011). The overall influence of the first shape factor on the lateral isolator stiffness was found to be negligible for the isolators considered in the study. Also, the magnitude and direction of the compressive stresses in both the vertical and lateral direction of the elastomer layers under pure compression were not affected by the shape factor value.

Mordini and Strauss (2008) performed a parametric static and dynamic finite element analysis study on the vertical and lateral behavior of FREI. The study considered both B-FREI and U-FREI. Different vertical loads, size of specimens, number of fiber layers and material constitutive models were also investigated in the study. The objective of this study was to obtain a better understanding of the mechanical behavior of FREI in order to confirm their ability to replace traditional steel reinforced elastomeric isolators.

Osgoei et al. (2014a) investigated the vertical response characteristics of FREI through three-dimensional finite element analysis. Circular isolators having the same dimensions, but different shape factor and in-plane tensile modulus reinforcement values were considered in the study. The results were compared with analytical solutions obtained using the ‘pressure solution’ method presented by Kelly and Calabrese (2012), and the ‘pressure approach’ method presented by Tsai (2006). Good agreement was found between the finite element model results and the analytical solutions for the deformed shapes of the elastomeric layers, and the overall vertical

stiffness. Osgoeei et al. (2014b) also performed three-dimensional finite element analysis to evaluate the lateral response of square U-FREI. Three isolators having different aspect ratios (R), defined as the ratio of isolator width to the total thickness of the isolator, were laterally deformed up to 200% of the total elastomer thickness in different directions. It was found that the effective lateral stiffness of U-FREI decreased significantly with an increase in the lateral deformation. It was also found that the minimum aspect ratio that results in stable rollover is dependent on the direction of applied lateral loading.

Research findings have shown that FREI possess unique advantages over SREI, including low weight, ease of installation, potential for mass production, simplicity of cutting to the desired size, no thick steel end plates, enhanced damping properties, high seismic isolation efficiency and lower stresses in the elastomer and fiber layers (Toopchi-Nezhad et al. 2008b,2009 (a&b); De Raaf et al. 2011; Foster 2011). Furthermore, the use of fabric as the reinforcement in elastomeric isolators is no longer prevented in the most recent version of CAN/CSA-S6 (2006) and is also permitted in AASHTO-LRFD (2012). Although there have been a number of recent research studies carried out on FREI, they have primarily focused on vertical loading and combined vertical and lateral loading. These types of loads/deformations are typically sufficient for building applications, but in order to extend the application of FREI to bridge structures requires an understanding of their behavior under rotational deformation. To date, the behavior of FREI under combined loads/deformations, such as vertical-rotational and vertical-rotational-lateral, have not been investigated.

The objective of this study is to investigate and compare the response of B-FREI and U-FREI when vertical and rotational loads/deformations are applied independently as well as in combination. This objective is achieved using finite element analysis, which permits both the

evaluation of isolator performance over a range of vertical pressures and angles of rotation and assessment of resulting stresses and strains within the elastomer and the reinforcement layers.

3.2. Finite Element Model

Finite element modeling was carried out on five isolators having the same material properties (see Table 3-1) but different geometric properties, as shown in Table 3-2. Two of the isolators investigated in this study (Isolator 1 & Isolator 4) are similar to isolators that were experimentally tested at the University of California, San Diego (Konstantinidis et al. 2008); however, they were reinforced with thin steel shims. All isolators had the same plan dimensions with length ($L = 375$ mm), and width ($W = 575$ mm). It can be observed from Table 3-2 that all five isolators had the same shape factor value. The effect of the shape factor on the rotational response of FREI, which is outside the scope of this study, has been investigated by Al-Anany and Tait (2015). The parameters varied in this study were the mean vertical pressure and the angle of rotation. The mean vertical pressure values considered were 1, 4.5, 7 and 10 MPa, which represent the specified upper and lower limits in CAN/CSA-S6 (2006) and AASHTO-LRFD (2012). The maximum imposed angle of rotation was limited to 0.05 radians, which corresponds to the expected maximum value for steel girder bridges.

The finite element analysis, employed to analyze infinitely long strip FREI isolators under vertical and rotational loads/deformations, was completed using the commercially available general-purpose finite element program MSC Marc (2013). A hyperelastic Neo-Hookean material model was used to represent the elastomer. This model is defined by two parameters representing the shear modulus (G_e) and bulk modulus (K_e) of the elastomer material, which are given in Table 3-1. The carbon fiber reinforcement was modeled as a linear elastic isotropic

material, which is typically defined by two constants, the elastic modulus (E_f) and Poisson's ratio (ν_f), which are listed in Table 3-1. A two-dimensional analysis was carried on the isolators based on the assumption of plane-strain behavior. All isolators were analyzed along the shorter plan dimension (i.e. 375 mm). Four-node quadrilateral plane-strain solid elements were used to model the rubber and the fiber layers. The size of elements used were selected so that each individual intermediate elastomer layer was represented by 12 elements in height and 375 elements along the length, which provides an adequate representation for the elastomer layers according to the mesh sensitivity analysis performed by previous researchers on the vertical and lateral response of the FREI (Osgooei et al. 2014a; Gerhafer et al. 2011).

A rigid wire having a control node with one degree of freedom in the vertical direction was defined at the top of the isolator to represent the upper contact support. Rotations were imposed through an auxiliary node with a single rotational degree of freedom, while a completely restrained rigid wire was defined at the bottom of the isolator to represent the lower contact support. Detachment between the isolator and the contact support surfaces were prevented for the bonded isolators by using the "Glue" contact model to simulate the contact between the contact supports and the B-FREI. For the unbonded isolators, a frictional contact surface represented by the "Touching" contact model was selected to simulate the interface between the contact supports and the U-FREI. This contact model allowed the unbonded isolator to detach from the top and bottom support surfaces; resulting in the development of only compressive and shear forces between the unbonded isolator and the contact support surfaces. The shear force was assumed to be transferred through a Coulomb friction mechanism with an assigned friction coefficient of unity. As the updated Lagrangian approach was used in the finite element analysis, the orientation of the coordinate system was updated during the analysis according to the new

deformed configuration and the stresses that developed during each increment of the analysis represent the true stresses. All isolators were loaded through the upper rigid wire until the target mean vertical pressure was achieved in a load control manner. The rotation was subsequently imposed through the upper rigid wire under displacement control. The loading procedure considered in this study replicates the in-situ boundary conditions that often occur over the life-time of a bridge.

3.3. Vertical Behaviour

Fig. 3-2 shows the relationship between the mean vertical pressure, P , and the vertical displacement, Δ_c , for the five isolators considered in this study. It can be observed that the vertical stiffness increases as the aspect ratio is increased. The vertical stiffness of an elastomeric isolator composed of a number of elastomer layers can be expressed as

$$K_v = \frac{E_c A}{t_r} \quad (1)$$

where A is loaded area of the isolator, t_r is the total thickness of the elastomer, and E_c is the compression modulus of the isolator, which represents the compression modulus of the reinforced elastomer. It can be also observed from Fig. 3-2 that the vertical stiffness was the same for the bonded isolator and unbonded isolator with the same aspect ratio. This indicates that the slippage at the top and bottom contact surfaces was negligible for the unbonded isolators considered in this study. The effect of surface slip on unbonded isolators (Kelly and Konstantinidis 2011) is beyond the scope of this study.

Fig. 3-3 compares the normalized compression moduli (E_c/E) of the isolators as a function of the mean applied vertical pressure obtained from finite element analysis. It can be observed that the value of the compressive modulus (and consequently vertical stiffness) is directly

proportional to the isolator aspect ratio, and that it increases with increased applied axial load. Based on the well-known approximate analytical “pressure solution” approach (Kelly and Konstantinidis 2011), the compression modulus, E_c , for a strip elastomeric isolator composed of incompressible elastomer layers between flexible reinforcements is given by

$$E_c = \frac{12G_e S^2}{(\alpha b)^2} \left(1 - \frac{\tanh \alpha b}{\alpha b}\right) \quad (2)$$

where b is half the isolator width (i.e. $375/2 = 187.5$). For the infinite strip case, the shape factor, S , can be expressed as:

$$S = \frac{W}{2t_e} = \frac{b}{t_e} = \frac{187.5}{12} = 15.63 \quad (3)$$

The parameter α represents the reinforcement flexibility and is defined as

$$\alpha = \sqrt{\frac{12G_e(1 - \nu_f^2)}{E_f t_f t_e}} \quad (4)$$

where t_f is the fiber layer thickness and t_e is elastomer layer thickness. The “pressure solution” approach is based on three main assumptions (Kelly and Konstantinidis 2011). The first two assumptions are kinematic; horizontal planes before a load is applied remain horizontal after a load is applied and vertical planes before a load is applied become parabolic plane after a load is applied. The third assumption is that the normal stresses (σ_{11} , σ_{22} , and σ_{33}), which develop in the elastomer after a load is applied, are approximately equal in magnitude. Accordingly, linear elastic behavior is assumed for the elastomer.

By assuming incompressibility the three orthogonal strain components sum to zero (Tsai and Kelly 2001)

$$\varepsilon_{xx} + \varepsilon_{yy} + \varepsilon_{zz} = 0 \quad (5)$$

where ε_{xx} , ε_{yy} and ε_{zz} are the components of strain in the three directions. The incompressibility assumption is considered to be suitable for elastomer layers having shape factor values in the range of 5–15 (Kelly 2002). The assumption of incompressibility leads to an overestimation of the compressive stiffness for elastomeric layers with high shape factors (Tsai and Lee 1998). Since the isolators considered in this study have a shape factor of approximately 15, which is in the transitional region between the incompressible and compressible assumption, the bulk compressibility effect is included (Kelly 1997) resulting in the following expression

$$\varepsilon_{xx} + \varepsilon_{yy} + \varepsilon_{zz} = -\frac{P}{K_e} \quad (6)$$

It can be observed from Eq. (6) that when K_e tends to infinity, the elastomer layer is considered to be incompressible. By employing the “pressure solution”, the compression modulus, E_c , of an elastomer layer, including the bulk compressibility effect, can be expressed as (Kelly 2002)

$$E_c = \frac{12G_e S^2}{(\beta b)^2 + (\alpha b)^2} \left(1 - \frac{\tanh \sqrt{(\beta b)^2 + (\alpha b)^2}}{\sqrt{(\beta b)^2 + (\alpha b)^2}} \right) \quad (7)$$

where β is defined as

$$\beta = \sqrt{\frac{12 G_e}{K_e t_e^2}} \quad (8)$$

Table 3-3 shows the vertical stiffness of the isolators obtained from finite element analysis, which is the same for bonded and unbonded isolators having the same aspect ratio, along with the values obtained from analytical solutions using Eqs. (2) and (6) for the calculation of the compression modulus values. It can be observed that the analytical values for the vertical stiffness are independent of the mean vertical pressure. This is because the “pressure solution” approach, which is based on small displacement theory, assumes the elastomer material behavior

to be linear-elastic isotropic, whereas a Neo-Hookean hyperelastic material, which exhibits nonlinear behavior (MSC 2000), has been used in the finite element analysis.

3.4. Rotational Behaviour

3.4.1. Moment-Rotation Response

The deformation response of Isolator 4 subjected axial and rotational loads is presented in Fig. 3-4. Under the application of pure axial load only (Fig. 3-4(b)) the isolator experiences uniform vertical deformation. Under this applied loading condition the elastomer layers bulge laterally at the edges. When small angles of rotation are imposed on the bonded and unbonded isolators, as shown in Fig. 3-4(c), the isolators remain in full contact with the supports but the compressive strain increases at one end (increased vertical deformation), and decreases at the other end (decreased vertical deformation) due to the differential vertical deformation. Under the application of intermediate angles of rotation, as shown in Fig. 3-4(d), the elastomer layers on the compressed side of both the bonded and unbonded isolators continue to bulge outward. However, on the uncompressed side of the isolators the deformation patterns of the bonded and unbonded isolators are observed to differ significantly. For the bonded isolator, tensile strains develop as detachment between the isolator and the contact supports is prevented. Conversely, for the unbonded isolator a gap develops between the isolator and the upper and lower support surfaces because the isolator is not bonded to the supports. As the angle of rotational is further increased, the size of the gap will continue to increase, resulting in a continuous change in the boundary condition and nonlinear rotational behavior. Finally, at large angles of rotation, as shown in Fig. 3-4(e), the compressive strain in the fiber reinforcement layers on the side of the bonded isolator under tension increase until they experience instability due to distortion/buckling. For the unbonded isolator, a bending deformation appears in the fiber

reinforcement layers in a transition zone that occurs between the compressed and the uncompressed portions of the isolator, and is observed to be most significant in the reinforcing layers that are nearest to the contact surfaces.

Fig. 3-5 compares the moment-rotation response curves for the five isolators obtained from finite element modeling under different mean compressive pressures. As seen in Fig. 3-5, the rotational behavior of the bonded isolators remains linear until buckling of the reinforcement occurs. The buckling is due to excessive deformation in the reinforcement on tension side of the isolator, which results in a significant decrease in the rotational capacity of bonded isolators. An examination of Fig. 3-5 indicates that the rotational response of the unbonded isolators can be divided into two stages. In the first stage, under small angles of rotation, the moment-rotation behavior is linear (similar to the bonded isolators) and independent of the axial stress as the supports remain in full contact with the isolator (i.e. no lift-off). In the second stage, at high angles of rotation, the unbonded isolators exhibit nonlinear behavior due to the separation (lift-off) because of the unbonded boundary conditions between the isolator and the supports, which results in a decrease in the rotational stiffness. Moreover, the rotational behavior of an unbonded isolator after lift-off occurs is directly related to the isolator aspect ratio and the axial compressive load. It can be observed from Fig. 3-5 that the rotational stiffness increases as the aspect ratio is increased and when the applied compressive load is increased.

The isolator rotational stiffness is used for verifying its ability in accommodating the applied rotation, checking isolator stability (Stanton et al. 2007) and estimating the buckling load (Stanton et al. 2007). Tsai and Kelly (2001) derived the following expression for the rotational stiffness, K_{θ} , of an isolator subjected to a bending moment, M , resulting in an angle of rotation, θ .

$$K_{\theta} = \frac{M}{\theta} = \frac{(EI)_{eff}}{t_r} \quad (9)$$

where the effective bending stiffness, $(EI)_{eff}$, is defined as

$$(EI)_{eff} = \frac{24G_e S^2}{\alpha^4 b} \left(1 + \frac{1}{3}(ab)^2 - \frac{\alpha b}{\tanh(\alpha b)} \right) \quad (10)$$

This rotational stiffness relationship is based on the analytical “pressure solution” approach and is derived for bonded isolators under pure bending. Fig. 3-5 shows the linear elastic behavior of isolators using the analytical solution given by Eq. (9). It can be observed from Fig. 3-5, that the rotational response determined from the analytical solution is in a good agreement with finite element results for the bonded isolators and for the unbonded isolators at small angles of rotation (prior to lift-off occurring). Good agreement is expected in the linear material and geometric response range when the unbonded isolators remain in a full contact with the support surfaces. At higher angles of rotation the response obtained from finite element analysis deviates substantially from that predicted by Eq. (9). It should be noted that the nonlinear response exhibited by the unbonded isolators considered in this study at larger rotation values is primarily due to lift-off (i.e. geometric nonlinearity), which results in a reduction in the rotational stiffness.

Since the analytical solution is derived for an isolator subject to pure bending (i.e. no axial stresses), it is of interest to investigate the rotational behavior of isolators under this particular type of loading. It is important to note that for pure bending vertical displacement control must be employed instead of vertical load control, such that the position of the loading surface is restrained vertically and restricted to rotate around the center of the top contact surface. Fig. 3-6 shows the moment-rotation response curves for both the bonded and unbonded isolators under pure bending (no applied axial load) up to 0.01 radians. It can be observed that there is excellent agreement between the bonded isolator behavior and the analytical solution. For the unbonded isolators the rotational stiffness is linear, however it is observed to be lower than that obtained for the bonded isolator and the analytical solution.

It is important to recognize that the rotational behavior of unbonded isolators under vertical displacement control is expected to differ from the rotational behavior observed under vertical load control. For unbonded isolators subjected to rotations applied under vertical displacement control, the initiation of lift-off (resulting in a decrease in the rotational stiffness) occurs when a rotation of any value is applied. Moreover, the linear moment-rotation behavior occurs because the position of the loading surface during rotation is constrained under displacement control so that the loaded portion of the isolator remains constant, which is not the case under vertical load control. It should be noted that under vertical load control the contact surface is allowed to move vertically up/down during the analysis in order to maintain the desired axial load, which is not the case under vertical displacement control as the vertical position of the loading surface is restrained to remain constant.

Fig. 3-7 shows the distribution of compressive stresses along the top surface of the bonded and the unbonded isolators under a rotation of 0.001 radians. It can be seen from Fig. 3-7 that both compressive and tensile stresses develop in the bonded isolators. Excellent agreement is also observed between the finite element results of the bonded isolators and the analytical solution by Tsai and Kelly (2001), which is based on the “pressure solution” for the distribution of stresses in the incompressible infinite strip elastomer layers under pure bending and is given as

$$\sigma(x) = \frac{12G_e b}{\alpha t_r^3} \left(\frac{\sinh \alpha x}{\sinh \alpha b} - \frac{x}{b} \right) \quad (11)$$

where x is the distance measured from the center of the isolator. For the unbonded isolators only compressive stresses develop over approximately 65% of the length of the isolator. At this level of applied rotation the maximum compressive stress is found to be approximately 15% larger in

all the unbonded isolators regardless of the aspect ratio value. However, no tensile stresses, which are associated with delamination and cavitation, develop.

3.4.2. Code Evaluation for Lift-off in Unbonded Isolators

Previous editions of certain bridge design codes (e.g. AASHTO 1989) specified a limit on the maximum rotation that could be imposed on an isolator. This maximum rotation was selected to be less than the critical rotation, which is defined by the angle that initiates nonlinear behavior in the moment-rotation response of unbonded isolators due to the occurrence of lift-off (AASHTO 1989). This limitation was specified as it was assumed that nonlinear behavior in the moment-rotation response could result in isolator instability, because beyond the critical rotation (i.e. initiation of nonlinearity) the rotational stiffness of the isolator typically decreases, which could lead to excessively large rotations and consequently isolator damage (AASHTO 1989). However, more recently it has been recognized that using unbonded isolators in order to allow lift-off may not result in the negative response described above (Stanton 2007). There are a number of reasons why there has been a shift away from limiting the maximum rotation to be less than the critical rotation. One reason is that isolators are designed to accommodate girder rotation, not to have a certain rotational stiffness, since rotational stiffness of the isolator is typically much less than the flexural stiffness of the girder (Constantinou et al. 2010). As a result, independent of the magnitude of rotational stiffness of the isolator, the level of rotation will be dictated by the girder. Therefore, the rotation imposed on the isolator is essentially applied in a displacement control mode manner, thus the rotational deformation applied on the isolator is equal to the girder end rotation. As such, the rotation experienced by the isolator is expected to be the same as the experienced by the girder. Another reason is that the lift-off of unbonded isolators prevents tensile stresses from developing on the uncompressed side of the

isolator. Finally, the stress and strain state in unbonded isolators after lift-off is less than in equivalent bonded isolators, as will be shown in the following sections.

Recent studies (Stanton et al. 2007) have found that the angle of rotation initiating debonding is higher than the maximum angle considered in this study (0.05 radians), which exceeds the expected largest angle of rotation to be experienced during the life-time of a typical bridge. As such, current design codes for bridges (i.e. AASHTO 2012) have removed restrictions against lift-off, but do place limits on the maximum shear strain that develops in the isolator. Research conducted by Stanton et al. (2007) confirmed that limiting the maximum shear strains was more appropriate than preventing lift-off. Moreover, to ensure isolator stability the ratio between the total width/length of the isolator to the total height of the intermediate elastomer layers of the isolator (also referred to as effective elastomer thickness) shall not be less than 3.0 (MTO-OPSS 1202). This ratio is greater than 3.0 for all the isolators considered in this study except Isolator 5, which was considered in order to investigate the behavior of an isolator having an aspect ratio less than that dictated by certain codes/standards. It should be noted that removing the restriction against lift-off eliminated one of the most serious challenges in the design of isolators (Stanton et al. 2007), which often existed during bridge construction when an isolator is subjected to small compressive loads and large rotations. Slender isolators were often selected in order to ensure lift-off was avoided; however, this had an adverse influence on isolator stability (Stanton et al. 2007).

3.5. Stresses in Elastomer

This section presents and discusses the stresses that develop in the elastomer in both the bonded and unbonded isolators investigated in this study under various angles of rotation. The reported stresses in the elastomer act parallel (σ_{11}) and perpendicular (σ_{22}) to the orientation of the fiber

reinforcement layers. Fig. 3-8 shows the normalized stress contours (σ_{22}/P) for Isolator 3, having an aspect ratio of 3.60, at angles of rotation: $\theta = 0$ (i.e. pure compression), 0.01, 0.03, and 0.05 radians under an average applied compressive stress (P), of 7 MPa. It can be observed from Fig. 3-8 that under vertical and rotational deformation, the magnitude of (σ_{22}) is essentially constant in the vertical direction. As the applied angle of rotation is increased the size of the compressed area decreases, resulting in an increase in the compressive stresses. The difference in the peak compressive stresses between the bonded and unbonded isolators increases as the applied angle of rotation is increased, with lower peak values occurring in the unbonded isolators. Also, at higher angles of rotation significant tensile stresses develop on one side of the bonded isolators whereas negligible tensile stresses are found to occur on the same side of the unbonded isolators. This is because no detachment is allowed for the bonded isolators, while lift-off is permitted for the unbonded isolators.

Fig. 3-9 presents the evolution of the normalized stress distribution (σ_{22}/P) at the center of the middle elastomer layer for Isolator 3 at different angles of rotation under an average applied vertical compressive stresses of 7 MPa. Under pure compression (i.e. $\theta = 0$), excellent agreement is observed between the finite element results and the analytical solution developed by Tsai and Kelly (2001), which is expressed as

$$\frac{\sigma(x)}{P} = \frac{ab (\cosh ab - \cosh ax)}{ab \cosh ab - \sinh ab} \quad (12)$$

From Fig. 3-9, it can be observed that for both the bonded and unbonded isolators the compressive stresses are shifted towards the compressed side of the isolator. This occurs in the bonded isolators as a result of the additional compressive stresses introduced from the induced moment. However, for the unbonded isolators the compressive stresses increase due to a reduction in the size of the compressed area. The results show that the maximum compressive

stress value is higher in the bonded isolator. For instance, the peak normalized stress (σ_{22}), which is 1.45 in both the bonded and unbonded isolators under pure compression (i.e. no rotation), increases by a factor of 2.30 and 2.78 at $\theta = 0.03$ and 0.05 , respectively, for bonded isolator and by a factor of 2.14 and 2.46 at $\theta = 0.03$ and 0.05 , respectively, for the unbonded isolator.

The normalized stress contours (σ_{11}/P) for Isolators 3 under a mean vertical pressure of 7 MPa at different angles of rotation are shown in Fig. 3-10. Similar to σ_{22} , the distribution of σ_{11} is independent of the vertical coordinate. An examination of Fig. 3-8 and Fig. 3-10 shows that (σ_{22} and σ_{11}) have approximately the same distribution and peak values. This indicates that the compressed side of the isolator is subjected to biaxial compression, while the uncompressed side of the isolator is subjected to significant biaxial tension for bonded isolators, and negligible biaxial tension for unbonded isolators. Even at higher angles of rotation, the difference in the values of both lateral (σ_{22}) and vertical (σ_{11}) stresses in a particular isolator is negligible. This observation confirms that the pressure distribution in the isolators follows the hydrostatic rule (i.e. $\sigma_{22} = \sigma_{11} = P_{\text{hydrostatic}}$), which is a key assumption in the pressure solution approach.

Fig. 3-11 shows the evolution of the normalized stress distribution (σ_{11}/P) along the length of the elastomer layer located at the mid-height of isolator 3 for different angles of rotation. As shown, the results from the finite element analysis are in excellent agreement with the analytical solution presented in Eq. (12). According to Fig. 3-11, as the angle of rotation is increased, the length of the compressed region decreases, and consequently the value of the peak compressive stress increases.

Fig. 3-12 and Fig. 3-13 show the variation of normalized peak stresses ($\sigma_{22,\text{max}}/P$ and $\sigma_{11,\text{max}}/P$) in the elastomer material, for rotations up to 0.05 radians, for all the isolators considered in this study. The stresses are normalized with respect to the applied compressive

stresses of 1, 4.5, 7, and 10 MPa. It can be seen in Fig. 3-12 that the maximum values of normalized stress (σ_{22}/P or σ_{11}/P) that develop as a result of applied rotation is always greater in a bonded isolator compared to an equivalent unbonded isolator (see Fig. 3-13). Additionally, the increase in stress due to rotation is more pronounced in unbonded isolators under lower compressive loads as a result of the earlier initiation of loss of compressive contact area, which is nearly negligible under high compressive loads because lift-off is delayed. This is due to the fact that lower compressive stresses causes lower vertical deformation in the isolator, which leads to the aforementioned earlier loss of contact. According to Fig. 3-12 and Fig. 3-13, at $\theta = 0.01$ radians, the peak normalized value of (σ_{22}/P) for bonded Isolator 1 is approximately 112%, 11%, 7%, and 5% higher relative to the unbonded case under average compressive stresses of 1, 4.5, 7, and 10 MPa, respectively.

The magnitude of normalized peak compressive stresses under combined axial and rotational deformation is highly dependent on the isolator aspect ratio. As the isolator aspect ratio is increased the value of the peak stress increases for a given angle of applied rotation. For example, under pure compression of 4.5 MPa, the peak normalized compressive stress in Isolator 1 and Isolator 5 are equal, while at 0.01 radians the peak normalized value of σ_{22}/P for Isolator 1, with a higher aspect ratio, is approximately 52% higher than for Isolator 5 for the bonded isolators. This difference decreases to approximately 29% for the unbonded isolator case. Furthermore, the magnitude of normalized peak stress (σ_{11}/P) is equal to a value of 1.45 for all isolators under pure compression, regardless of the compressive stress value. However, when the angle of rotation is increased to 0.03 radians, the peak normalized value of σ_{11}/P for bonded Isolator 4 increased to 7.20 and 2.50 under an average compressive stress of 1 MPa and 4.5 MPa,

respectively. On the other hand, under the same compressive stress values, the peak normalized value of (σ_{11}) for unbonded Isolator 4 increased to 3.27 and 2.23, respectively.

3.6. Shear Strain

Excessive shear strain can lead to delamination between the elastomer layers and the reinforcement. As a result, shear delamination is considered to be the most important potential mode of failure (Stanton et al. 2007). The contours of shear strain (γ_{12}) in Isolator 3 (bonded and unbonded) are shown in Fig. 3-14. These contours are presented when the selected isolator is subjected to $P = 7$ MPa, and $\theta = 0, 0.01, 0.03, 0.05$ radians. As shown, the peak shear strain due to axial and rotational deformations occurs at the same location, which is at the top and bottom outer edges of the elastomer layer. Under pure compression, the shear strains are the same in both the bonded and unbonded isolators. However, when rotations are applied the values of shear strain increase significantly and differences in values between the bonded and unbonded values can be observed. As shown in Fig. 3-14, this difference increased from 0% at 0 radians to approximately 53% at 0.05 radians.

Fig. 3-15 and Fig. 3-16 show the variation of peak shear strain in all isolators under the different considered levels of applied vertical compressive load, and for all angles of rotation considered in the study. It can be observed that the peak value of shear strain is identical in all isolators under a given vertical load level for the case of pure compression, regardless the isolator aspect ratio and boundary conditions. When the applied vertical load is increased from 1 MPa to 10 MPa, the maximum shear strain value increases by a factor of 6. Moreover, the rotational deformation induces additional shear strain between the elastomer layers and reinforcement. As seen in Fig. 3-15 and Fig. 3-16, the maximum value of shear strain increases

significantly when the angle of rotation is increased. This increase is more significant in the bonded isolators having higher aspect ratio values. For example, under 10 MPa and zero applied rotation (pure compression) the peak value of shear strain in all isolators is approximately equal to 0.99. However, when an angle of rotation of 0.05 radians is applied, Isolator 4 experiences an increase in shear strain of approximately 225%, whereas, Isolator 5 experiences an increase of 189%. For the unbonded isolators, and under same applied rotation, the peak shear strain value increases by 132% and 114% in Isolator 4 and Isolator 5, respectively.

3.7. Tensile Strain in Fiber Reinforcement

Elastomeric isolators employ reinforcement in order to increase their compressive stiffness by confining the elastomer layers. The strain that develops in the fiber (ϵ_{fiber}) can be either tension or compression, depending on the stresses that develop in the elastomer, as shown in Fig. 3-17. When the isolator is compressed vertically (which is the typical loading condition experienced) tensile strains are introduced in the fiber reinforcement, which limit bulging of the elastomer layers (see Fig. 3-17a). Conversely, compressive strains will develop in the fiber reinforcement when the elastomer is under tensile loading (see Fig. 3-17b).

Fig. 3-18 shows the strain contours (tensile/compressive) developed in the fiber layers of Isolator 3 due the applied vertical load and rotational deformations. As can be seen from these figures, at lower angles of rotation, the magnitudes and distributions of fiber strain are similar for the bonded and unbonded isolators. However, at larger rotational deformations, for example 0.05 radians as shown in Fig. 3-18, the peak fiber strain in the bonded isolator is found to increase significantly relative to the unbonded isolator. The increase in the compressive fiber strain in the bonded isolator is due to the high tensile stresses in the elastomer layers in the uncompressed side of the isolator that occurs as a result of the moment that develops from the applied rotation.

High compressive strain in the fiber reinforcement leads to excessive reinforcement deformation/buckling. It is important to note that if the fiber buckles it is not expected to yield. As such, no permanent damage to the reinforcement is expected and it is anticipated that it would return to its original shape upon unloading. The compressive strains that develop in the fiber reinforcement in an unbonded isolator occur primarily after the initiation of lift-off as a result of the reinforcement being deformed at a location between the compressed and uncompressed portions of the isolator.

Fig. 3-19 and Fig. 3-20 show the variation in the peak fiber strain (ϵ_{fiber}) in the fiber reinforcement of each isolator for different applied vertical pressures with respect to rotational deformation. It can be observed in Fig. 3-19 and Fig. 3-20 that the peak fiber strain that develops for the case of pure compression is not dependent on the aspect ratio. This is because when no rotational deformation is induced the aspect ratio has a negligible effect on (σ_{11}), and since all the isolators considered in this study have the same elastomer thickness the reinforcement experiences the same level of tension. It can also be observed that the rate of increase in peak fiber strain due to rotation is significantly influenced by the aspect ratio of the isolator and the boundary conditions. For example, for $P = 4.5$ MPa with no applied rotation the peak tensile strain value is approximately 0.23% in bonded Isolator 4 and increases by approximately 635% when a rotation of 0.05 radians is applied, however the increase was only 204% for bonded Isolator 5. Conversely, when a 0.05 radian rotation is applied to unbonded Isolator 4 and Isolator 5 the increase in peak strain is approximately 65% and 52%, respectively.

3.8. Comparison of Stresses and Strains in Bonded and Unbonded Isolators

It has been shown that the stresses and strains that develop in the unbonded fiber reinforced elastomeric isolators studied are smaller relative to the equivalent bonded isolators. This is due to

the fact that unbonded isolators can separate from the contact surfaces under excessive displacements of these surfaces. Table 3-4 presents the ratio of maximum response in a bonded isolator relative to the response of the equivalent unbonded isolator under the same loading conditions. The ratio is defined as:

$$\text{Ratio} = \frac{\text{Response of Bonded Isolator}}{\text{Response of Unbonded Isolator}} \quad (13)$$

This comparison was carried out at the maximum angle of rotation reached by the bonded isolator. It can be observed that the stresses and strains in a bonded isolator are much higher than the equivalent unbonded isolator. The most significant difference (i.e. largest ratio) is in the tensile stresses that developed in the elastomer layers on the uncompressed side of the bonded isolator. As shown in Table 3-4, the relation between the factor of increase in the response of bonded isolators and the isolator aspect ratio is directly proportional. Conversely, the relation is inversely proportional with the magnitude of axial compressive stresses applied on the isolator, because lift-off is delayed for these isolators as previously mentioned. Additionally, with the application of rotational deformations the compressive strains that develop in the reinforcement of the bonded isolators due to tensile stresses in the elastomer layers is significantly higher than the compressive strains that develop in the equivalent unbonded isolators due to bending of the reinforcement due to lift-off. Moreover, as observed in Table 3-4, the shear strain in bonded isolators is always higher than the equivalent unbonded isolators, which confirms that permitting the contact supports to lift-off from the isolator surface is beneficial as it limits/delays the angle of rotation that is expected to result in delamination between the elastomer layers and the reinforcement.

3.9. Discussion and Conclusions

Finite element modeling was employed to analyze infinitely long strip fiber reinforced elastomeric isolators (FREI) under vertical and rotational loading. FREI were modeled to simulate both bonded and unbonded boundary conditions between the top and bottom surfaces of the isolators and the corresponding support surfaces. The primary goal of the finite element analysis was to (1) investigate the vertical and rotational behavior of FREI; (2) evaluate the performance of isolators with different aspect ratios under different axial loads and angles of rotation; and (3) assess the resulting stress and strain states. The isolators considered in this study had a shape factor of 15.63, while their aspect ratios were 7.21, 4.81, 3.60, 2.88, and 2.40. All isolators were vertically loaded up to a mean compressive pressure of 1, 4.5, 7 and 10 MPa, which covers the limits given by CAN/CSA-S6 (2006) and AASHTO-LRFD (2012). Additionally, all isolators were rotationally deformed by angles of rotation up to the 0.05 radians, which is the maximum expected rotation for steel girder bridges.

Excellent agreement was found between the finite element results and the analytical “pressure solution” approach (Tsai and Kelly 2001) for the following:

- Vertical behaviour of isolators (pure compression).
- Distribution of stresses developed in elastomer layers under pure compression.
- Rotational behaviour of both bonded isolators and unbonded isolators (but before the occurrence of lift-off).
- Distribution of stresses developed in elastomer layers of bonded isolators under pure rotation (i.e. no axial stresses).

According to the results from this FE study, the following conclusions can be drawn regarding the response of the unbonded isolators relative to the bonded isolators considered:

- i. No difference in the vertical behaviour.
- ii. Able to accommodate larger angles of rotation.
- iii. Reduced compressive stress demand on the elastomer.
- iv. Negligible tensile stress demand on the elastomer.
- v. Significant reduction in the shear strain on the bond between the elastomer and fiber reinforcement layers.
- vi. Considerably lower tensile/compressive strain demand on the fiber reinforcement layers.

In general, it was noted that isolators with lower aspect ratios had lower normal stresses in the elastomer, strains in the reinforcement, and shear strain between the elastomer and the fiber reinforcement under combined vertical and rotational loading. However, a lower aspect ratio also resulted in lower vertical and rotational isolator stiffness values. It was also noted that excessive tensile stresses on the uncompressed side of the isolators led to distortion/buckling of the reinforcement, which is expected to be temporary and recoverable upon unloading.

The findings presented here are part of a larger research program investigating the viability of using FREI as seismic isolators for bridge structures. Ongoing research is being carried out to experimentally investigate the behavior of unbonded fiber reinforced elastomeric isolators, having lower shape factor values, under combined vertical and rotational loading.

Acknowledgements

The authors would like to gratefully acknowledge the support provided by the Ontario Ministry of Research and Innovation (MRI), and the Natural Sciences and Engineering Research

Council of Canada (NSERC). Additionally, the authors are grateful for the support provided by MSC Software Corporation.

References

AASHTO. (1989). *Standard Specifications for Highway Bridges*, Washington, D.C.

AASHTO. (2012). *American Association of State Highway and Transportation Officials. LRFD Bridge Design Specifications*, Washington, D.C.

Al-Anany Y., Tait M. (2015). “A Study on the Rotational Behaviour of Bonded and Unbonded Fiber Reinforced Elastomeric Isolators”, *11th Canadian Conference on Earthquake Engineering*, Victoria, British Columbia, Canada, 21-24 July 2015.

Caltrans (1994). *Bridge Memo to Designers. Section 7: Bridge Bearings*. California Department of Transportation, Sacramento, California.

CAN/CSA-S6-06. (2006). *Canadian Highway Bridge Design Code*. Canadian Standard Association. Ontario.

CAN/CSA-S6-14. (2014). *Canadian Highway Bridge Design Code*. Canadian Standard Association. Ontario.

Constantinou M., Kalpakidis I., Filiatrault A., Ecker Lay R. (2010). *LRFD-based analysis and design procedures for bridge bearings and seismic isolators*. Report No. MCEER-11-0004, Multidisciplinary Center for Earthquake Engineering Research, University at Buffalo, State University of New York, Buffalo, New York.

De Raaf M., Tait M., Toopchi-Nezhad H. (2011). “Stability of fiber reinforced elastomeric bearings in an unbonded application”. *J Comp Mater*; 45(18):1873–84.

Foster B. (2011) *Base isolation using stable unbonded fibre reinforced elastomeric isolators (SU-FREI)*. Master's t.hesis. Hamilton: McMaster University.

Ph.D. Thesis - Yasser Mohammed Al-Anany; McMaster University - Civil Engineering

Gerhaher U., Strauss A., Bergmeister K. (2011). "Numerical modeling of elastomeric bearings in structural engineering", *Advances in Materials Sciences*;11(3): 51-63.

Kelly J. (1997). *Earthquake-resistant design with rubber*. 2nd ed. London: Springer-Verlag.

Kelly J. (1992). "Analysis of fiber-reinforced elastomeric isolators". *Journal of Seismology and Earthquake Engineering*; 2(1): 19–34.

Kelly J. (2002). "Seismic isolation systems for developing countries". *Earthquake Spectra*;18(3): 385–406.

Kelly J., Konstantinidis D. (2007). "Low-cost seismic isolators for housing in highly seismic developing countries", *ASSISi 10th World conference on seismic isolation, energy dissipation and active vibrations control of structures*, Istanbul; 28–31; May 2007.

Kelly J., Konstantinidis D. (2011). *Mechanics of rubber bearings for seismic and vibration isolation*. Chichester, UK: Wiley.

Kelly J., Lai J. (2011). "The use of tests on high-shape-factor bearings to estimate the bulk modulus of natural rubber". *The Journal of the Anti-Seismic Systems International Society*; 2(1):21–33.

Kelly J., Calabrese A. (2012). *Mechanics of fiber reinforced bearings*. Pacific Earthquake Engineering Research Center, PEER, Berkeley, California; 2012/101.

Konstantinidis D., Kelly J., Makris N. (2008). *Experimental investigations on the seismic response of bridge bearings*. Report No. EERC-2008/02, Earthquake Engineering Research Center, University of California, Berkeley.

Konstantinidis D., Kelly J. (2012). Two Low-Cost Seismic Isolation Systems. *15th World Conference on Earthquake Engineering*. Lisbon, Portugal, September 24– 28.

LaFave J., Fahnestock L., Foutch L., Steelman D., Revell J., Filipov E. (2013). *Experimental investigations of the seismic response of bridge bearings*. Report No. FHWA-ICT-13-002, Illinois Center for Transportation, University of Illinois at Urbana-Champaign, Urbana.

Lee D. (1994). *Bridge Bearings and Expansion Joints*. E & FN Spon, London, UK.

Mordini A, Strauss A. (2008). “An innovative earthquake isolation system using fibre reinforced rubber bearings”. *Engineering Structures*; 30(10): 2739-51.

Mori A., Moss P., Cooke N., Carr A. (1999). “The Behavior of Bearings Used for Seismic Isolation under Rotation and Axial Load”. *Earthquake Spectra*; 15(2): 225–44.

MTO. OPSS 1202. (2008). Material Specification for Bearings – Elastomeric Plain and Steel Laminated. Ontario Ministry of Transportation, Toronto, Ontario.

Muscarella J., Yura J. (1995). *An Experimental Study of Elastomeric Bridge Bearings with Design Recommendations*. Research Report No. 1304-3, Center for Transportation Research, Bureau of Engineering Research, the University of Texas at Austin, Austin.

MSC Software Corporation (2000). *Nonlinear finite element analysis of elastomers*. Technical paper. Los Angeles, CA: MSC Software Corporation.

MSC. Marc. (2013) Santa Ana, CA: MSC Software Corporation.

Naeim F., Kelly J. (1999). *Design of seismic isolated structures: From theory to practice*. John Wiley & Sons, New York.

Osgooei P., Tait M., Konstantinidis D. (2014a). “Three-dimensional finite element analysis of circular fiber-reinforced elastomeric bearings under compression”. *Compos Struct*; 108: 191–204.

Osgooei P., Tait M., Konstantinidis D. (2014b). “Finite Element Analysis of Unbonded Square Fiber-Reinforced Elastomeric Isolators (FREIs) under Lateral Loading in Different Directions”. *Compos Struct* 2014; 113: 164–173.

Ramberger G. (2002) *Structural Bearings and Expansion Joints for Bridges*. International Association for Bridges and Structural Engineering. IABSE, Zurich, Switzerland.

Stanton J., Roeder C., Mackenzie-Helnwein P., White C., Kuester C., Craig B. (2007). *Rotation Limits for Elastomeric Bearings*. Report No. NCHRP 596, Transportation Research Board, National Cooperative Highway Research Program, Washington, D.C.

Toopchi-Nezhad H, Tait M., Drysdale R. (2008a). “Testing and modeling of square carbon fiber-reinforced elastomeric seismic isolators”. *Struct Control Health Monit*; 15(6): 876–900.

Toopchi-Nezhad H., Tait M., Drysdale R. (2008b). “Lateral response evaluation of fiberreinforced neoprene seismic isolators utilized in an unbonded application”. *J Struct Eng*; 134(10): 1627–37.

Toopchi-Nezhad H., Tait M., Drysdale R. (2009a). “Shake table study on an ordinary low-rise building seismically isolated with SU-FREIs (stable unbonded fiber-reinforced elastomeric isolators)”. *Earthq Eng Struct Dyn*; 38(11): 1335–57.

Toopchi-Nezhad H., Drysdale R., Tait M. (2009b) Parametric study on the response of stable unbonded fiber-reinforced elastomeric isolators (SU-FREIs). *J Compos Mater*; 43(15): 1569–87.

Toopchi-Nezhad H., Tait M., Drysdale R. (2011). “Bonded versus unbonded strip fiber reinforced elastomeric isolators: finite element analysis”. *Compos Struct*; 93(2): 850–9.

Toopchi-Nezhad H., Drysdale R., Tait M. (2012). “Influence of thickness of individual elastomer layers (first shape factor) on the response of unbonded fiber-reinforced elastomeric bearings”. *J Compos Mater*; 47(27): 3433-50.

Tsai H, Lee C. (1998) Compressive stiffness of elastic layers bonded between rigid plates. *Int J Solids Struct*; 35(23): 3053–69.

Tsai H., Kelly J. (2001). *Stiffness analysis of fiber-reinforced elastomeric isolators*. Pacific Earthquake Engineering Research Center, PEER, Berkeley, California; 2001/5.

Tsai H. (2006). “Compression stiffness of circular bearings of laminated elastic material interleaving with flexible reinforcements”. *Int J Solids Struct*; 46(11): 3484–97.

Table 3-1: Material properties of the isolators

Elastomer	Fiber
Shear Modulus (G_e) = 0.80 MPa	Elastic Modulus (E_f) = 30 GPa
Bulk Modulus (K_e) = 2000 MPa	Poisson's ratio (ν_f) = 0.20

Table 3-2: Geometric properties of the isolators

Properties	Isolator 1	Isolator 2	Isolator 3	Isolator 4	Isolator 5
Elastomer Thickness (Top & Bottom Outer Layers)	6 mm				
Elastomer Thickness (Inner Layers)	12 mm				
Number of Intermediate Elastomer Layers	3	5	7	9	11
Total Elastomer Thickness (including cover)	48 mm	72 mm	96 mm	120 mm	144 mm
Effective Elastomer Thickness (excluding cover)	36 mm	60 mm	84 mm	108 mm	132 mm
Fiber Layer Thickness	1 mm				
Number of Fiber Layers	4	6	8	10	12
Total Fiber Thickness	4 mm	6 mm	8 mm	10 mm	12 mm
Bearing Height	52 mm	78 mm	104 mm	130 mm	156 mm
Shape Factor	9.46	9.46	9.46	9.46	9.46
Second Shape Factor	10.41	6.25	4.46	3.47	2.84
Aspect Ratio (R)	7.21	4.81	3.60	2.88	2.40

Table 3-3: Vertical stiffness value obtained from finite element analysis and analytical solutions

Isolator	Mean Vertical Pressure [MPa]	Finite Element K_v [kN/mm]	Analytical	
			Incompressible K_v [kN/mm]	Compressible K_v [kN/mm]
1 (R = 7.21)	1	2266	2583	1927
	4.5	2317		
	7	2363		
	10	2426		
2 (R = 4.81)	1	1428	1722	1285
	4.5	1462		
	7	1493		
	10	1536		
3 (R = 3.60)	1	1042	1292	963
	4.5	1068		
	7	1091		
	10	1123		
4 (R = 2.88)	1	821	1033	771
	4.5	841		
	7	860		
	10	885		
5 (R = 2.40)	1	677	861	642
	4.5	694		
	7	709		
	10	731		

Table 3-4: Ratio of maximum stress and strain in a bonded isolator relative to an unbonded isolator

		P = 1 MPa				P = 4.5 MPa				P = 7 MPa				P = 10 MPa						
	θ_{max} (rad.)	Ratio [%]				Ratio [%]				Ratio [%]				Ratio [%]						
		σ_{22} T C	σ_{11} T C	γ_{12}	ϵ_{fiber} T C	σ_{22} T C	σ_{11} T C	γ_{12} T C	ϵ_{fiber} T C	σ_{22} T C	σ_{11} T C	γ_{12} T C	ϵ_{fiber} T C	σ_{22} T C	σ_{11} T C	γ_{12} T C	ϵ_{fiber} T C			
Isolator 1 (R = 7.21)	0.018	202.14 2.9	245.45 2.97	2.39	15.08 35.14	0.024	91.67 1.53	87.50 1.50	2.13	3.51 15.27	0.026	67.22 1.30	64.44 1.30	1.84	2.37 11.16	0.025	34.00 1.12	32.35 1.12	1.67	1.14 1.48
Isolator 2 (R = 4.81)	0.023	157.35 2.7	151.43 2.72	2.28	2.56 8.80	0.032	75.01 1.39	68.64 1.35	1.59	1.82 7.47	0.039	38.33 1.22	36.67 1.22	1.62	3.32 9.63	0.034	23.50 1.13	22.64 1.13	1.48	1.11 1.29
Isolator 3 (R = 3.60)	0.029	115.86 2.5	112.07 2.52	2.19	11.30 18.22	0.039	44.83 1.27	44.14 1.27	1.46	3.47 8.67	0.050	26.67 1.13	26.01 1.13	1.55	4.49 11.04	0.043	14.72 1.08	13.65 1.08	1.43	1.10 1.33
Isolator 4 (R = 2.88)	0.033	105.56 2.4	101.85 2.40	2.11	8.09 13.50	0.050	23.25 1.25	22.03 1.25	1.68	4.63 10.45	0.050	15.75 1.09	12.50 1.18	1.47	2.04 3.54	0.050	9.67 1.05	8.97 1.06	1.40	1.09 0.97
Isolator 5 (R = 2.40)	0.037	91.23 2.1	89.47 2.21	2.10	5.89 10.58	0.050	11.00 1.19	17.50 2.21	1.45	2.01 5.10	0.050	11.00 1.08	10.25 1.09	1.39	1.15 2.04	0.050	2.80 1.03	2.60 1.02	1.35	1.05 0.81

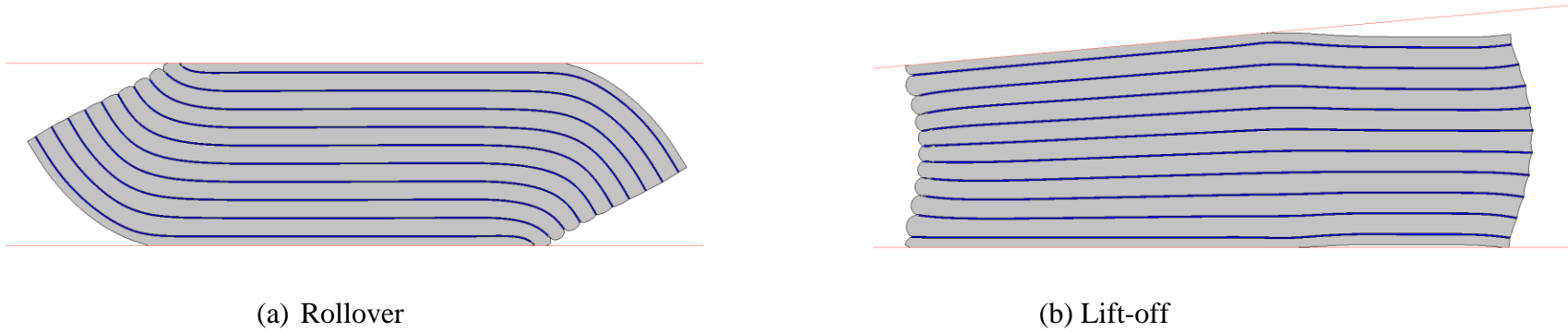


Fig. 3-1: Deformation patterns of U-FREI

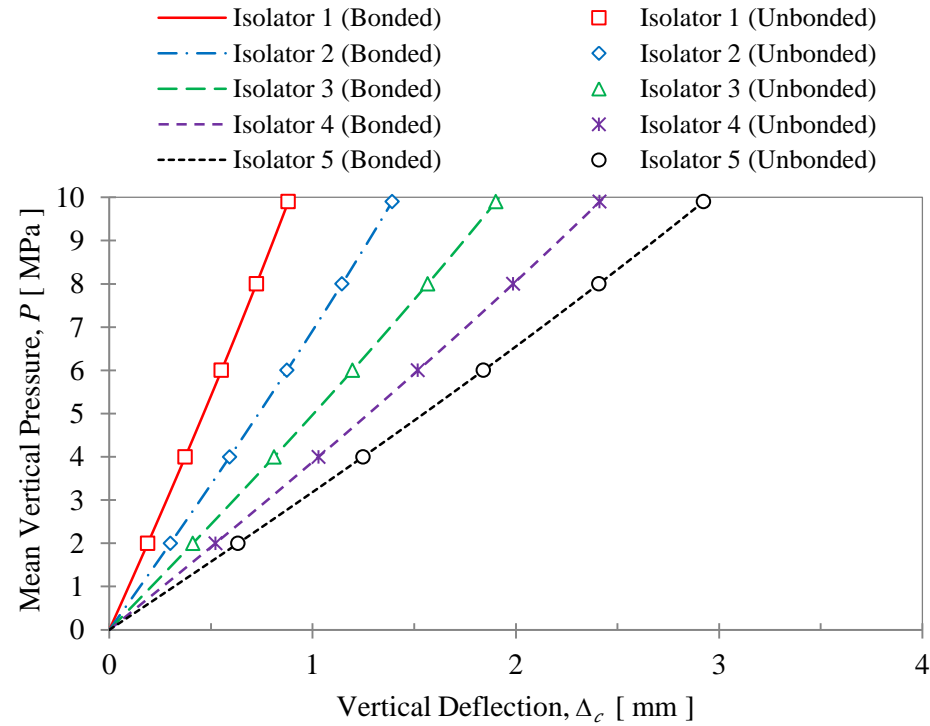


Fig. 3-2: Influence of aspect ratio on vertical response

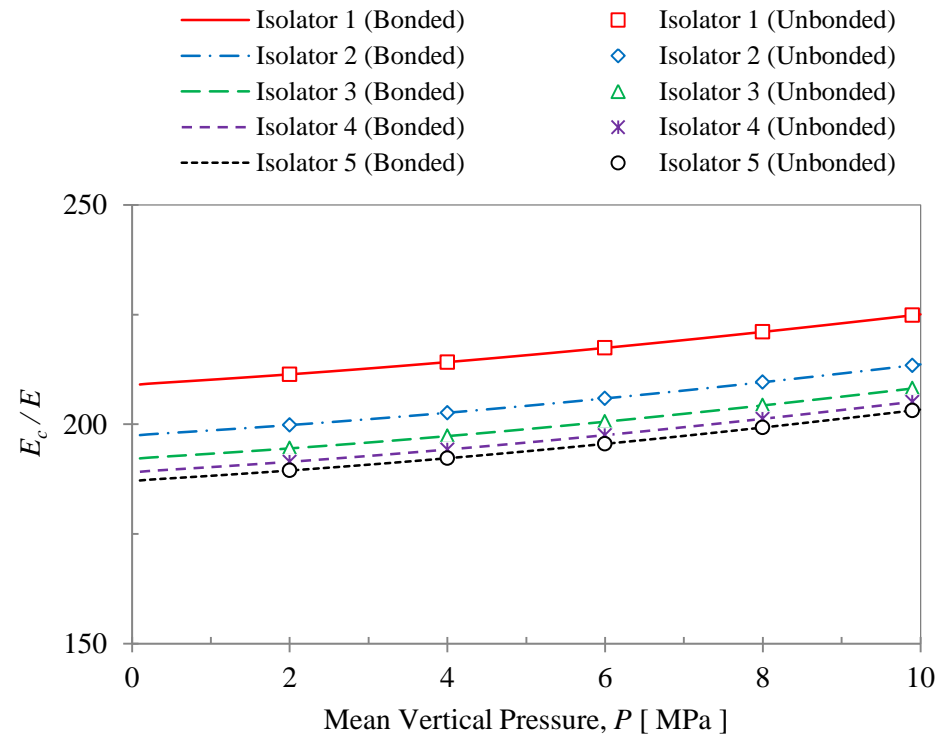


Fig. 3-3: Variation of normalized compression modulus (E_c/E) with mean vertical pressure (P)

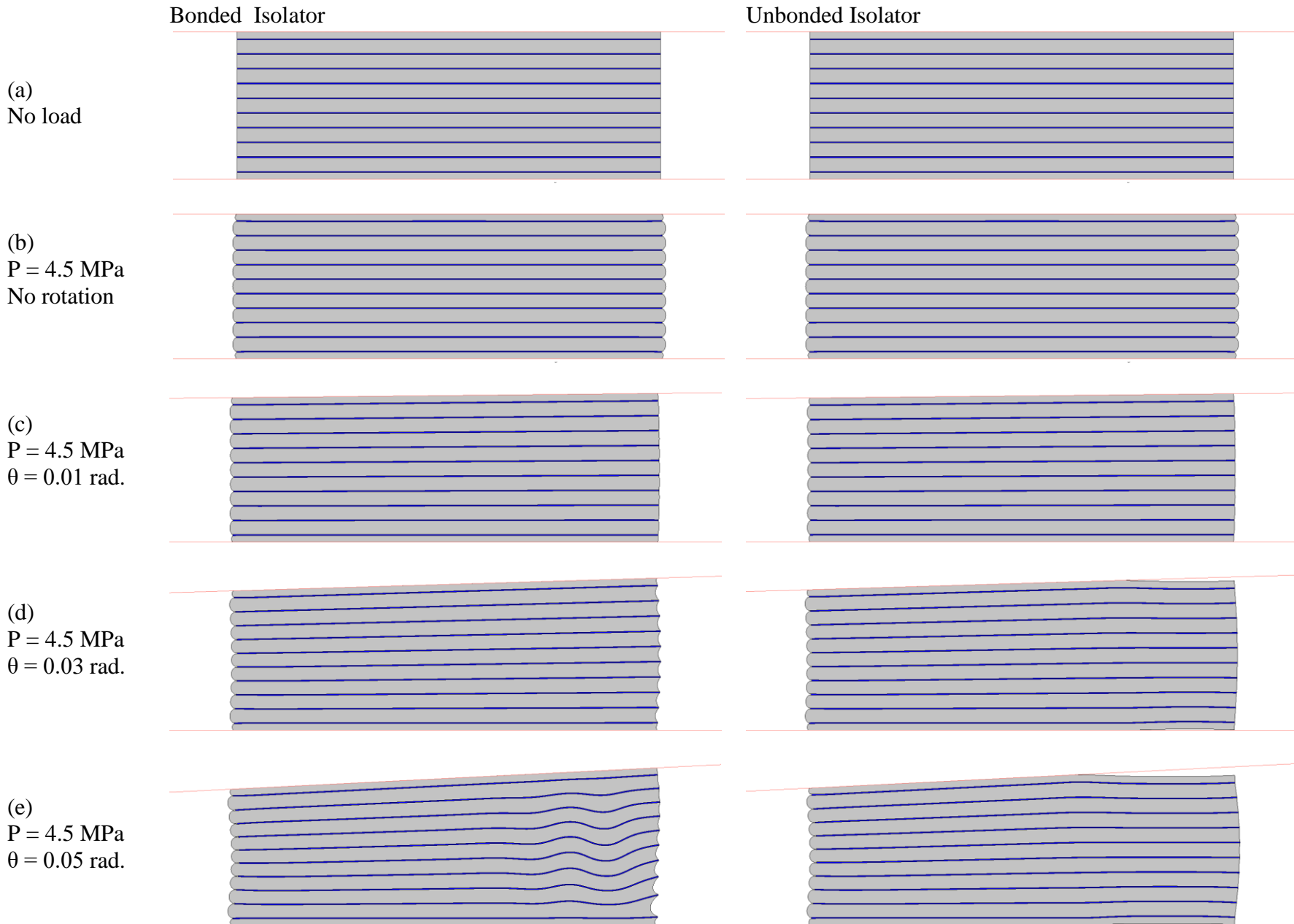


Fig. 3-4: Deformation progress of *Isolator 4*.

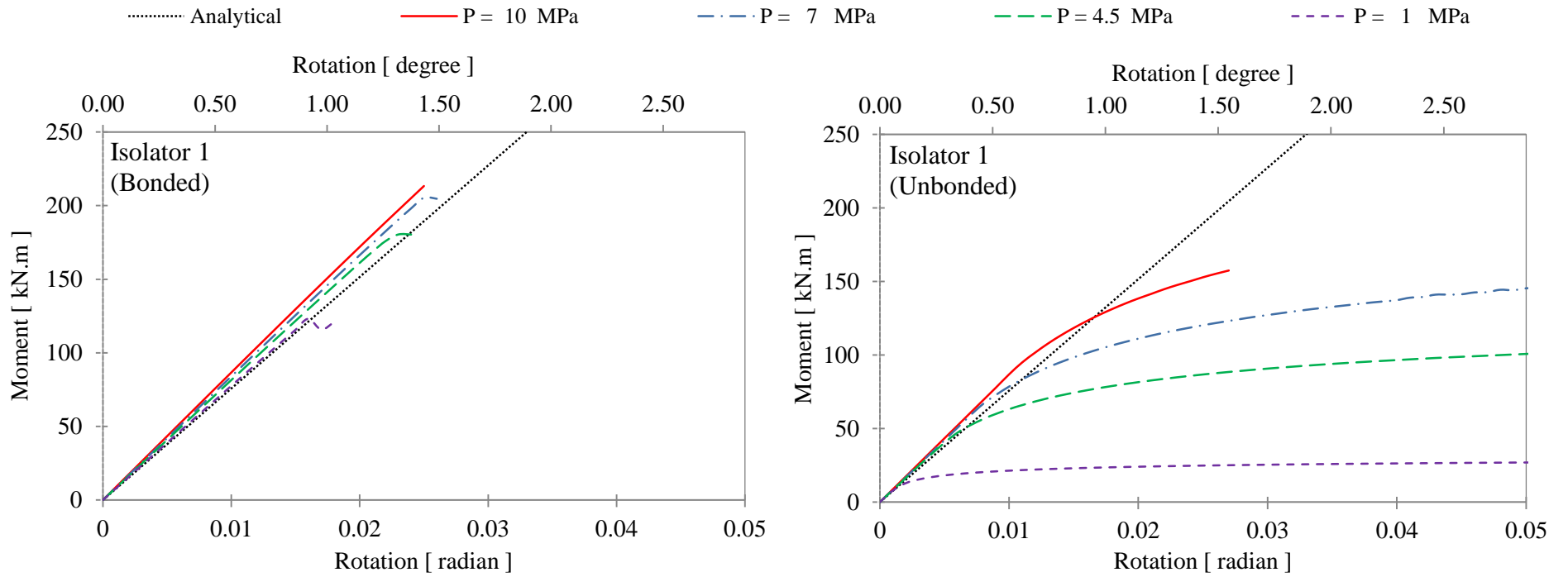
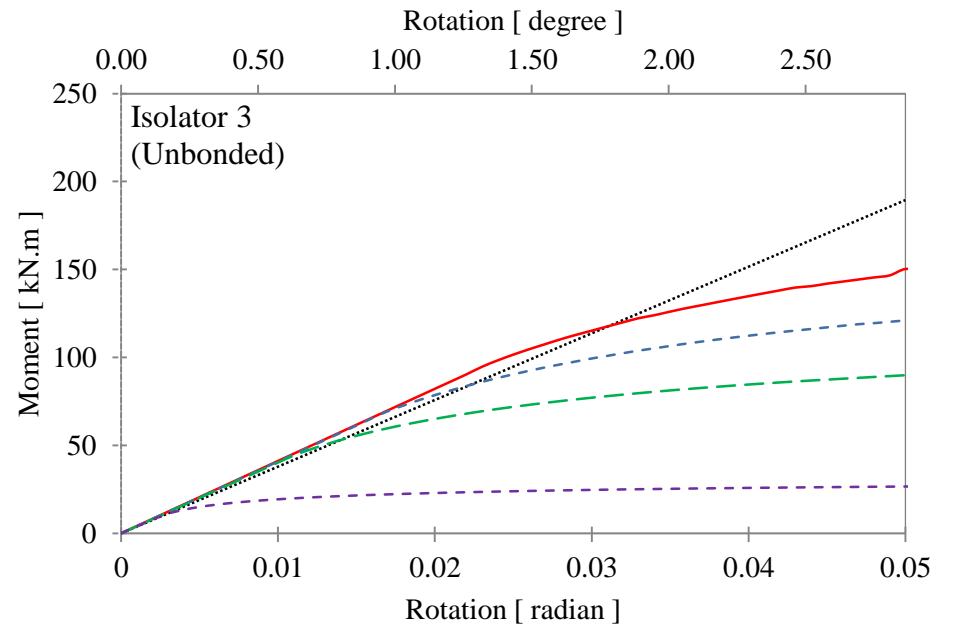
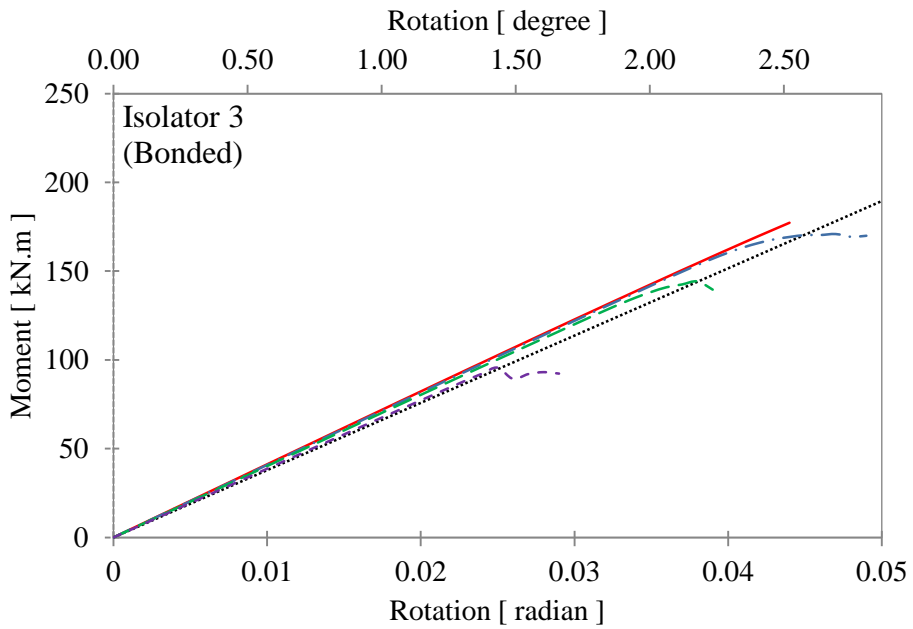
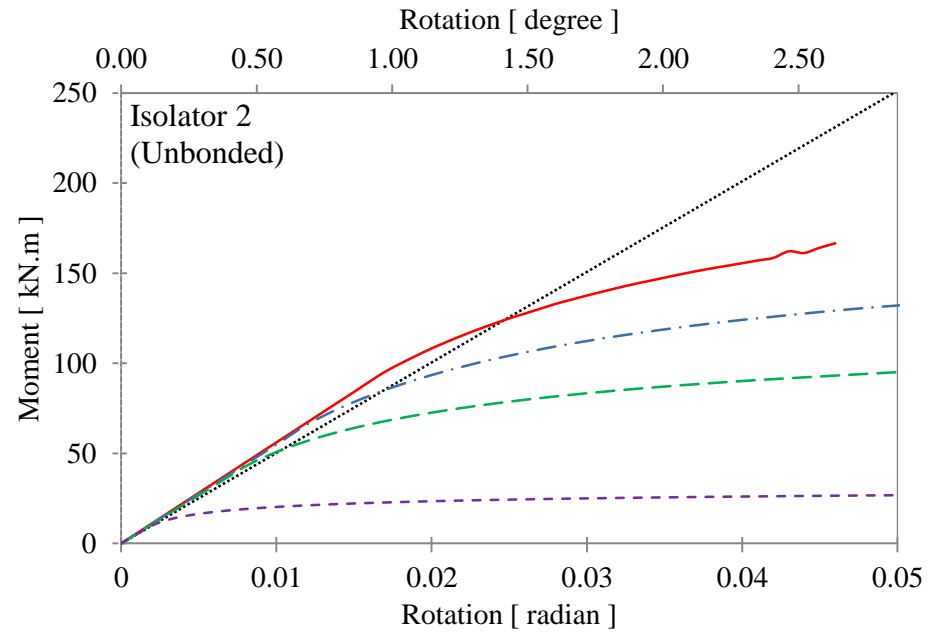
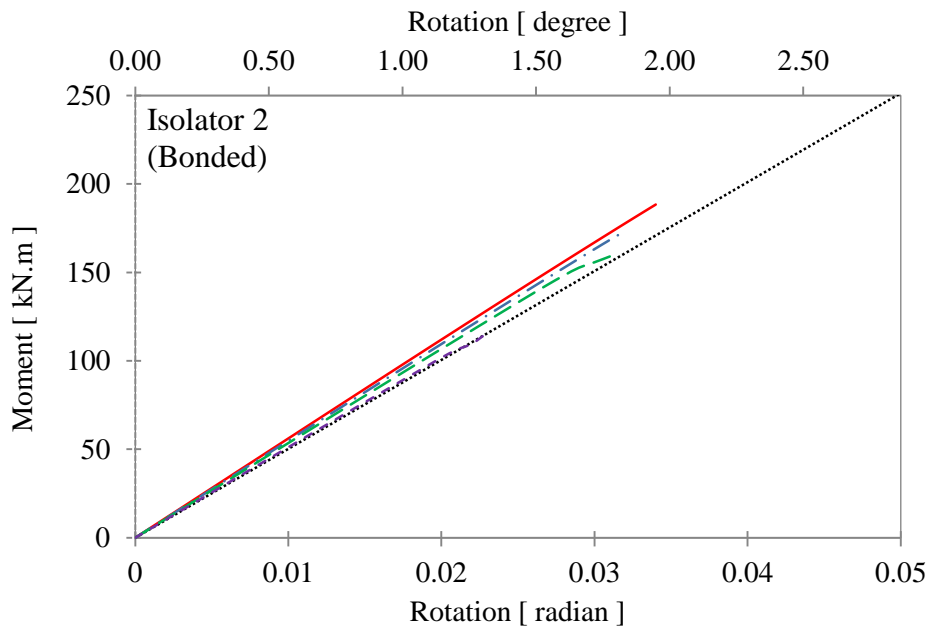


Fig. 3-5: Moment-rotation response under different compressive loads



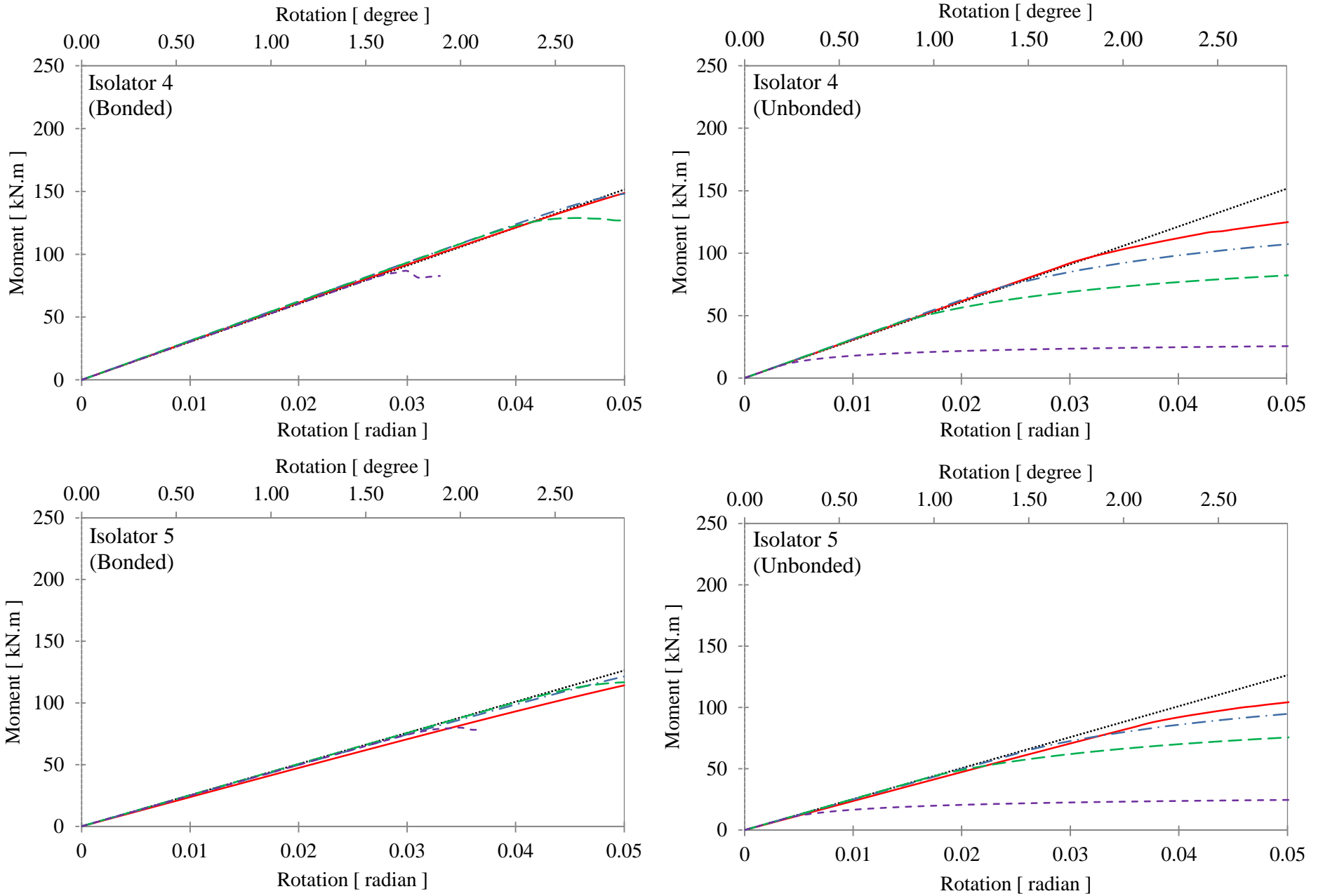


Fig. 3-5: Moment-rotation response under different compressive loads (continued)

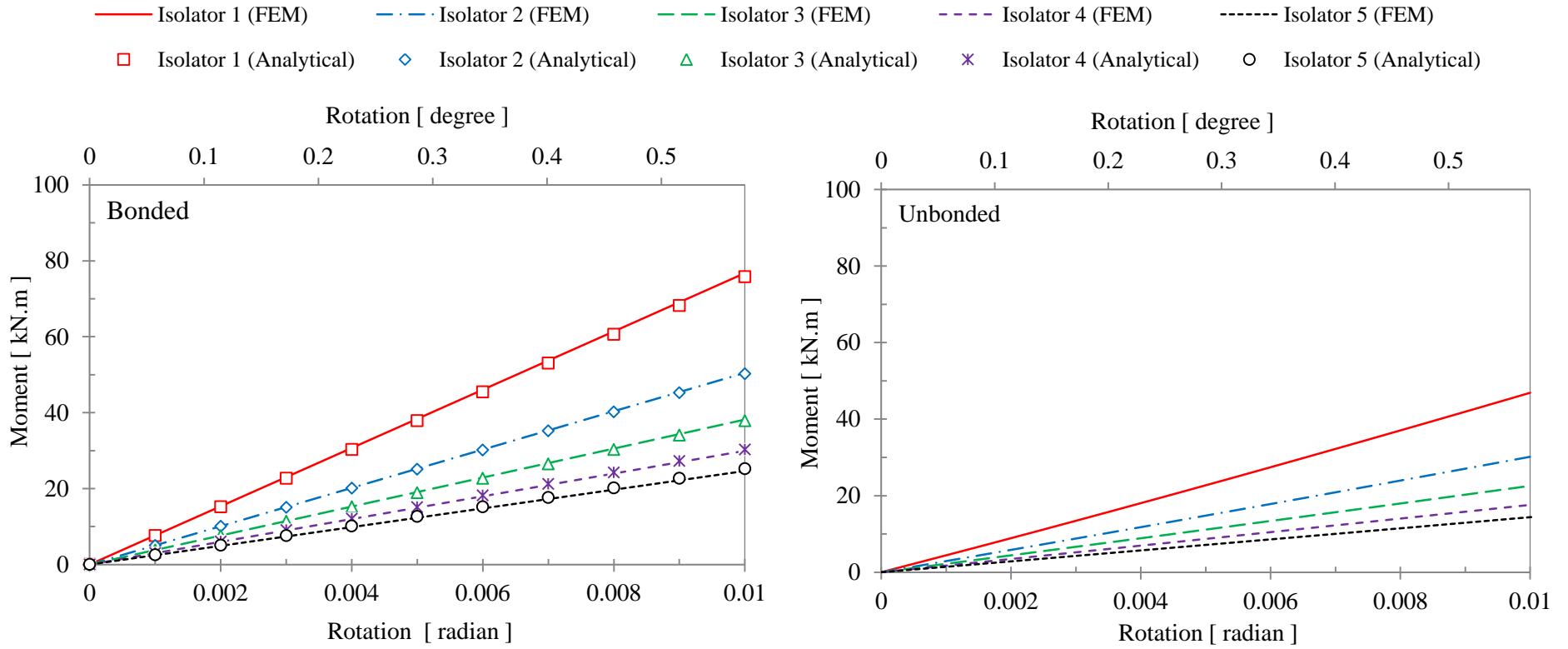


Fig. 3-6: Moment-rotation response under pure rotation (*i.e. no axial loads*)

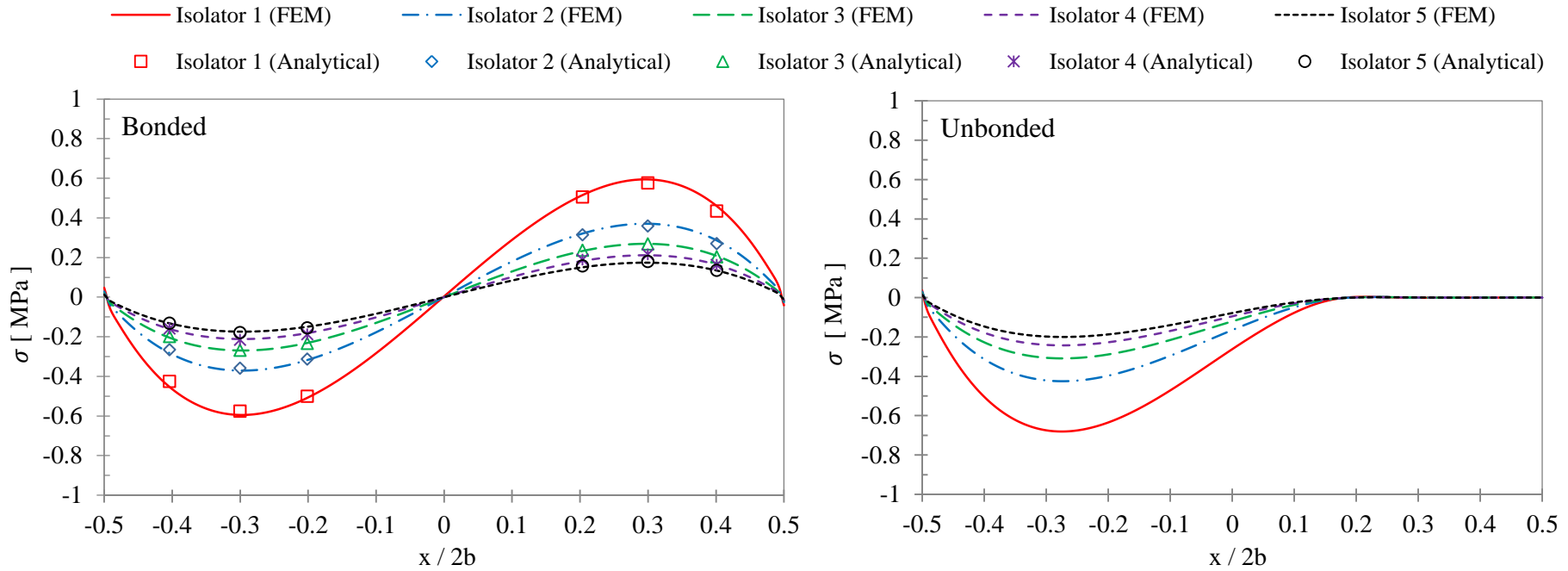


Fig. 3-7: Compressive stress distribution along the top surface of the isolators under a rotation of 0.001 radians (*vertical displacement control*)

Rotation

Bonded Isolator

Unbonded Isolator

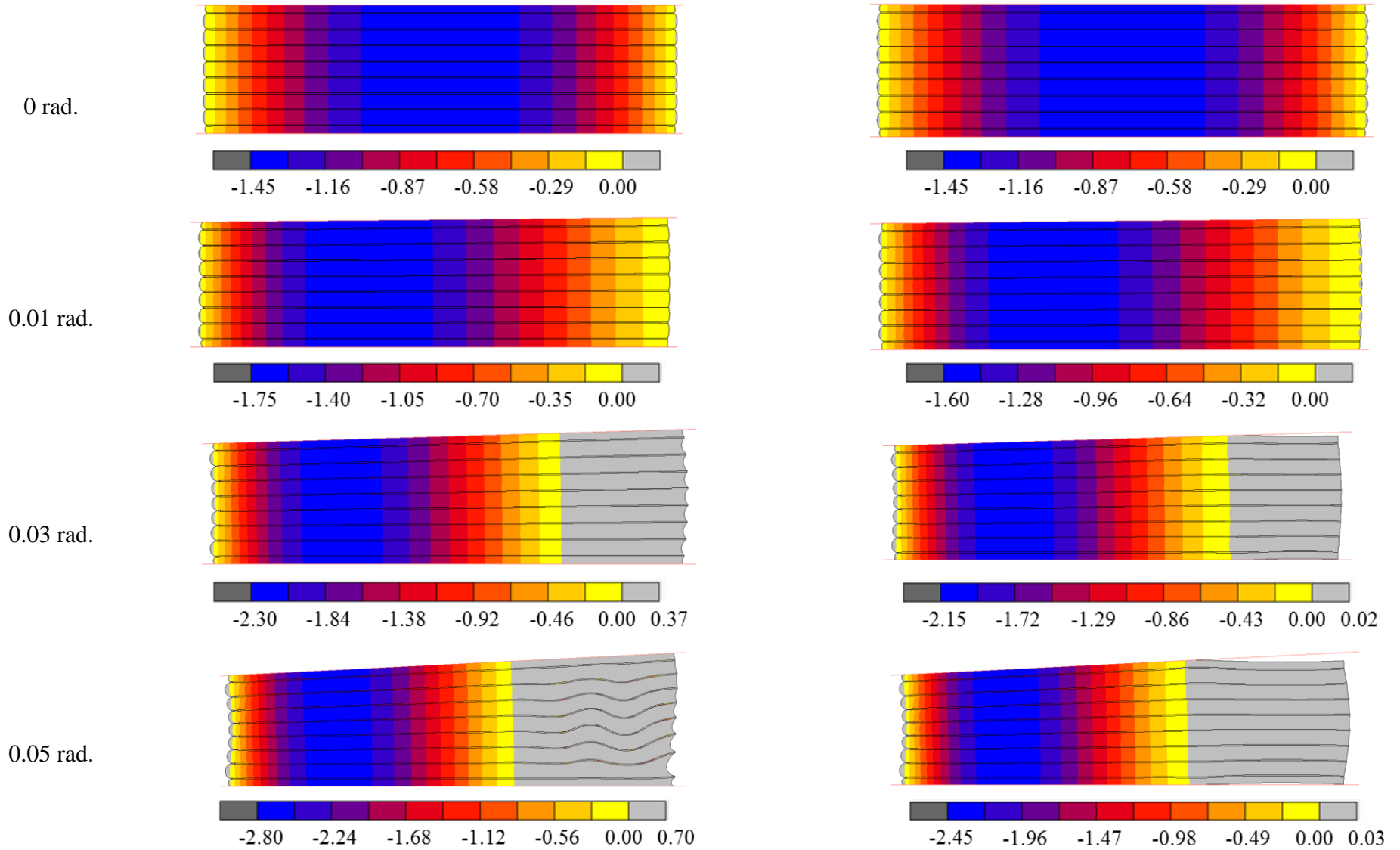


Fig. 3-8. Normalized stresses (σ_{22} / P) in *Isolator 3* under average compressive stress of 7 MPa

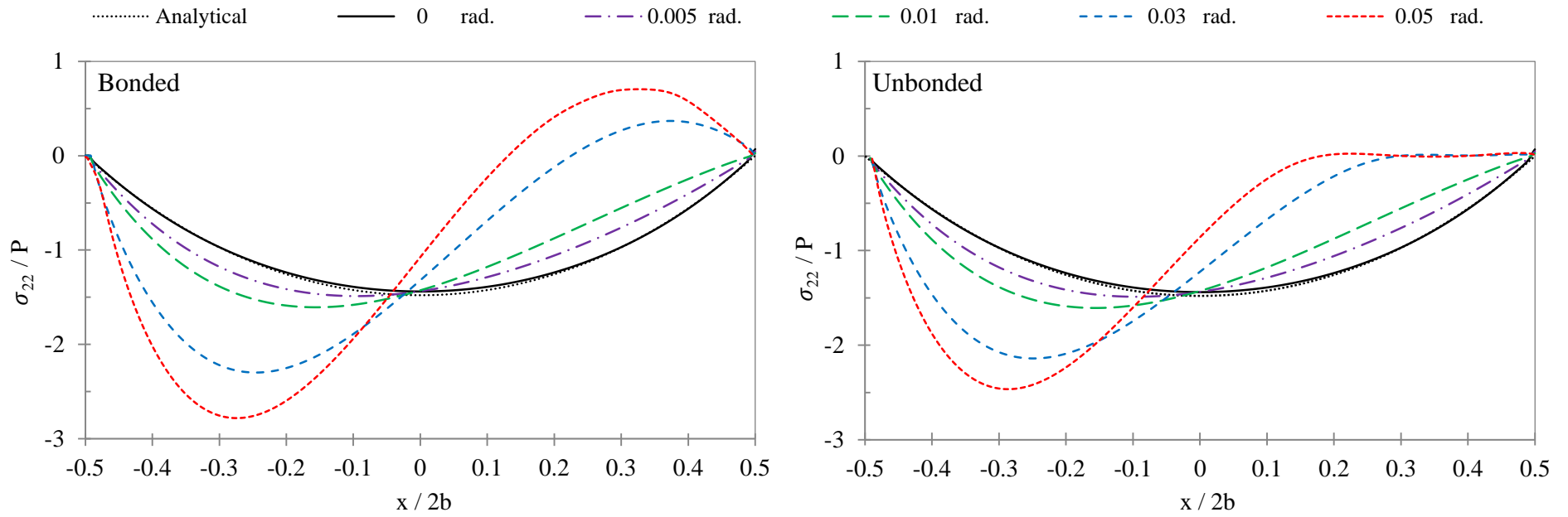


Fig. 3-9: Profile of normalized stress (σ_{22} / P) distribution along the intermediate elastomer layer for *Isolator 3* ($P = 7$ MPa)

Rotation

Bonded Isolator

Unbonded Isolator

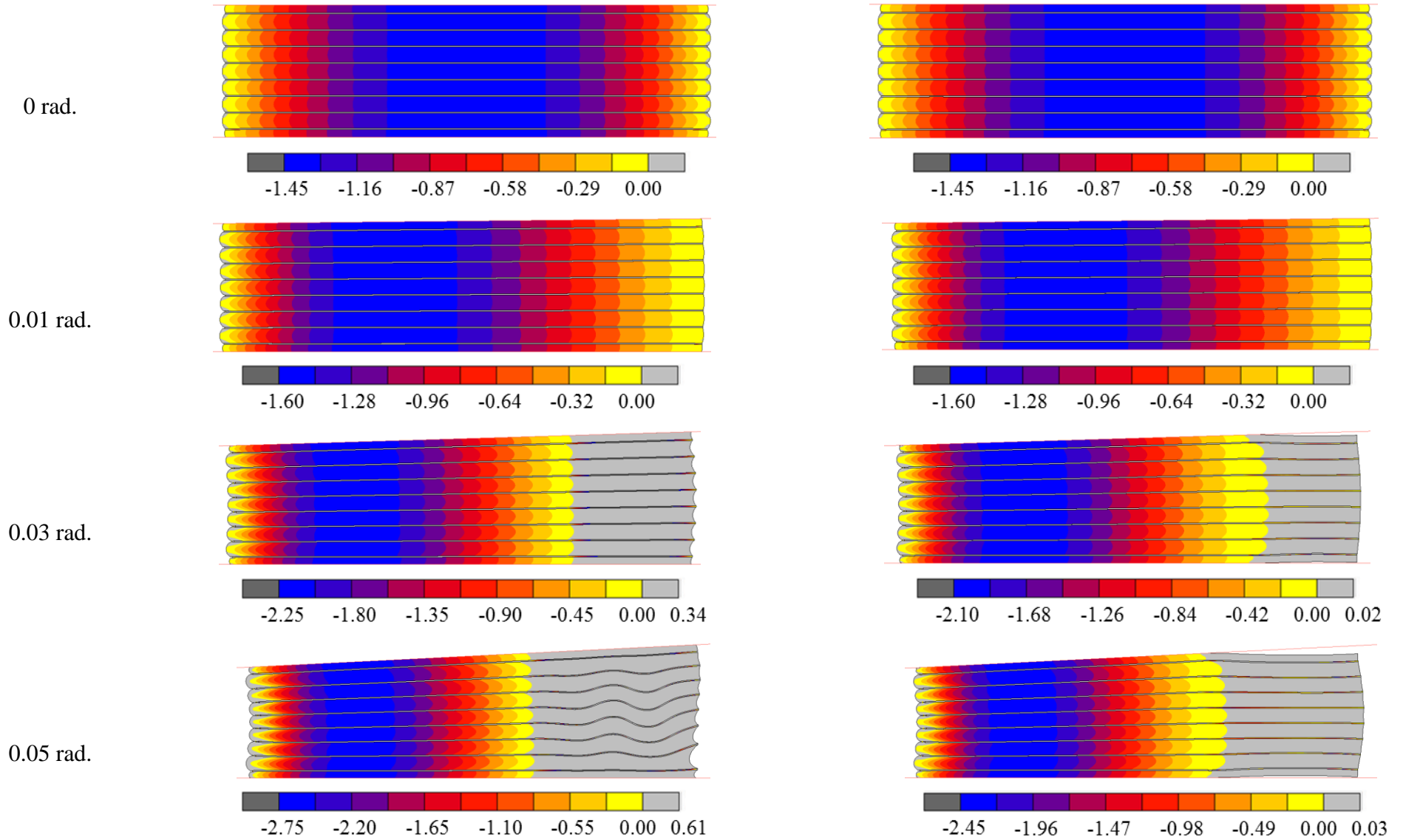


Fig. 3-10: Normalized stresses (σ_{11}/P) in *Isolator 3* under an average compressive stress of 7 MPa.

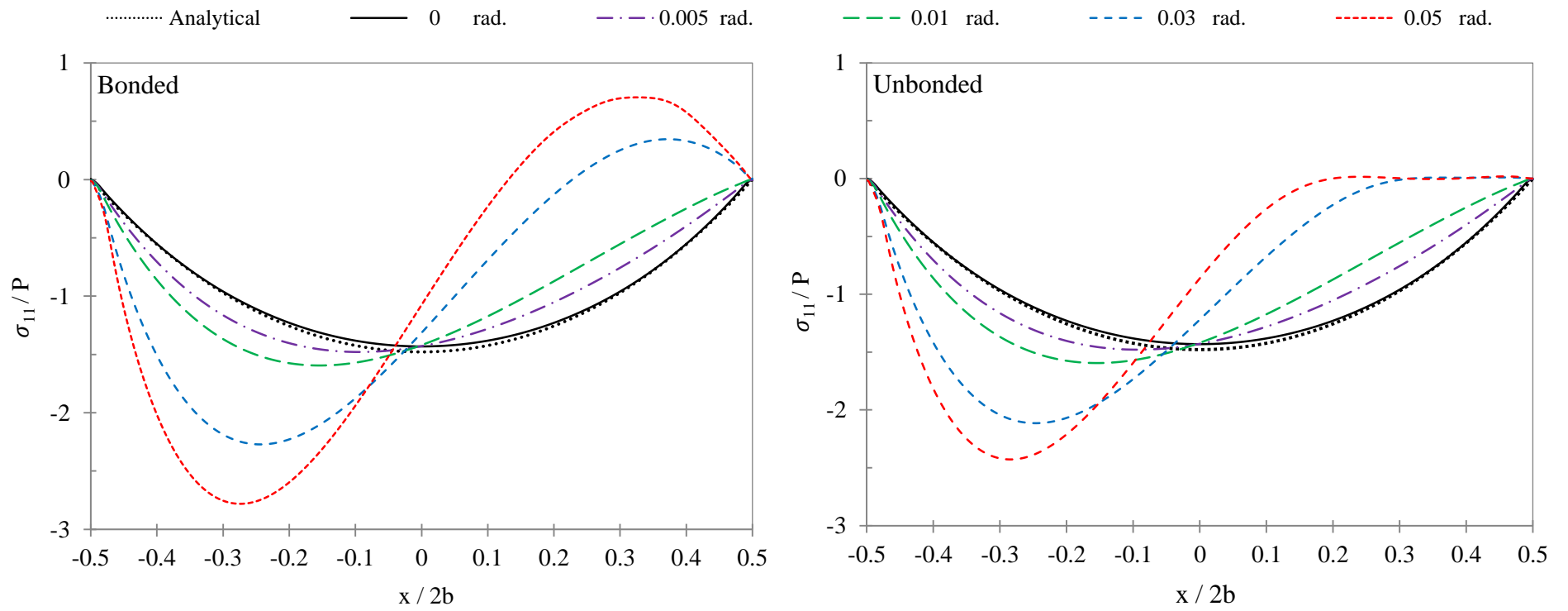


Fig. 3-11: Profile of normalized stress (σ_{11}/P) distribution along the intermediate elastomer layer for *Isolator 3* ($P = 7$ MPa)

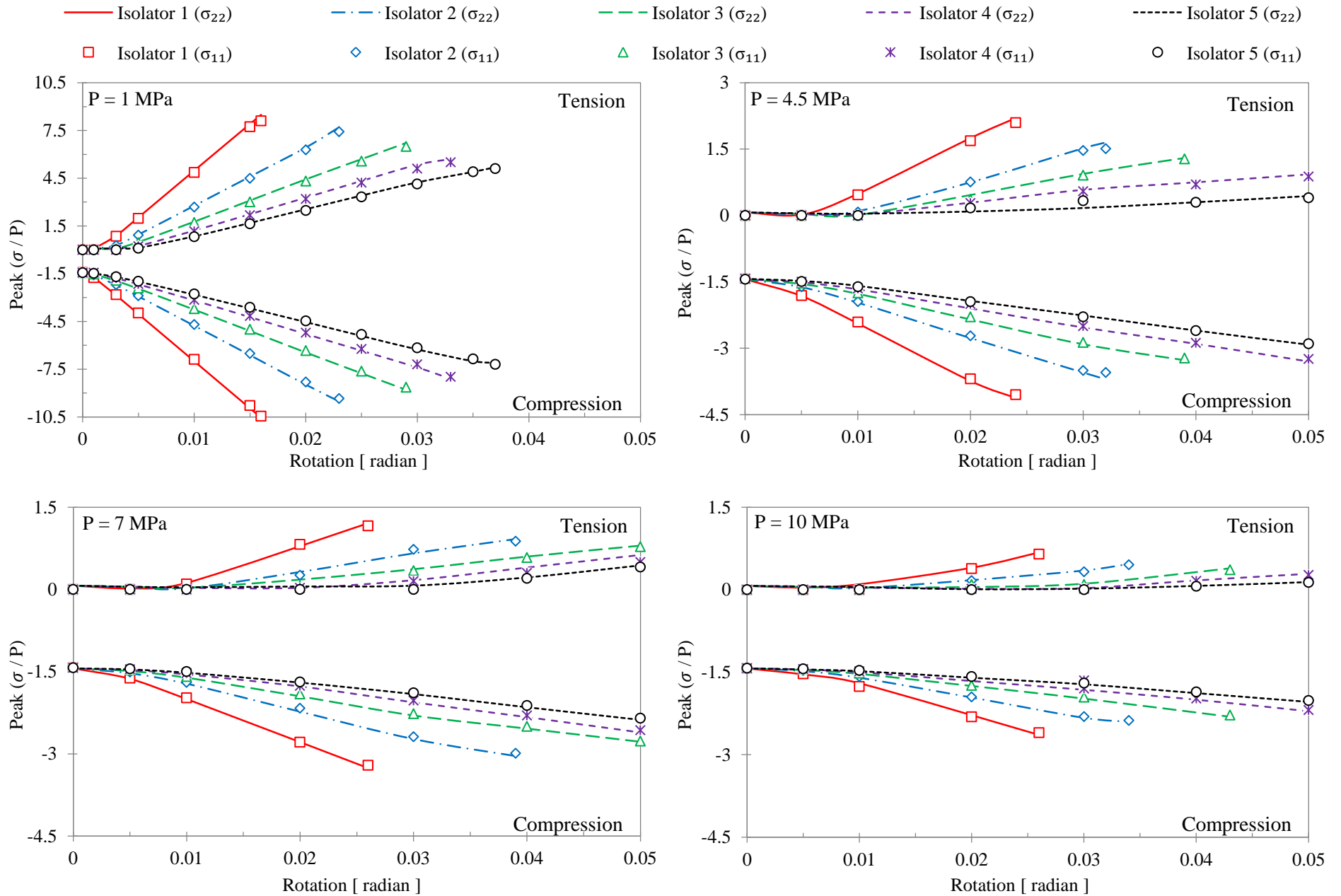


Fig. 3-12. Profile of normalized peak stresses (σ / P) in the bonded isolators

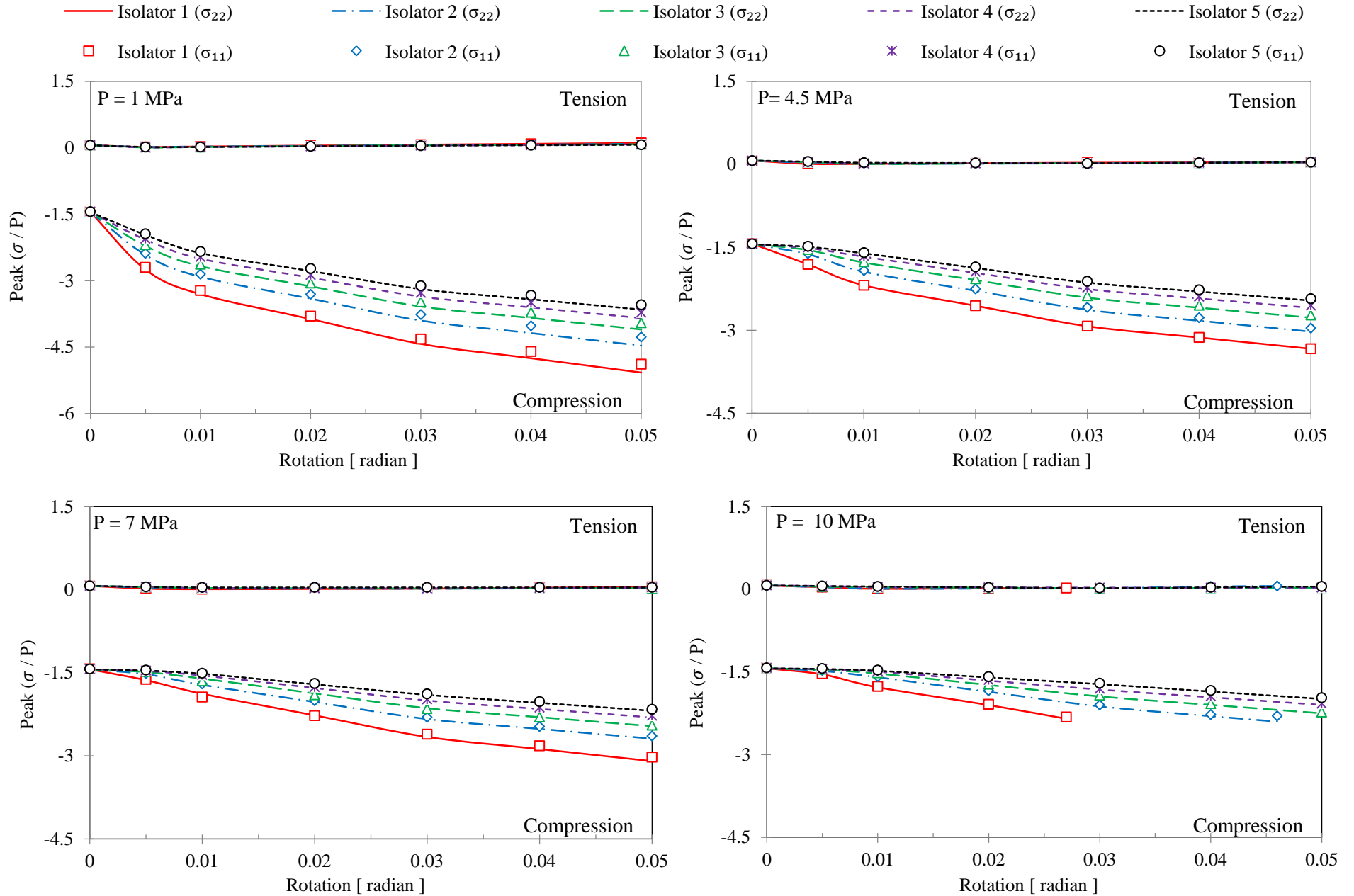


Fig. 3-13: Profile of normalized peak stresses (σ/P) in the unbonded isolators

Rotation

Bonded Isolator

Unbonded Isolator

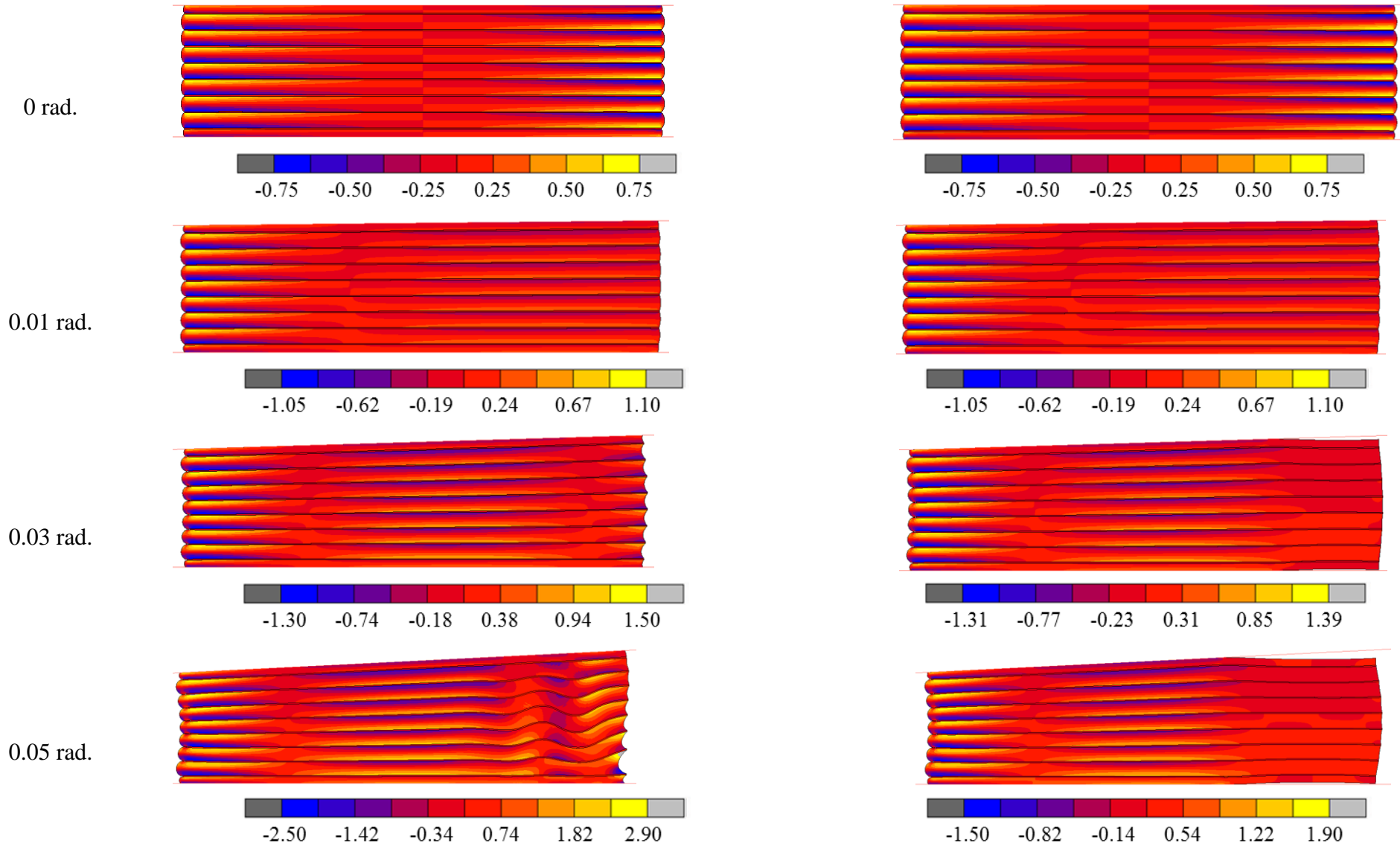


Fig. 3-14: Shear strains (γ_{12}) in *Isolator 3* under average compressive stress of 7 MPa

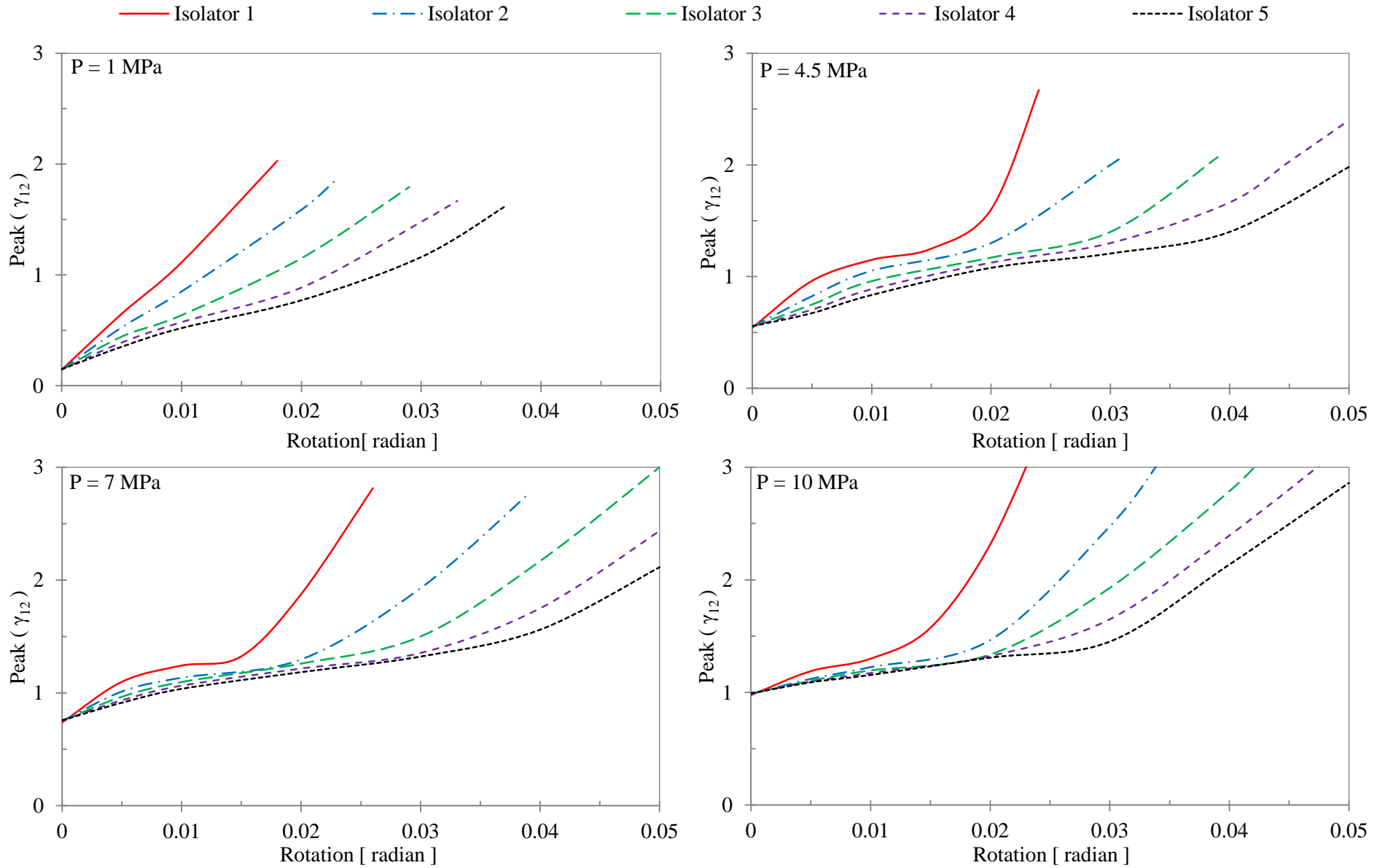


Fig. 3-15: Variation of peak shear strain (γ_{12}) in the bonded isolators

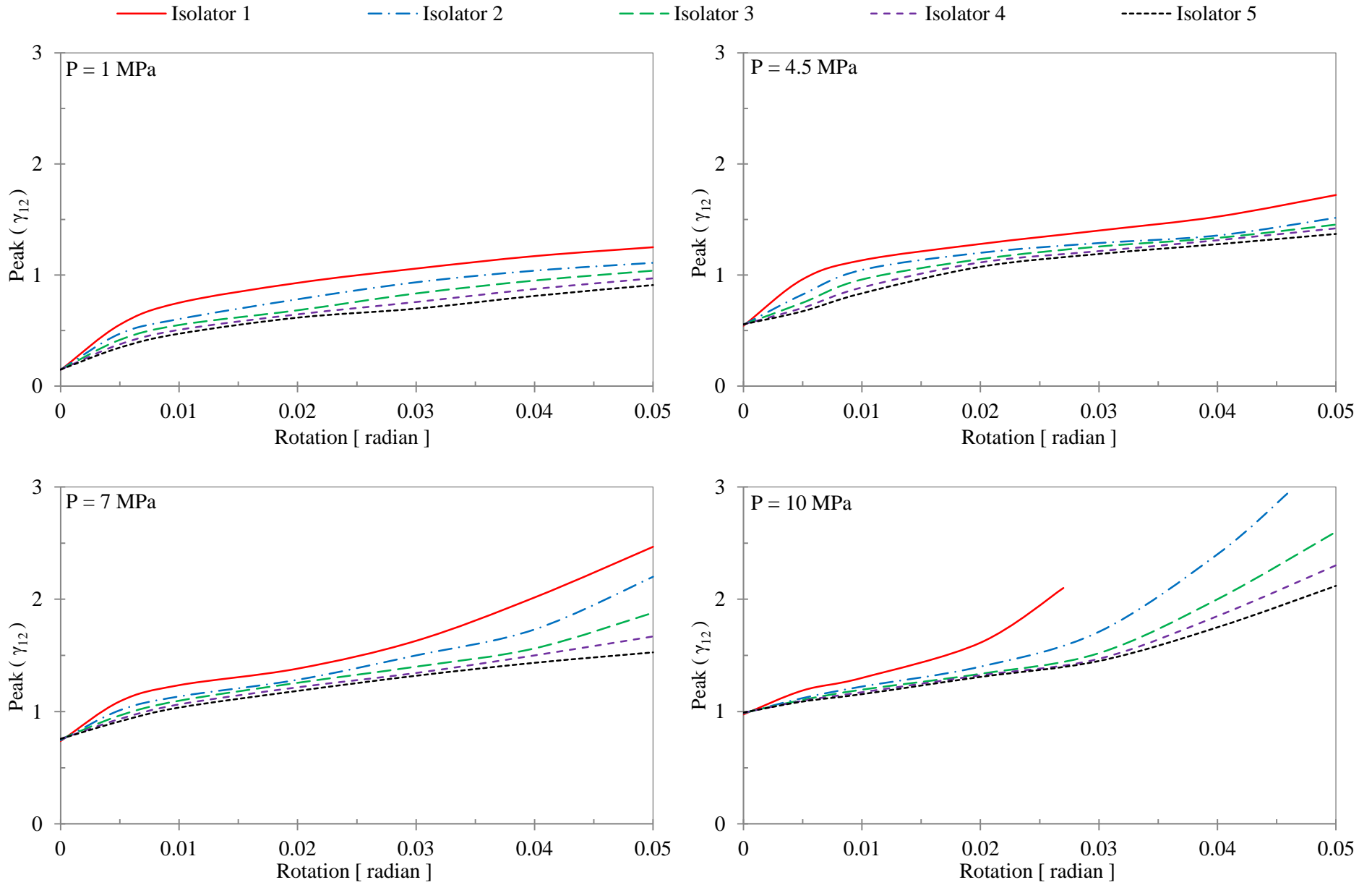
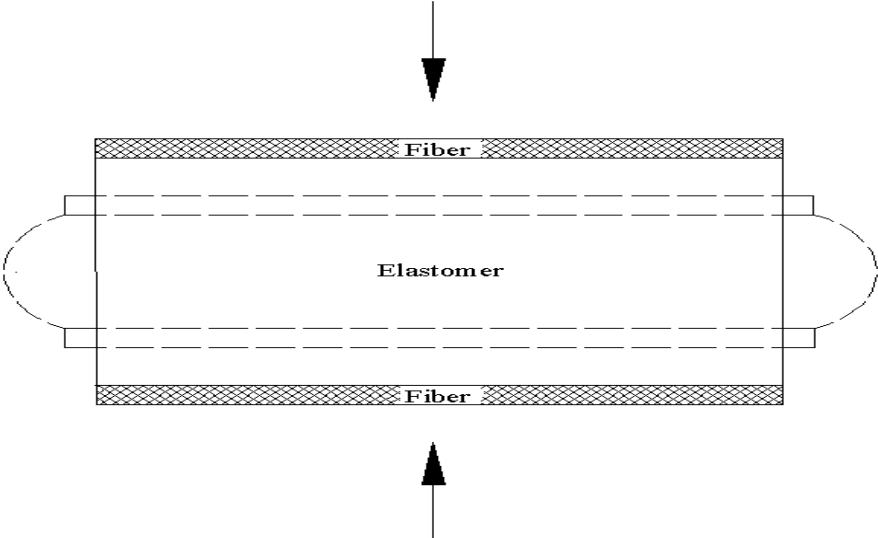
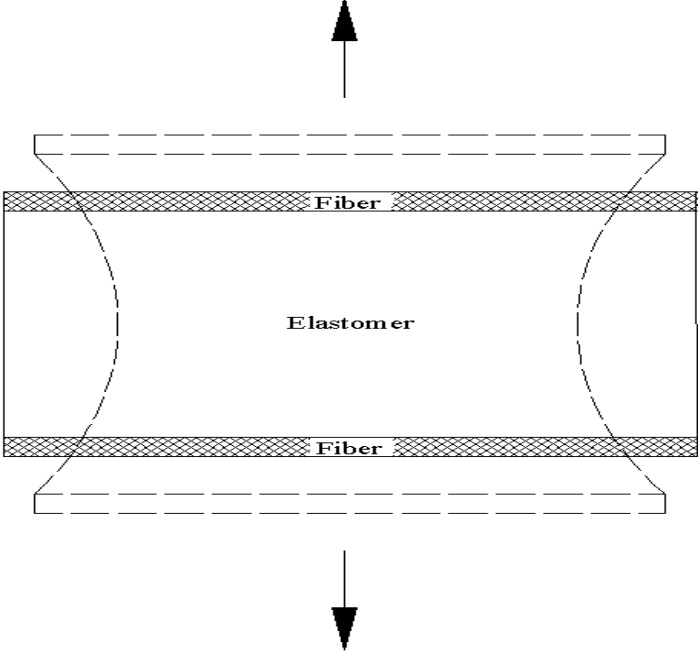


Fig. 3-16: Variation of peak shear strain (γ_{12}) in the unbonded isolators



(b) Tensile strain

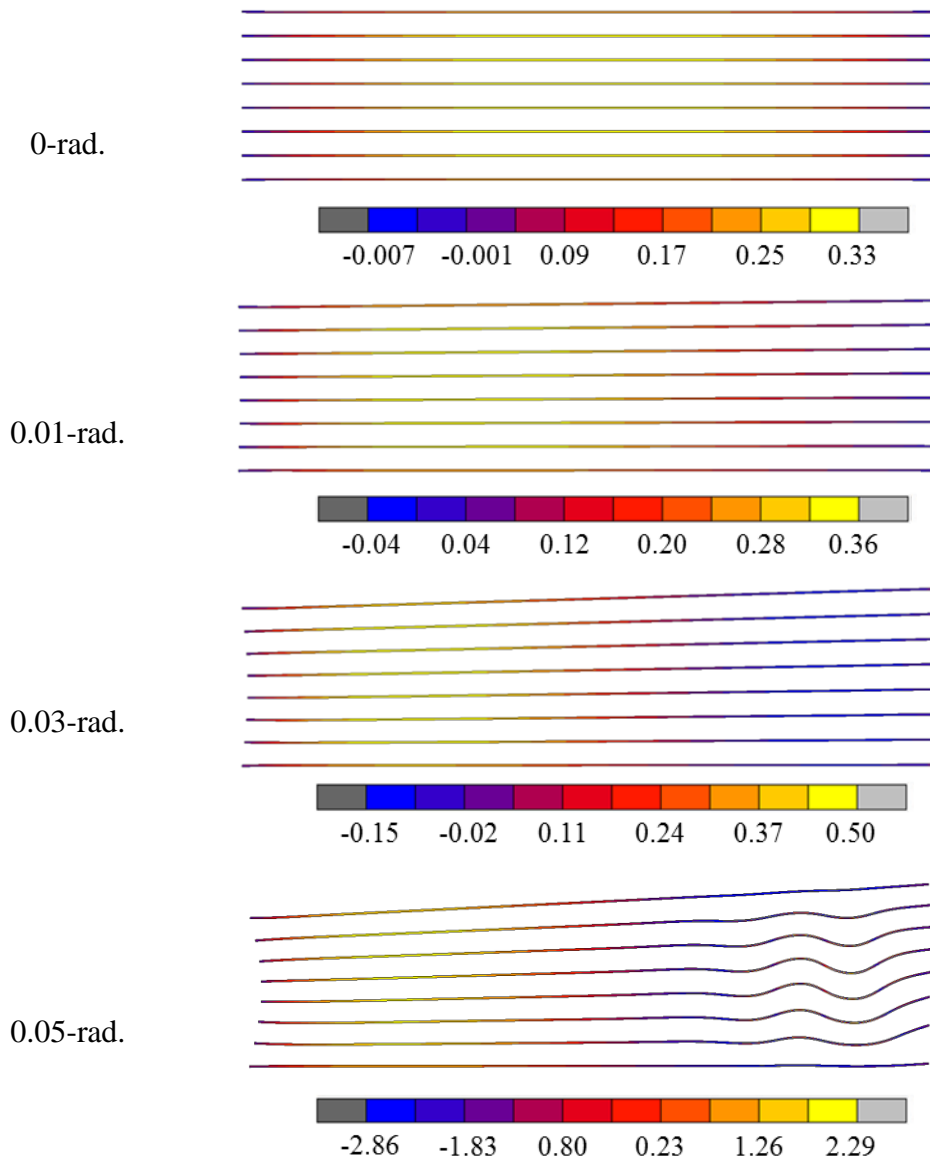


(a) Compressive strain

Fig. 3-17. Deformation of isolator and resulting strain in fiber reinforcement

Rotation

Bonded Isolator



Unbonded Isolator

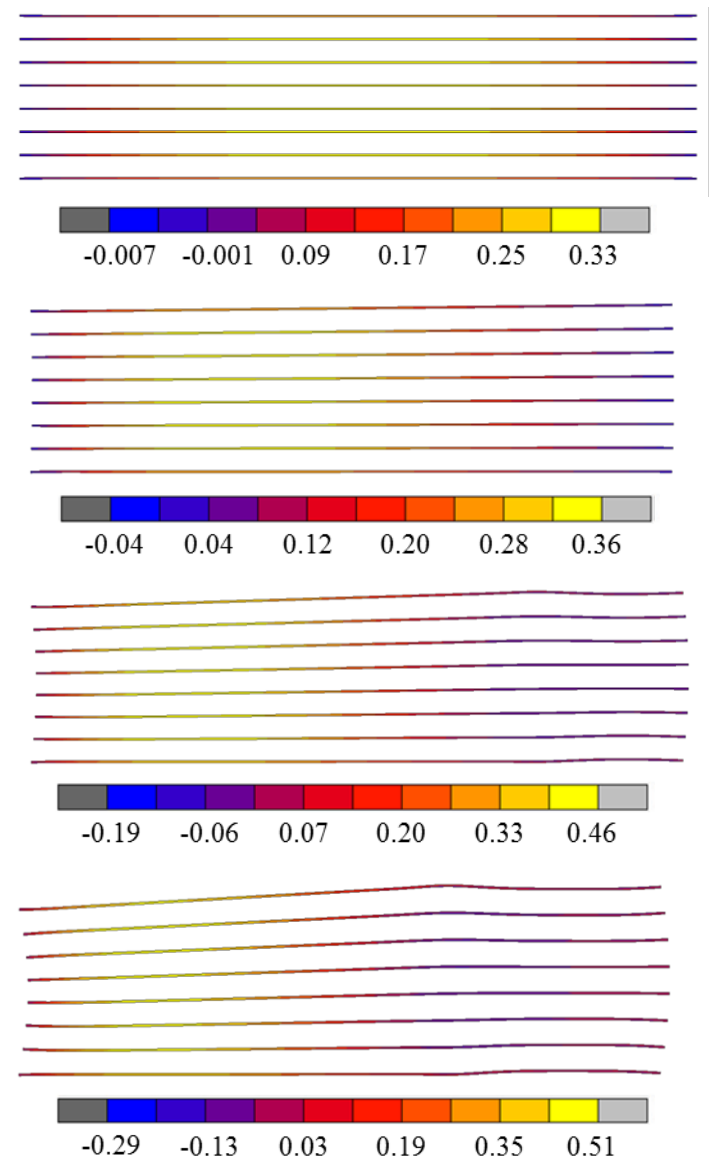


Fig. 3-18: Reinforcement strains ($\% \epsilon_{\text{fiber}}$) in *Isolator 3* ($P = 7$ MPa)

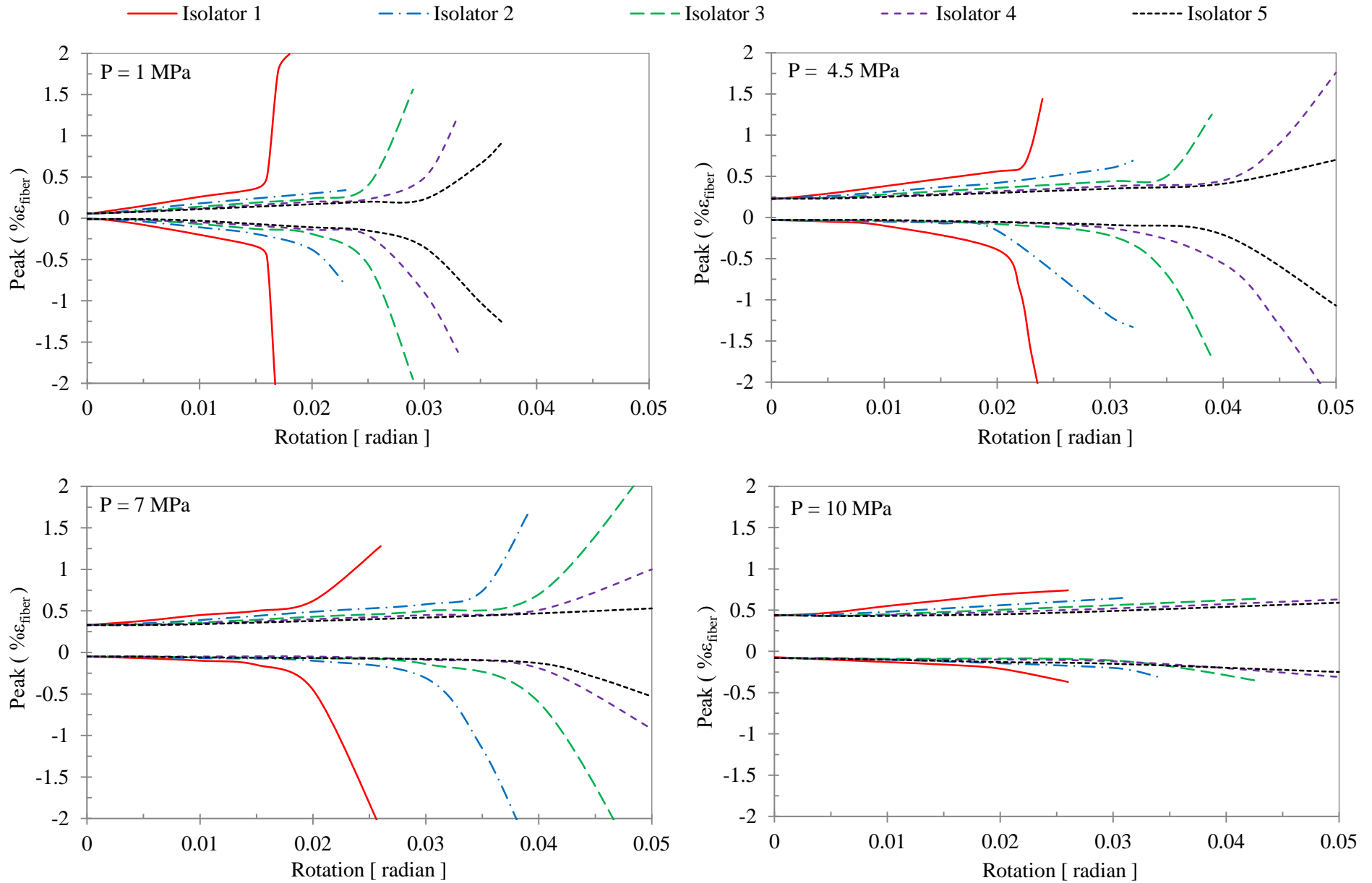


Fig. 3-19: Variation of peak fiber strain ($\% \epsilon_{\text{fiber}}$) in the bonded isolators

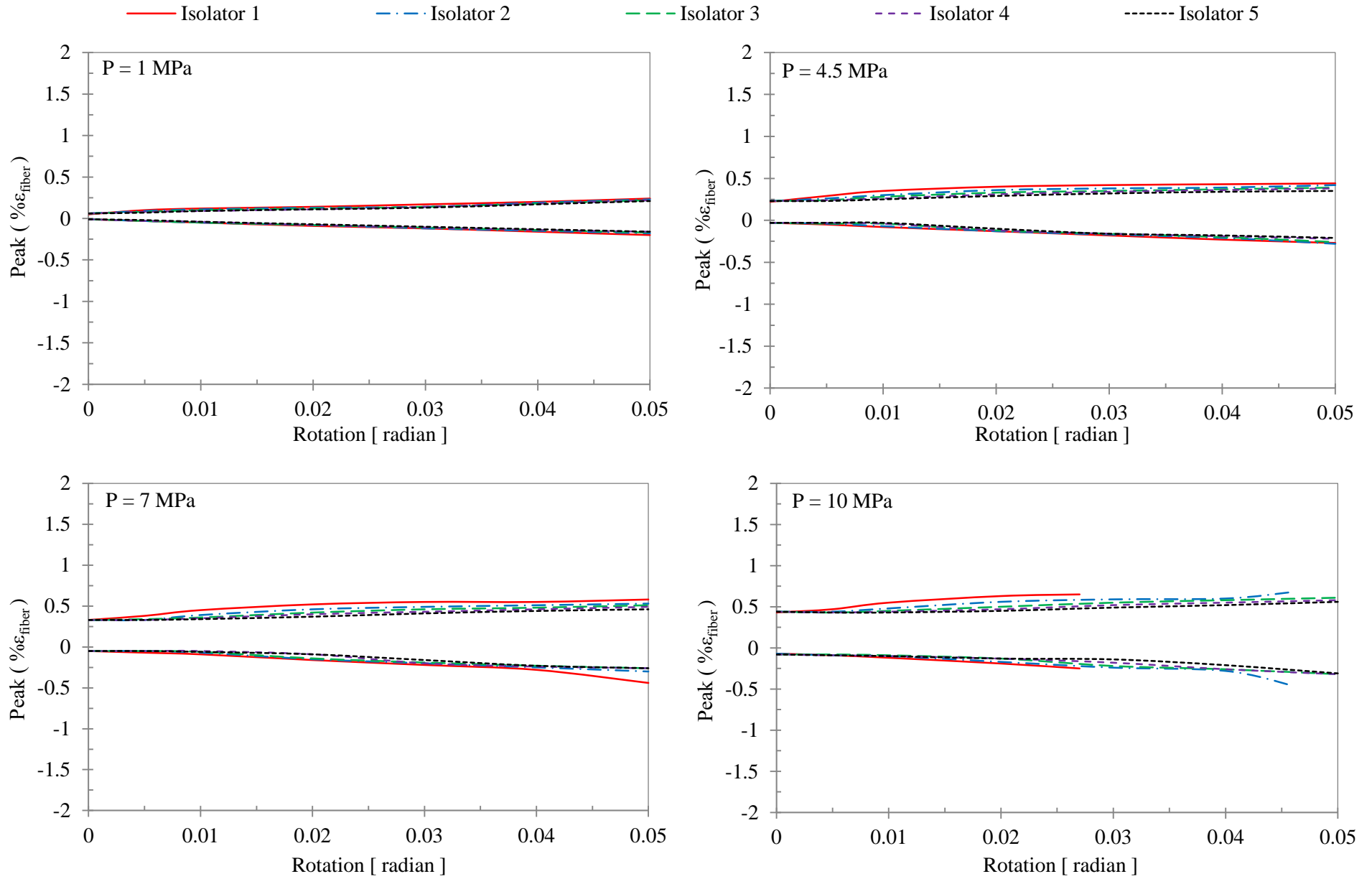


Fig. 3-20: Variation of peak fiber strain ($\% \epsilon_{\text{fiber}}$) in the unbonded isolators

Chapter FOUR

Experimental Assessment of Fiber Reinforced Elastomeric Isolators for Bridge Applications

Abstract

Fiber reinforced elastomeric isolators (FREI) can be implemented in a variety of structures, including buildings and bridges. FREI consists of alternating layers of elastomer and fiber fabric (often carbon fiber). The main role for the fiber reinforcement is to limit the bulging of the elastomer layers, and is the dominant parameter affecting the vertical stiffness. Compared to tradition steel-reinforced elastomeric isolators (SREI), the use of fabric reinforcement could potentially lead to a substantial reduction in both weight and manufacturing costs. To date, FREI have been tested under either vertical loading or combined vertical and lateral loading. Although, these loading scenarios are typically sufficient for building applications, extending the use of FREI to bridges requires an understanding of their behaviour under rotational deformation. This paper presents results from an experimental study conducted to 1) investigate the behaviour of FREI under different types of loads/deformations expected in bridge applications and; 2) determine the viability of FREI as bridge bearings. The test program covered a range of axial loads, lateral displacements as well as angles of rotations. In general, under a different of loading scenarios, U-FREI has shown considerable success in resisting loads and accommodating deformations with no damage/delamination of the isolators observed.

4.1. Introduction

Bearings are an important element in bridge design as they are responsible for transmitting the loads from and accommodating deformations between the superstructure (i.e. deck/girder) to the substructure (i.e. piers/columns). CAN/CSA-S6 Canadian Highway Bridge Design Code (CHBDC) (CSA 2014) and American Association of State Highway and Transportation Officials (AASHTO 2012) LRFD Bridge Design Specifications, define bridge bearings as: "a structural device that transmits loads while facilitating translation and/or rotation". As such, in addition to deformations in the vertical and lateral directions, which bearings/isolators are typically subjected to in building applications, the bearings will also experience rotational deformations in bridge applications (Lee 1994). Accordingly, bridge bearings should have sufficient stiffness in the vertical direction to transmit dead and live loads and also be able to accommodate the lateral and/or rotational deformations induced in the girders. The failure of bridge bearings may lead to accelerated bridge deterioration or cause damage to the bridge (AASHTO-LRFD 2012). Accordingly, damage is prohibited in bridge bearings under any anticipated loading condition.

The selection of a bearing type depends on several factors, including the predicted loading, geometry, maintenance, available clearance, deflection, displacement and rotation demands, availability, policy, designer preference, and cost (Caltrans 1994). Standard bridge bearings can be categorized as either high load multi-rotational (HLMR) bearings (pot, disc and spherical) or elastomeric bearings (Ramberger 2002). Pot bearings comprise elastomeric pads confined within a steel cylinder (pot). Disc bearings are similar to pot bearings, except that the elastomeric pad is replaced with annular shaped urethane disc. Spherical bearings consist of a concave plate mounted on a convex base. In general, HLMR bearings have the ability to provide high vertical and rotational capacity. The lateral movements are typically accommodated through

a separate sliding interface between a polytetrafluoroethylene (PTFE) disk and a stainless steel plate.

The major component of an elastomeric bearing is the elastomeric pads. The pads can be used directly without being reinforced (i.e. plain elastomeric bearings), or they can be laminated with reinforcement having a high tensile capacity in order to increase the vertical stiffness of the bearing by limiting bulging of the elastomer. According to the Caltrans Bridge Memo to Designers (1994): “reinforced elastomeric bearings should be considered the preferred type of bearing for all structures”.

Elastomeric bearings, which are typically reinforced with steel shims (steel reinforced elastomeric isolators (SREI)), can alternatively use fiber fabric (fiber reinforced elastomeric isolators (FREI)) as the reinforcing material. A number of studies have been conducted to investigate the viability of replacing SREI with FREI (Kelly 1999 & 2002; Moon et al. 2002; Mordini and Strauss 2008; Toopchi-Nezhad et al. 2008 (a&b)).

Unbonded-fiber reinforced elastomeric isolators (U-FREI), which have no rigid end plates, are FREI that are simply placed between the superstructure and the substructure with no connection/fastening mechanism. This lack of mechanical connection between the bearing and the superstructure/substructure, removal of the thick end plates and lack of flexural rigidity in the fiber reinforcement allows the bearing to undergo a unique rollover deformation pattern when subjected to lateral deformations (shown in Fig. 4-1a), and lift-off under large rotational deformations (shown in Fig. 4-1b). Numerical studies (Toopchi-Nazhad et al. 2011; Al-Anany and Tait (2015a&b)) have shown that the unbonded connection eliminates the occurrence of significant tensile stresses in the bearing under lateral and rotational deformations. As such, the fastening of elastomeric isolators to the upper and lower contact supports introduces tensile

stresses, which can initiate/accelerate bearing damage when subjected to lateral and rotational deformations. However, an important characteristic of the unbonded bearing is that it should remain stable (i.e. a positive lateral tangential stiffness to be maintained when deformed laterally) during rollover (ASCE 2010).

Compared to U-FREI, SREI are relatively heavy due to the rigid steel end plates and steel reinforcement shims. The manufacturing cost of SREI is also high due to the labour intensive manufacturing process (Kelly and Konstantinidis 2007). Replacing the steel reinforcement with fiber can reduce the weight, as fiber is a much lighter material. Additionally, the use of fiber reinforcement could also lead to a potential reduction in manufacturing cost as individual isolators can be readily cut from large sheets. In general, U-FREI possess several unique characteristics such as: low weight, ease of installation, potential for mass production, simplicity of cutting to desire size, no thick steel end plates, superior damping properties, high seismic isolation efficiency and lower stresses in the elastomer and fiber layers (Toopchi-Nezhad et al. 2008a). These features make the U-FREI a viable option over traditional isolators in different bridge applications, such as accelerated bridge construction. Finally, it should be noted that the most recent versions of CAN/CSA-S6 (2014) and AASHTO-LRFD (2012) permit the use of fabric as the reinforcing material in elastomeric isolators.

4.2. Background

Experimental and numerical studies have been carried out to investigate the vertical, rotational, and lateral response of SREI and FREI for building and bridge applications. Muscarella and Yura (1995) conducted an experimental study on steel reinforced elastomeric bridge bearings. The purpose of the study was to evaluate elastomeric bearing performance on the basis of

different parameters (e.g. elastomer hardness, shape factor, and reinforcing shim orientation). Several different types of experimental tests were performed, including vertical and rotational stiffness tests. Results from the vertical tests showed that the shape factor (S) defined as the ratio between loaded area and the area free to bulge, had a greater effect on the vertical stiffness. Additionally, the orientation of the steel reinforcement (i.e parallel or tilted) was found to have a negligible effect on the compression modulus. Results from rotational testing showed that an increase in the shape factor and/or rubber hardness resulted in an increase in the rotational stiffness and decrease in the rotational capacity of the bearing. It was also observed that an increase in the applied compressive stress led to an increase in both the rotational stiffness and rotational capacity.

Mori et al. (1999) evaluated the behaviour of steel reinforced elastomeric bearings under compressive loads. The bearings were designed to be used as seismic isolators for bridges. It was found that the relation between the vertical force and displacement of all the tested bearings was nearly linear under different levels of applied compressive load. However, a nonlinear behaviour was observed for some bearings at higher compressive strains of approximately 4%. It was postulated that the change in vertical behaviour from linear to nonlinear was dependent on the rubber hardness and the shape factor of the bearing.

Kelly (2001) performed an experimental and theoretical study on elastomeric bearings reinforced with fiber (instead of steel) by analyzing their mechanical properties in the vertical direction. The study was carried out on isolators with high shape factors in order to include the effect of rubber compressibility. Experimental test results showed a nonlinear increase in the vertical stiffness with an increase in the level of the vertical load (stresses) applied on the

bearing. Findings from this study confirmed the feasibility of replacing the steel reinforcement in the conventional elastomeric bearings with lighter fiber material.

Warn et al. (2007) investigated the vertical response of a quarter-scale bonded SREI used for seismic isolation of bridges. The study was conducted on two different types of steel reinforced bearings: low-damping rubber (LDR) and lead-rubber (LR) bearings. The parameters varied in the study included the amplitude of the applied vertical load (stress), vertical loading rate, and lateral offset. A small increase in vertical stiffness was observed with an increase in either the amplitude of applied vertical load (stress) and/or the vertical loading rate. Conversely, an increase in the amplitude of the applied lateral offset resulted in a significant reduction in the vertical stiffness as a result of a reduction in the compressed area of the isolator. The vertical effective damping was found to be approximately 1% and 2% for LDR and LR bearings, respectively. In addition, good agreement was found between experimental results and theoretical values of vertical stiffness, if elastomer compressibility and lateral offset were accounted for in the analytical solution.

Al-Anany and Tait (2015b) conducted a two-dimensional finite element study on bonded FREI (B-FREI) and U-FREI. The objective of this study was to evaluate and compare the vertical and rotational response of B-FREI and U-FREI. The isolators that were investigated all had the same shape factor, but different aspect ratio values, defined as the ratio between the total length and height. The amplitude of the applied vertical load and angle of rotation were varied. In general, for the bearings considered the stress demand on both the elastomer and the fiber reinforcement were considerably lower for U-FREI relative to the B-FREI. No difference in vertical response was observed between B-FREI and U-FREI, which indicated negligible slippage, occurred at the top and bottom contact surfaces. However, the U-FREI were able to

accommodate higher angles of rotations (i.e. higher rotational capacity) compared to the B-FREI. In addition, good agreement was found between the finite element results and the analytical “pressure solution” approach (Tsai and Kelly 2001), particularly for the B-FREI under vertical and rotational response, and also for the rotational response of U-FREI prior to the initiation of lift-off.

4.3. Experimental Test Program

4.3.1. Properties of the Bearing Specimens

A total of four quarter-scale bearings with plan dimensions of 70×70 mm and a total thickness of 20.6 mm were cut from a larger $150 \text{ mm} \times 150 \text{ mm}$ fiber reinforced elastomeric pad as shown in Fig. 4-2. Each bearing consisted of 7 layers (5 intermediate layers and 2 outer cover layers) of a soft compound of natural rubber with a hardness of 55 Durometer, Shore A (ASTM 2010). The thickness of each individual intermediate rubber layer (t_e) was 3.18 mm and the 2 outer cover layers were 1.59 mm thick. The bearings were reinforced with plain weave (bidirectional) carbon fiber fabric having a thickness (t_f) of 0.25 mm.

Accordingly, the total thickness of the rubber (t_r) and fiber was approximately 19.05 mm and 1.50 mm, respectively. The shape factor was determined to be 5.50, which is within the typical range for bridge bearings ($3 < S < 8$) (Stanton et al. 2007). The aspect ratio, AR , defined as the ratio between the total length/width and total height, was 3.4. Additionally, the ratio between the total length/width and the total thickness of the intermediate rubber layers ($5 \times 3.18 \text{ mm} = 15.9 \text{ mm}$) was 4.40. It is important to note that certain bridge standard specifications (e.g. OPSS 1202) require the latter ratio to be more than 3 in order to ensure the stability of the bearing under the expected loading conditions during the life time of the bridge. The main specifications for the bearings investigated in this study are listed in Table 4-1.

4.3.2. Employed Test Apparatus

All the bearings were tested using the 3-degree of freedom (3DOF) bearing test apparatus shown in Fig. 4-3. The primary components of the apparatus are a loading beam, a pedestal, and a reaction frame. The loading beam is controlled using three hydraulic actuators. The two vertical actuators, which are located at either end of the top beam, control the vertical load and angle of rotation applied on the isolator. The third actuator, which is oriented in the horizontal direction, controls the lateral movement of the loading beam.

The tested bearings were located between the upper and lower loading platens. The upper loading platen was attached to the loading beam. The lower loading platen was supported on two thick steel plates, which were mounted on the pedestal. The feedback for vertical loading was generated from 2 three-axis load cells located between the two thick plates (i.e. underneath the bearing). The rotational angle of the loading beam was controlled/measured using string potentiometers, which were connected to each actuator. High precision laser transducers, which were attached to each of the four corners of the upper platen, were used to measure the vertical bearing deformations.

4.3.3. Organization of the Test Program

A series of testing were conducted on the bearing specimens in accordance with the procedures outlined in ISO-22762 (ISO 2010). The main objective of this study was to investigate the behaviour of fiber reinforced elastomeric bearing under different loading scenarios that are expected to occur over the lifetime of a bridge. The three major parameters varied in this test program were the vertical load, lateral offset, and rotation angle.

The vertical testing was conducted in four phases. For each phase, the bearings were subjected to five different vertical loads (P), which resulted in average vertical stress values of (σ_v) of 2, 4, 6, 8, and 10 MPa on the bearings under pure compression. The first phase investigated the effect of different levels of vertical load, the second phase investigated the effect of lateral offset, the third phase investigated the influence of static rotation, and the fourth investigated the rotational response of the bearings under cyclic rotation.

During the first three phases of vertical testing the bearings were monotonically loaded under load control to the target vertical load level (P). Subsequently, a vertical load consisting of three full cycles at amplitude of $\pm 20\% P$ at a rate of 0.2 Hz was applied. The lateral offset and static rotation (i.e. phase 2 and 3) were applied to the specimen after applying the vertical load, P , but prior to cycling the load vertically on the specimen. For the last phase, the bearings were subjected to nine rotational cycles, 3 cycles at each of the 3 rotational amplitudes under a constant vertical applied load. The experimental results of each testing phase will be covered in the following sections.

It is worth noting that very few studies focusing on the effects of rotation have been reported in the literature due to the anticipated cost and challenges associated with the design, development, and construction of a suitable test apparatus (Stanton et al. 2007).

4.4. Experimental Results

4.4.1. Phase 1: The effect of axial load on vertical response

One of the main functions of bearings is to support and transmit the vertical loads from the superstructure to the substructure, without altering the elevation of the bridge slab. The bearings must be able to support the expected vertical loads, the most prevalent of these being permanent dead loads (e.g. superstructure components, pavement, and railings) as well as live loads related

to the movement of vehicles and pedestrians. Accordingly, bridge design codes set limits for the maximum design vertical loads depending on the type of the bearing and the expected rotational and lateral deformations. Often a minimum vertical load limit is also specified in an effort to prevent adverse effects, such as bearing slippage, which may occur under low vertical load with/without excessive horizontal or rotational deformation (IRICEN 2006).

The primary objective of this section is to investigate the influence of vertical load on the vertical response of bearings. This was accomplished through the application of different levels of vertical load to the bearings. The vertical load levels applied during this phase were 9.8, 19.6, 29.4, 39.2, and 49 kN. The loading procedure followed during this phase is shown in Fig. 4-4. The vertical load (P) – vertical displacement (Δ_v) response curves for Bearing 1 are shown in Fig. 4-5. As anticipated, the bearings experienced a degree of run-in prior to the full development of the vertical stiffness (K_v). Run-in, which does not occur in steel reinforced elastomeric isolators (SREI), is present until the individual fibers become straight and taut under the applied vertical load (Kelly 2008). It is recognized that run-in effects are not expected to occur in the SREI.

Figure 4-6 shows the vertical hysteresis loops recorded for Bearing 1 during the vertical cyclic loading. It can be observed that the bearing exhibits some residual strains after the first cycle. It is postulated that this residual strain is due to stress relaxation (i.e. softening) associated with the elastomer layers and breakage of links within elastomer material under repeated loading (referred to as the Mullins effect) (Marckmanna 2002). The virgin properties of the bearing before experiencing any loading are known as unscragged properties. It should be noted that scragging has been observed to occur under both vertical and lateral loading/deformation (Toopchi-Nezhad et al. 2008b).

The influence of vertical load on vertical stiffness can be observed from Figure 4-7a, which presents the average stiffness determined at the third cycle (i.e. scragged stiffness) for all four bearings along with the corresponding standard deviation. The primary mechanical properties of interest evaluated during each phase are the vertical stiffness and vertical damping. The vertical stiffness was determined from the maximum and minimum vertical forces ($F_{v,max}$ and $F_{v,min}$) and displacements ($\Delta_{v,max}$ and $\Delta_{v,min}$) observed over the vertical hysteresis loop corresponding to the third cycle (i.e. scragged cycle), and was calculated as follows (ISO 2010)

$$K_v = \frac{F_{v,max} - F_{v,min}}{\Delta_{v,max} - \Delta_{v,min}} \quad (1)$$

The low standard deviation values at each load level, which can be observed in Fig. 4-7a, indicate the measured vertical stiffness for all bearings were in excellent agreement. This was expected as all bearing specimens were cut from the same pad. Accordingly, the average value of all four bearings will be used throughout this study to represent the results due to the negligible relative error between them. According to Fig. 4-7a, the value of the vertical stiffness for the bearings has an almost linear dependency on the value of applied load (i.e. vertical stiffness). Increasing the load by a factor of 5 from 9.6 kN to 49 kN led to an increase in vertical stiffness by factor of approximately 2. The increase in vertical stiffness is anticipated to be beneficial in resisting larger severe loads. The nonlinear vertical stiffness behaviour of the bearings is primarily due to the nonlinearity properties of the elastomer (Pouriayevali 2011).

In addition, the corresponding vertical vibrational frequencies was calculated using the following relation

$$f_v = \frac{1}{2\pi} \sqrt{\frac{K_v g}{P A}} \quad (2)$$

where g is the gravitational acceleration and A is the isolator plan area. Using Eq. 2, the vertical frequencies were found to range from 17 to 29 Hz, which is considered to be satisfactory for isolation applications. Figure 4-7b shows the calculated vertical damping values, which were found to range from 1.0% to 1.4%, depending on the amplitude of the axially applied load. The vertical damping ratio was calculated as follow

$$\zeta_v = \frac{1}{2\pi} \left[\frac{W_D}{(|F_{v,max} - F_{v,min}| |\Delta_{v,max} - \Delta_{v,min}|)} \right] \quad (3)$$

where W_D represents the dissipated energy (area within the hysteresis loop)

4.4.2. Phase 2: The effect of lateral offset on vertical response

In addition to supporting vertical loads, bridge bearings must be able to accommodate the laterally induced motions that occur between the superstructure (deck/girder) and substructure (abutment/pier) of the bridge. Large lateral forces can develop when the relative movement between the superstructure and substructure is restrained, particularly for very wide curved and skewed bridges (AASHTO-LRFD). Lateral movement in the bridge superstructure occurs as a result of temperature change (expansion and contraction), creep and shrinkage, elastic shortening due to prestressing and traffic loading (AASHTO-LRFD). The lateral movement is limited in most bridge design codes (e.g. CAN/CSA-S6 and AASHTO-LRFD) to be less than half the total elastomer thickness (i.e. $< 0.50 t_r$) in order to prevent the occurrence of contact loss between the bearing and the contact surfaces and also to prevent delamination between elastomer layers under continuous loading (i.e. fatigue). Thus, it is important to investigate the vertical behaviour of bearings under lateral displacements up to a value of $0.50 t_r$.

The objective of this section is to investigate the influence of lateral offset on the vertical stiffness and damping of FREI. During this phase of the study the vertical behaviour was studied

under lateral offsets of 0, 0.25 and 0.50 t_r . The loading procedure followed during this phase of the study is shown in Fig 4-8. The variation of the average vertical stiffness for all four bearings, determined at the third cycle, is shown in Fig. 4-9. While the vertical hysteresis loops for the three lateral offsets measured from Bearing 1 for the 5 different levels of vertical load are shown in Fig. 4-10. It is observed from Figs. 4-9 and 4-10 that the lateral offset has no significant effect on the vertical response of the bearings. It is postulated that under lateral deformations the tautness of the fibers increases coupled with geometric nonlinearity effects mitigate the expected reduction in vertical stiffness. It should be noted that the vertical stiffness of a bonded steel reinforced isolator has been found to reduce even under small lateral displacement up to 0.5 t_r as a result on the moment induced (Warn et al. 2007).

An important design requirement is that bearing should remain stable (i.e. maintain a positive lateral tangential stiffness) over the entire lateral displacement range until full rollover occurs. Figure 4-11 presents the measured lateral force (F_L) for Bearing 1 prior to the application of the vertical cyclic load. It can be observed that the bearing exhibits a linear response and stable behaviour up to the considered lateral offset. The lateral behaviour is similar to that of a bonded isolator because of the high aspect ratio of the bearing and the relatively low applied lateral displacement amplitude. However, nonlinear softening is expected to occur at higher displacements (i.e. $> 0.50 t_r$), which are typically required in bearings when designed as seismic isolators (Van Engelen et al. 2014).

4.4.3. Phase 3: The effect of static rotation on vertical response

Rotational deflections of a bridge superstructure are an important aspect that must be considered during the design of bridge bearings (CAN/CSA-S6 2014; AASHTO-LRFD 2012). These rotations may occur due to dead loads, live traffic loads, and/or misalignment during installation.

Additionally, the bearings can be subjected to significant rotations during a particular stage of construction. For example, Roeder and Stanton (1997) indicate that the largest rotation experienced by a bridge bearing over its lifetime may occur as a result of the initial camber in a prestressed concrete girder (i.e. prior to being loaded). Although bridge design codes (e.g. CAN/CSA-S6 2014 and AASHTO-LRFD 2012) do not specify a specific maximum rotational value that can be applied to the bearing, limits are specified for the maximum shear strains within the elastomer layers of the bearing due to the imposed rotation.

This section examines the influence of static rotation on the vertical behaviour of FREI, with a particular focus on vertical stiffness. The following static rotations were imposed on the test specimens: 0, 0.01, 0.02, and 0.03 radians using the loading procedure shown in Fig. 4-12. The effect of static rotation on the vertical stiffness of the bearings is presented in Fig. 4-13. As shown, the static rotation was found to significantly decrease the vertical stiffness at lower vertical load levels (see Fig. 4-14a), due to lift-off, which occurs when there is a loss of contact between the bearing and the loading plates, resulting in a reduction in the vertically loaded area (see Fig. 4-1). The lift-off leads to an increase in the compressive stresses on the loaded side of the bearing (where contact is maintained), while on the unloaded side (where there is a loss of contact) the stresses are significantly reduce. However, under the application of higher vertical load no significant change was observed in the values of vertical stiffness (see Fig. 4-14b) as lift-off is delayed or completely eliminated.

4.4.4. Phase 4: The effects of axial load and angle of rotation on rotational response

Knowing the rotational response of a bearing is important in order to determine if it can accommodate the expected level of applied rotation and to estimate the vertical load that may initiate buckling in the bearing (Kelly and Konstantinidis 2011). Accordingly, the objective of

this phase of the study is to experimentally investigate the rotational response of U-FREI. The effect of aspect ratio and shape factor on the rotational response of U-FREI, which has previously been investigated by Al-Anany and Tait (2015a&b), is beyond the scope of this study.

Three amplitudes of applied rotation were considered in the study (i.e. 0.01, 0.02, and 0.03 rad.) and were applied in a cyclic manner as shown in Fig. 4-15. The moment-rotation response curves for Bearing 1 under vertical loads of 9.8, 19.2, 29.4, 39.2, and 49 kN are presented in Fig. 4-16. It is observed that the amplitude of the vertical load applied on the bearing influences the shape of the hysteresis loops, which affects the effective rotational stiffness and damping values. The magnitude of vertical load is an important parameter, as it affects the initiation of lift-off. For example, when the vertical load is reduced from 19.2 kN to 9.8 kN a significant reduction in the rotational stiffness is observed to occur due to lift-off (see Fig. 4-17a). However, under higher vertical load levels lift-off is prevented and as a result the change in the rotational stiffness is much less. It can be observed from Fig. 4-17 that both the effective rotational stiffness (k_{θ}) and rotational damping (ζ_{θ}) are dependent upon the amplitude of the applied vertical load and angle of rotation.

4.5. Comparison of Measured and Theoretical Vertical Stiffness

This section compares the values of the vertical stiffness obtained from experimental test results with theoretical values determined using an analytical method that is based on the “pressure solution” approach. The pressure solution approach, which includes the effects of reinforcement flexibility and the rubber compressibility, has been used by Kelly and Van Engelen (2015) to derive the vertical stiffness of elastomeric bearings. The vertical stiffness (K_v) of an elastomeric isolator with a plan area (A) and composed of a number of elastomer layers with total thickness (t_r) is given by

$$K_v = \frac{E_c A}{t_r} \quad (4)$$

According to Kelly and Van Engelen (2015), the compression modulus (E_c) of a square pad can be expressed as

$$E_c = 1536 G S^2 \sum_{n=1,3,5,\dots}^{\infty} \frac{1}{\alpha^2 + \beta^2 + n^2 \pi^2} \frac{1}{n^2 \pi^2} \left(1 - \frac{\tanh(\lambda)}{\lambda}\right) \quad (5)$$

The dimensionless parameter (λ) is defined as

$$\lambda = \frac{\sqrt{\alpha^2 + \beta^2 + n^2 \pi^2}}{2} \quad (6)$$

where α represents the influence of reinforcement flexibility, and is defined as

$$\alpha^2 = \frac{384 G S^2 t_e}{E_f t_f} \quad (7)$$

and β represents the effects of rubber compressibility, and is expressed as

$$\beta^2 = \frac{192 G S^2}{K} \quad (8)$$

where E_f is the elastic modulus of the fiber, and K is the bulk modulus of the elastomer. Table 4-2 presents the material properties of the bearings. The effective shear modulus was calculated based on the experimental results of the four bearing specimens considered in the study by using the following relation

$$G = \frac{K_L t_r}{A} \quad (9)$$

Table 4-3 compares the experimentally determined values of vertical stiffness with the analytical value obtained from Eq. (4). It is observed that the analytical solution is in good agreement with the values determined experimentally under intermediate levels of vertical load (i.e. 19.6 kN). However, an overestimation is observed when compared to value at 9.8 kN, which

is postulated to be because the fibers were not yet fully straight and taut under this low vertical load level. While, the underestimation in vertical stiffness observed at higher vertical loads (i.e. 29.4, 39.2, and 49 kN) is assumed to be due to nonlinearity in both material (nonlinear behaviour of rubber shear modulus) and geometry (change in elastomer layers thickness). Good agreement is observed between the experimental results and analytical solution at lower design limits of most bridge design codes. Also, since the vertical stiffness increases with increased applied load, this implies that analytical solutions can be sufficiently used for a preliminary estimation/design of the vertical stiffness of U-FREI

4.6. Conclusion

A series of vertical and rotational testing had been performed on quarter scale unbonded Fiber reinforced elastomeric isolators (U-FREI) using a 3 DOF bearing test apparatus. The main objective of the study was to investigate the viability of using U-FREI as bridge bearings. Accordingly, the test program included different vertical load levels, lateral offsets and static rotations expected to occur during the lifetime of a bridge. The main conclusions that can be drawn from this study for the considered FREI are:

- 1- An increase in the applied vertical load level resulted in an increase in the vertical stiffness and rotational stiffness, but a reduction in the lateral stiffness.
- 2- The lateral offsets up to 0.50 % t_r , which is the maximum considered for the design of bridge bearings, did not have a significant effect on the vertical behaviour.
- 3- The static rotations led to a reduction in vertical stiffness at lower vertical load levels due to lift-off. However, static rotations were not observed to have a significant effect on the vertical stiffness under higher vertical load levels.

- 4- Results indicate that bearings can accommodate rotations induced by the bridge deck/girder as they exhibited a stable rotational response during rotational cyclic testing.
- 5- Good agreement was found between the experimental results and the analytical solution, particularly at vertical loads corresponding to lower boundaries in bridge design codes.

Further experimental studies are required to investigate the influence of parameters such as the shape factor and aspect ratio on the response of U-FREI.

Acknowledgements

Financial support from the Natural Sciences and Engineering Research Council (NSERC) of Canada is gratefully acknowledged. Support was also provided by the McMaster University Centre for Effective Design of Structures (CEDs) funded through the Ontario Research and Development Challenge Fund (ORDCF).

References

- Al-Anany Y., Tait M. (2015a). A Study on the Rotational Behaviour of Bonded and Unbonded Fiber Reinforced Elastomeric Isolators, *11th Canadian Conference on Earthquake Engineering*, Victoria, British Columbia, Canada, 21-24 July 2015.
- Al-Anany Y., Tait M. (2015b). "A numerical study on the compressive and rotational behavior of fiber reinforced elastomeric isolators (FREI)" *Composite Structures*: 133: 1249-1266.
- AASHTO. (2012). *American Association of State Highway and Transportation Officials. LRFD Bridge Design Specifications*, Washington, D.C.

- ASCE. American Society of Civil Engineers. (2010). *Minimum Design Loads for Buildings and other Structures*, ASCE/SEI 7-10. New York.
- ASTM. (2010). The American Society for Testing and Material. *Standard Test Method for Rubber Property-Durometer Hardness*. ASTM D2240. The American Society for Testing and Material.
- CAN/CSA-S6-06. (2014). *Canadian Highway Bridge Design Code*. Canadian Standard Association, Ontario.
- Caltrans. (1994). *Bridge Memo to Designers. Section 7: Bridge Bearings*. California Department of Transportation, Sacramento, California.
- IRICEN. (2006). *Indians Railways Institute of Civil Engineering*. Bridge Bearings. M. R. & Co.
- ISO. (2010). *Elastomeric seismic-protection isolators*. ISO 22762, Geneva.
- Kelly J. (1999). "Analysis of fiber-reinforced elastomeric isolators", *Journal of Seismology and Earthquake Engineering*; 2(1): 19–34.
- Kelly J. (2002). "Seismic isolation systems for developing countries", *Earthquake Spectra*; 18(3): 385–406.
- Kelly J. and Konstantinidis D. (2007). "Low-cost seismic isolators for housing in highly-seismic developing countries." *10th World Conference on Seismic Isolation, Energy Dissipation and Active Vibrations Control of Structures*, Istanbul, Turkey, May 28-31.
- Kelly J., Konstantinidis D. (2011). *Mechanics of rubber bearings for seismic and vibration isolation*. Chichester, UK: Wiley.
- Kelly J., Van Engelen N. (2015). *Single Series Solution for the Rectangular Fiber-Reinforced Elastomeric Isolator Compression Modulus*. Pacific Earthquake Engineering Research Center, PEER, Berkeley, California; 2015/03.

Lee D. (1994). *Bridge Bearings and Expansion Joints*, E & FN Spon, London, UK.

Marckmann G., Verron E., Gornet L., Chagnon G., Charrier P., Fort P. (2002), “A theory of network alteration for the Mullins effect”, *Journal of the Mechanics and Physics of Solids*; 50 (9): 2011-2028.

Moon B., Kang G., Kang B., Kelly J. (2002). “Design and manufacturing of fiber reinforced elastomeric isolator for seismic isolation”, *Journal of Materials Processing Technology*; 130(131): 145–150.

Mordini A, Strauss A. (2008). “An innovative earthquake isolation system using fibre reinforced rubber bearings”, *Engineering Structures*; 30(10): 2739–51.

Mori A., Moss P., Cooke N., Carr A. (1999). “The Behavior of Bearings Used for Seismic Isolation under Rotation and Axial Load”, *Earthquake Spectra*; 15(2): 225–44.

MTO. OPSS 1202 (2008). *Material Specification for Bearings – Elastomeric Plain and Steel Laminated*. Ontario Ministry of Transportation, Toronto, Ontario.

Muscarella J., Yura J. (1995). *An Experimental Study of Elastomeric Bridge Bearings with Design Recommendations*. Research Report No. 1304-3, Center for Transportation Research, Bureau of Engineering Research, The University of Texas at Austin, Austin, TX.

Pouriyaveali H., Guo Y., Shim V. (2011). “A visco-hyperelastic constitutive description of elastomer behaviour at high strain rates”, *Procedia Engineering*; 10: 2274–2279.

Ramberger G. (2002). *Structural Bearings and Expansion Joints for Bridges*. International Association for Bridges and Structural Engineering. IABSE, Zurich, Switzerland.

Roeder C., Stanton J. (1997). *Steel Bridge Bearing Selection and Design Guide*. National Steel Bridge Alliance, Highway Structures Design Handbook, Vol. II, Ch 4, AISI, Washington DC.

- Stanton J., Roeder C., Mackenzie-Helnwein P., White C., Kuester C., Craig B. (2007). *Rotation Limits for Elastomeric Bearings*. Report No. NCHRP 596, Transportation Research Board, National Cooperative Highway Research Program, Washington, D.C.
- Toopchi-Nezhad H., Tait M., Drysdale R. (2008a). “Testing and modeling of square carbon fiber reinforced elastomeric seismic isolators”, *Structure Control Health Monitoring*; 15(6): 876–900.
- Toopchi-Nezhad H., Tait M., Drysdale R. (2008b). “Lateral Response Evaluation of Fiber-Reinforced Neoprene Seismic Isolators Utilized in an Unbonded Application”, *Journal of Structural Engineering*; 134(10): 1627-1637.
- Tsai H., Kelly J. (2011) Stiffness analysis of fiber-reinforced elastomeric isolators. Pacific Earthquake Engineering Research Center, PEER, Berkeley, California; 2001/5.
- Van Engelen, N., Tait, M., Konstantinidis, D. (2014). “Model of the Shear Behavior of Unbonded Fiber-Reinforced Elastomeric Isolators”, *Journal of Structural Engineering*; 144(7): 04014169.
- Warn G., Whittaker A., Constantinou M. (2007). “Vertical Stiffness of Elastomeric and Lead–Rubber Seismic Isolation Bearings”, *Journal of Structural Engineering*; 133(9): 1227–1236.

Table 4-1: Test specimen specifications

	Value (mm)
Width (a)	70
Length ($2b$)	70
Total Bearing Height (h)	20.6
Total Thickness of Intermediate Elastomer Layers (t_{eff})	15.9
Aspect Ratio ($2b / h$)	3.4
Effective Aspect Ratio ($2b / t_{eff}$)	4.4
Shape Factor (S)	5.5

Table 4-2: Material properties of the bearings

Elastomer	Fiber
Shear Modulus (G) = 0.86 MPa	Elastic Modulus (E_f) = 20 GPa
Bulk Modulus (K) = 2000 MPa	Poisson's ratio (ν_f) = 0.20

Table 4-3: Comparison of the experimental results with the analytical solution

Axial Load (kN)	<u>K_V (kN/mm)</u>		
	Experimental	Analytical	Error (%)
9.8	31.2		29.81
19.6	39.7		2.02
29.4	45.9	40.5	-11.76
39.2	51.3		-21.05
49.0	58.9		-31.24

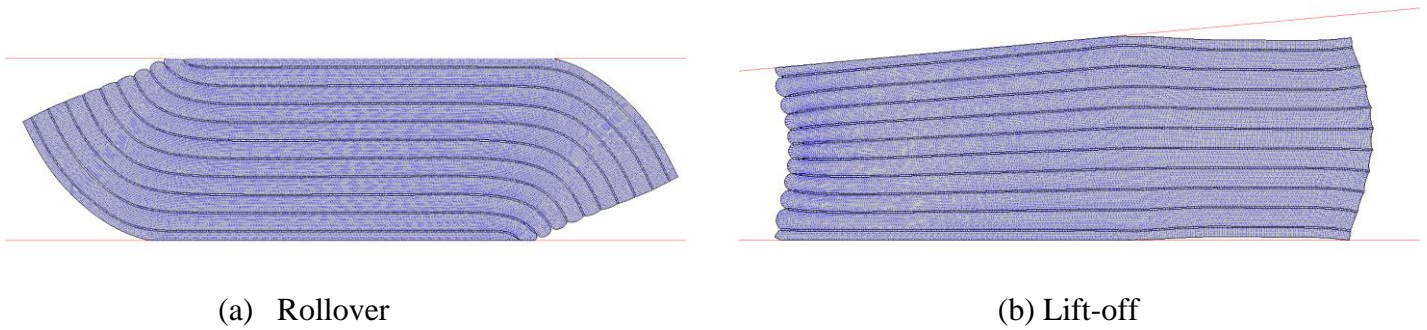
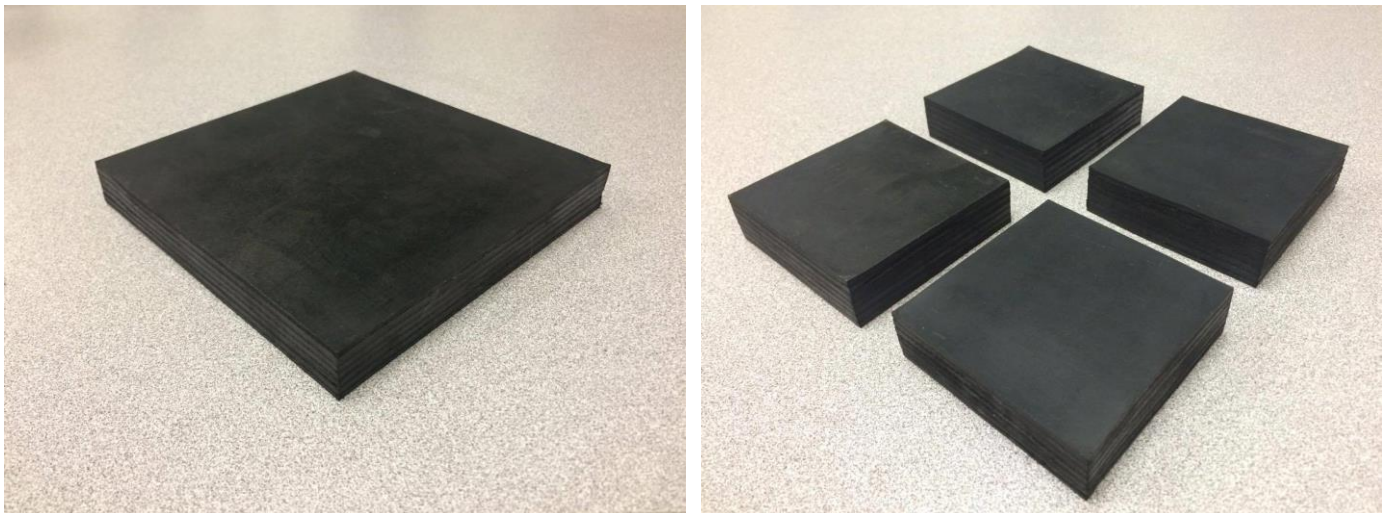


Fig. 4-1: (a) Lateral and (b) rotational deformation patterns of U-FREI



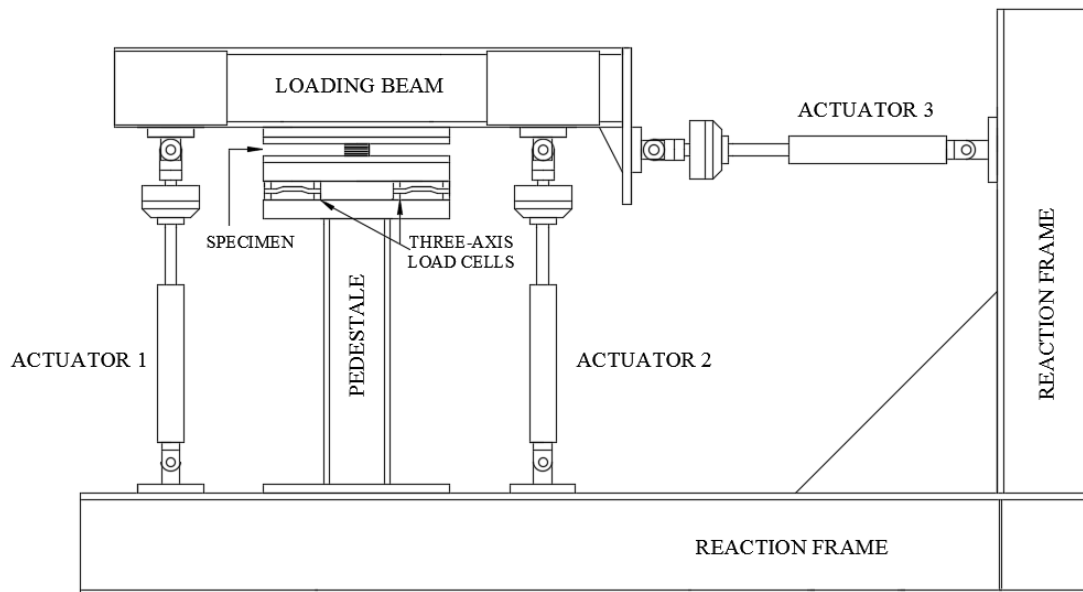
(a) FREI pad

(b) Individual U-FREI specimens

Fig. 4-2: U-FREI specimens tested in the study



(a)



(b)

Fig. 4-3: The 3 DOF test apparatus: (a) photograph; (b) schematic

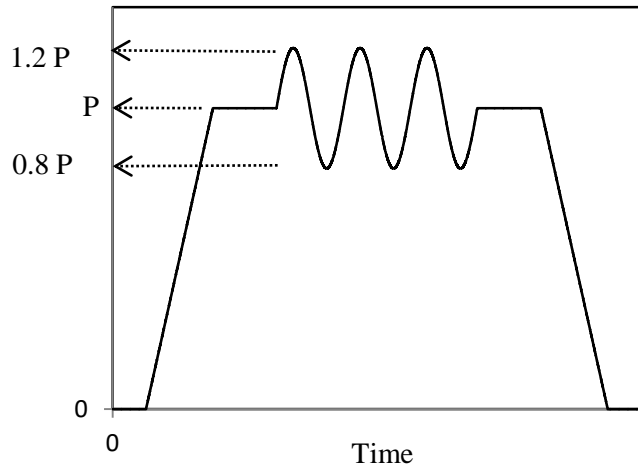


Fig. 4-4: Applied vertical load time history for phase 1

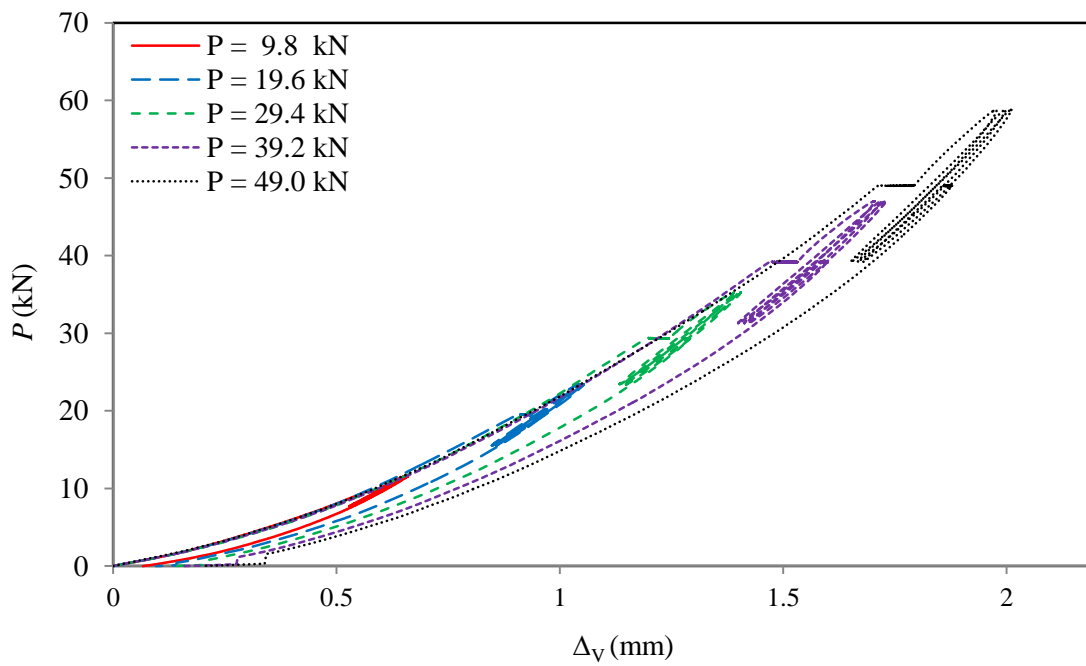


Fig. 4-5: Vertical compressive load (P) versus vertical displacement (Δ_v) response curves for Bearing 1

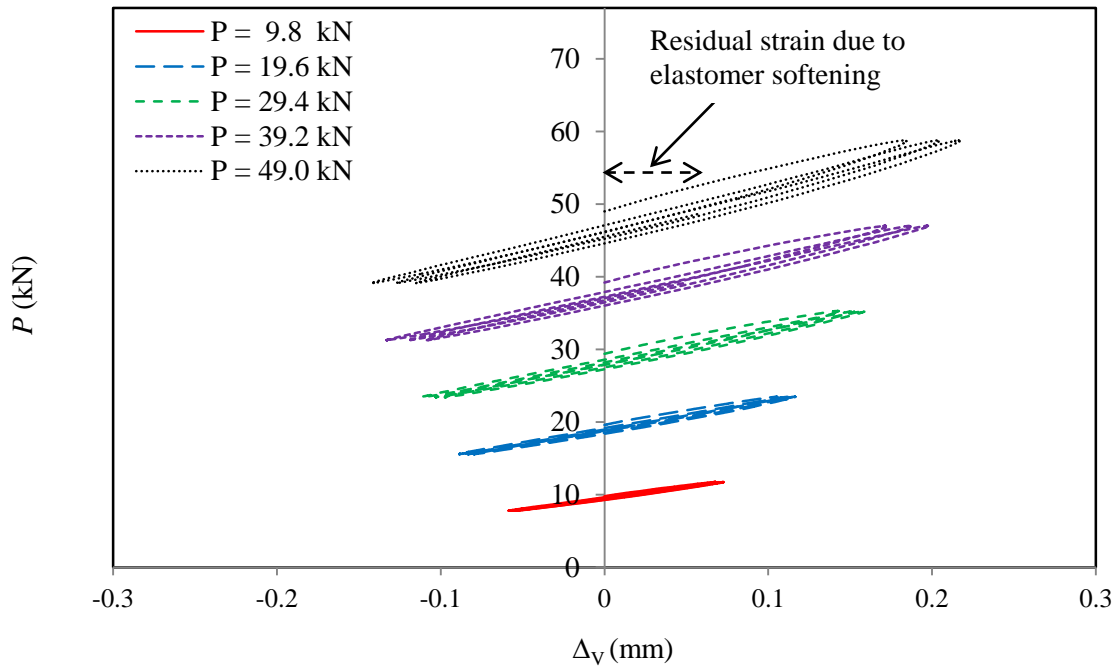


Fig. 4-6: Vertical hysteresis loops for Bearing 1 under different axial loads

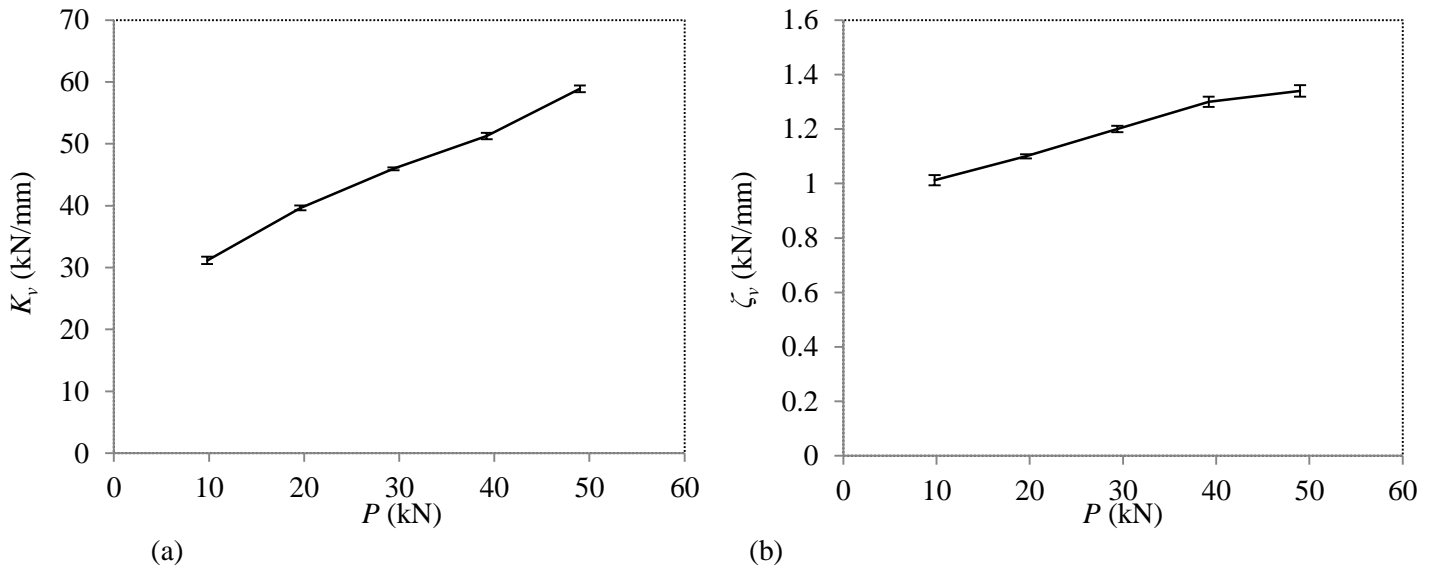


Fig. 4-7: Influence of applied vertical load on the: (a) vertical stiffness; (b) vertical damping

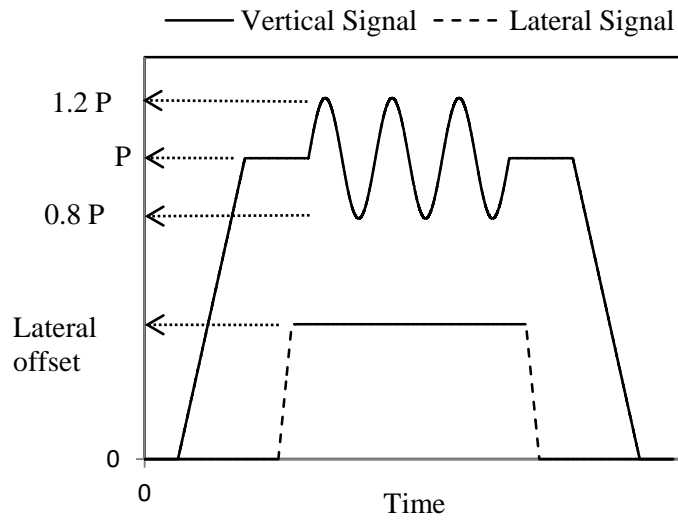


Fig. 4-8: Applied vertical and lateral load time histories for phase 2

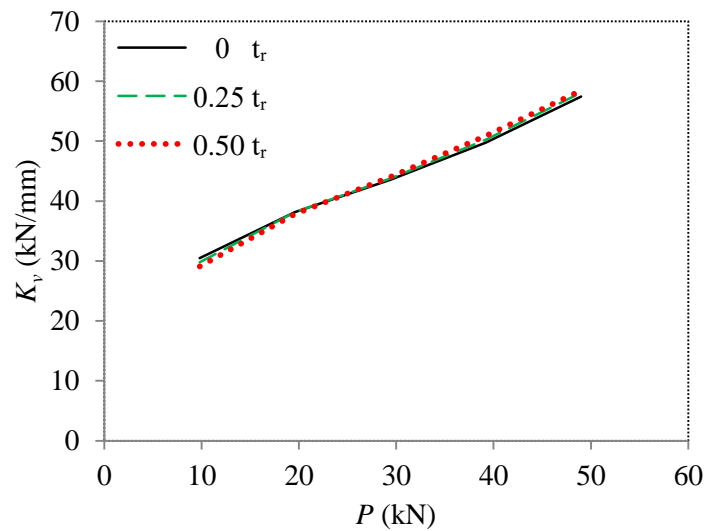
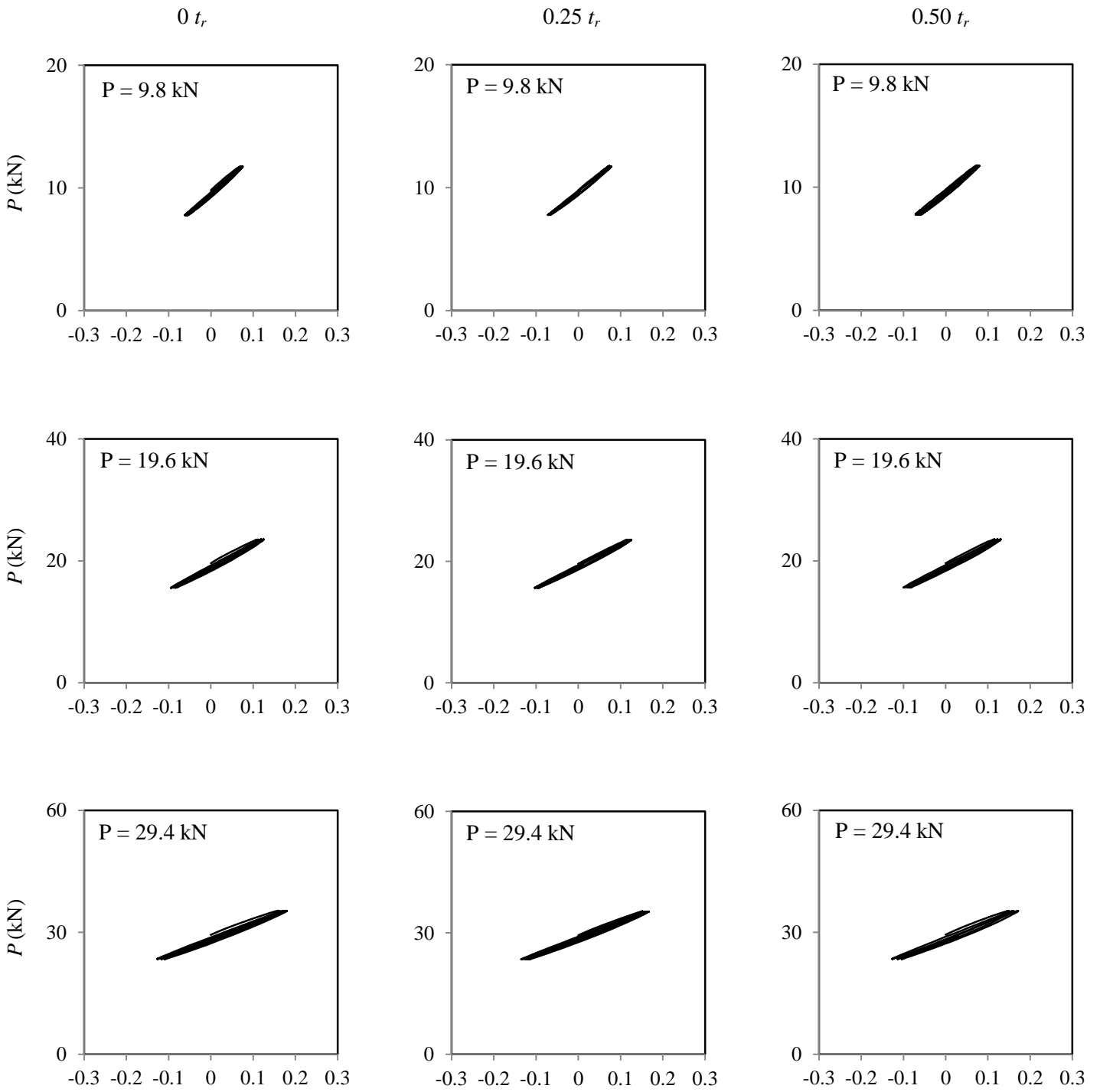


Fig. 4-9: Influence of lateral offset on the vertical stiffness



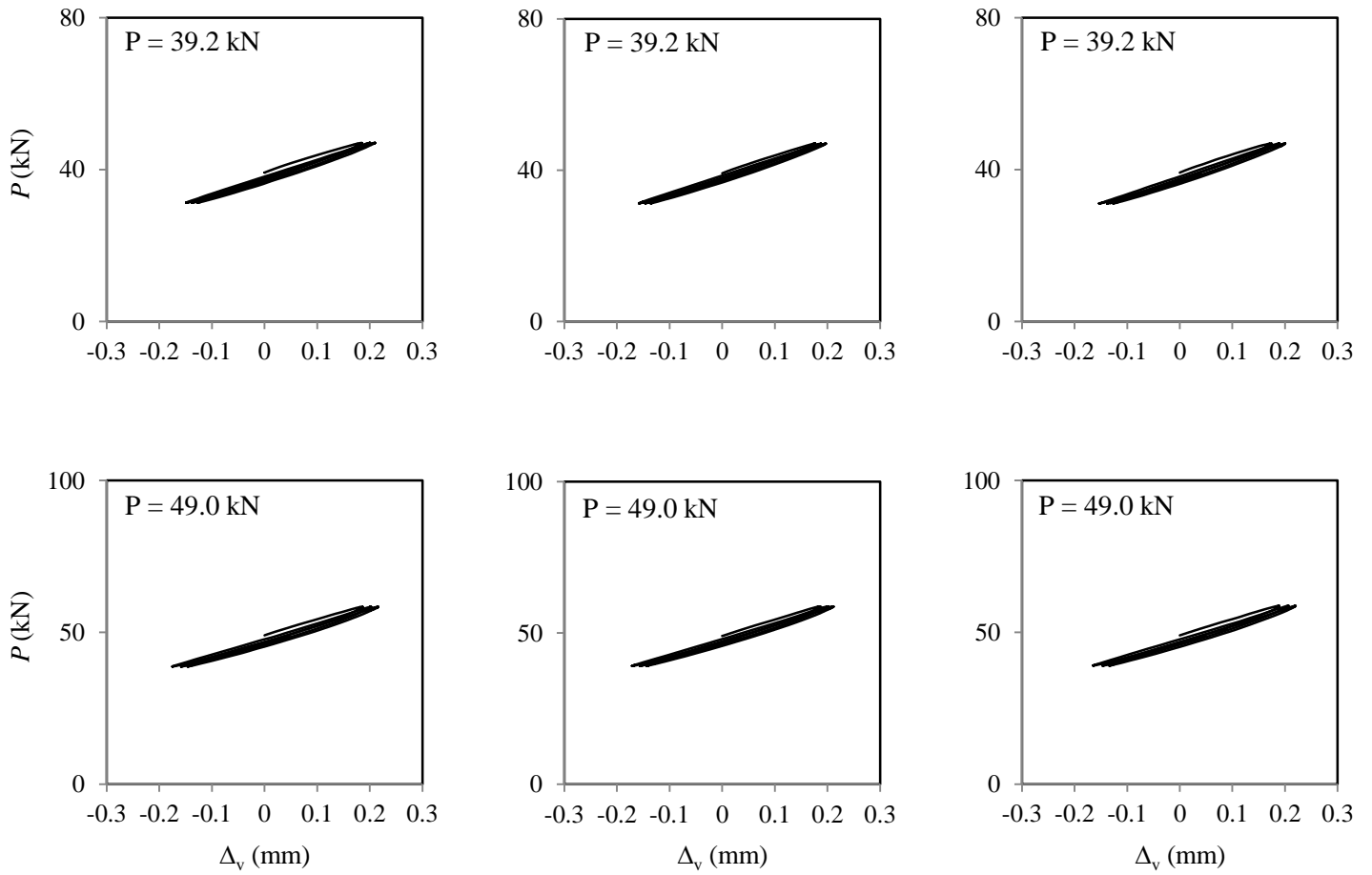


Fig. 4-10: Vertical hysteresis loops for Bearing 1 corresponding to different vertical loads and lateral offsets

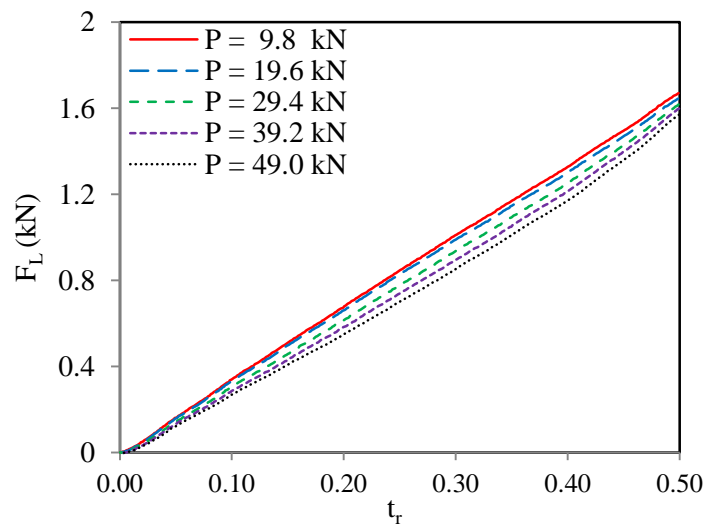


Fig. 4-11: Lateral response of Bearing 1 up to lateral displacement amplitude of $0.50 t_r$

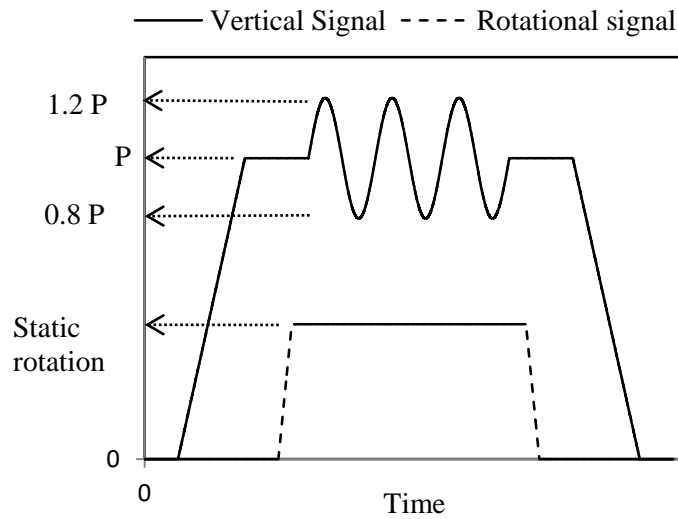


Fig. 4-12: Applied vertical and lateral load time histories for phase 3

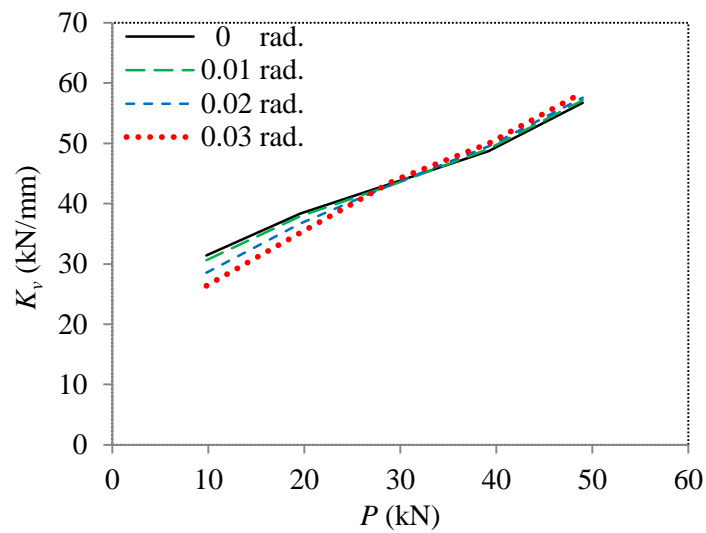


Fig. 4-13: Influence of static rotation on the vertical stiffness

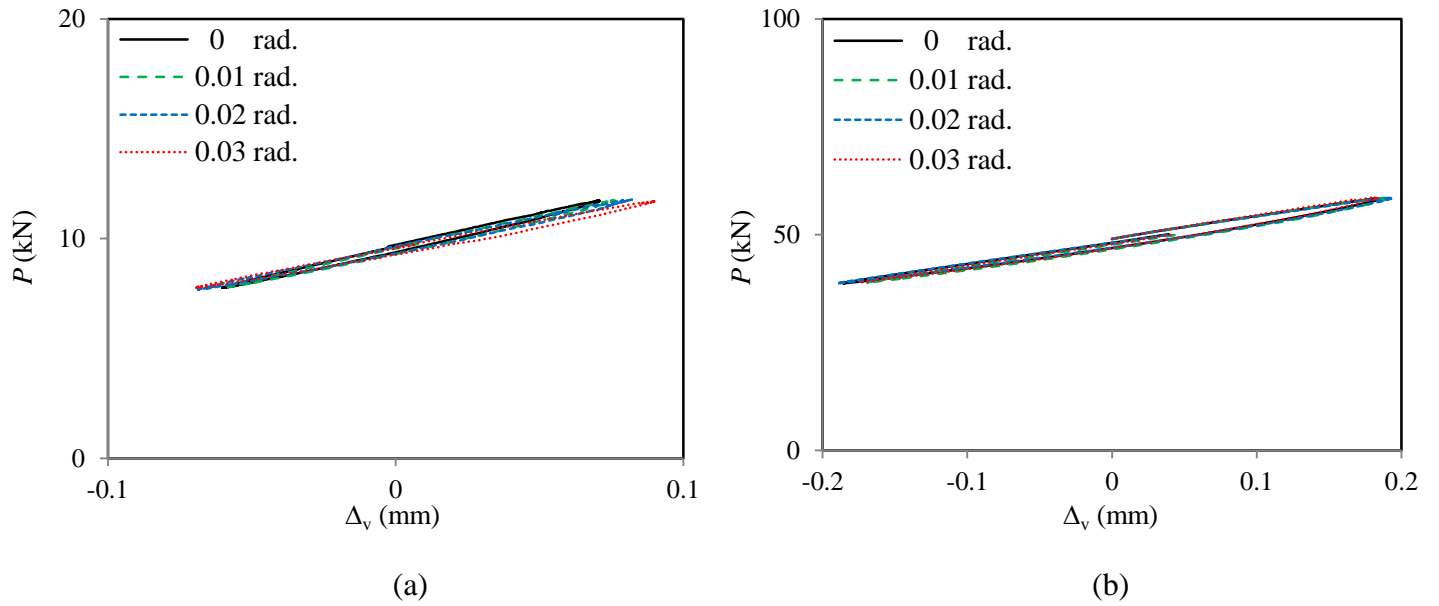


Fig. 4-14: Vertical hysteresis loops for Bearing 1 corresponding to different static rotations under a (a) 9.8kN and (b) 49kN vertical loads

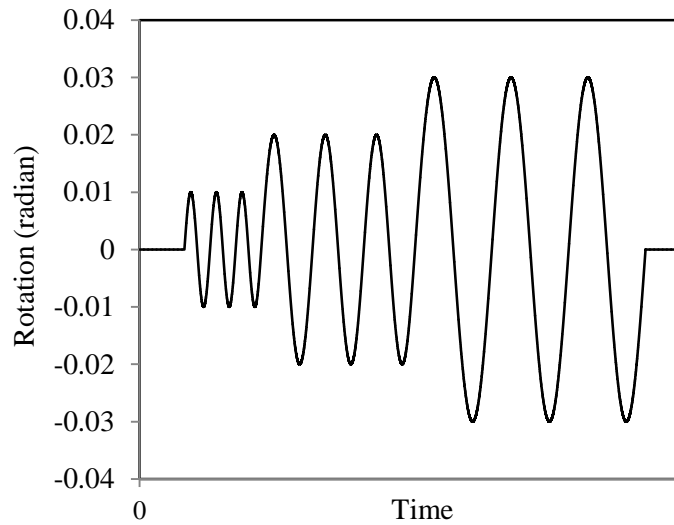
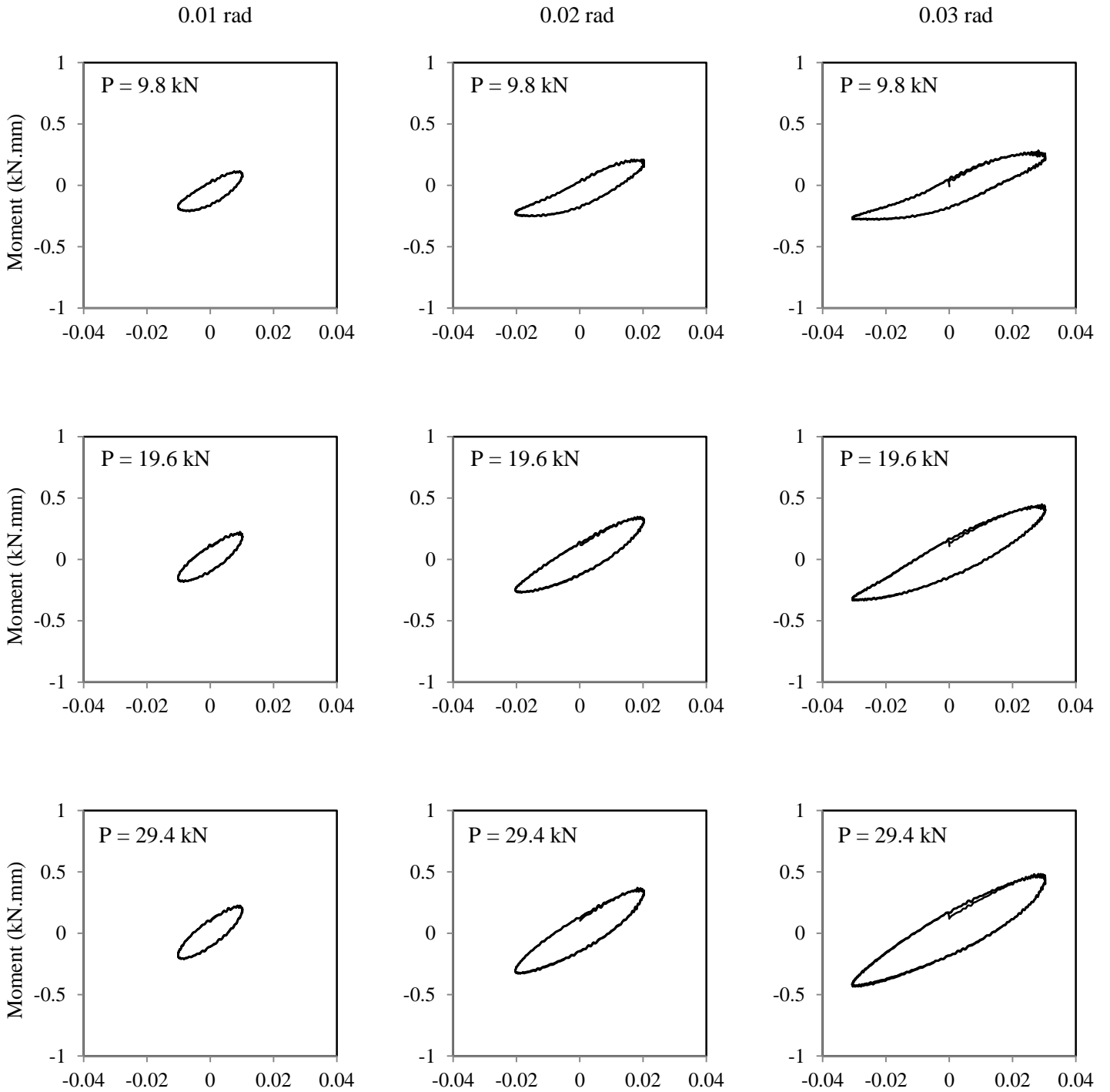


Fig. 4-15: Applied rotational loading time history for phase 4



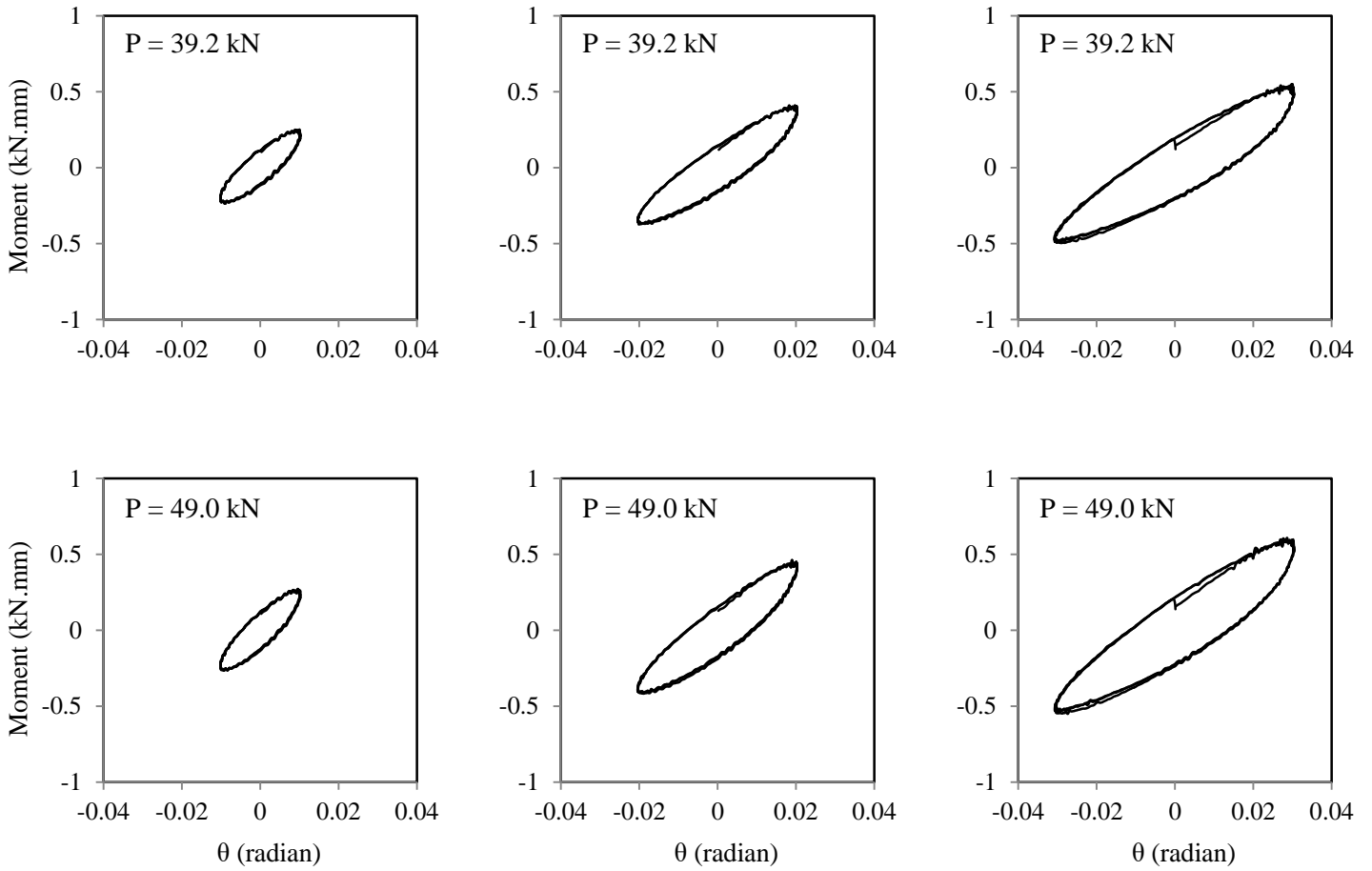


Fig. 4-16: Moment-rotation response for Bearing 1

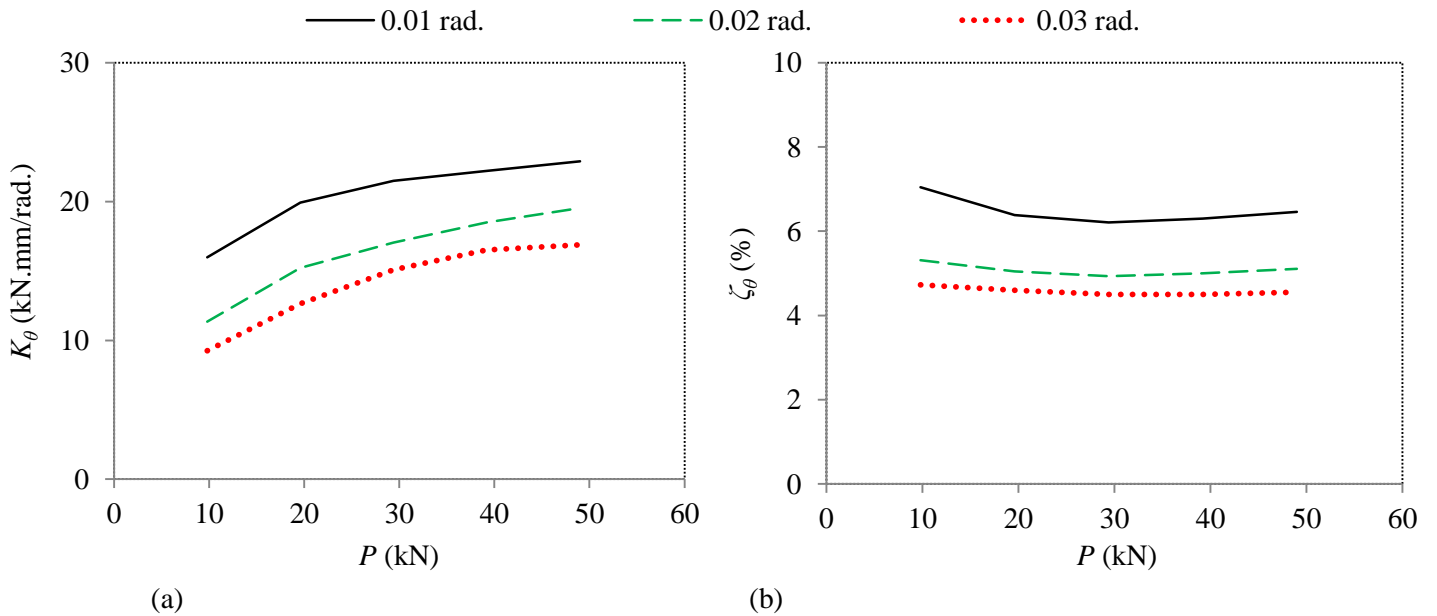


Fig. 4-17: Influence of axial load and angle of rotation on the (a) rotational stiffness; (b) rotational damping (graphs represent the determined values at the third cycle)

Chapter FIVE

Fiber Reinforced Elastomeric Isolators for the Seismic Isolation of Bridges

Abstract

Unbonded-fiber reinforced elastomeric isolators (U-FREI) have been proposed as a viable alternative to traditional steel reinforced elastomeric isolators (SREI) for use in low-rise building base isolation systems. The viability of U-FREI for this particular application was confirmed through an extensive evaluation of their lateral response under the condition of no rotational deformations of the loading supports. In order to extend the use of U-FREI to bridge applications the consideration of rotational deformation in the analysis is necessary as it is an important component in bridge isolator design. Currently, no data exists in the literature for investigating the influence of rotational deformation on the lateral response of U-FREI, to the best of authors' knowledge. Accordingly, an experimental and numerical study was completed on U-FREI to investigate their lateral behaviour under a range of vertical loads and rotational deformations in order to determine their suitability as a seismic isolator for bridges. The lateral stiffness and damping were computed experimentally for different levels of vertical pressure, angles of rotations and lateral deformations. Additionally, the resulting stress and strain state within the isolators under peak deformations was also evaluated numerically via 3D modeling and presented in this study.

5.1. Introduction

Earthquakes are one of the most devastating types of natural disasters, which often result in loss of life, a large number of structural failures, and significant socio-economic costs. As it is not possible to prevent earthquakes from occurring, designers must focus on mitigating their effects. This can be accomplished by either increasing the capacity/ductility of the structure or decreasing the seismic demand placed on the structure. While increasing the capacity/ductility of a structure has traditionally been the approach employed, it is not always the most effective (Jangid 2004). Alternatively, decreasing the seismic demand placed on the structure can be achieved through base isolation, and is considered to be one of the most effective methods to reduce seismic induced damage (Naeim and Kelly 1999).

Base isolation in bridge applications can be achieved by introducing low lateral stiffness elements, which are able to adequately support the vertical loads, between the superstructure (i.e. deck/girder) and substructure (i.e. pier/ abutments) as shown in Fig. 5-1. When these flexible elements are used to accommodate non-seismic induced rotations and lateral deformations experienced by the girders, they are typically referred to as bearings. However, they are often referred to as isolators when employed to reduce and redistribute seismic induced lateral forces (i.e. base isolation). Their low lateral stiffness shifts the period of the structure into the displacement sensitive region, where the resulting inertial forces are significantly reduced. This results in a reduction in the seismic demand on the structural elements.

The loading demands on bridge bearings have increased due to continued developments in bridge design, such as the introduction of frames with much larger spans and innovative forms (ex. curved and skewed girders) (Caltrans 1994). In order to handle this increase, improvements to existing bearing types and the development of new bearings types are needed. Consequently,

recent research efforts have focused on replacing conventional isolators with more innovative types that can accommodate larger loads and deformations (Konstantinidis et al. 2008).

There are two primary types of seismic isolators: (1) sliding, and (2) elastomeric (Kunde and Jangid 2006). The sliding isolation system is based on the transmission of lower shear forces to the structure through a medium with a low friction coefficient that is placed between the structure and its foundation. Sliding isolators are typically either pure friction isolators or friction pendulum isolators (Girish and Pranesh 2013). Elastomeric isolators, which have the combination of high stiffness in the vertical direction as well as rotational and horizontal flexibility, are among the most widely used type of seismic isolator. Elastomeric isolators are reinforced with steel plates, which result in a high vertical stiffness by limiting the bulging in elastomer layers. They are typically divided into three isolator types: low-damping natural rubber (LDR) isolators, lead-plug rubber (LPR) isolators and high-damping natural rubber (HDR) isolators (Naeim and Kelly 1999).

A significant amount of research had been carried out to investigate the effectiveness of the aforementioned isolators (i.e. sliding and elastomeric) for the seismic isolation of bridges. Tsopeles et al. (1988(a&b)) investigated the ability of sliding isolation systems to significantly reduce the seismic force transmitted to a bridge during a seismic event. Ghobarah and Ali (1988) studied the effectiveness of LPR isolators for the seismic isolation of a typical three span highway bridge. Wesolowsky and Wilson (2003) showed that isolators can decrease the accelerations and forces in cable-stayed bridges, which usually exhibit long natural periods due to their flexible cable-superstructure systems. Matsagar and Jangid (2006) conducted a comparative numerical study on the seismic response of bridges isolated by friction pendulum, LDR and LPR isolators, and it was found that the seismic response of base-isolated bridges was

highly influenced by the type and properties of the isolator employed. Jangid (2004) evaluated the effect of using LPR isolators on the bidirectional seismic behaviour of bridges, and it was noted that neglecting the bidirectional interaction of LRP isolator restoring forces would result an underestimation in the isolator displacements.

5.2. Background

When fiber is used as the reinforcement for elastomeric isolators as a replacement for steel, the isolators are called Fiber Reinforced Elastomeric Isolators (FREI). FREI have potential advantages over traditional steel reinforced elastomeric isolators, including reduced manufacturing costs (Konstantinidis and Kelly 2012), increased corrosion resistance, and lower stress demand on the bond between the reinforcement and elastomer (Toopchi-Nezhad et al. 2008 (a&b)). Moreover, in addition to the intrinsic damping of the elastomer, another source of energy dissipation is also provided via the interaction between the individual fibers within the fiber reinforcement layers (Toopchi-Nezhad et al. 2009 (a&b)).

Fiber reinforced elastomeric isolators can be unbonded (U-FREI), partially bonded (PB-FREI) or bonded (B-FREI) to both the superstructure and substructure. The variation in the deformation patterns between the bonded and unbonded isolator types can be observed in Figs.5-2 and 3. An unbonded isolator experiences *rollover* when displaced laterally (see Fig. 5-2a), and *lift off* under excessive rotational deformations (see Fig. 5-2b). These deformation patterns (i.e. rollover and lift off) occur due to the lack of flexural rigidity provided by the fiber fabric reinforcement and also because of the unbonded boundary conditions. It can be observed from Fig. 5-3 that different deformation patterns occur if the isolator is bonded to the upper and lower platens. In general, unbonded isolators possess unique advantages over traditional bonded

isolators under large lateral deformations (Toopchi-Nezhad et al. 2011) and large rotational deformations (Al-Anany and Tait 2015 (a&b)), such as:

- i- Higher seismic isolation efficiency due to the significant reduction in lateral stiffness due to lateral rollover.
- ii- Lower compressive stress demand on elastomer material as well as lower tensile stress demand on the fiber reinforcement.
- iii- Reduced peeling stress demand on the bond between rubber and the fiber reinforcement layers as a result of the significant reduction in the shear strain demand.

A recent experimental research study by Al-Anany and Tait (2016a) found that U-FREI are capable of resisting large vertical loads and can accommodate lateral and rotational deformations under different loading scenarios that a bridge bearing is expected to experience over its design lifespan. Furthermore, no damage/delamination of the isolators was observed during the experimental study. However, the influence of rotational loads/deformations on the lateral response of U-FREI has not been investigated to date. The behaviour of U-FREI under such combined deformations must be determined in order to extend its utilizations to the seismic isolation of bridges. As such, the objective of this study is to investigate the lateral behaviour of U-FREI under a range of different rotational deformation amplitudes and vertical loads. The first section of this paper reports on the experimentally evaluated lateral response of U-FREI both with and without rotational deformations, including the effects of vertical loads and isolator aspect ratio. The second section describes the findings from a three-dimensional finite element (FE) analysis, including the resulting stress and strain state of the experimentally tested isolators.

5.3. Experimental Program

5.3.1. Isolators specimens

A total of three quarter-scale U-FREI test specimens, having different geometric properties as shown in Table 5-1, were constructed and tested in the Applied Dynamics Laboratory (ADL) at McMaster University. Each specimen consisted of layers of natural rubber elastomer reinforced with bi-directional plain weave carbon fiber fabric. The intermediate elastomer layers had a thickness that was twice as large as the outer most elastomeric layers, which served as the top and bottom covers. All three isolators were cut from a single fiber-reinforced elastomeric pad with dimensions of $140 \times 140 \times 20.6$ mm (shown in Fig. 5-4).

In general, the behaviour of a U-FREI is predominantly influenced by its shape factor, S , and aspect ratio, AR . Both of these parameters must be properly selected in order to attain sufficient vertical and rotational stiffness (Al-Anany and Tait 2015 (a&b)) and maintain a stable response under different levels of lateral deformation (Toopchi-Nezhad et al. 2008 (a&b)). The aspect ratio, which has a significant effect on the lateral response of a U-FREI, is defined as ratio between the total length/width and the total thickness of the isolator. The shape factor, which is the dominant parameter affecting the vertical response, is defined as the ratio between loaded area and the area free to bulge. The in plane dimension (direction of lateral testing) was varied, as shown in Table 5-1, in order to investigate the behaviour of U-FREI having aspect ratios of 2.5, 3.5, and 4.5. In addition, the out of plane dimension of all three isolators were also varied in order to maintain a constant shape factor value of 6.0. A shape factor of 6.0 falls within the range of typical values used in bridges applications (i.e. $3 < S < 8$) (Stanton et al. 2007).

5.3.2. Test Apparatus

A three-degree of freedom test apparatus was used to carry out the experimental testing, as shown in Fig. 5-5. The main components of the test apparatus include the loading beam, pedestal, and reaction frame as shown in Fig. 5-6. Three hydraulic actuators (2 vertical + 1 lateral), denoted as 1, 2, and 3 (see Fig. 5-6), were used to apply vertical, rotational, and lateral deformations on the test specimen. The vertical pressure (i.e. vertical loads) was applied under load control while both the lateral and rotational deformations (i.e. angles of rotational) were applied under displacement control.

5.3.3. Test program

In order to investigate the influence of static rotation on the lateral behaviour their response under different levels of rotational deformation were studied a total of 27 experimental tests were conducted on the U-FREI specimens. The parameters varied during the application of cyclic lateral displacements were the vertical load (P) and the static rotation (θ). Different levels of vertical load were applied in order to reach corresponding mean vertical compressive stresses (ratio between vertical load and the isolator plan area), σ_v , of 2.0, 6.0, and 10.0 MPa under pure compression. The values of applied static rotations were 0, 0.015, 0.03 radians.

The loading procedure used in this part of the study is shown in Fig. 5-7. The isolator was first loaded monotonically up to the target vertical load level. The top-loading beam was then rotated until the required value of static rotation was reached. Next, a total of 12 lateral cycles representing four different lateral amplitudes of magnitude 0.25, 0.50, 1.00, and 1.50 t_r were applied at a lateral loading rate of 76 mm/s. Finally, the isolator was unloaded (monotonically) and the isolator was removed from test apparatus and visually inspected for damage.

5.4. Experimental Program - Results and Discussion

Figure 5-8 shows the lateral load-displacement response (hysteresis loops) of the isolators under different vertical pressures and applied rotations. The loops are normalized per unit width of the isolator and elastomer shear modulus (G_e) value of 0.86 MPa, which was calculated based on the average experimental results of the three isolators. It is observed that the lateral response of U-FREI is dependent on the amplitude of the applied lateral displacement. Under small lateral displacements, the isolator remains in complete contact with the upper and lower surfaces, resulting in a near linear response. Under moderate displacements, the isolator rolls off the loading surfaces leading to a reduction in the loaded shear area, which results in a nonlinear decrease in the effective lateral stiffness (Van Engelen et al. 2014) [22]. The ability of U-FREI to rollover is a consequence of the unbonded connection and the negligible flexural rigidity of the fiber reinforcement. However, as the lateral displacement is further increased, the initially vertical sides of the isolator begin to make contact with the upper and lower loading surfaces (see Fig. 5-2a), resulting in a stiffening in the lateral response.

A small variation in the response under vertical pressures of 2 MPa and 6 MPa for Isolator 1 and Isolator 2 can be observed in Fig. 5-8. Negligible difference in the hysteresis loops can be observed at 10 MPa and for Isolator 3 under all three pressures. The application of a rotational deformation to the isolator could result in lift-off (Al-Anany and Tait 2015b) and consequently a reduction in the effective shear area. However, it can be observed from Fig. 5-8 that all the isolators maintained a stable rollover response (i.e. tangential stiffness remains positive) over all cycles up to the maximum lateral displacement of $1.5 t_r$ and under all angles of applied rotation considered in this study, including the maximum rotation of 0.03 radians.

5.4.1. Effects of rotational deformation on lateral stiffness

Figure 5-9 shows the effect of lateral displacement amplitude on the lateral stiffness (K_L) for the isolators considered in this study. The lateral stiffness is determined based on the peak response of lateral loads (F_L) and displacements (U) observed over each cycle, using the following relation

$$K_L = \frac{F_{L,max} - F_{L,min}}{U_{max} - U_{min}} \quad (1)$$

The effective lateral stiffness of the isolators is found to decrease as the applied lateral displacement is increased due to the reduction in the effective shear area. This behaviour is considered beneficial during the occurrence of earthquakes, particularly moderate (design) earthquakes (Foster 2011) [23], since a reduction in lateral stiffness results in an increase in the isolated period of the structure. This is expected to improve isolation efficiency as it further shifts in the structure's fundamental period away from the predominant periods associate with earthquakes. Additionally, the displacement demand on the isolator is limited by the stiffening response at larger lateral displacements as the effective lateral stiffness increases due to the initiation of contact between the supports and originally vertical faces of the isolator. In general, the effective lateral stiffness also reduces as the applied vertical load and angle of rotation are increased, particularly for isolators with lower aspect ratio values (see Fig. 5-9). Furthermore, it has been shown by Al-Anany et al. (2016b) that the vertical stiffness of the isolator can be maintained even under higher values of lateral offsets up to $1.50 t_r$.

Table 5-2 lists the corresponding isolated periods of the tested isolators using the effective lateral stiffness values determined from the third cycle, based on the following equation

$$T = 2\pi \sqrt{\frac{P/g}{K_L}} \quad (2)$$

where g is the gravitational acceleration. As previously mentioned, the lateral stiffness of U-FREI, which directly influences the time period, is primarily dependent on the amplitude of lateral displacement and applied vertical load. Accordingly, for the isolators investigated in this study the isolated periods are found to range between 0.40 and 1.45 seconds. This corresponds to full-scale isolated periods of 0.80 to 2.90 seconds (i.e. scale factor of 2.0). As a large number of bridges have a fundamental period in the range of 0.2 to 1.0 seconds (Kunde and Jangid 2003), using the U-FREI considered in this study for the isolation of bridges could lead to a sufficiently large shift in the fundamental period that would result in a sizeable reduction in the seismic accelerations and forces on the bridges (Jangid 2004).

5.4.2. Effects of rotational deformation on lateral damping

Results presented in Fig. 5-10 show the influence of lateral displacement amplitude on the lateral damping of the isolators. The lateral damping was determined based on the area within the hysteresis loop (W_D), using the following equation

$$\zeta_L = \frac{2}{\pi} \left[\frac{W_D}{K_L(|U_{max}| + |U_{min}|)^2} \right] \quad (3)$$

As shown, the lateral damping was found to range from a minimum value of 7.5% to a maximum value of 13%, 14%, and 16% for Isolator 1, 2, and 3, respectively, which implies an increase in lateral damping with a reduction of the isolator aspect ratio. Additionally, an increase in the applied angle of rotation and vertical load were found to increase the lateral damping. A sufficient level of energy dissipation (damping) is needed in order to control isolator

displacement amplitude. The advantage of damping in reducing isolator displacement is significant in bridges, where large displacements can lead to damage of the expansion joints (Constantinou et al. 2011). Therefore, in addition to the ability of the U-FREI considered in this study to provide adequate seismic isolation periods, they are also able to produce sufficient damping to limit displacement demands.

5.5. Finite Element Modelling

5.5.1. Model description and evaluation

Three-dimensional finite element (FE) modelling of the experimentally tested isolators was completed using the commercially available general-purpose program MSC Marc (2013). The FE analysis was employed in order to analyze the isolators under the critical loads/deformations considered during the experimental program. The primary objective of the FE study was to evaluate and assess the resulting stress and strain state in the isolators when subjected to the largest vertical loads (i.e. 10 MPa), rotational deformations (i.e. 0.03 radians), and lateral deformation (i.e. $1.5 t_r$) considered in the experimental program.

The elastomer was represented by an eight-node isoparametric quadrilateral brick element (element type 74) with dimensions of $1.50 \text{ mm} \times 1.50 \text{ mm} \times 0.75 \text{ mm}$. The elastomer material was represented by a simplified single-parameter Mooney-Rivlin material model (i.e. Neo-Hookean). This hyperelastic model considers the elastomer compressibility and is defined by two parameters: the shear modulus, G_e , and bulk modulus, K_e . A membrane element with zero flexural rigidity and with linear elastic isotropic material properties was used to represent the fiber reinforcement, which was assumed to have zero flexural rigidity. The linear model employed for the fiber reinforcement is defined by two constants: the elastic modulus, E_f , and Poisson's ratio, ν_f . The material properties considered for modelling the isolators are listed in

Table 5-3. While the value representing the fiber reinforcement elastic modulus (E_f) of 23 GPa was selected based on uniaxial tensile tests results.

The top and bottom loading supports were modelled as rigid surfaces. The unbonded contact between the isolators and the loading supports were simulated using the “Touching” contact model, which allows the nodal points at the top and bottom of the cover layers of the elastomer that are in contact with the supports to detach under sufficiently large lateral and rotational deformations when no normal compression stress exists. Accordingly, the shear forces along the contact interface between the isolator and the supports were transferred through a Coulomb friction mechanism. The friction coefficient was selected to be equal to one in order to prevent any slippage.

Table 5-4 compares the lateral stiffness of the isolators obtained from the experimental with the FE modelling results. Although the presented FE model considered a constant value for the shear modulus of the elastomer, which is characterized by strain dependency, the FE modelling provided a reasonable estimate to the lateral stiffness values over the entire range of lateral displacements with the error ranging between approximately -3% and 9%. This level of agreement provides confidence in the accuracy of the presented model and its ability to capture the isolator lateral response.

5.6. Results and Discussions of FE Modelling

This section investigates the resulting normal stresses (σ_{11} , σ_{22} , and σ_{33}) and shear strain (γ_{12}) that develop in the three isolators. The stresses monitored are those generated according to the local axis of the elastomer layer (see Fig. 5-11), rather than the global axis. Additionally, the 3D analyses were completed using the Updated Lagrangian (UL) formulation, which allows the

deformed configuration at the last completed increment to be the reference for the current configuration.

5.6.1. Normal stresses σ_{11} , σ_{22} , and σ_{33}

This section investigates the normal stresses that develop within the isolator as it is subjected to vertical, rotational and lateral deformations. Accordingly, the stresses are presented at four different phases. Phase I represents the deformation of the isolator under a mean compressive stress, σ_v of 10 MPa. Next, an angle of rotation equal to 0.03 radians is introduced in Phase II. Finally, Phase III and Phase IV represent the isolator under loading conditions of Phase I and Phase II, but when subjected to either a positive or negative lateral deformation of $1.5 t_r$. These four phases represent the maximum deformation experienced by the isolators in this study.

Figures 5-12, 5-13, and 5-14 presents the contours of normalized normal stresses σ_{11} , σ_{22} , and σ_{33} , developed within Isolator 1, 2, and 3, respectively, during the four phases considered. The three orthogonal stresses have been normalized with respect to the mean vertical stress σ_v and only half of the isolator is shown. It can be observed that the difference in distribution and peak values of the normalized stresses in the three considered orthogonal directions in a particular isolator is negligible. This observation confirms that the hydrostatic rule can be used to define the pressure distribution in the isolators under the considered deformation.

As seen in Figs. 5-12, 5-13, and 5-14, an applied angle of rotation leads to an increase of the normal stresses on the loaded side of the isolator due to a reduction in the size of the loaded area. However, insignificant tensile stresses are found to occur on the unloaded side of the isolator due to the detachment of the isolator from the contact supports. Additionally, the rate of increase in the peak stresses under different patterns of deformation is a factor of the isolator aspect ratio and also the ratio of plan dimensions of the isolator (i.e. ratio of length, $2b$, to width, a).

As an example, under a mean vertical stress of 10 MPa (i.e. Phase I), the peak normalized value of stresses for Isolator 2 with a plan dimension ratio of 0.89 (i.e. rectangular) and Isolator 3 with a plan dimension ratio of 0.35 (i.e. longer strip) is equal to 1.90 and 1.70, respectively. This trend is in agreement with the theoretical solutions for predicting the stress values (Tsai and Kelly 2001). Additionally, the increase in the peak value of normal stresses due to the application of rotational deformation was approximately 28.9%, 13.2%, and 2.9% for Isolator 1 and 2, and 3, respectively. This is due to the fact that the decrease in the isolator aspect ratio results in an increase in the isolator flexibility and thus its ability to accommodate the applied rotation without lift-off (i.e. losing contact area). However, under lateral deformation, the reduction in the contact area becomes more evident for isolators with lower aspect ratios. For instance, the increase in the peak value of normal stresses in the rotated isolators under lateral deformation was found to be approximately 6.1%, 11.6%, and 22.8% for Isolator 1 and 2, and 3, respectively.

5.6.2. Shear strain γ_{12}

A primary cause of failure in bridge bearings/isolators has been reported to be due to shear delamination of reinforcement from the elastomer layers (Stanton et al. 2007). Consequently, bridge design codes, such as CAN/CSA-S6 Canadian Highway Bridge Design Code (CHBDC) (CSA 2014) and the American Association of State Highway and Transportation Officials, Bridge Design Specifications, (AASHTO-LRFD 2012), specify a limit on the sum of the shear strains that developed within the isolator under vertical, rotational, and lateral deformation.

Figure 5-15 presents the shear strain γ_{12} contours at the center of isolators for Phase I through Phase VI. It can be observed that the orientation of the peak shear strain varies according to the loading condition applied on the isolator. Under pure vertical deformation, the peak shear strains are observed to occur at the edges of the elastomer layers (i.e. $x = \pm b$), however, under

rotational deformation, the peak values continue to increase at the edge location, but on the loaded side of the isolator. Finally, it should be noted that under lateral deformation, shear strains with higher values are localized at the corner of the top and bottom elastomer layers in the contact zone between the isolator and the loading plate.

5.7. Conclusion

This research paper investigates the effect of coupled vertical-rotational deformation on the lateral response of Unbonded-Fiber-Reinforced Elastomeric Isolators (U-FREI). The investigation was carried out experimentally using a 3 DOF test apparatus and numerically using the commercially available finite element software MSC Marc (2013). The test apparatus employed for the experimental testing was designed to apply deformations in three different directions (i.e. vertical, rotational, and lateral) independently and/or in combination. Thus, it was able to conduct different loading conditions on the isolators expected during the lifetime of a bridge. The novelty of the experimental testing was based on the ability to include the effect of the rotational deformation, which is considered an important aspect in bridge bearings/isolators design, on the lateral response of the isolators. Additionally, three-dimensional finite element modelling was performed on the isolators in order to evaluate the stresses and strains that develop under the peak applied load and deformations. The three isolators considered in this study had in-plane aspect ratios of 2.5, 2.5, and 4.5, but a constant shape factor of 6.0 was maintained.

The main findings from the experimental study are:

- 1- A rotational deformation up to 0.03 radians had a negligible effect on the lateral response of all isolators in general, but was with the least significant for isolators with lower aspect ratios.

- 2- Increasing both the applied vertical load as well as the angle of rotation on the isolator caused a slight decrease in the lateral stiffness and small increase in the lateral damping.
- 3- The isolation periods of the considered isolators varied according to the values of the applied vertical loads and angle or rotation, with a maximum calculated value of approximately 2.90 sec.

Based on results from FEM the following main conclusions were drawn:

- 1- The hydrostatic rule can be used to define the distribution of pressures that are developed within the elastomeric isolators, not only vertical deformation, but also if under coupled vertical-lateral-rotational deformation.
- 2- Decreasing the aspect ratio of the isolator delay the occurrence of lift-off, this results in a lower rate of increase in the normal stresses and shear strains under rotational deformation. However, it also results in a larger rate of increase in stresses and strains developed within the isolator when subjected to lateral deformations.

Acknowledgements

This research was carried out as part of the mandate of the Centre for Effective Design of Structures (CEDs) at McMaster University. The support of the Natural Sciences and Engineering Research Council (NSERC) of Canada and the Ontario Ministry of Research and Innovation (MRI) is gratefully acknowledged.

References

AASHTO. (2012). *American Association of State Highway and Transportation Officials. LRFD Bridge Design Specifications*, Washington, D.C.

Al-Anany Y., Tait M. (2015a). "A Study on the Rotational Behaviour of Bonded and Unbonded Fiber Reinforced Elastomeric Isolators", *11th Canadian Conference on Earthquake Engineering*, Victoria, British Columbia, Canada, 21-24 July 2015.

Al-Anany Y., Tait M. (2015b). "A numerical study on the compressive and rotational behavior of fiber reinforced elastomeric isolators (FREI)", *Composite Structures*; 133: 1249-1266.

Al-Anany, Y., Tait M. (2016a). "An experimental study of the vertical and rotational behavior of unbonded fiber-reinforced elastomeric isolators (U-FREI) for bridge applications", *Composites part B: Engineering*, under review.

Al-Anany Y., Van Engelen N., Tait M. (2016b). "An experimental investigation on the vertical and lateral behavior of unbonded fiber-reinforced elastomeric isolators", *ASCE Journal of Composites for Construction*, under review.

Caltrans. (1994). *Bridge Memo to Designers. Section 7: Bridge Bearings*. California Department of Transportation, Sacramento, California.

CAN/CSA-S6-14. (2014). *Canadian Highway Bridge Design Code*. Canadian Standard Association. Ontario.

Constantinou M., Kalpakidis I., Filiatrault A., Ecker Lay R. (2011). *LRFD-based analysis and design procedures for bridge bearings and seismic isolators*. Report No. MCEER-11-0004, Multidisciplinary Center for Earthquake Engineering Research, University at Buffalo, State University of New York, Buffalo, New York.

Foster B. (2011). *Base isolation using stable unbonded fibre reinforced elastomeric isolators (SU-FREI)*. Master's thesis. Hamilton: McMaster University.

Ghobarah A., Ali H. (1988). "Seismic performance of highway bridges", *Engineering Structures*; 10(3):157-166.

Girish M., Pranesh M. (2013). "Sliding Isolation Systems: State-of-the-Art Review", *IOSR Journal of Mechanical and Civil Engineering (IOSR-JMCE)*; ISSN : 2278-1684: 30–35.

Jangid R. (2004). "Seismic response of isolated bridges", *Journal of Bridge Engineering*, 9(2): 156–166.

Konstantinidis D., Kelly J., Makris N. (2008). *Experimental investigations on the seismic response of bridge bearings*. Report No. EERC-2008/02, Earthquake Engineering Research Center, University of California, Berkeley.

Konstantinidis D., Kelly J. (2012). “Two Low-Cost Seismic Isolation Systems”, *15th World Conference on Earthquake Engineering*, Lisbon, Portugal, September 24– 28; 2012.

Kunde M., Jangid R. (2003). “Seismic behavior of isolated bridges: A-state-of-the-art review”, *Electronic Journal of Structural Engineering*; 3(2): 140–169.

Kunde M., Jangid R. (2006). “Effects of Pier and Deck Flexibility on the Seismic Response of Isolated Bridges”, *ASCE Journal of Bridge Engineering*, 11(1): 109–121.

Matsagar V., Jangid R. (2006). “Seismic response of simply supported base-isolated bridge with different isolators”, *International Journal of Applied Science and Engineering*; 4 (1), 53-69.

MSC. Marc. (2013). Santa Ana, CA: MSC Software Corporation.

Naeim F., Kelly J. (1999). *Design of Seismic Isolated Structures: From Theory to Practice*. John Wiley & Sons Inc., New York.

Stanton J., Roeder C., Mackenzie-Helnwein P., White C, Kuester C., Craig B. (2007). *Rotation Limits for Elastomeric Bearings*. Report No. NCHRP 596, Transportation Research Board, National Cooperative Highway Research Program, Washington, D.C.

Toopchi-Nezhad H., Tait M., Drysdale R. (2008a). “Testing and modeling of square carbon fiber-reinforced elastomeric seismic isolators”, *Structural Control and Health Monitoring*; 15(6): 876–900.

Toopchi-Nezhad H., Tait M., Drysdale R. (2008b). “Lateral response evaluation of fiber-reinforced neoprene seismic isolators utilized in an unbonded application”, *ASCE Journal of Structural Engineering*; 134(10): 1627–37.

Toopchi-Nezhad H., Drysdale R., Tait M. (2009a). “Parametric study on the response of stable unbonded fiber-reinforced elastomeric isolators (SU-FREIs)”, *Journal of Composite Materials*; 43(15):1569–87.

Toopchi-Nezhad H., Tait M., Drysdale R. (2009b). “Shake table study on an ordinary low-rise building seismically isolated with SU-FREIs (stable unbonded fiber-reinforced elastomeric isolators)”, *Earthquake Engineering and Structural Dynamics*; 38(11): 1335–57.

Toopchi-Nezhad H., Tait M., Drysdale R. (2011). “Bonded versus unbonded strip fiber reinforced elastomeric isolators: finite element analysis”, *Composite Structures*; 93(2): 850–9.

Tsai H., Kelly J. (2001). *Stiffness analysis of fiber-reinforced elastomeric isolators*. Pacific Earthquake Engineering Research Center, PEER, Berkeley, California; 2001/5.

Tsopelas P., Constantinou M., Kim Y., Okamoto S. (1996a). “Experimental study of FPS system in bridge seismic isolation”, *Earthquake Engineering and Structural Dynamics*; 25(1), 65–78.

Tsopelas P., Constantinou M., Okamoto S., Fujii S., Ozaki D. (1996b). “Seismic performance of highway bridges”, *Engineering Structures*; 18(4):301-310.

Van Engelen N., Tait M., Konstantinidis D. (2014). “Model of the Shear Behavior of Unbonded Fiber-Reinforced Elastomeric Isolators”, *ASCE Journal of Structural Engineering*; 141(7): p.04014169.

Wesolowsky M., Wilson J. (2003). “Seismic isolation of cable-stayed bridges for near-field ground motions”, *Earthquake Engineering and Structural Dynamics*; 32: 2107–26.

Table 5-1: Geometric properties of the test specimen (all units are in mm)

	Isolator 1	Isolator 2	Isolator 3
Length ($2b$)	87.75	68.25	48.75
Width (a)	61.20	76.20	138.00
Total height of bearing (h)	19.5	19.5	19.5
Aspect ratio (R) = $2b / h$	4.5	3.5	2.5
Shape Factor	6	6	6

Table 5-2: Fundamental isolated period for the ¼ scaled isolators in seconds

<i>Isolator 1</i>										
	$\sigma_v = 2$ MPa			$\sigma_v = 6$ MPa			$\sigma_v = 10$ MPa			
θ (rad.) =	0	0.015	0.03	0	0.015	0.03	0	0.015	0.03	
0.25	0.40	0.42	0.43	0.70	0.72	0.73	0.92	0.93	0.93	
U/t_r	0.50	0.44	0.46	0.47	0.78	0.79	0.81	1.03	1.03	1.04
1.00	0.50	0.51	0.53	0.85	0.87	0.89	1.11	1.13	1.13	
1.50	0.51	0.52	0.53	0.86	0.87	0.88	1.09	1.10	1.10	
<i>Isolator 2</i>										
	$\sigma_v = 2$ MPa			$\sigma_v = 6$ MPa			$\sigma_v = 10$ MPa			
θ (rad.) =	0	0.015	0.03	0	0.015	0.03	0	0.015	0.03	
0.25	0.41	0.43	0.46	0.72	0.74	0.76	0.94	0.95	0.94	
U/t_r	0.50	0.46	0.47	0.50	0.79	0.82	0.84	1.05	1.06	1.06
1.00	0.52	0.54	0.55	0.89	0.92	0.93	1.14	1.17	1.17	
1.50	0.53	0.55	0.56	0.91	0.92	0.94	1.15	1.17	1.17	
<i>Isolator 3</i>										
	$\sigma_v = 2$ MPa			$\sigma_v = 6$ MPa			$\sigma_v = 10$ MPa			
θ (rad.) =	0	0.015	0.03	0	0.015	0.03	0	0.015	0.03	
0.25	0.42	0.42	0.42	0.75	0.76	0.76	1.03	1.03	1.02	
U/t_r	0.50	0.47	0.47	0.47	0.84	0.86	0.86	1.19	1.20	1.18
1.00	0.56	0.56	0.57	0.99	1.02	1.03	1.39	1.40	1.37	
1.50	0.59	0.59	0.60	1.06	1.06	1.07	1.45	1.41	1.39	

Table 5-3: Material Properties of the modeled isolators

Elastomer material	Fiber material
Shear Modulus (G) = 0.86 MPa	Elastic Modulus (E) = 23 GPa
Bulk Modulus (K) = 2000 MPa	Poisson's ratio (ν) = 0.20

Table 5-4: Error in (%) for the calculated stiffness between the Experimental and FEM results

<i>Isolator 1</i>			
U/t_r	Exp.	FEM	Error (%)
0.25	4.05	3.84	5.2
0.50	3.26	3.25	0.3
1.00	2.78	2.86	-3.0
1.50	2.92	2.88	1.3
<i>Isolator 2</i>			
U/t_r	Exp.	FEM	Error (%)
0.25	3.08	2.90	5.8
0.50	2.43	2.42	0.5
1.00	1.99	2.04	-2.6
1.50	1.99	1.94	2.7
<i>Isolator 3</i>			
U/t_r	Exp.	FEM	Error (%)
0.25	1.90	1.74	8.6
0.50	1.41	1.38	2.1
1.00	1.04	1.04	-0.3
1.50	1.02	0.93	9.2

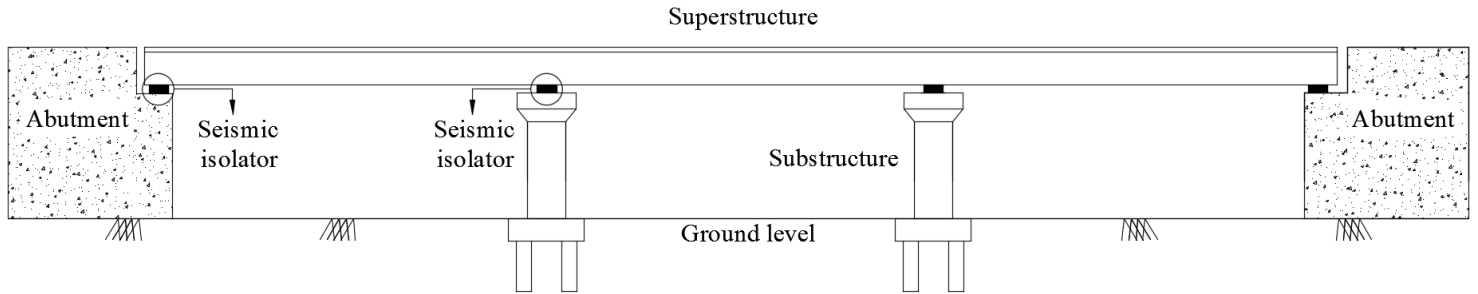


Fig. 5-1: Typical seismically isolated bridge.

Under *Vertical + Lateral* deformation

Under *Vertical + Rotational* deformation

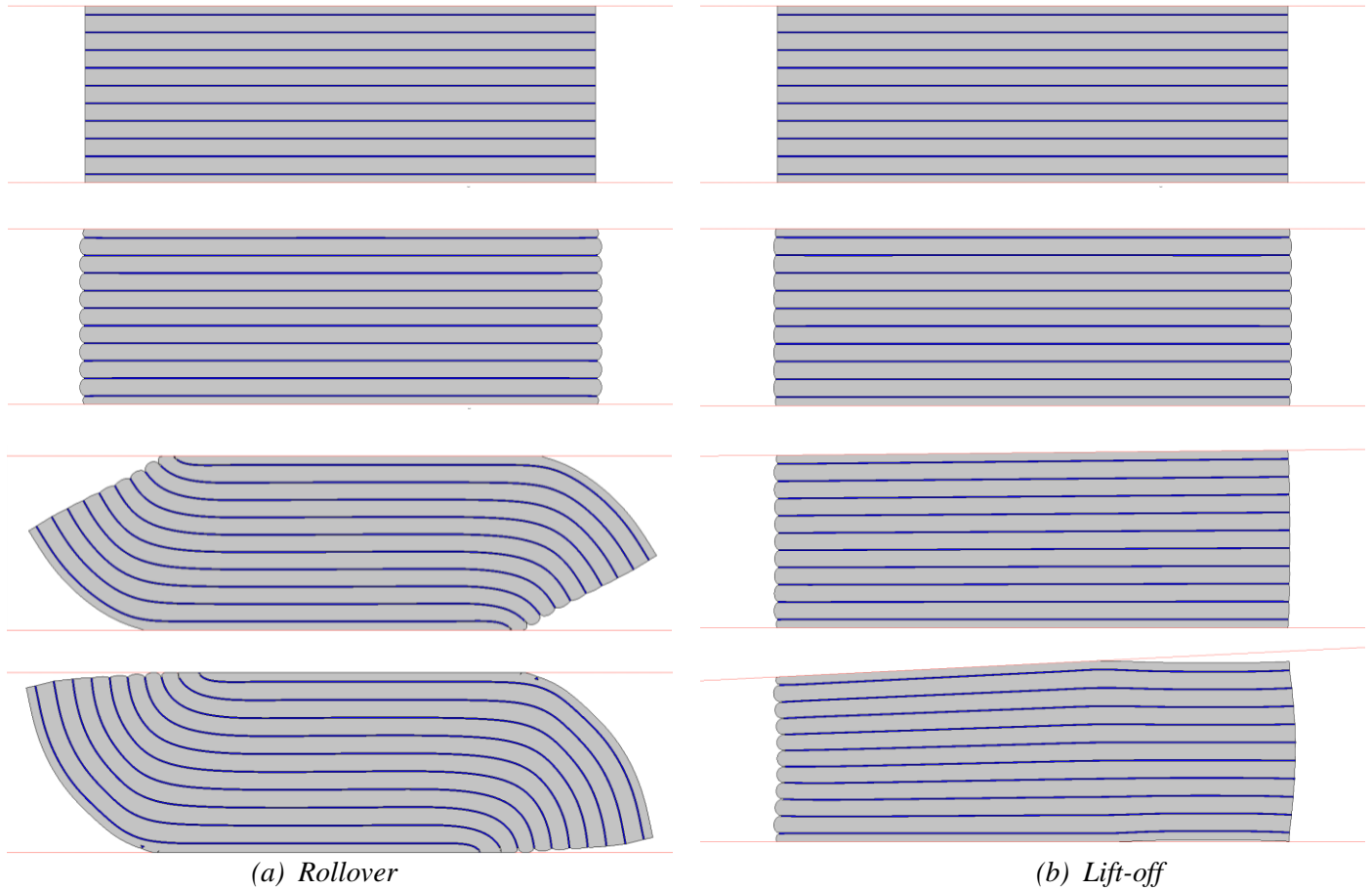
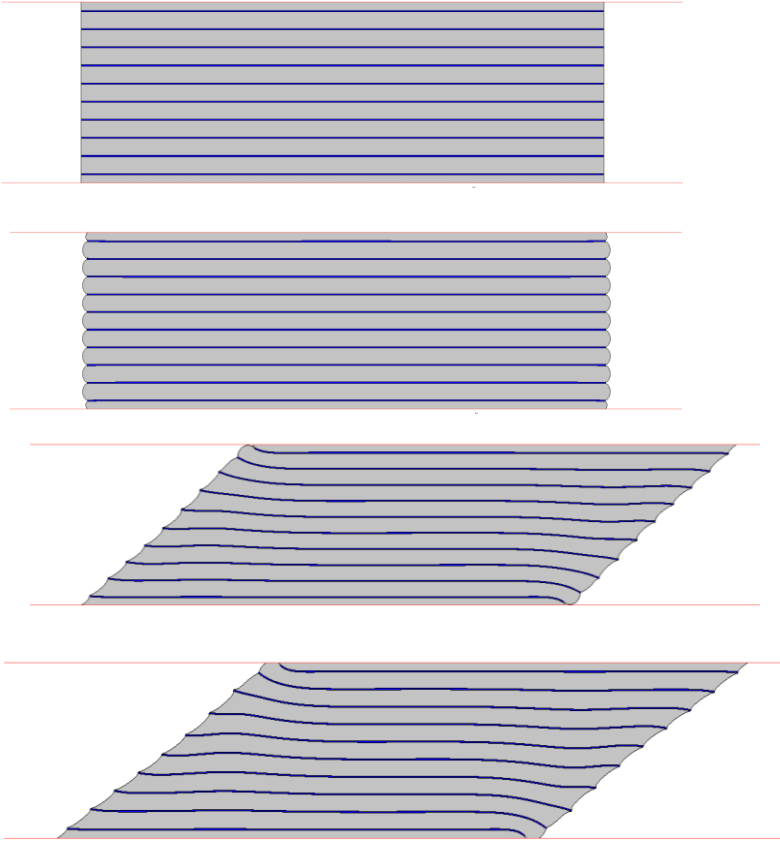


Fig. 5-2: Deformation patterns of U-FREI (i.e. unbonded).

Under *Vertical + Lateral* deformation



Under *Vertical + Rotational* deformation

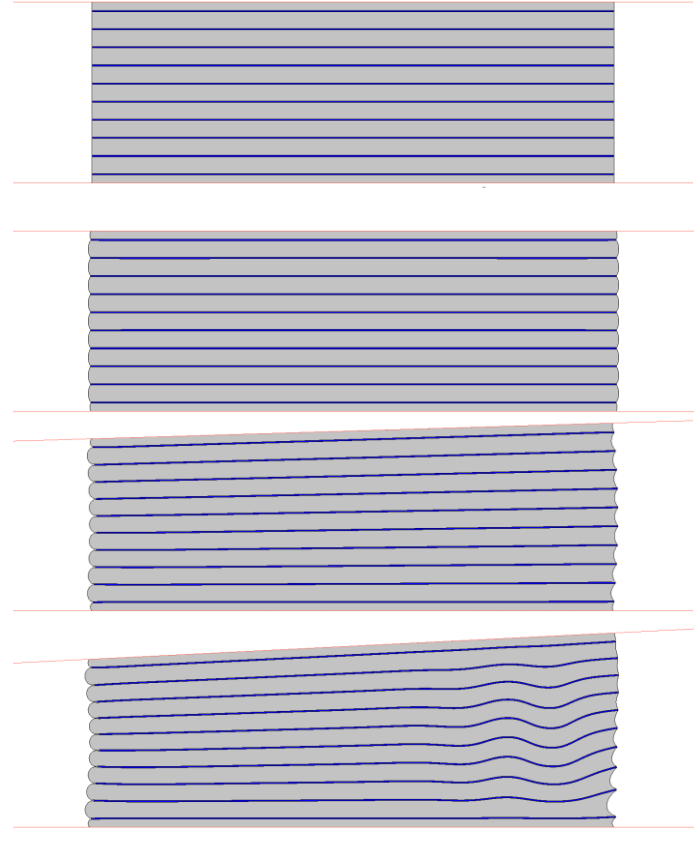


Fig. 5-3: Deformation patterns of B-FREI (i.e. bonded).

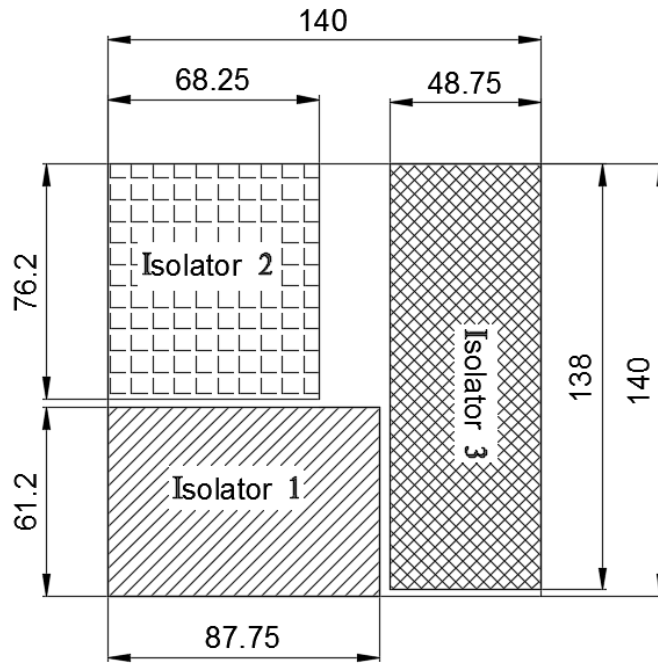


Fig. 5-4: Sketch of the original pad before cutting the isolators (all dimensions are in mm)



Fig. 5-5: Photograph of the three-degree of freedom test apparatus.

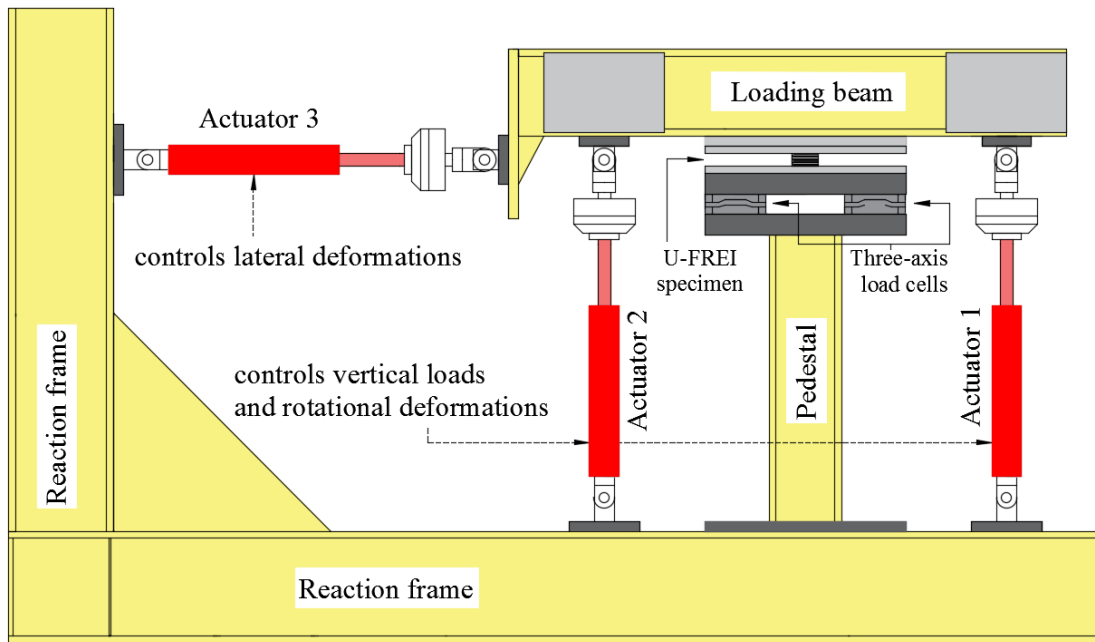


Fig. 5-6: Schematic of the three-degree of freedom test apparatus.

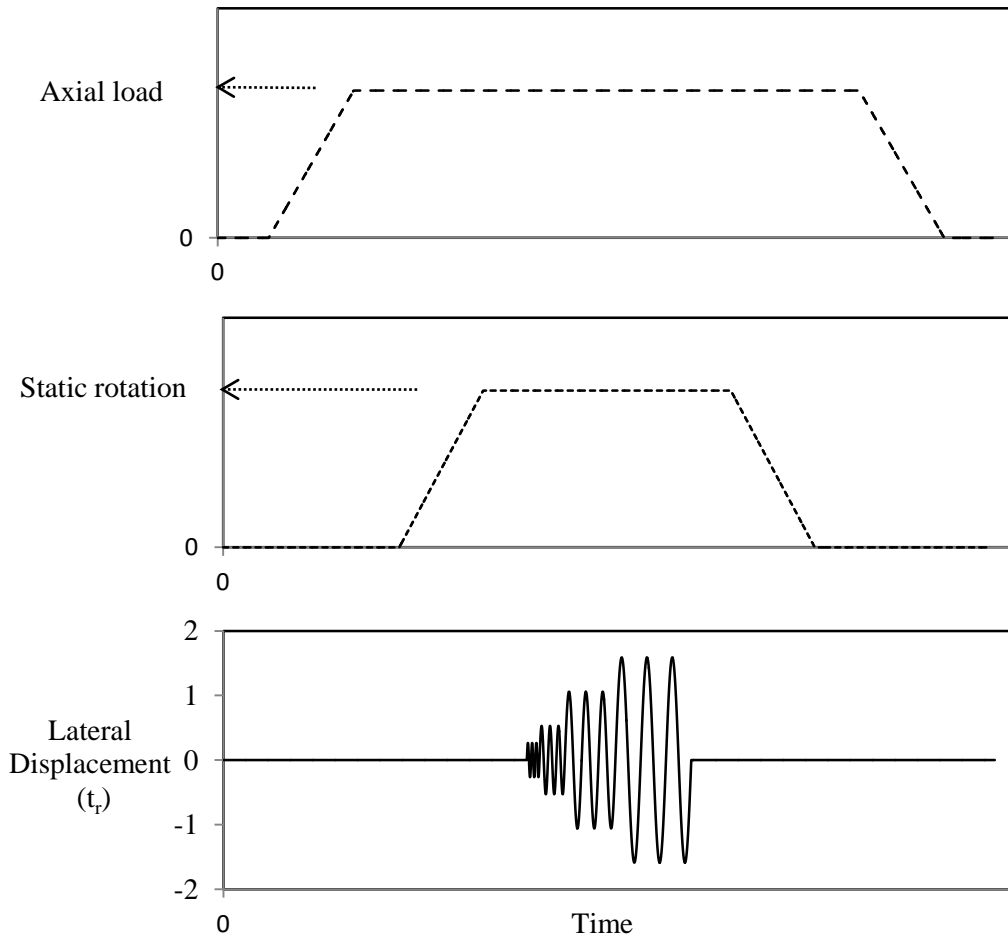


Fig. 5-7: The input signal time history.

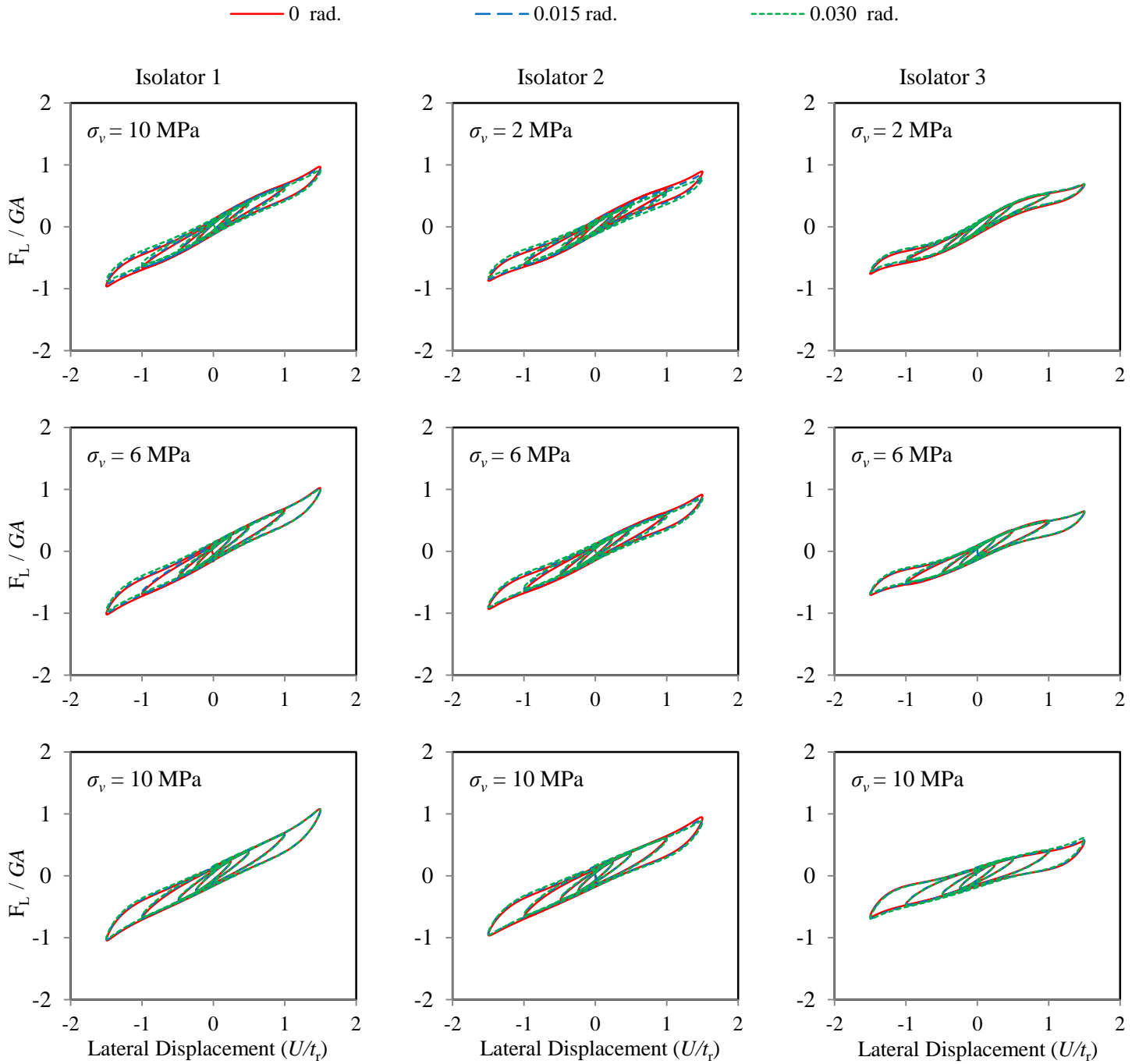


Fig 5-8: Lateral hysteresis loops

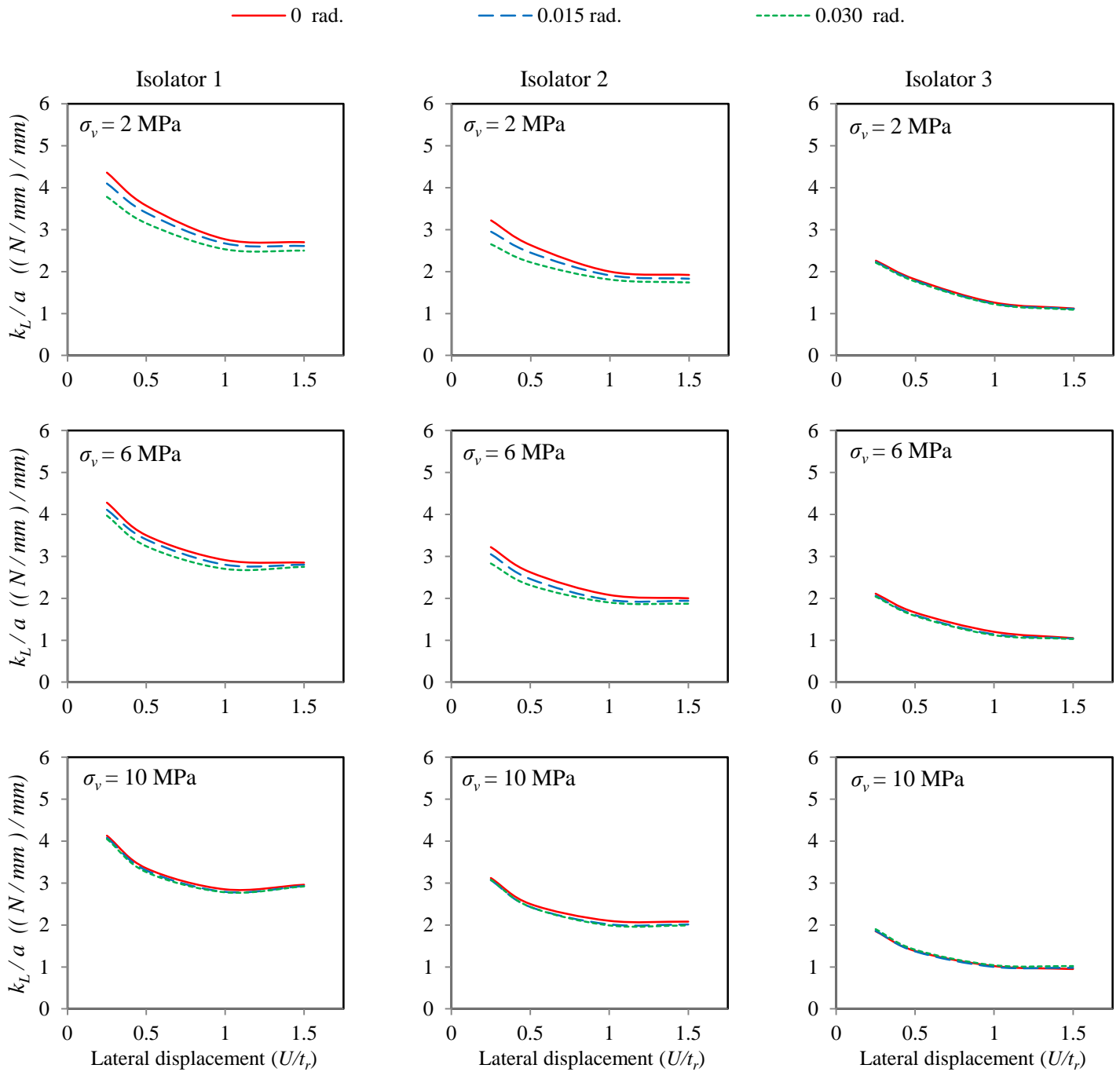


Fig 5-9: Variation in lateral stiffness (K_L) for all isolators

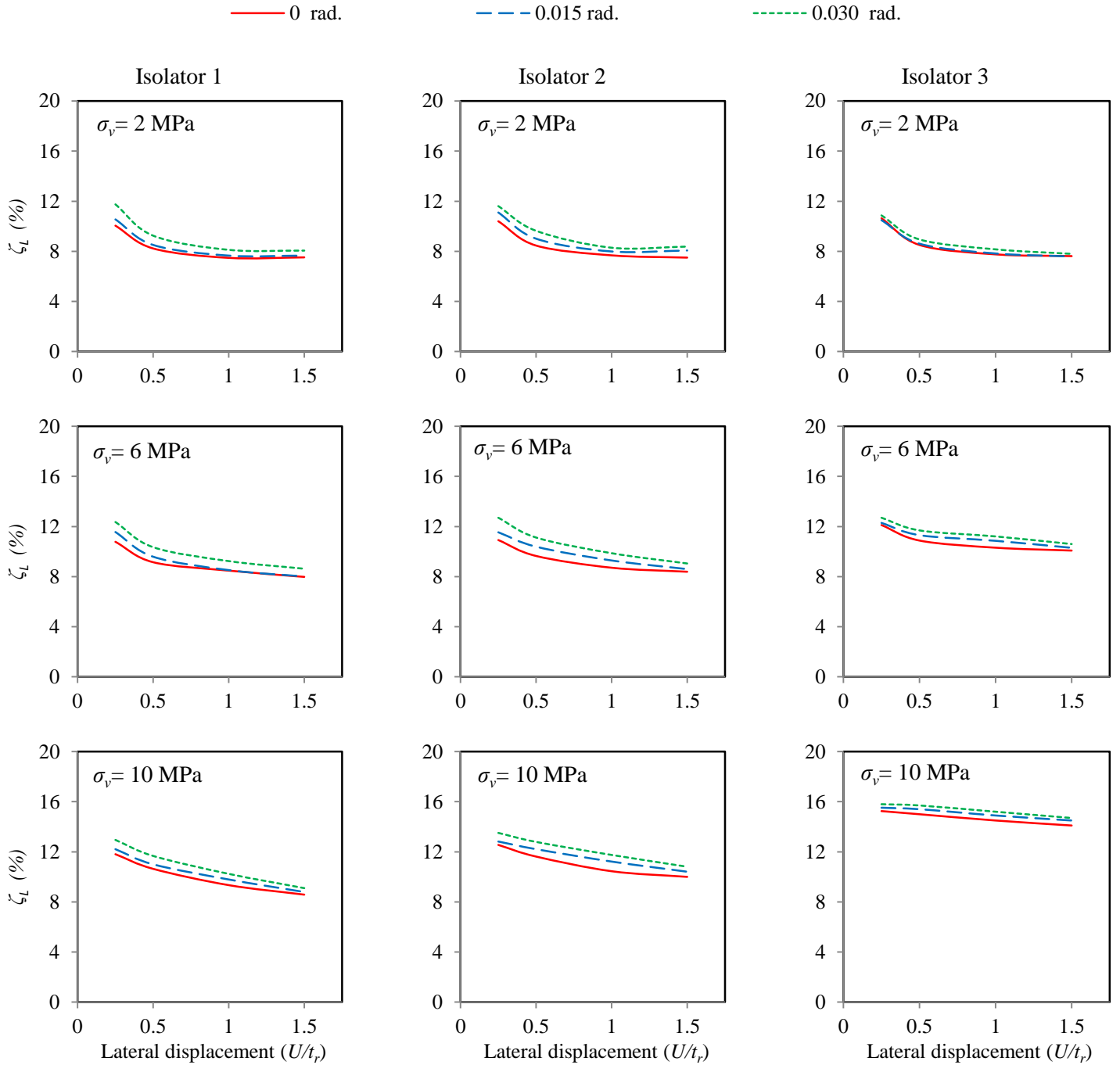


Fig 5-10: Variation in isolator lateral damping (ζ_L).

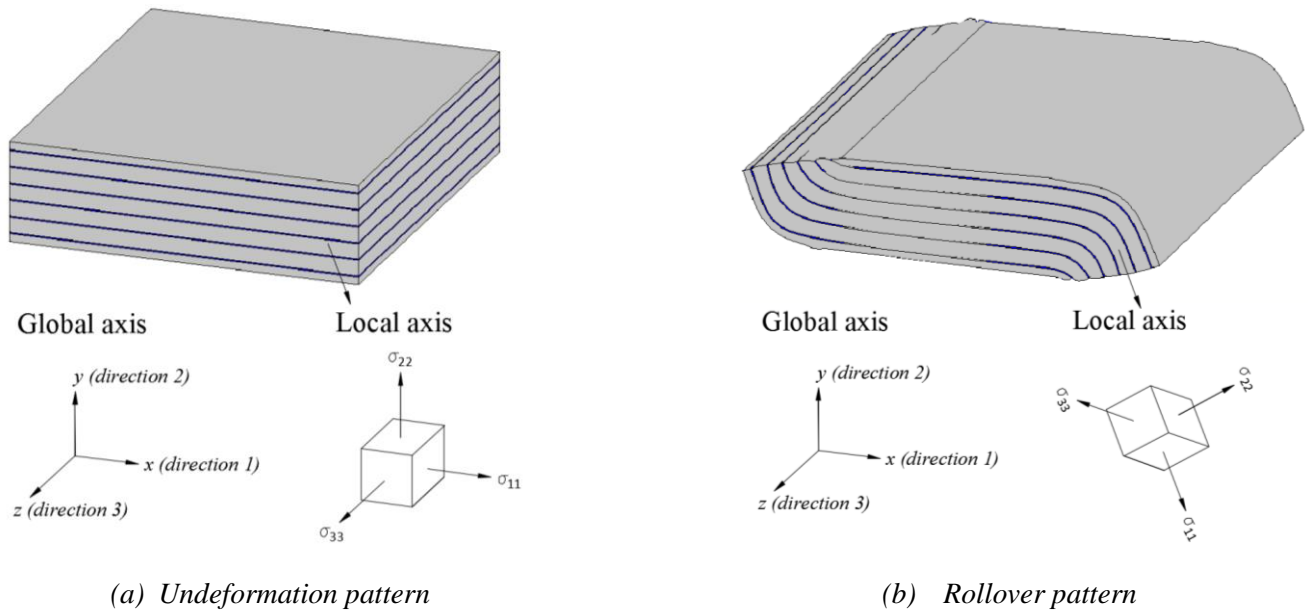


Fig. 5-11: Definition of Stresses.

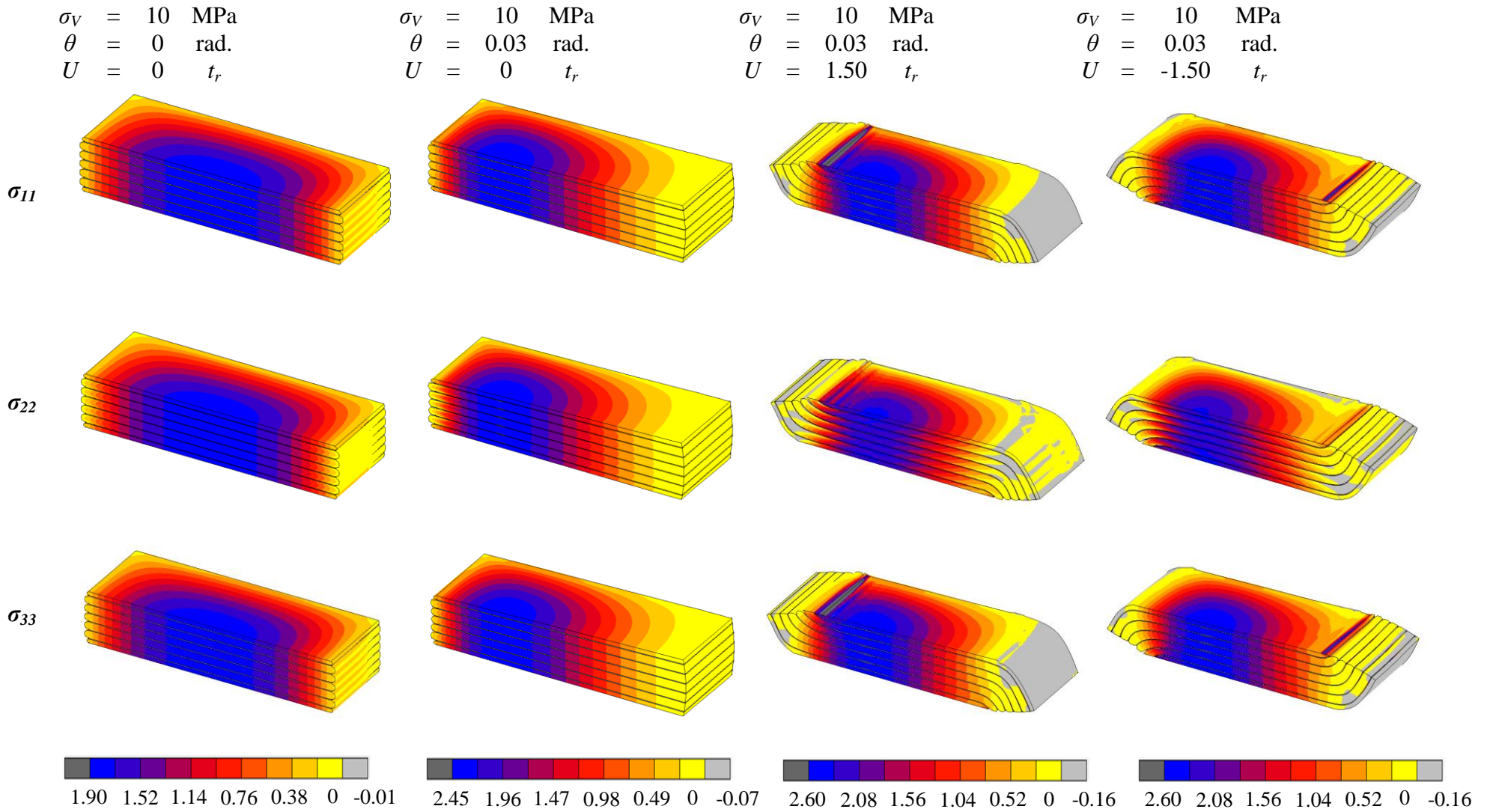


Fig 5-12: Contours of normalized stresses (σ / σ_V) in *Isolator 1*

$$\begin{aligned} \sigma_V &= 10 \text{ MPa} \\ \theta &= 0 \text{ rad.} \\ U &= 0 \text{ } t_r \end{aligned}$$

$$\begin{aligned} \sigma_V &= 10 \text{ MPa} \\ \theta &= 0.03 \text{ rad.} \\ U &= 0 \text{ } t_r \end{aligned}$$

$$\begin{aligned} \sigma_V &= 10 \text{ MPa} \\ \theta &= 0.03 \text{ rad.} \\ U &= 1.50 \text{ } t_r \end{aligned}$$

$$\begin{aligned} \sigma_V &= 10 \text{ MPa} \\ \theta &= 0.03 \text{ rad.} \\ U &= -1.50 \text{ } t_r \end{aligned}$$

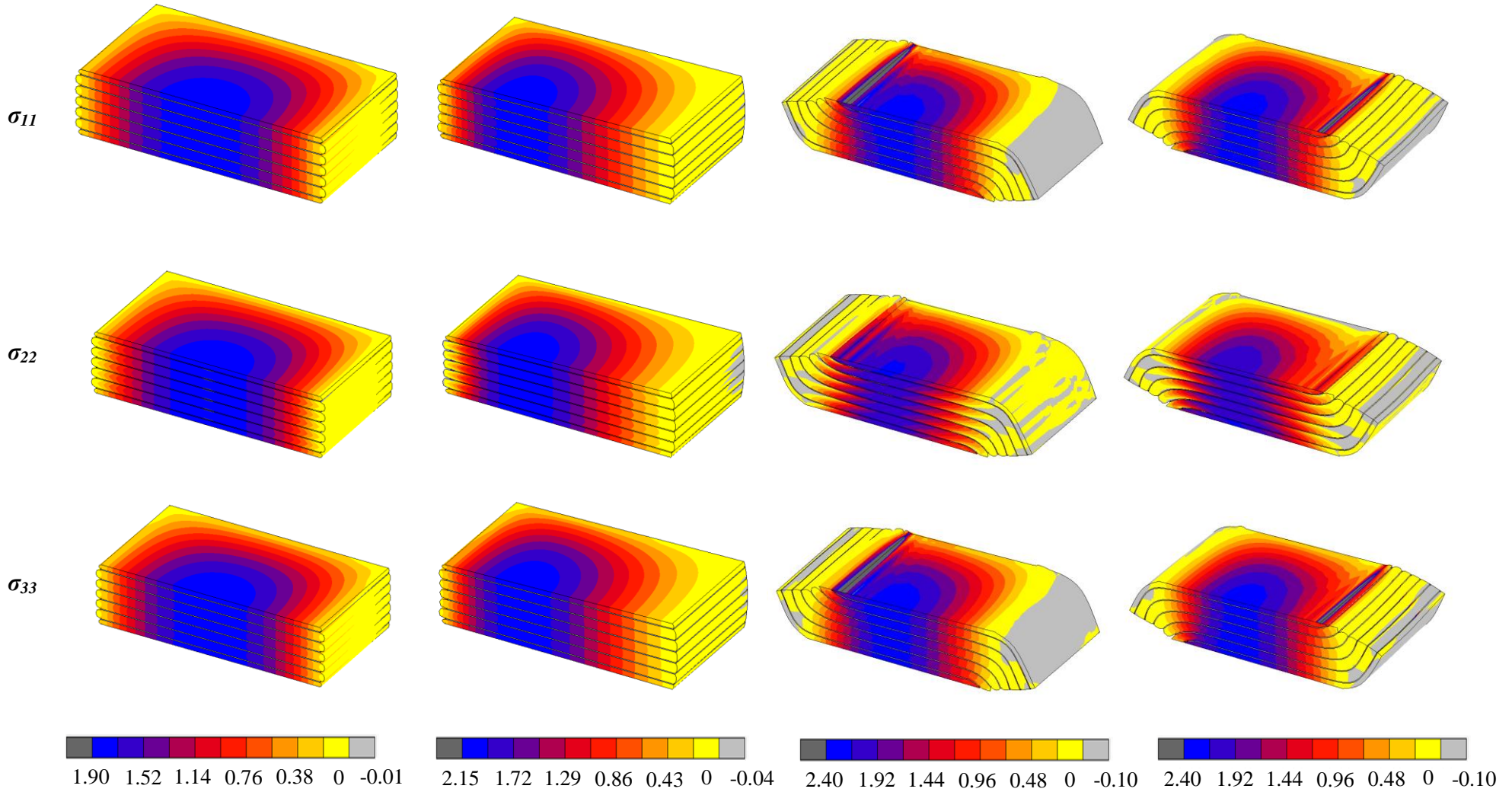


Fig 5-13: Contours of normalized stresses (σ / σ_V) in *Isolator 2*

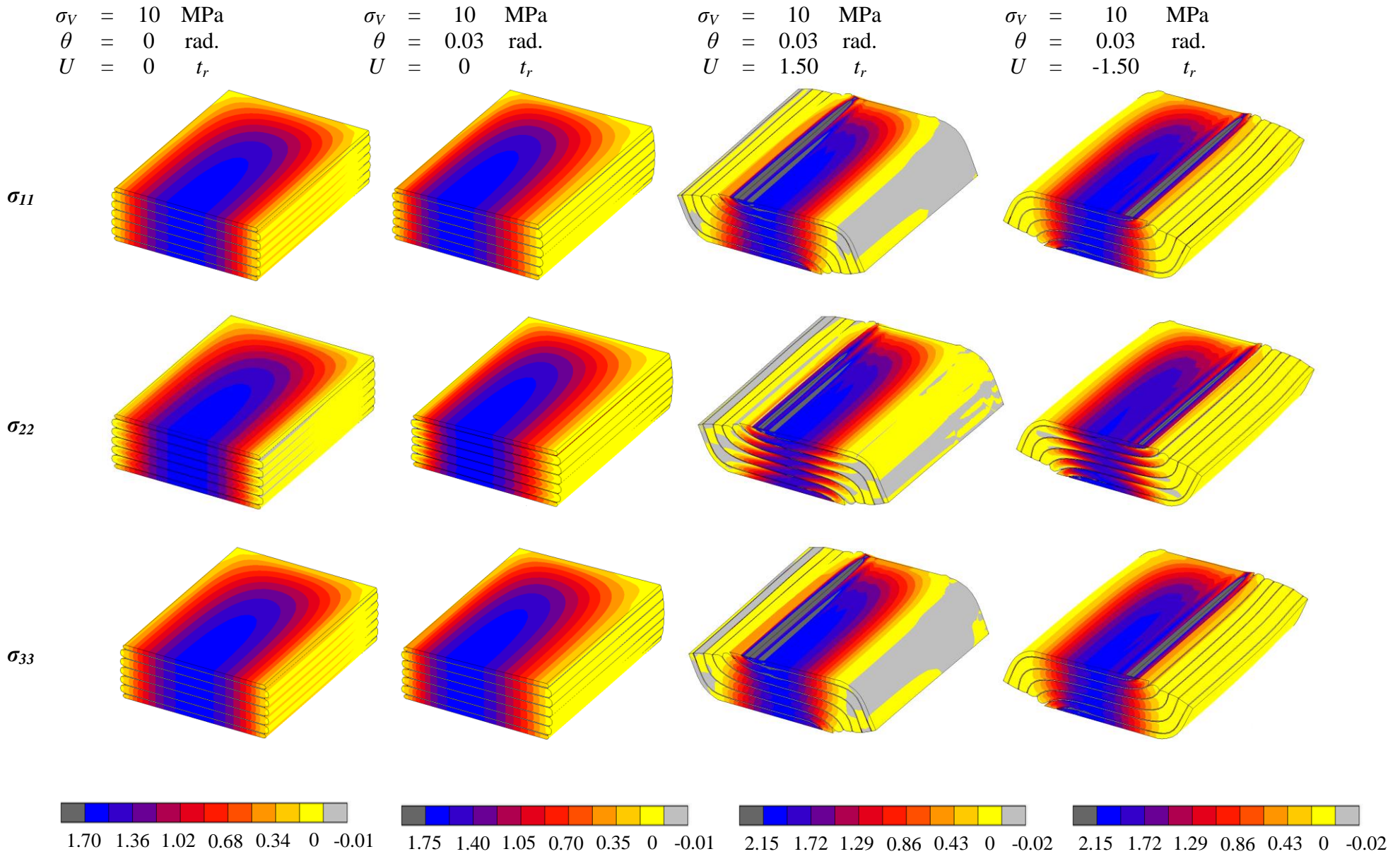


Fig 5-14: Contours of normalized stresses (σ / σ_V) in *Isolator 3*

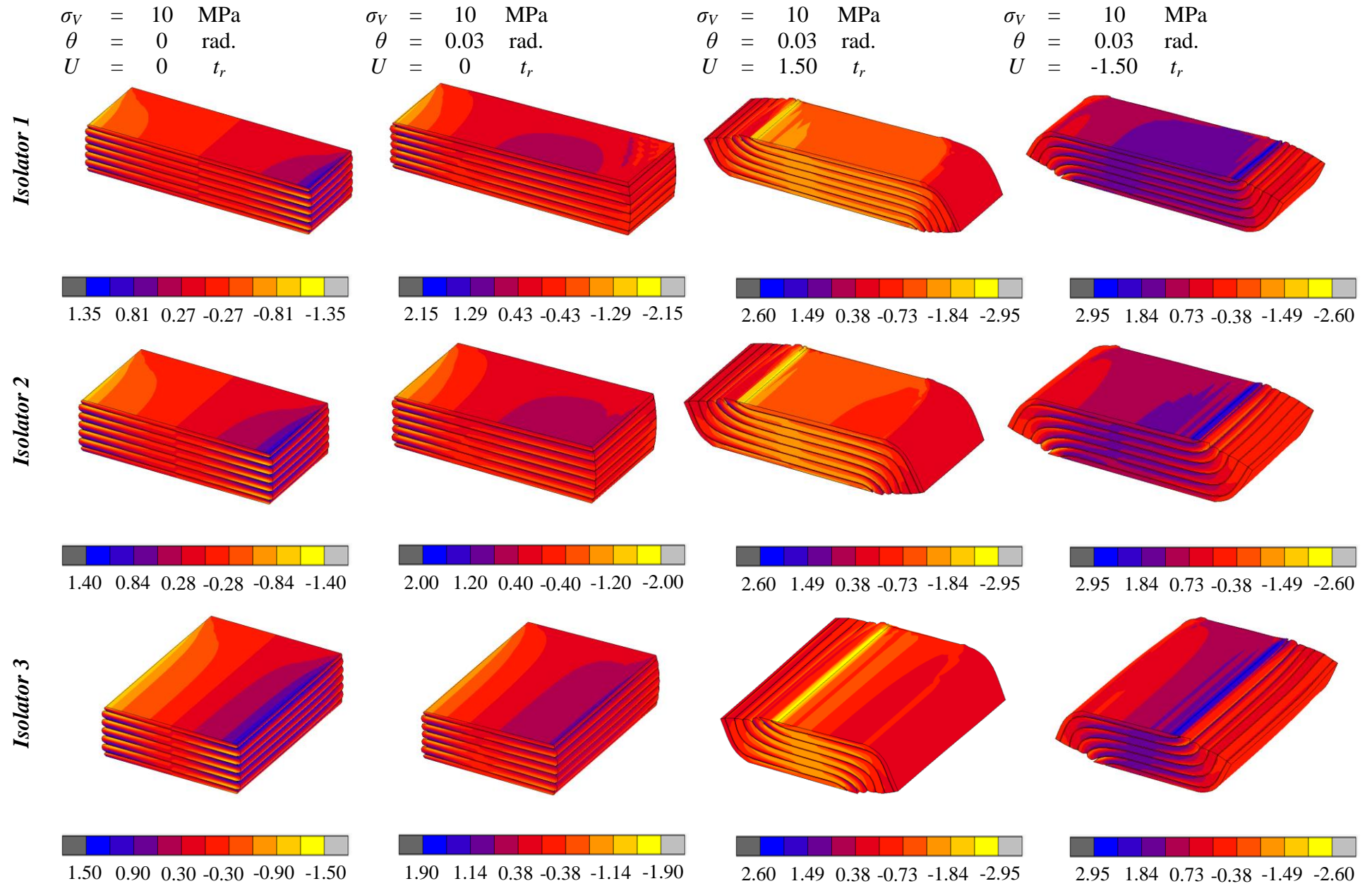


Fig 5-15. Contours of shear strain (γ_{12})

Chapter SIX

Modeling and Evaluation of Seismically Isolated Bridge Using Unbonded Fiber Reinforced Elastomeric Isolators

Abstract

Seismic isolation is a structural technique used to mitigate seismic induced damage in bridges. Traditionally, the design approach employed to protect bridges from earthquakes is by increasing their ductility and/or seismic capacity. However, the goal of seismic isolation is to reduce the seismic demands on the bridge by shifting its fundamental period away from the earthquake's predominant periods. An Unbonded-Fiber Reinforced Elastomeric Isolator (U-FREI) is a relatively new type of elastomeric bearing that can be implemented as a seismic isolator for bridges. U-FREI possess beneficial characteristics including their potentially low-cost and light-weight. Individual U-FREI can be rapidly produced as they can be easily cut from large sheets to the required size and shape, which is an attractive feature for accelerated bridge construction. The objective of this paper is to introduce a non-iterative analytical model to simulate the lateral response of U-FREI. The isolator model is utilized to investigate the seismic response of a typical highway bridge isolated using U-FREI and compare it to a traditional non-isolated bridge. Nonlinear time history analysis was conducted for the two bridge cases to compare the base shears, deck accelerations, and displacements developed in the piers and seismic isolators. The isolated bridge demonstrated a resilient seismic behavior where all the bridge components remained elastic with no damage or residual deformation. The analytical results indicate that the seismic demand of the isolated-bridge is reduced up to 77% and 84% in terms of accelerations and base shear, respectively, as compared to the non-isolated bridge.

6.1. Introduction

The observed number of bridge failures during major seismic events confirms that they are extremely vulnerable to the damaging effects of earthquakes. This highlights the importance of seismic design of bridges and accurate estimation of seismic demands, especially for performance based design (Moustafa and Mosalam 2015). Traditional earthquake-resistant design approaches aim to increase the ductility and/or capacity of a structure. However, the destructive effects of seismic events on bridges (e.g. Kobe 1995) have shown that this approach is insufficient and not the most effective (Jangid 2004). On the other hand, the seismic isolation approach has been found to be more efficient for seismic mitigation (Ghobarah and Ali 1988; Tsopelas et al. 1996; Wesolowsky and Wilson 2003; Jangid 2004; Buckle et al. 2006 & 2011; Siqueira et al. 2014). Seismic isolation can be accomplished by placing laterally flexible isolators between the bridge superstructure (i.e. deck/girders) and the substructure (i.e. piers/bents). By placing these seismic isolators, the bridge superstructure is decoupled from the excessive lateral excitations induced at its base (i.e. substructure). This results in a significant reduction in the transmission of forces between the bridge superstructure and substructure (Kelly 1997; Naeim and Kelly 1999). This reduction on forces allows the bridge to remain in the elastic range and eliminates the occurrence of plastic hinges at the top and bottom of piers as shown in Fig. 6-1. The seismic performance of a bridge can be significantly improved by introducing isolators with low lateral stiffness that are capable of shifting the dominant period of the structure to the displacement sensitive region. Accordingly, the inertial forces are highly reduced, and this is accompanied by a reduction in deformation and stresses in structural elements (Constantinou et al. 2011).

A Steel-Reinforced Elastomeric Isolator (SREI), which comprise elastomeric pads reinforced with steel plates, is widely used for seismic isolation of structures (Kelly and Konstantinidis 2011). The properties of the elastomeric pads highly influence the isolator lateral response, while the role of the steel plates is to increase the vertical stiffness by controlling the bulging of the elastomeric pads under gravity loads. More recently, design codes for bridges (e.g. CHBDC 2014 and AASHTO 2012) have allowed the use of fiber fabric, which has comparable mechanical properties to steel in tension, for reinforcing the elastomeric pads. This type of isolator is denoted as a Reinforced Elastomeric Isolator (FREI). The replacement of steel with fiber can lead to a relative reduction in both weight and manufacturing costs of the isolator allowing it to be economically installed in typical structures.

Another benefit of using FREI is that individual isolators could be manufactured rapidly as they can be cut from large sheets to the required size and shape (i.e. rectangular and circular) using a standard band-saw or water jet cutter. This feature facilitates a number of potential applications where cutting and fine adjustment of the isolator dimensions on site may be required in order to minimize construction time. An example of this potential required on-site adjustment of the isolator would be in Accelerated Bridge Construction (ABC) applications. Typically, the employed types of seismic connections for ABC are energy-dissipated connections, capacity-protected connections, and/or deformation elements (Marsh et al. 2011). As the FREI connection allows this type of isolator to be manufactured and installed in a time saving manner, it is considered to be a viable deformation element that can be employed in ABC.

The upper and lower surfaces of FREI can be either bonded or unbonded to the substructure and superstructure. Early investigations have revealed that unbonded FREI (U-FREI) can effectively protect a structure and its non-structural components from moderate and

strong seismic events (Kelly 1999; Toopchi-Nezhad et al. 2009a; Van Engelen 2015). As a result of the unbonded boundary conditions and lack of flexural rigidity of the fiber fabric reinforcement, U-FREI can detach from the loading supports and experience rollover under large lateral deformations (see Fig. 6-2) and lift-off under excessive rotational deformations. Therefore, this study focuses only on U-FREI. Two parameters that influence the response of U-FREI are the shape factor and the aspect ratio. The shape factor is defined as the ratio between loaded area and the area free to bulge. It is a parameter that strongly influences the vertical and rotational response (Al-Anany and Tait 2015a). The aspect ratio is defined as the ratio of isolator width to the total height of the isolator. It is the controlling parameter for the stable rollover response of FREI under lateral deformation (Van Engelen et al. 2014).

A number of experimental and analytical studies have been carried out to investigate the potential application of U-FREI in improving the seismic performance of structures, particularly in low-rise buildings. Toopchi-Nezhad et al. (2009a) evaluated the effectiveness of U-FREI for mitigation of seismic induced forces by conducting a shake table study on a reduced-scale structure comprised of a two-story one-bay moment-resisting steel frame. The response of the frame, when it is non-isolated and when it is seismically isolated with U-FREI, was evaluated and compared. It was found that the measured roof accelerations, base shear, total drift in the seismically isolated building were 24–32%, 30–35%, and 28–42% of the corresponding values in the fixed base building, respectively. More recently, Osgooei et al. (2015) investigated and compared, via time history analysis, the seismic response of a 2-story reinforced concrete shear wall structure non-isolated and seismically-isolated using U-FREI. Results from these analyses showed that a large reduction can be achieved in base shear, roof acceleration, and roof drift ratio for the seismically-isolated building.

Focusing on bridge applications, Al-Anany and Tait (2015a,b) and Al-Anany et al. (2016a,b) have investigated, via experimental testing, the response of individual U-FREI to determine if it can meet the criteria stated in CHBDC 2014 and AASHTO 2012. In addition, the resulting stress and strain state within the isolator was evaluated and assessed via numerical modeling. It was found that U-FREI can provide satisfactory behavior under the different types of loads/deformations in the vertical, rotational and lateral directions expected in bridge applications.

The objective of this study is to develop a numerical model for the lateral behavior of U-FREI and utilize it to analytically compare the seismic response of a non-isolated bridge to a similar bridge isolated with U-FREI. The non-isolated bridge refers to a bridge where its superstructure is monotonically attached to the substructure at the top of the piers; while it slides on ordinary frictionless seat bearings located at the abutments (see Fig. 6-3a). For the seismically-isolated bridge, the isolators are placed on the top of the bents (i.e. the cap beam and columns) and abutments (see Fig. 6-3b), which leads to full-isolation for the entire superstructure from the substructure.

All the bridge elements were designed to satisfy the provisions of NBCC (2010) and CHBDC (2014) for a site in Victoria, Canada. Nonlinear time history analysis was conducted under a range of ground motions to determine the efficiency of U-FREI for the seismic isolation of bridges. The bridge modeling and finite element simulations were done using the open source finite element platform OpenSees (McKenna et al. 2000). Details of the bridge and U-FREI modeling, selected ground motions, and analysis results and discussions are presented in the following sections.

6.2. Bridge and Isolator Model

A three-dimensional OpenSees model of a typical three-span highway bridge was developed and used for the time history analyses as shown in Fig. 6-4. This section defines the methodology followed and type of elements and materials used in OpenSees for modeling the bridge superstructure and substructure as well as the new proposed model for the U-FREI.

6.2.1. Idealization of the bridge substructure and superstructure

The bridge substructure is comprised of two seat-type abutments and two three-column bents with circular reinforced concrete (RC) columns that support integral bent cap beams. The bent caps span the entire bridge width and, in turn, support the box-girder superstructure. Thus, the bridge superstructure is supported on two abutments and two transverse bridge frames (three columns and a bent cap beam). The bent cap beam is considered to be integrated with the superstructure box-girder only for the non-isolated bridge. For the seismically-isolated bridge, the bent cap is located beneath the superstructure (i.e. attached to columns) and the seismic isolators are located between the bent cap and the box-girder. In the seismically-isolated case, the box-girders are connected with rigid diaphragms at the bents' locations. The height of the bridge columns (h_c) is maintained the same in this study (see Fig. 6-3) to allow direct comparisons between the non-isolated and the isolated bridges.

The “NonlinearBeamColumn” element available in OpenSees is used to model the columns and bent cap beams. This nonlinear element is defined by fiber sections, which are discretized into smaller regions for which the material stress-strain response is integrated to obtain global component behavior (McKenna et al. 2000). The fiber section is subdivided into concrete patches and steel layers as illustrated in Fig. 6-5a. The patches (cover and core) are

defined using one of the available concrete material models, while the steel layers are defined using a reinforcing steel material in order to create the full RC section.

Two materials from OpenSees *Concrete02* and *Steel02* are used to define the material characteristics of the concrete and reinforcing steel, respectively. *Concrete02* and *Steel02* are uniaxial materials with uniaxial stress-strain (or force-deformation) relationships. *Concrete02* (Yassin M. 1994) is able to capture the nonlinear behavior of concrete in compression as well as a linear tension softening behavior as illustrated in Fig. 6-5a. The reinforcing bars are modeled using *Steel02* (Filippou 1983), which has a bilinear behavior with kinematic strain hardening (see Fig. 6-5b).

The superstructure of the bridge, which refers to a typical RC box-girder, is modeled using linear elastic elements. This is because bridge superstructures are capacity protected elements that are required to remain elastic under vertical and lateral seismic loads (AASHTO 2011). The section properties (e.g. area, inertia...etc.) of the box-girder equivalent cross-section are defined using the dimensions and reinforcement design from Moustafa and Mosalam (2015). The inelastic nonlinear behavior of the bridge is concentrated only in the columns, which are the fuse components allowed by design codes to develop plastic hinges under excessive ground motions. This means that the cap beam is also designed as a capacity protected member that remains elastic when the bridge columns reaches their over strength capacity (AASHTO 2011).

6.2.2. Idealization of the U-FREI Behaviour

The lateral behavior of U-FREI consists of three main stages as shown in Fig. 6-6. At lower lateral displacement amplitudes, the isolator is still in full contact with the supports, which results in a linear behavior similar to that of a bonded isolator. At intermediate lateral amplitudes, there is a gradually increasing loss of contact with the supports, leading to a

softening behavior in the lateral response. Under large lateral displacements, contact between the originally vertical faces of the isolator and the supports occur, resulting in a stiffening behavior.

Several models have been employed to describe the nonlinear force-displacement behavior of U-FREI. However, most of these models are iterative and amplitude-dependent (Toopchi-Nazhad et al. 2009; Manzoori and Toopchi-Nezhad 2016). In this study, a non-iterative rate-independent *Takeda-Elastic* model has been developed to represent the lateral response of the U-FREI. The model comprises a Takeda-based bilinear plastic model (Takeda et al. 1970) in parallel with a nonlinear elastic spring as shown in Fig. 6-7. A beneficial feature of this model is that the *Takeda-Elastic model* parameters can be directly determined from the effective lateral stiffness and damping values without the need to directly fit to the entire hysteresis loops. It is worth noting that a similar concept was employed to capture the U-FERI lateral behavior but using pivot elements available in SAP2000 by Osgooei et al. (2015). Thus, the proposed model in this study builds on the Osgooei et al. (2015) model and provides immediate and practical implementation in OpenSees as explained next.

Assuming a bilinear Takeda-hysteresis model with an initial stiffness of k_1 , post yield stiffness of k_2 , a yield displacement of u_y , the force of the Takeda-based bilinear model is equal to:

$$\begin{aligned} F_{TA} &= k_1 u_y & u < u_y \\ F_{TA} &= k_1 u_y + k_2 (u - u_y) & u \geq u_y \end{aligned} \quad (1)$$

Using a fifth order polynomial to describe the nonlinear elastic spring (NES), the relationship between the force of the nonlinear elastic spring, F_{NES} , and the isolator displacement, u , can be written as follows:

$$F_{NES} = a_1 u + a_2 u^3 + a_3 u^5 \quad (2)$$

where a_i are the polynomial parameters. Accordingly, the effective stiffness k_{eff} of the proposed *Takeda-Elastic* model can be expressed as:

$$k_{eff} = \frac{F_{TA} + F_{NES}}{u} \quad (3)$$

where,

$$\begin{aligned} k_{eff} &= k_1 + a_1 + a_2 u^2 + a_3 u^4 & u < u_y \\ k_{eff} &= (k_1 - k_2) \frac{u_y}{u} + k_2 + a_1 + a_2 u^2 + a_3 u^4 & u \geq u_y \end{aligned} \quad (4)$$

Additionally, the effective damping β_{eff} when the lateral displacement u is greater than u_y can be expressed as

$$\beta_{eff} = \frac{1}{4\pi} \left[\frac{(k_1 u_y + k_2 (u - u_y)) \cdot 2 \left(u - \frac{k_1 u_y + k_2 (u - u_y)}{k_1} \right)}{k_{eff} \cdot u^2} \right] \quad (5)$$

The model parameters can be determined by minimizing the error between the values of the effective stiffness and effective damping ratio determined experimentally with those calculated from Eqs. (4) and (5). Thus, experimental data is still required to calibrate the proposed model parameters, but only once for a given isolator. In this study, the model parameters were calibrated using results from an experimental test conducted on a reduced-scaled U-FREI specimen. The test used a 3 degree-of-freedom (DOF) bearing test apparatus (see Fig. 6-8a) to determine the lateral response of the considered isolator. The test specimen was made up from natural rubber with a shear modulus more reflective of that used for bridges applications. The physical plan dimensions of the tested isolator is approximately equal to 70 mm \times 70 mm, and its total height is equal to 20.6 mm. This total height is comprised of a total rubber thickness t_r equal to 19 mm in addition to the fiber reinforcement thickness of 1.60 mm. Fig. 6-8b presents the experimental lateral response of the considered isolator under a range of lateral displacement amplitudes and under a mean compressive stresses σ_v of 6 MPa. As shown

in Fig. 6-8b, the force is normalized with respect to the isolator plan area A and shear modulus G , which was experimentally determined to be 0.86 MPa. The lateral displacement is normalized with respect to the total rubber thickness t_r .

For the analytical case study presented herein, the geometric properties of the tested isolator were scaled up by a factor of 4 to maintain an average vertical stress of 6 MPa on each isolator placed between the bridge superstructure and substructure. The dimensions of the $\frac{1}{4}$ scale tested model as well as the considered prototype isolator are presented in Table 6-1.

Table 6-2 shows the analytical model parameters calculated using Eqs. (4) and (5) in order to match the effective stiffness and damping obtained from experimental test results. Furthermore, it is noted that the effects of any rotational deformations for the girder on the lateral response of U-FREI is neglected because research investigations showed that it does not have a significant effect on the lateral behavior of the considered type of isolators (Al-Anany et al. 2017).

To implement the *Takeda-Elastic* isolator model in OpenSees, two “ZeroLength” elements represented by *Hysteretic* and *MultiLinear* materials connected in parallel. In order to ensure the adequacy of the selected element and material model for the U-FREI, the modeled isolators were independently subjected to cyclic loading under displacement control using OpenSees, similar to the experimentally conducted tests. Fig. 6-8b compares the measured hysteretic behavior with the simulated behaviour obtained from OpenSees. Good agreement is found between the experimental and analytical behavior for the proposed *Takeda-Elastic* model using the parameters given in Table 6-2. The ratios of the results determined from the analytical *Takeda-Elastic* model to the experimental values over each cycle are compared in Table 6-3. The table shows that the differences were found to be within 5%. This demonstrates overall good

agreement with the experimental results and validates the use of the developed seismic isolator model for the case study considered in the paper.

6.3. Ground Motion Records

A total of twenty ground motions (see Table 6-4) were employed in the nonlinear time history analysis of prototype bridge model. The ground motions used for this study were originally extracted from the strong ground motions database of PEER-NGA-2 (Pacific Earthquake Engineering Research Center). The main criterion for selecting the considered ground motions was based on the work by Baker et al. (2011) for selecting standardized sets of ground motions that would meet user-specific needs. Accordingly, the earthquakes were selected from a list provided by Baker et al. (2011) for a set of broadband ground motions for a rock site with a magnitude range between 5.7 and 7.9 MPa as would be expected in a typical hazard scenario in Victoria, Canada. The twenty ground motions were scaled to have a 5% damped response spectra (see Fig. 6-9a) that matches a design-basis earthquake (DBE) spectrum for Victoria, Canada (see Fig. 6-9b). Moreover, following the CHBDC (2014) guidelines, all site class factors were assumed to be unity as the reported shear wave velocities for the selected earthquakes were within the limit of 760 m/sec. The scaling was conducted to minimize the difference between the values of spectral accelerations of the scaled ground motions with the DBE spectrum over the range of the two expected natural periods corresponding to the non-isolated and totally-isolated bridge models. Two sets of analyses were conducted in this study which considered each of the horizontal components of the selected ground motions applied independently, i.e. one set of the analysis applied the ground motions in the longitudinal direction of the bridge, while the second set was applied in the transverse direction. It is noted that only uniaxial earthquake loading was considered, either in the transverse or longitudinal directions independently, because the U-FREI

behavior under combined transverse and longitudinal lateral loading was not evaluated experimentally.

The natural period of vibration for the non-isolated bridge was determined from a preliminary modal analysis carried out in OpenSees, and was found to be approximately 0.35 sec and 0.50 sec in the longitudinal and transverse direction, respectively. The natural period range for the totally-isolated bridge was calculated according to ASCE (2010) based on the minimum and maximum values of the effective stiffness of the isolation system, and was found to be in a range of 1.50-1.90 seconds.

In addition to the considered DBE, two additional levels of earthquake hazards were considered: strength (service) level earthquake (SLE) and maximum credible earthquake (MCE). According to CHBDC (2014), DBE represents mid-hazard level earthquakes with 5% probability of exceedance in 50 years (975-year return period). SLE represents low hazard level earthquakes with 10% probability of exceedance in 50 years (475-year return period), and MCE represents high hazard level earthquakes with 2% probability of exceedance in 50 years (2,475-year return period). Thus, after the ground motions were selected based on the DBE spectrum, their amplitudes were multiplied by $1/3$ and $3/2$ in order to simulate the MCE and SLE hazards levels, respectively, according to the provisions of ASCE (2010).

6.4. Results and Discussion

This section presents the nonlinear time history analysis results of the non-isolated and isolated bridge cases and the response parameters that influence the seismic performance of bridges during earthquakes. The emphasis is placed on studying the base shear in the substructure, the acceleration at the superstructure deck level, and the displacement demands in seismic isolators. All the response parameters were studied independently in the two orthogonal directions as the

sets of uniaxial ground motions were applied in the longitudinal and transverse directions, respectively. Due to the bridge symmetry, and because of the nature of substructure-to-superstructure connection, the analysis results are presented for one of the two bridge bents, (i.e. the bent-cap and three-columns frame). The force and displacement responses are shown for the full bent, the moment and curvature responses are selected for one of the bent columns with largest demands, and the absolute recorded acceleration is shown for the center of the bridge deck. The response histories and seismic demand comparisons for the isolated and non-isolated bridges are presented next.

6.4.1. Response Histories

A comparison between the base shear histories of the both the non-isolated and isolated bridge under the MCE hazard level of *Earthquake 11* (see Table 6-4) is normalized with respect to the bridge weight and shown in Fig. 6-10. It is shown that U-FREI is very effective and significantly reduces the base shear in the bridge columns. The figure compares the response in both transverse and longitudinal directions where the observed difference in the base shear is due to the variation in the bridge flexibility in both directions. However, the difference in the response for the isolated bridge in the longitudinal and transverse direction is not as much as in case of non-isolated bridge. This is attributed to the fact that in both cases, the bridge vibrates as a nearly rigid body on the isolators.

Similar time histories plots presenting the effectiveness of the U-FREI in reducing the absolute deck acceleration response are shown in Fig. 6-11. As expected, the implementation of seismic isolators that have very low lateral stiffness relative to the columns led to a significant reduction in the acceleration response as a result of the large shift in time period. This observation suggests that an additional energy dissipation mechanism for the excessive energy

resulting from the ground motions is provided by the U-FREI, which reduces the superstructure accelerations as well as the substructure base shear. It can also be concluded from Figs. 6-10 and 11 that the higher demands on the non-isolated bridge make it seismically more vulnerable than the equivalent isolated bridge.

Fig. 6-12 illustrates the observed deck displacement at the top of the bent cap beam of one of the two bents in the case of the non-isolated bridge. The figure shows that a non-favorable scenario of post-earthquake residual displacement and permanent damage is expected in the case of non-isolated bridge. These residual displacements are a result of the excessive inelastic deformations experienced by the bridge columns, particularly under MCE level. It is important to note that residual displacement is one of the critical aspects used to assess the usability/functionability of the bridge for immediate use after an earthquake. Excessive residual displacements and permanent damage can also lead to expensive repair schemes or complete demolition of a bridge. A good example of this is the 1995 Kobe earthquake, where a large number of bridges were demolished due to excessive residual damage in the columns that exceeded acceptable residual displacement limits. Accordingly, new resilient bridge designs are currently sought where immediate use of bridges after earthquake events is desired. Thus, seismic isolation features an excellent solution for infrastructure resiliency.

To demonstrate the efficiency of U-FREI in eliminating any residual displacements or damage, Fig. 6-13 shows the deck displacements in the case of the isolated bridge. Larger lateral displacements were observed in the isolated bridge compared to the non-isolated bridge but no residual displacements occurred. However, these large lateral displacements are entirely accommodated by the U-FERI rather than the bent columns (see Fig. 6-1). Accordingly, very low seismic demands are developed in the bridge superstructure and substructure, where both

behave as two decoupled rigid bodies. As such, the transmitted force between the superstructure and substructure is highly dependent on the effective lateral stiffness of the employed isolation system, which is already very low compared to the bent-cap-columns system. It is also to be noted that the zero residual displacements in the isolated bridge are attributed to the restoring forces in the isolation system, which re-centers the bridge deck above the bent-cap beam.

6.4.2. Seismic Demands Comparison

In addition to the response histories comparison shown above, the peak response values are summarized and compared in this subsection. Fig. 6-14 presents the mean values from the 20 ground motions of the peak base shear (V_{maximum}) developed in a single bent in the non-isolated and isolated bridges for each of the three hazard levels. The peak response is plotted for both longitudinal and transverse directions. The values are normalized with respect to the total gravity loads (W_b) on the three-column bent. It can be observed from Fig. 6-14 that the isolation of the bridge using U-FREI results in a reduction in the shear forces developed within the substructure piers when compared to the non-isolated bridge. For the three earthquake hazard levels, the reduction in the mean value of the peak shear in the substructure was found to be up to 68% and 77% for the longitudinal and transverse directions, respectively.

Furthermore, the significant reduction in the isolated bridge base shear (Fig. 6-14) was sufficient to decrease the peak base shear under all considered earthquakes to below the elastic limit ($\sim 0.43W_b$), i.e. before initiation of yielding or the formation of any plastic hinges in the bridge columns. Thus, the behavior of the non-isolated bridge remained within the elastic envelope as demonstrated by the normalized column force-deformation relationship and column moment-curvature relationship shown in Fig. 6-15a and 6-15b, respectively. However, for the non-isolated bridge, yielding and hysteretic damage was observed for most earthquake ground

motions. This yielding was particularly evident at the DBE and MCE level as shown for one of the selected ground motions (MCE of Earthquake 11) in Fig. 6-15.

Nevertheless, it should be noted that if it is desired to design the non-isolated bridge columns not to exceed the elastic design limits, this requires a significant increase in the column size and capacity. Thus, designing a non-isolated bridge to resist severe earthquake elastically is considered uneconomical (Ghobarah and Ali 1988). However, under the same loading conditions, columns located in base-isolated bridge are designed for much lower forces, which leads to economical and compact cross sections. Additionally, increasing the ductility and/or capacity of the piers is not as effective as seismic isolation due to significant post-earthquake repair costs (Jangid 2004).

Fig. 6-16 shows the mean values for the peak accelerations that are recorded in the center of the bridge superstructure deck in the longitudinal and transverse directions. For the three hazard levels, seismic isolation using U-FREI resulted in a reduction in the deck acceleration by at least 71% and 84% in the longitudinal and transverse direction, respectively. It is noted from Figs. 6-14 and 6-16 that more significant reduction in pier base shear and deck acceleration is observed in the transverse direction when compared to the longitudinal direction as summarized in Fig. 6-17. The reduction in base shear was found to be higher in the transverse direction by an approximate value of 21%, 17% and 12% for the SLE, DBE, and MCE hazard levels, respectively, compared to the equivalent values observed in the longitudinal direction. Similarly, the corresponding reduction in the deck acceleration was higher in the transverse direction by 24%, 18%, and 16% for the SLE, DBE, and MCE hazard levels, respectively. Thus, it can be concluded that the characteristics of the bridge (i.e. stiff/flexible) plays a crucial role in controlling the isolation efficiency of U-FREI. A stiffer bridge experiences more reduction in its

seismic demand if it is seismically isolated. In addition, it is important to note that the soil site (i.e. hard rock) considered in this study is another important factor that contributed to the observed significant reduction. This means that a lower reduction or even a different response could be exhibited if the same isolator was employed in a more flexible bridge located in a soft soil condition that is capable of highly increasing the energy transmitted to the bridge, particularly at lower frequencies (Ghobarah and Ali 1988). While only a relatively stiff bridge on hard rock soil condition was considered in this study to demonstrate the effectiveness of U-FERI, other bridge and soil conditions should be considered in future studies.

Finally, Fig. 6-18 shows the values of the peak U-FERI displacements developed in the bridge superstructure as a result of seismic isolation. The results are presented for the three hazard levels considered in the study and for all of the 20 considered ground motions in both longitudinal and transverse directions. As expected, the displacement range for the isolators is directly proportional to the hazard level of the applied ground motion. This observation is in agreement with the provisions of ASCE (2010) for the calculation of minimum and maximum displacements of the seismic isolator employed. As also expected, the displacements developed in the transverse direction are higher than for longitudinal direction. This is due to the flexibility of the bridge in the longitudinal direction, which allows a portion of the displacement demand to be accommodated by the piers. On the other hand, it should be noted that an excessive increase in the displacement response in the bridge superstructure due to the usage of seismic isolators may lead to damage of the bridge expansion joints (Constantinou et al. 2011). Thus, if further reduction in the isolated bridge deck displacement is desired, additional energy dissipation devices connected between the bridge superstructure and substructure can be employed (Syngellakis 2013).

6.5. Summary and Conclusions

In this paper, an analytical model, called the *Takeda-Elastic model*, was developed to simulate the lateral response of U-FREI. The model comprises a parallel combination of a bilinear Takeda Hysteresis Model and a nonlinear elastic spring. Both components are represented by simplified parameters that were accurately calibrated using experimental test results. Advantages of the proposed model are that it is non-iterative, it can accurately predict the effective stiffness and damping of the modeled isolator at each lateral displacement amplitude, and it does not require fitting over the entire experimentally obtained hysteresis loops for calibration. A nonlinear time history analysis framework was conducted on a typical highway bridge to utilize the developed *Takeda-Elastic* model and investigate the effectiveness of U-FREI bridge seismic isolation. Two different types of bridges were considered for analysis: a non-isolated bridge that has a monolithic connection between the superstructure and substructure, and an isolated bridge, which is isolated by U-FREI at bents and abutments. The seismic analysis of the bridges was carried out for 20 earthquake ground motions and three earthquake hazard levels (SLE, DBE, and MCE).

The main findings of this study are as follows:

- The peak response values of columns base shear and deck accelerations show a significant reduction in the isolated bridge when compared with the results for the corresponding non-isolated bridge. The reduction in the peak values of the bents base shear of the isolated bridge was in the range of 59% to 67% in the longitudinal direction, and in the range of 72% to 77% in the transverse direction as compared to the non-isolated bridge. The reduction in the peak value of the absolute acceleration at the deck

level was in range of 61% to 70% and 76% to 84% in the longitudinal and transverse direction, respectively, as compared to the non-isolated bridge.

- All the bridge components, particularly the columns, remained within its elastic range with no yielding or plastic hinge damage in the isolated bridge. Moreover, no residual displacements or permanent deformation are developed in the isolated bridge, so expensive post-earthquake repair or traffic down time are eliminated. Thus, bridge isolation using U-FREI is an attractive solution for the development of resilient infrastructure systems.
- A slight increase in terms of the isolator lateral rollover was developed when the isolators are used in the stiffer direction of the bridge. Similarly, the seismic demand reduction relative to the non-isolated bridge case varies with the bridge stiffness.
- Overall, this paper shows that U-FREI has the potential to efficiently improve the seismic response in highway bridges during a seismic event. U-FREI is characterized by low weight, potentially low cost, and can be employed in a reduced time manner, which is an attractive feature for accelerated bridge construction applications. However, the study focused on a relatively stiff bridge on a hard rock soil condition. Thus, it is recommended that additional future studies examine the influence of flexibility in bents and decks along with the effects of different soil conditions and soil-structure interaction to fully characterize the effectiveness of U-FREI use in highway bridge seismic isolation.

Acknowledgements

The authors would like to gratefully acknowledge the support provided by the Ontario Ministry of Research and Innovation (MRI), and the Natural Sciences and Engineering Research Council of Canada (NSERC). Additionally, the authors are grateful for the support provided by MSC Software Corporation.

References

- AASHTO. (2012). *American Association of State Highway and Transportation Officials. LRFD Bridge Design Specifications*, Washington, D.C.
- AASHTO. (2011). *Guide Specifications for LRFD Seismic Bridge Design*, 2nd ed., American Association of State Highway and Transportation Officials, Washington, D.C.
- Al-Anany Y, Tait M. (2015a). "A Study on the Rotational Behavior of Bonded and Unbonded Fiber Reinforced Elastomeric Isolators", *11th Canadian Conference on Earthquake Engineering*, Victoria, British Columbia, Canada, 21-24 July.
- Al-Anany Y, Tait M. (2015b). "A numerical study on the compressive and rotational behavior of fiber reinforced elastomeric isolators (FREI)". *Composite Structures*, 133: 1249-1266.
- Al-Anany Y., Tait M., Torrie M., Sciascetti A. (2016a). "The Vertical, Rotational and Lateral Response of Unbonded Fiber Reinforced Elastomeric Isolators", *Annual Conference of the Canadian Society for Civil Engineering (CSCE)*, London, Ontario, June 1-4, 2016.
- Al-Anany Y., Van Engelen N., Tait M., Konstantinidis D. (2016b). "Examination of Fiber Reinforced Elastomeric Isolators for Bridge Applications", *International Joints and Bearings Research Council*, Atlanta, Georgia, USA, 25-29 September.
- Al-Anany Y., Tait M., Moustafa M., Torrie M. (2017). "A study on the Response of Fiber Reinforced Elastomeric Isolators Under Combined Loading", *16th World Conference on Earthquake Engineering (16WCEE)*, Chile, 9-13 January, 2017.
- ASCE. (2010). American Society of Civil Engineers. *Minimum Design Loads for Buildings and other Structures*, ASCE/SEI 7-10. New York: American Society of Civil Engineers.
- Baker J., Lin T, Shahi S. (2011). *New ground motion selection procedures and selected motions for the PEER transportation research program*. PEER Report 2011/03, Pacific Earthquake Engineering Research Center, University of California, Berkeley.

Buckle I., Constantinou M., Dicleli M., Ghasemi H. (2006). *Seismic Isolation of Highway Bridges*. Special Publication MCEER-06-SP07, Multidisciplinary Center for Extreme Events Research, University at Buffalo, Buffalo NY, 171pp.

Buckle, I. G., Moustafa Al-Ani, Eric Monzon. (2011). *Seismic isolation design examples of highway bridges*. NCHRP Project: 20-7.

CHBDC. (2014). *Canadian Highway Bridge Design Code*. CAN/CSA-S6. Canadian Standard Association. Ontario.

Constantinou M., Kalpakidis I., Filiatrault A., Ecker Lay R. (2011). *LRFD-based analysis and design procedures for bridge bearings and seismic isolators*. Report No. MCEER-11-0004, Multidisciplinary Center for Earthquake Engineering Research, University at Buffalo, State University of New York, Buffalo, New York.

Filippou F., Popov E., Bertero V. (1983). *Effects of Bond Deterioration on Hysteretic Behavior of Reinforced Concrete Joints*. Report EERC 83-19, Earthquake Engineering Research Center, University of California, Berkeley.

Ghobarah A., Ali H. (1988). "Seismic performance of highway bridges", *Engineering Structures*, 10(3): 157-166.

Jangid R. (2004). "Seismic response of isolated bridges." *Journal of Bridge Engineering*, 9(2): 156–166.

Kelly J., Konstantinidis D. (2011). *Mechanics of rubber bearings for seismic and vibration isolation*. Chichester, UK: Wiley.

Kelly J. (1999). "Analysis of fiber-reinforced elastomeric isolators", *Journal of Seismology and Earthquake Engineering*, 2(1):19–34.

Yassin M. (1994). *Nonlinear Analysis of Prestressed Concrete Structures under Monotonic and Cycling Loads*, Ph.D. dissertation, University of California, Berkeley.

McKenna F., Fenves G., Scott M., Jeremic B. (2000). *Open System for Earthquake Engineering Simulation (OpenSees)*, Pacific Earthquake Engineering Research Center, University of California, Berkeley, CA.

Manzoori A., Toopchi-Nezhad H. (2016). "Application of an Extended Bouc-Wen Model in Seismic Response Prediction of Unbonded Fiber-Reinforced Isolators", *Journal of Earthquake Engineering*.

Marsh M., Wernli M., Garrett B., Stanton J., Eberhard M., Weinert M. (2011). *Application of Accelerated Bridge Construction connections in Moderate-to-High Seismic Regions*. NCHRP Report 698. Transportation Research Board, Washington, DC.

Moustafa M., Mosalam K. (2015). "Seismic response of bent caps in as-built and retrofitted reinforced concrete box-girder bridges", *Engineering Structures*; 98: 59-73.

Naeim F., Kelly J. (1999). *Design of Seismic Isolated Structures: From Theory to Practice*. John Wiley & Sons.

NBCC. (2010). *National Building Code of Canada*. Institute for Research in Construction, National Research Council of Canada: Ottawa.

Osgoee P., Tait M., Konstantinidis D. (2015). “Non-iterative computational model for fiber-reinforced elastomeric isolators”, *Engineering Structures*, in press.

Osgoee P., Tait M., Konstantinidis D. (2015). “Seismic Isolation of a Shear Wall Structure Using Rectangular Fiber-Reinforced Elastomeric Isolators”, *Journal of Structural Engineering*, p.04015116.

PEER Ground Motions, Pacific Earthquake Engineering Research Center, Strong Ground motion Database, University of California at Berkeley, USA. (last date accessed 04/2016).

SAP2000 version 16.0.0 [Computer software]. Berkeley, CA, Computers and Structures.

Siqueira G., Sanda A., Paultre P., Padgett J. (2014). “Fragility curves for isolated bridges in eastern Canada using experimental results”, *Engineering Structures*; 74, 311-324.

Syngellakis S. (2013). *Seismic Control Systems: Design and Performance Assessment*. Wit Press.

Takeda T., Sozen M., Nielsen N. (1970). “Reinforced concrete response to simulated earthquakes”, *Journal of the Structural Division*; 96(12): 2557-2573.

Toopchi-Nezhad H., Tait M., Drysdale R. (2009a). “Shake table study on an ordinary low-rise building seismically isolated with SU-FREIs (stable unbonded fiber-reinforced elastomeric isolators)”, *Earthquake Engineering & Structural Dynamics*; 38(11): 1335–57.

Toopchi-Nezhad H., Tait M. Drysdale R. (2009b). “Simplified analysis of a low-rise building seismically isolated with stable unbonded fiber reinforced elastomeric isolators”, *Canadian Journal of Civil Engineering*; 36(7): 1182-1194.

Tsopelas P., Constantinou M., Okamoto S., Fujii S., Ozaki D. (1996). “Seismic performance of highway bridges”, *Engineering Structures*; 18(4): 301-310.

Van Engelen, Niel C., Konstantinidis D., Tait M. (2015). “Structural and nonstructural performance of a seismically isolated building using stable unbonded fiber reinforced elastomeric isolators”, *Earthquake Engineering & Structural Dynamics*; 45(3): 421-439.

Wesolowsky M., Wilson J. (2003). “Seismic isolation of cable-stayed bridges for near-field ground motions”, *Earthquake Engineering & Structural Dynamics*; 32(13): 2107–26.

Table 6-1: Specifications of the U-FREI specimen

	¼ scale model	Prototype model
Width (a)	70 mm	280 mm
Length ($2b$)	70 mm	280 mm
Total rubber thickness (t_r)	18 mm	72 mm
Total height of bearing (h)	20.6 mm	82.4 mm
Aspect ratio (R)	3.4	3.4
Shape Factor (S)	5.6	5.6

Table 6-2: Parameters of the *Takeda-Elastic Model*

Parameter	Value
k_1 (N/mm)	1800
k_2 (N/mm)	120
u_y (mm)	6
a_1 (N/mm)	370
a_3 (N/mm ³)	-0.015
a_5 (N/mm ⁵)	9.20×10^{-7}

Table 6-3: Comparison of the predicted analytical response solution to the experimental results

U / t_r	$K_{experimental}$	$K_{analytical}$	Error	$\beta_{experimental}$	$\beta_{analytical}$	Error
(%)	(N/mm)	(N/mm)	(%)	(%)	(%)	(%)
25	1045	1066	2	12.3	12.9	5
50	752	760	1	12.8	13.2	3
100	577	577	0	11.9	12.3	3
150	534	534	0	11.1	11.2	1
200	645	645	0	8.2	8.4	2

Table 6-4: The selected ground motion records

ID	Earthquake	Year	Station	Magnitude
1	Coyote Lake	1979	Gilroy Array #6	5.74
2	Imperial Valley-06	1979	Cerro Prieto	6.53
3	Victoria_ Mexico	1980	Cerro Prieto	6.33
4	Taiwan SMART1(45)	1986	SMART1 E02	7.30
5	Loma Prieta	1989	Gilroy - Gavilan Coll.	6.93
6	Loma Prieta	1989	Gilroy Array #6	6.93
7	Loma Prieta	1989	San Jose - Santa Teresa Hills	6.93
8	Northridge-01	1994	Burbank - Howard Rd.	6.69
9	Northridge-01	1994	LA - Chalon Rd	6.69
10	Northridge-01	1994	LA - Wonderland Ave	6.69
11	Northridge-01	1994	Santa Susana Ground	6.69
12	Northridge-01	1994	Vasquez Rocks Park	6.69
13	Kocaeli_ Turkey	1999	Gebze	7.51
14	Kocaeli_ Turkey	1999	Izmit	7.51
15	Chi-Chi_ Taiwan	1999	TCU129	7.62
16	Sitka_ Alaska	1972	Sitka Observatory	7.68
17	Hector Mine	1999	Heart Bar State Park	7.13
18	Denali_ Alaska	2002	Carlo (temp)	7.90
19	Chi-Chi_ Taiwan-03	1999	TCU138	6.20
20	Chi-Chi_ Taiwan-06	1999	TCU129	6.30

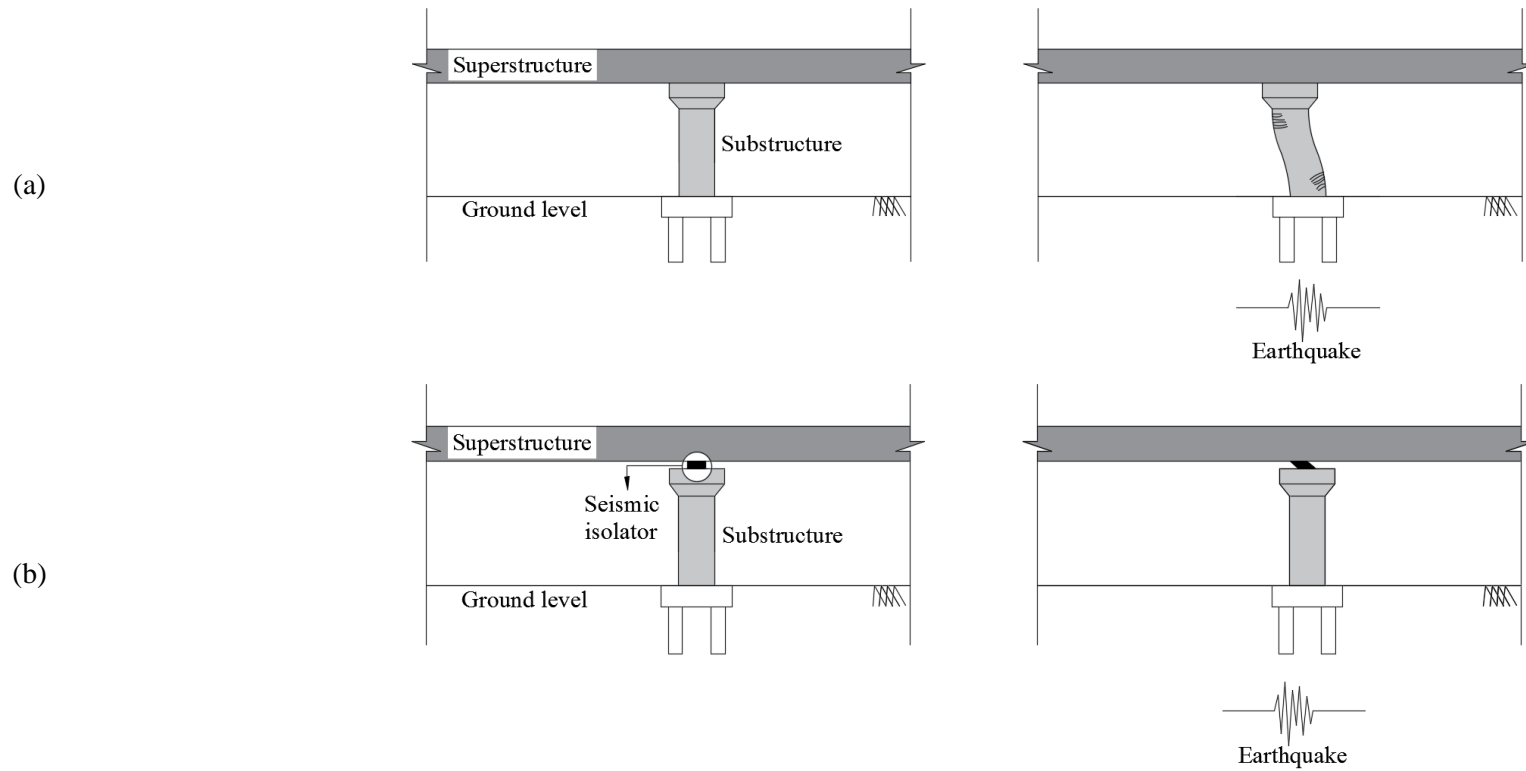


Fig. 6-1: A comparison between:
(a) non-isolated bridges (deformation occurs in substructure);
and (b) isolated bridges (deformation occurs in seismic isolators)

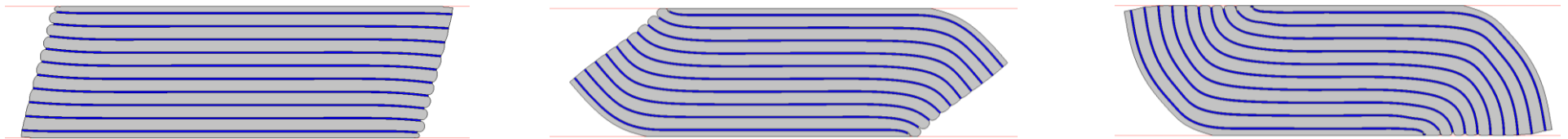


Fig. 6-2: Deformation progress of *rollover* in U-FREI under lateral deformation

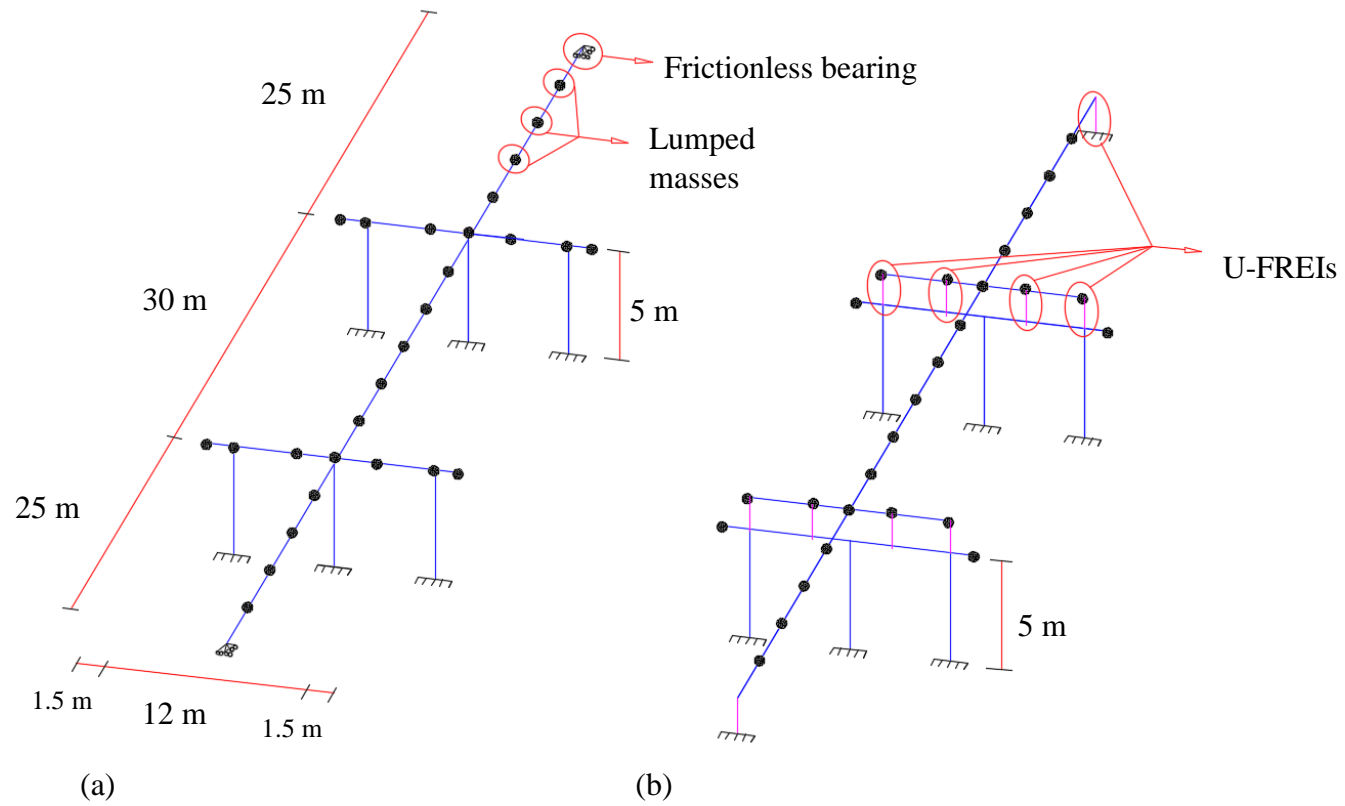


Fig. 6-4: The three-dimensional bridge model: (a) non-isolated, (b) isolated.

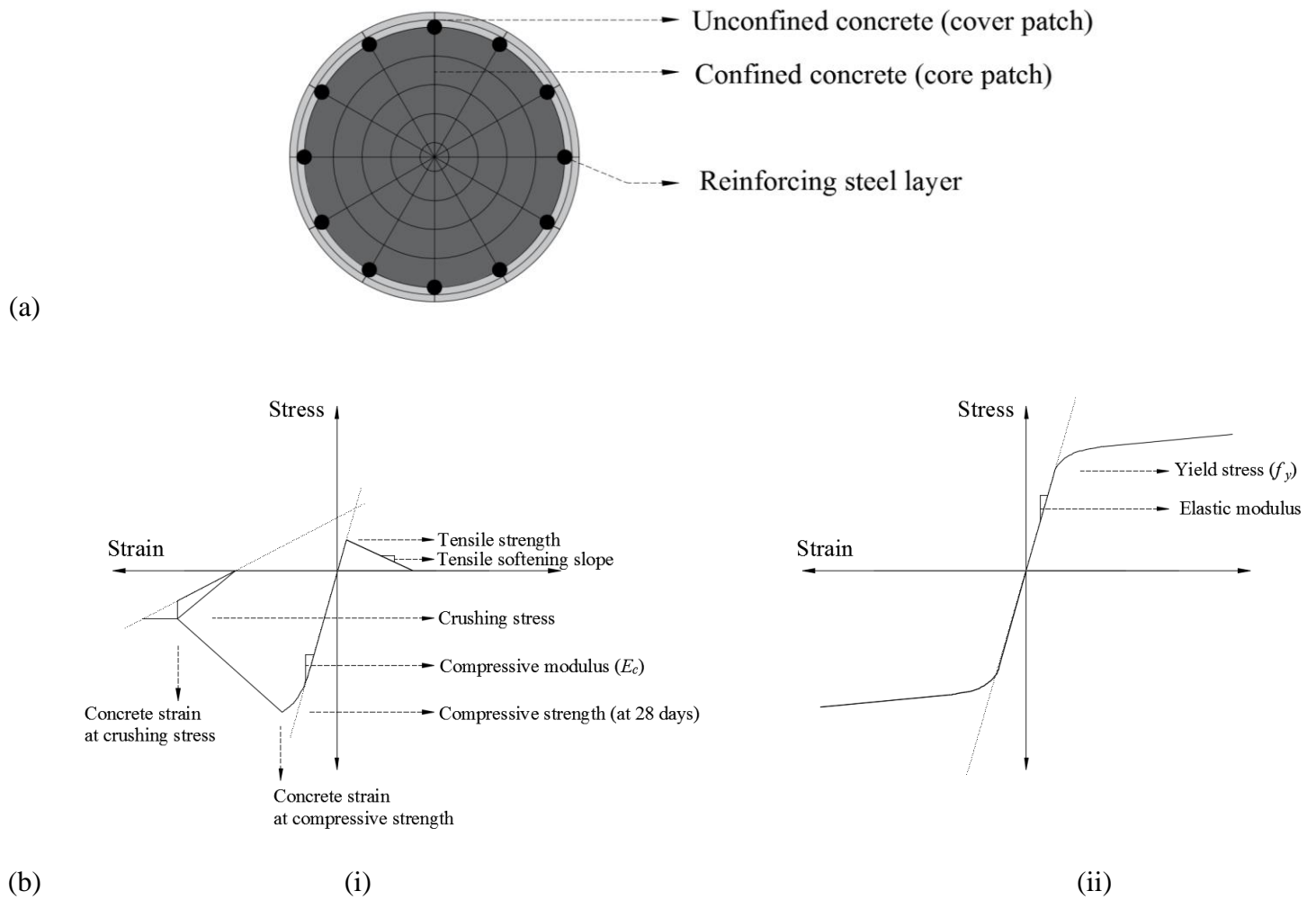


Fig. 6-5: (a) A typical OpenSees fiber-section defined for RC circular column; (b) the stress-strain relationship of: (i) *concrete-02*; (ii) *steel-02* as defined in OpenSees

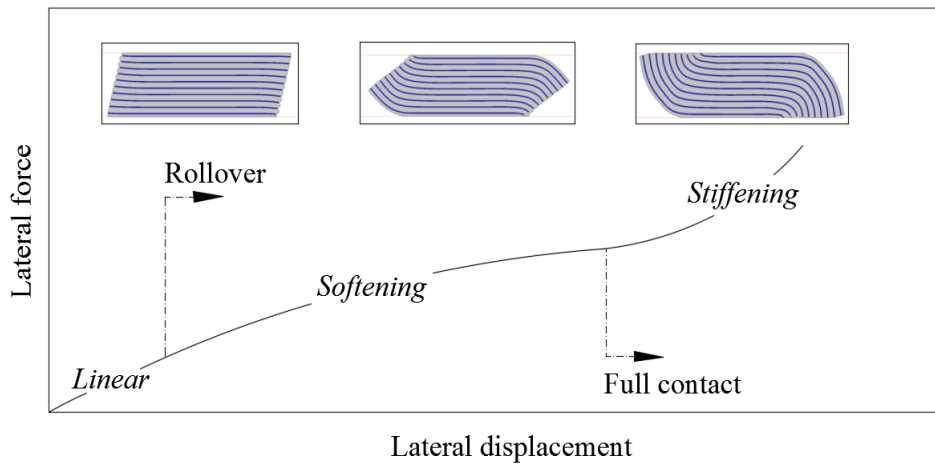


Fig. 6-6: Schematic illustration of typical load-displacement curve of an unbonded FREI

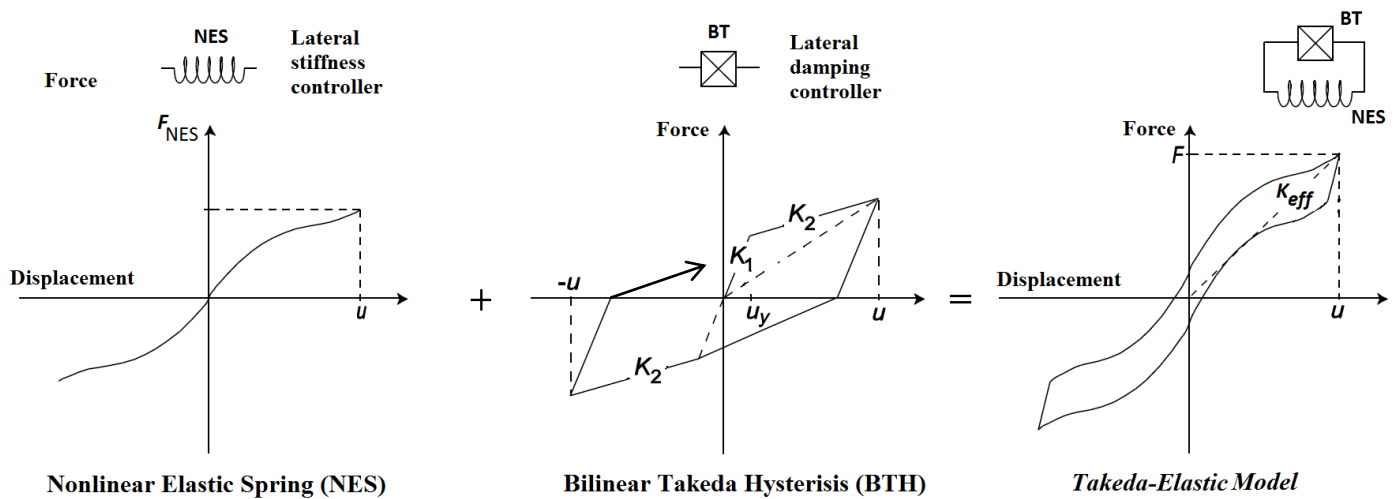
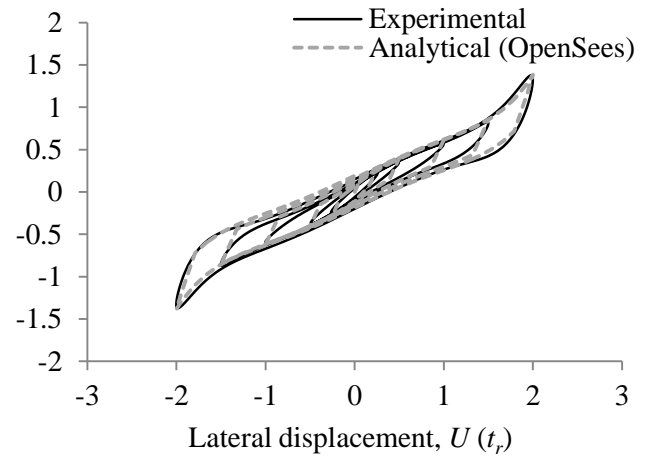


Fig. 6-7: Illustration of the proposed *Takeda-Elastic* model

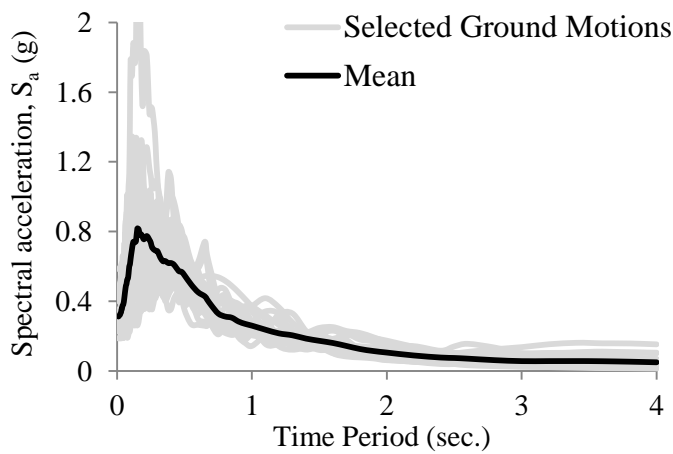


(a)

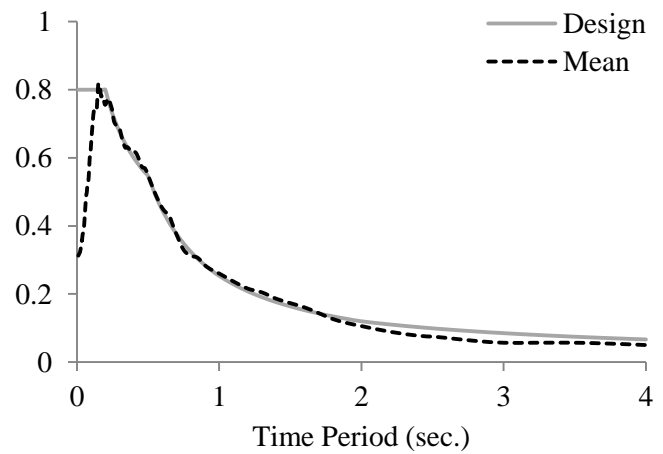


(b)

Fig. 6-8: (a) The 3DOF employed test apparatus; (b) Comparison of the experimentally obtained response of the U-FREI with the prediction of the *Takeda-Elastic* model



(a)



(b)

Fig. 6-9: (a) Scaled pseudo-acceleration response spectra of the 20 selected ground motions (Damping = 5%); (b) comparison of the mean scaled acceleration response spectrum of the selected ground motions with the CHBDC (2014) design response spectrum at Victoria City Hall, Canada.

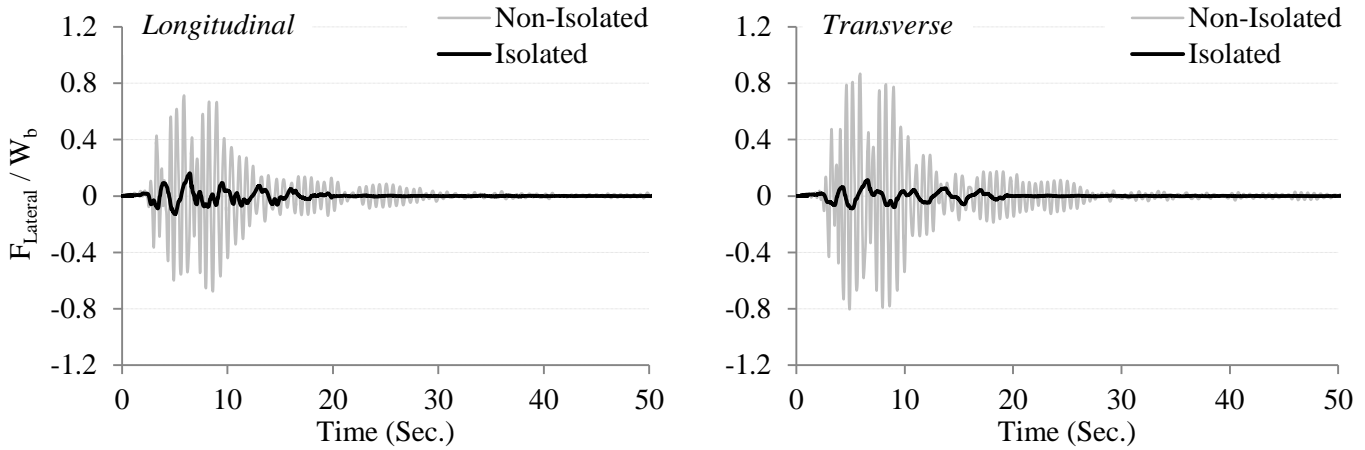


Fig. 6-10: Longitudinal and transverse response histories of normalized base shear when subjected to Earthquake 11 at MCE level

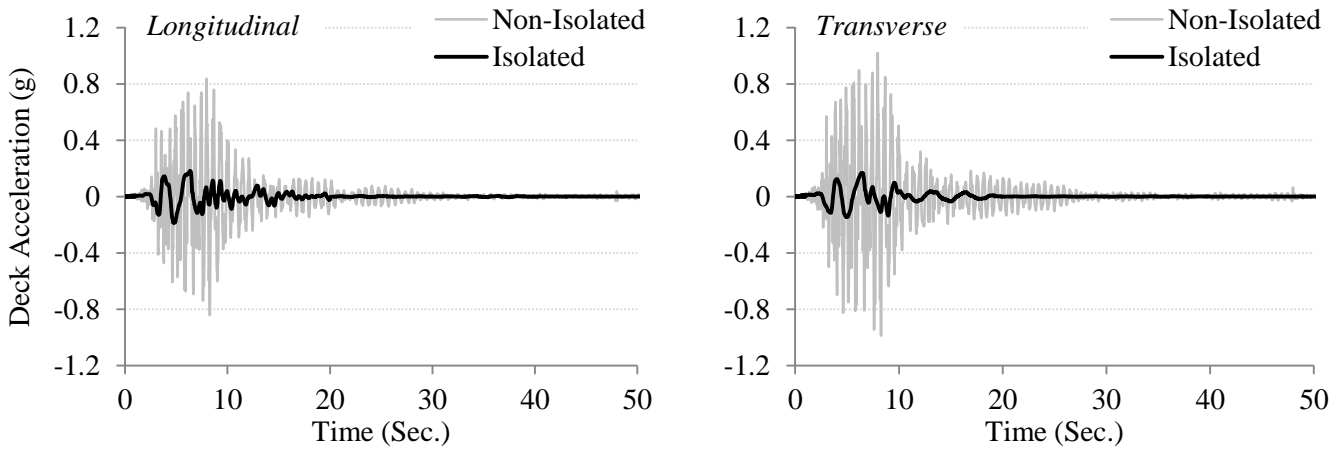


Fig. 6-11: Longitudinal and transverse response histories of deck acceleration when subjected to Earthquake 11 at MCE level

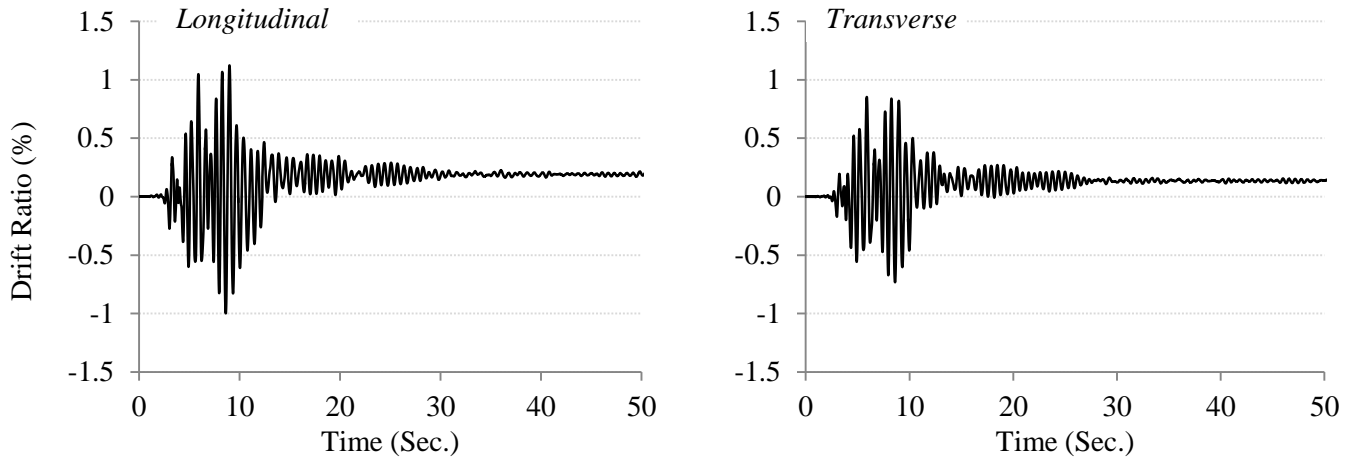


Fig. 6-12: Deck drift ratio for non-isolated bridge when subjected to Earthquake 11 at MCE level

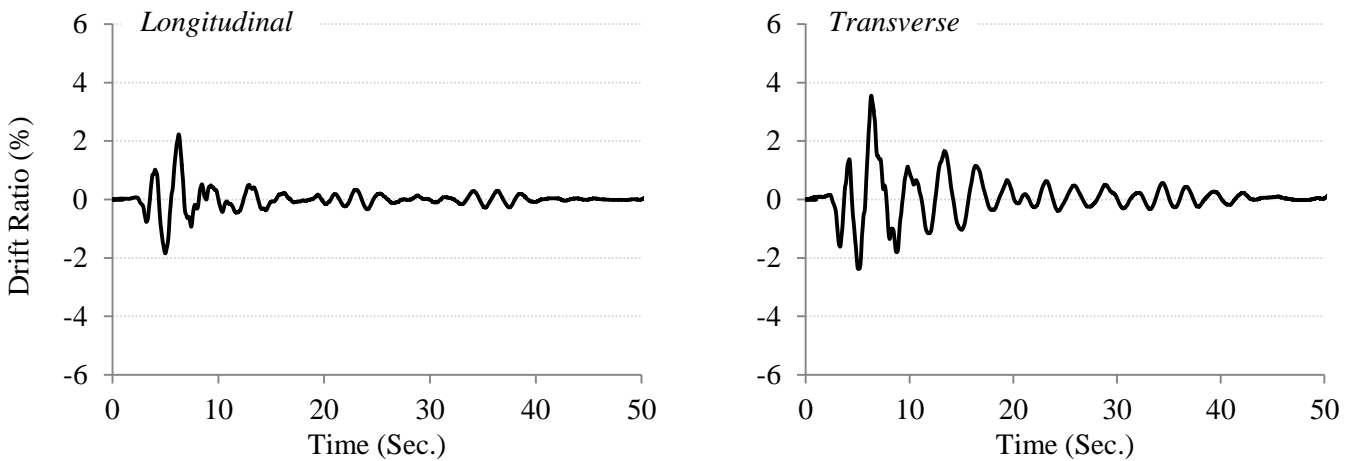


Fig. 6-13: Deck drift ratio for isolated bridge when subjected to Earthquake 11 at MCE level

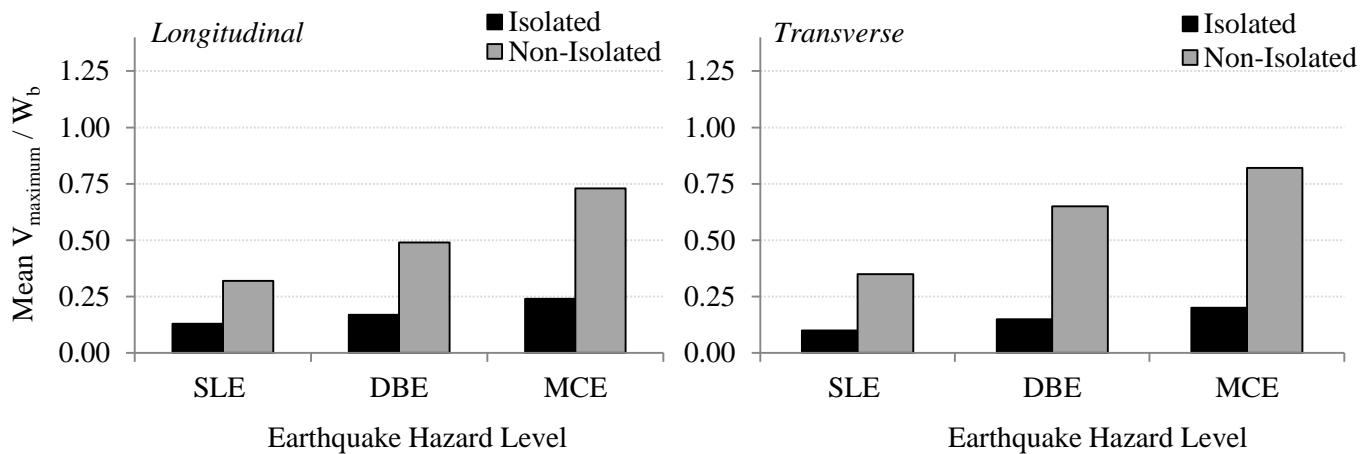


Fig. 6-14: Comparison of the mean values from all 20 ground motions of the normalized peak bent base shear for the longitudinal and transverse directions

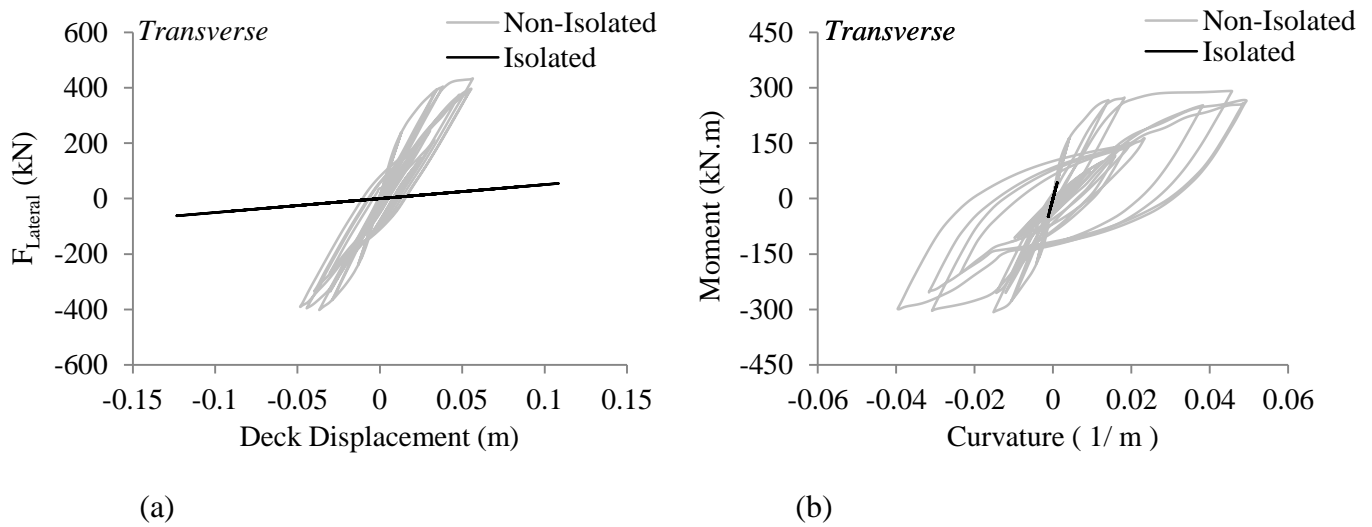


Fig. 6-15: (a) Force-displacement; (b) moment-curvature relationship for a single bent cap of both bridges when subjected to Earthquake 11 at MCE level

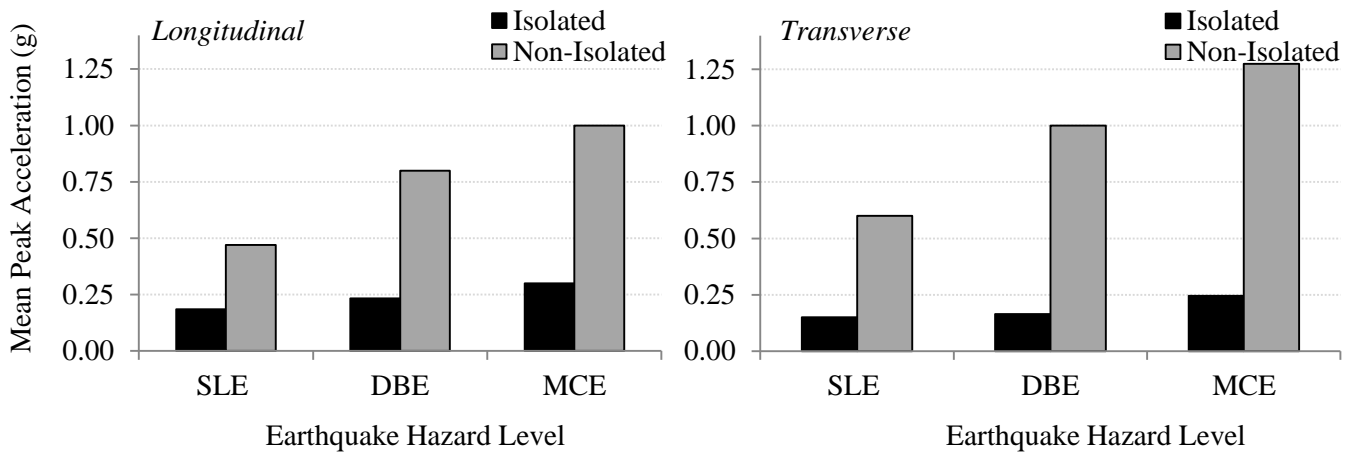


Fig. 6-16: Comparison of the mean values of the peak acceleration at the deck level from all 20 ground motions for the longitudinal and transverse directions

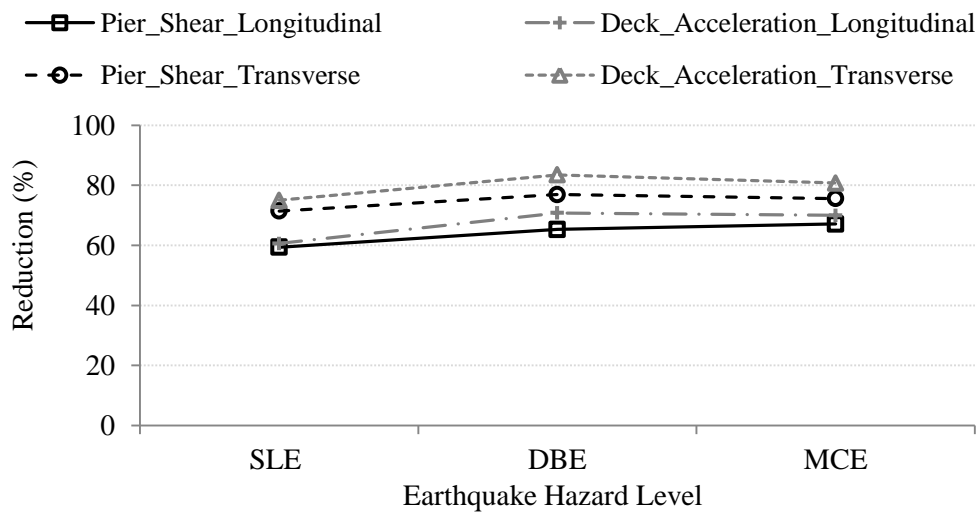


Fig. 6-17: Reduction (%) in the seismic demand of the bridge in both longitudinal and transverse directions

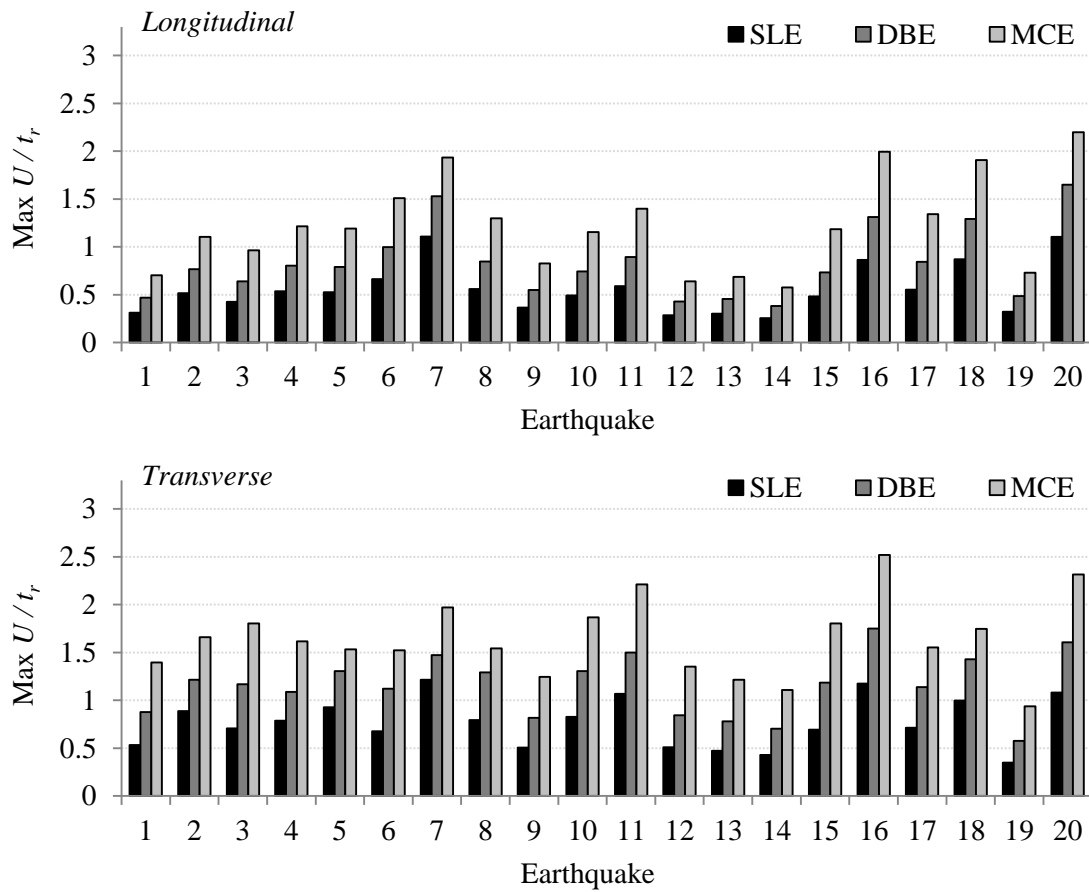


Fig. 6-18: Normalized peak isolation displacement for each of the considered 20 ground motions

Chapter SEVEN

SUMMARY, CONCLUSIONS AND RECOMMENDATIONS

7.1 Summary

The demand on bridge bearings/isolators has increased due to rapid developments in bridge design. In order to handle this increase in demand, researchers continue to focus on the development of new bearings. One of the critical aspects in selecting a bridge bearing, in addition to having sufficient vertical stiffness and lateral flexibility, is its ability to accommodate the rotational deformations induced by the bridge superstructure. A potential cost effective isolation system to enhance the seismic performance of ordinary low-rise buildings is comprised of unbonded-fiber reinforced elastomer isolators (U-FREI). However, there is a lack of experimental data available in the literature focusing on the influence of rotational deformation on the response of U-FREI. Most research conducted on U-FREI has focused on building applications rather than bridge applications. As such, the objective of this study is to investigate the efficiency of U-FREI to be employed in bridge applications as a bridge bearing as well as to seismically isolate vulnerable bridges.

To achieve this objective a set of comprehensive and numerical studies were carried out under a wide range of vertical loads, rotational deformations, and lateral deformations. All the loads and deformations were picked to represent loading scenarios that would be expected to occur under daily traffic loads and under seismic events. The experimental program was conducted in the Applied Dynamics Laboratory (ADL) at McMaster University using a three-degree of freedom (3DOF) bearing test apparatus, which is capable of applying vertical, rotational, and lateral loads, both separately and in combination. The U-FREI specimens were $\frac{1}{4}$

scale and fabricated from two different types of elastomer: natural and synthetic (i.e. neoprene). In addition, 2D and 3D finite element analyses were carried out using the commercially available general-purpose finite element program MSC Marc in order to evaluate and assess the resulting stress and strain state within the isolators. Finally, a mathematical model was developed to simulate the lateral response of U-FREI. This model was subsequently used to represent U-FREI in evaluating the seismic response of a typical three spans highway bridge, which was modeled using the open source finite element platform OpenSees (open system for earthquake engineering simulations).

7.2 Conclusions

i. Rotational Response

- U-FREI are able to accommodate rotational deformation angles up to 0.03 rad. via a stable rotational response with no delamination between elastomer and fiber or any other type of visible damage.
- The unbonded boundary condition of the U-FREI allows the uncompressed side of the isolator to detach from the contact supports (i.e. *lift-off*).
- One of the major advantages of the occurrence of *lift-off* is the fact that it reduces the development of tensile stresses in the uncompressed side of the isolator that may lead to damage.
- The level of vertical stresses applied on the U-FREI controls the initiation of *lift-off*, which subsequently influences the shape of the rotational hysteresis loops. As such, the softening type behaviour in the rotational response is much less significant under higher load levels as lift-off is delayed.

- The effective rotational damping ratio of U-FREI was determined to range between approximately 4% and 7%.

ii. Vertical Response

- U-FREI possess sufficient vertical stiffness and can adequately resist and transmit vertical loads from the bridge superstructure to its substructure.
- An increase in vertical loading frequency results in a directly proportional increase in the value of the vertical stiffness.
- An increase in the amplitude of the vertically applied load leads to an increase in the vertical stiffness of the isolator.
- The influence of static lateral offsets up to $1.5 t_r$ (total elastomer thickness) on the vertical stiffness is negligible. This behaviour was postulated to be due to the fact that lateral offsets results a significant nonlinearity in bearing geometry and elastomer.
- The effect of static rotations on the vertical stiffness of U-FREI is more significant under lower axial loads as a result of the earlier initiation of contact area loss (i.e. *lift-off*).
- Under large vertical loads, the effect of static rotations of the vertical stiffness is insignificant as *lift-off* is delayed.
- The values of vertical stiffness obtained experimentally were found to be in good agreement with the recently introduced theoretical solutions introduced by Kelly and Van Engelen (2015) for determining the vertical stiffness of square and rectangular elastomeric bearings, which include elastomer compressibility and reinforcement extensibility. However, since theoretical solutions were based on small displacement theory, the best agreement was found at low vertical stresses (i.e. 4 MPa).

- The effective vertical damping ratio of U-FREI was determined to range between approximately 1% and 3%.

iii. Lateral Response

- The influence of rotational deformations on the lateral response of U-FREI is negligible, but is least significant for isolators with lower aspect ratios.
- U-FREI with an aspect ratio of 2.50 could exhibit a stable lateral response even if subjected to rotational deformations up to 0.03 rad.
- In general, the increase in the levels of vertical loads as well as the increase in the applied angle of rotation on the isolator caused a slight decrease in the lateral stiffness and small increase in the lateral damping.
- The effective isolation period of the U-FREI investigated was calculated to be in the range of 0.80 to 2.90 seconds.
- The effective lateral damping ratio of U-FREI was determined to range between approximately 7.5% and 16%.

iv. Finite Element Modeling of the U-FREI via MSC Marc

- The end boundary conditions were found to have a negligible effect of on the vertical stiffness of the modeled U-FREI.
- Good agreement was found between the values of vertical stiffness with the approximate analytical “pressure solution” approach (Tsai and Kelly 2001) for both the B-FREI and U-FREI.

- For rotational stiffness, good agreement with the theoretical approach is found for B-FREI, while for U-FREI, significant deviation is found after the occurrence of *lift-off*.
- The rotational response of bonded FREI is linear up to failure.
- The rotational response of U-FREI is linear up to the occurrence of *lift-off* because the isolator is still in full contact with the supports (i.e. similar to B-FREI). While a nonlinear response in the rotational response is observed after *lift-off* due to the change in gap between the isolator and loading plate under rotational deformation.
- The rotational behaviour of U-FREI after the occurrence of *lift-off* is directly related to the isolator aspect ratio and the amplitude of the vertical load.
- The rotational stiffness of FREI increases as the aspect ratio is increased and as the applied vertical load is increased.
- The tensile stresses that occurs in the uncompressed side of the B-FREI leads to significant compressive strains in the fiber layers, which may results in excessive distortion (buckling) of the fiber reinforcement. On the other hand, U-FREI are always able to accommodate larger angles of rotation because separation of the isolator from the contact supports is permitted under excessive rotational deformations.
- The stress/strain demand on the elastomer material, fiber reinforcement, and bond between rubber and fiber was found to be considerably lower in the U-FREI when compared to the equivalent bonded-FREI.

v. Finite Element Modeling of a Typical Highway Bridge via OpenSees

- The developed non-iterative *Takeda-Elastic* model can simulate the lateral response of U-FREI, both the lateral stiffness and lateral damping.
- The parameters of the *Takeda-Elastic* model can be evaluated using the effective stiffness and damping values that are determined experimentally, avoiding the need to carry out fitting, for example using least squares, directly to the hysteresis loops.
- A reduction in the seismic demand of a typical highway bridge isolated with U-FREI was found to be in the range of 60% - 80% in the longitudinal and transverse directions.
- U-FREI can be employed as a potential cost-effective seismic isolation system in different bridge applications (e.g. accelerated bridge construction).

7.3 Recommendations for future studies

- A comprehensive cost-benefit analysis study on U-FREI compared to SREI in particular and other seismic isolation systems in general. The study should not be limited to manufacturing cost, but should also include the cost of installation and life-cycle performance.
- An investigation of the influence of fiber reinforcement on the lateral damping of the U-FREI. This can be accomplished by an experimental study on U-FREI with similar elastomer, but different types of fiber reinforcement properties, such as: thickness, volume of fiber to elastomer, weave type, and weave direction.
- Bi-directional experimental testing of U-FREI in order to investigate the effect of rollover in one direction on altering the lateral response in the other direction. Such a study would

allow the nonlinear finite element analysis completed in Chapter 6 to be replicated but under all three components of earthquake excitation.

- The inclusion of bridge design parameters such as: the flexibility in the piers and girders and the effects of soil-structure interaction on the seismic isolation adequacy of U-FREI for typical highway bridge considered in Chapter 6. Furthermore, a numerical investigation should also be conducted on the effectiveness of U-FREI in seismically isolating different bridge types (e.x. cable-stayed bridge) beyond the typical highway bridge.
- Comprehensive assessment of the long-term natural aging effects on the mechanical properties of U-FREI.
- Employing U-FREI in an existing bridge and performing structural health monitoring evaluation on the real performance of the bridge.

References

Kelly J., Van Engelen N. (2015). *Single Series Solution for the Rectangular Fiber-Reinforced Elastomeric Isolator Compression Modulus*. Pacific Earthquake Engineering Research Center, PEER, Berkeley, California; 2015/03.

Tsai H., Kelly J. (2001). *Stiffness analysis of fiber-reinforced elastomeric isolators*. Pacific Earthquake Engineering Research Center, PEER, Berkeley, California; 2001/5.